

**TUNING MATERIAL PROPERTIES VIA PEPTIDE DESIGN AND  
PHOTOPOLYMERIZATION OF SELF-ASSEMBLED PEPTIDE BASED  
HYDROGELS**

by

Ronak Rughani

A dissertation submitted to the Faculty of the University of Delaware in  
partial fulfillment of the requirements for the degree of Doctor of Philosophy in  
Chemistry and Biochemistry

Summer 2009

Copyright 2009 Ronak Rughani  
All Rights Reserved

**TUNING MATERIAL PROPERTIES VIA PEPTIDE DESIGN AND  
PHOTOPOLYMERIZATION OF SELF-ASSEMBLED PEPTIDE BASED  
HYDROGELS**

by

Ronak Rughani

Approved:

\_\_\_\_\_  
Klaus Theopold, Ph.D.  
Chair of the Department of Chemistry and Biochemistry

Approved:

\_\_\_\_\_  
George H. Watson, Ph.D.  
Interim Dean of the College of Arts and Sciences

Approved:

\_\_\_\_\_  
Debra Hess Norris, M.S.  
Vice Provost for Graduate and Professional Education

I certify that I have read this dissertation and that in my opinion it meets the academic and professional standard required by the University as a dissertation for the degree of Doctor of Philosophy.

Signed:

---

Joel P. Schneider, Ph.D.  
Professor in charge of dissertation

I certify that I have read this dissertation and that in my opinion it meets the academic and professional standard required by the University as a dissertation for the degree of Doctor of Philosophy.

Signed:

---

Joseph M. Fox, Ph.D.  
Member of dissertation committee

I certify that I have read this dissertation and that in my opinion it meets the academic and professional standard required by the University as a dissertation for the degree of Doctor of Philosophy.

Signed:

---

Darrin J. Pochan, Ph.D.  
Member of dissertation committee

I certify that I have read this dissertation and that in my opinion it meets the academic and professional standard required by the University as a dissertation for the degree of Doctor of Philosophy.

Signed:

---

Randall L. Duncan, Ph.D.  
Member of dissertation committee

## **ACKNOWLEDGMENTS**

Though only my name is printed on the cover of this dissertation with a new title “Ph.D.”, there are many people including my family, friends and mentors who have contributed and supported me to achieve this honor. I am very grateful to all those people who have made this achievement possible and because of whom my educational experience has been one that I will cherish forever.

First, I would like to express my deepest gratitude to my advisor Dr. Joel P. Schneider who gave me the freedom to explore research avenues on my own and at the same time guiding me to learn and recover from my mistakes. As a patient and supportive mentor, not only has he helped me in time of crisis but has also trained me to face the challenges yet to come. Under his guidance, I got an opportunity to learn how to become an independent scientist and am very proud to have been part of his research group.

I would also like to thank my interdisciplinary committee members, Dr. Darrin J. Pochan, Dr. Joseph M. Fox and Dr. Randall L. Duncan, for helping me to look at my research from different perspectives. I truly appreciate their valuable suggestions on both levels, scientific as well as professional development.

I am also very grateful to all the past members of the Schneider group whose previous research efforts helped me progress in my research work. To all the

currents members, thank you for all the your help through suggestions, scientific discussions and constructive criticisms.

My special thanks to Dr. Karthikan Rajagopal for all the support, encouragement and guidance since my first day in the lab and Monica Branco, a great friend, who has always been there to listen, give advice, explain rheology, correct grammar in my manuscripts and for all the fun times. Dr. Danny Ramadan, my best friend and family, for always being there especially in times of crisis. I couldn't have done it without all of you.

I am also thankful to all the faculty and administrative staff of the Department of Chemistry and Biochemistry at University of Delaware for their assistance and making my graduate study comfortable.

Most importantly, none of this would have been possible without the love, patience and support from my family. I am also very thankful to my extended family who have supported me throughout my career and helped me whenever possible.

## **DEDICATION**

I dedicate this dissertation to my family, to whom I am highly indebted.....

My father, Vinod Rughani, who taught me the importance of hard work and dedication, and has always, supported me.

My brother Prमित, my sister-in-law Shabana, my niece and nephew Simone and Ayaan for all their support and the sacrifices they have made so that I could succeed in getting my Ph.D.

My fiancé, Hiral Modi, who came into my life as a pillar of support half way into my Ph.D. and has always been there for me. I am very lucky to have her as my life partner.

Above all, to my mother, the late Champa Rughani, who instilled in me values such as patience and perseverance, and taught me the importance of education. Although she was long gone, her teachings and values have always guided me through every step I have taken to achieve my goals.

## TABLE OF CONTENTS

LIST OF TABLES .....	xii
LIST OF FIGURES .....	xiii
ABSTRACT .....	xxii
<b>Chapter 1. Molecular Design of <math>\beta</math>-Hairpin Peptides for Material Construction .....</b>	<b>1</b>
1.0 Introduction .....	1
1.1 <i>De Novo</i> Designed Self-Assembling $\beta$ -hairpins .....	4
1.1.1 Amino Acid Substitutions at the Hydrophilic Face .....	8
1.1.2 Amino Acid Substitution at the Hydrophobic Face .....	9
1.1.3 Importance of Hydrogen Bonding and Hydrophobic Contacts .....	11
1.1.4 Importance of Turn Region Residues .....	13
1.2 Functional Materials from Self-Assembling $\beta$ -Hairpins .....	14
1.2.1 Mimics of Extracellular Matrix .....	14
1.2.2 Injectable Delivery .....	16
1.2.3 Antibacterial Activity .....	16
1.2 Thesis Objective .....	17
<b>Chapter 2. Enhancing the Mechanical Properties of Designed Self-Assembling <math>\beta</math>-Hairpin Peptides via Photopolymerization .....</b>	<b>24</b>
2.0 Introduction .....	24
2.1 Folding, Self-Assembly and Hydrogelation of MAX1 at Physiologically Relevant Conditions .....	27
2.2 N-Terminus Modification of MAX1 .....	30
2.2.1 Design of N-Acryloyl MAX1 (M1NA) .....	30
2.2.2 Folding, Self-Assembly and Hydrogelation .....	31
2.2.3 Optimization of Photopolymerization Parameters .....	33
2.2.4 Effect of Irradiation on Mechanical Properties of MAX1 Hydrogel .....	34

2.2.5 Increase in Mechanical Properties of Hydrogels upon Photopolymerization .....	35
2.3 Hydrophilic Face Modification of MAX1 .....	38
2.3.1 Intrafibrillar Crosslinking via Polymerization of Lysine-Dienes .....	38
2.3.1.1 Peptide Design.....	40
2.3.1.2 Folding, Self-Assembly and Photopolymerization of Peptide Solutions .....	42
2.3.1.3 Monitoring Photopolymerization of Self-Assembled Peptide using CD and UV Spectroscopy.....	45
2.3.1.4 Mechanical Properties of Photopolymerized Hydrogels .....	48
2.3.1.5 Shear Recovery and Subsequent Photopolymerization of Hydrogels.....	50
2.3.1.6 Conclusions .....	53
2.3.2 Interfibrillar Crosslinking via Polymerization of Ne-Acryloyl-L-Lysine.....	54
2.3.2.1 Peptide Design.....	55
2.3.2.2 Effect of Photopolymerization on $\beta$ -Sheet Structure of Peptide Hydrogels.....	58
2.3.2.3 Mechanical Properties of Photopolymerized Hydrogels .....	59
2.3.2.4 Shear Recovery and Subsequent Photopolymerization of Hydrogels.....	61
2.3.2.5 Nanoscale Structure Analysis.....	64
2.3.2.6 Effect of Gelation Time on Mechanical Properties of Photopolymerized Hydrogels.....	66
2.3.2.7 Peptide Concentration Dependent Mechanical Rigidity of Hydrogels.....	67
2.3.2.8 Conclusions .....	70
2.3.3 Experimental Section .....	71
<b>Chapter 3. Fabricating Mechanically Robust Peptide-Polymer Hydrogels via Photopolymerization .....</b>	<b>81</b>
3.0 Introduction .....	81

3.1 Construction of Mechanically Rigid Hydrogels via the Formation of Crosslinked Network of Peptide and Divinylbenzyl PEG .....	82
3.1.1 Design and Fabrication Strategy of Peptide-Polymer Hydrogels.....	84
3.1.2 Synthesis of Divinylbenzyl PEG (PEGDVB) .....	85
3.1.3 Mechanical Properties of Single Network Hydrogels.....	86
3.1.4 Shear Recovery and Polymerization of Pre-formed Hydrogels.....	87
3.1.5 Compression Analysis of Photopolymerized Hydrogels .....	94
3.1.6 Cytocompatibility of Hydrogel Surfaces.....	97
3.1.7 Potential Advantage of MKA-based Hybrid Hydrogels over Polymer Hydrogels for Tissue Engineering Applications.....	99
3.1.8 Conclusions .....	100
3.2 Construction of Interpenetrating Network Hydrogels of Self-Assembled Peptide and Polymerized PEG-Diacrylate Network.....	101
3.2.1 Interpenetrating Network Hydrogels.....	103
3.2.2 Design and Fabrication of Peptide-Polymer IPN Hydrogels .....	105
3.2.3 Compression Analysis of Peptide-Polymer IPN Hydrogels.....	107
3.2.4 Conclusions .....	112
3.3 Experimental Section.....	114
<b>Chapter 4. Design and Characterization of Self-Assembling Three-Stranded <math>\beta</math>-sheet Peptides.....</b>	<b>124</b>
4.0 Introduction .....	124
4.1 Design of a Three-Stranded Self-Assembling Peptide .....	127
4.2 Folding, Self-assembly and Bulk Material Properties of a <i>De Novo</i> Designed Three-Stranded $\beta$ -sheet Hydrogel .....	133
4.2.1 Temperature Triggered Folding and Self-Assembly .....	133
4.2.2 Temperature Triggered Hydrogelation.....	135
4.2.3 Triggered Folding, Self-Assembly and Hydrogelation under Physiologically-relevant Conditions .....	142
4.2.4 Cytocompatibility of EMAX2 Hydrogels .....	146
4.2.5 Conclusions .....	149
4.3 Comparing the Self-Assembly and Material Properties of a Three-Stranded Peptide (EMAX2) and a $\beta$ -Hairpin Peptide (MAX1) .....	150
4.3.1 Temperature Triggered Folding and Self-Assembly .....	151
4.3.2 Temperature Triggered Hydrogelation.....	153

4.3.3 Peptide Sequence, Hydrophobicity and Material Properties.....	157
4.3.4 Folding, Self-Assembly and Hydrogelation under Physiologically relevant Conditions.....	158
4.4 Conclusions .....	161
4.5 Experimental Section.....	162
<b>Chapter 5. Role of Turn Sequence in Modulating the Mechanical     Properties of Three-Stranded Peptide Hydrogels .....</b>	<b>178</b>
5.0 Introduction .....	178
5.1 Turns in Proteins and Peptides .....	179
5.2 <i>De novo</i> Designed $\beta$ -turns.....	180
5.3 Turn Sequence dependent Self-Assembly and Hydrogelation.....	181
5.3.1 Design of Turn Sequence Peptides .....	182
5.3.2 Folding, Self-Assembly and Hydrogelation of EMAX Peptides.....	182
5.4 Conclusions .....	189
5.5 Experimental Section.....	191
<b>Chapter 6. Role of Cell Culture Conditions in Enhancing the Mechanical     Properties of Self-Assembled <math>\beta</math>-Hairpin Peptide Hydrogels as a     Function of Time .....</b>	<b>197</b>
6.0 Introduction .....	197
6.1 Self-Assembly and Hydrogelation of MAX1 under Cell Culture Conditions .....	198
6.2 Increase in Storage Modulus of MAX1 Hydrogels over Time: Effect of Normal Aging.....	200
6.3 Effect of Sodium Bicarbonate on the Kinetics of Self-Assembly and Hydrogelation of MAX1 .....	201
6.4 Influence of Gaseous Carbon Dioxide on Storage Modulus of MAX1 Hydrogels .....	206

6.5 Role of Dissolved Carbon Dioxide on Storage Modulus of MAX1 Hydrogels .....	209
6.6 Conclusions .....	210
6.7 Experimental Section.....	212
<b>Chapter 7. Conclusions .....</b>	<b>217</b>

## LIST OF TABLES

Table 2.1 Dynamic time sweep experiment data of 1 wt% MKA hydrogels showing physical gelation time dependent increase in storage modulus upon photopolymerization .....	68
Table 2.2 Concentration dependent mechanical rigidity of MKA hydrogels before and after photopolyemrization at pH 7.4 and 37 °C.....	69
Table 3.1 Literature examples of different types of IPNs and their compressive moduli .....	104
Table 4.1 Differences between MAX1 and EMAX2.....	158
Table 5.1 Sequences of three-stranded peptides with identical or mixed turn regions.....	182
Table 5.2 Properties of Three-Stranded Turn Sequence Peptides .....	189

## LIST OF FIGURES

Figure 1.1 Self-assembled structures derived from peptide amphiphiles (red: hydrophilic, green: hydrophobic) (a) Diblock amphiphile (b) Facial amphiphile .....	2
Figure 1.2 (a) Environmentally triggered folding, self-assembly, and non-covalent fibril crosslinking leading to hydrogelation. (b) $\beta$ -hairpin structure of MAX 1 comprised of two $\beta$ -strands of alternating valine (green) and lysine (red) residues connected via a type II' $\beta$ -turn.....	4
Figure 1.3 Factors affecting (a) folding and (b) self-assembly of $\beta$ -hairpin peptides .....	7
Figure 1.4 Structure-based design of MAX1. Modifications to the hydrophilic, hydrophobic, and turn regions to create new peptides with tailored properties.....	15
Figure 2.1 Possible modifications of the amphiphilic MAX1 $\beta$ -hairpin.....	27
Figure 2.2 (a) Circular dichroism wavelength spectrum of a 1 wt% MAX1 hydrogel at pH 7.4 (50 mM BTP, 150 mM NaCl) and 37 °C after a 1hr gelation time. (b) $[\theta]_{216}$ measured as a function of time (1 wt% MAX1, pH 7.4, 37 °C).....	28
Figure 2.3 Dynamic time sweep measurement of 1 wt% MAX1 at pH 7.4 (50 mM BTP, 150 mM NaCl) at 37 °C. [6 rad/s, 0.2% strain].....	29
Figure 2.4 Design and synthesis of M1NA peptide.....	30
Figure 2.5 (a) Circular dichroism wavelength spectrum of a 1 wt% M1NA hydrogel at pH 7.4 (50 mM BTP, 150 mM NaCl) and 37 °C after a 1hr gelation time. (b) $[\theta]_{216}$ measured as a function of time (1 wt% M1NA, pH 7.4, 37 °C).....	31

Figure 2.6 Rheological measurements of 1 wt% M1NA at pH 7.4 (50 mM BTP, 150 mM NaCl) and 37 °C. (a) Dynamic time sweep experiment showing evolution of storage modulus ( $G'$ ) as a function of time (b) Dynamic frequency sweep measurement showing the storage ( $G'$ ) and loss ( $G''$ ) modulus values as a function of angular frequency.....	32
Figure 2.8 Changes in temperature and viscosity of standard viscosity oil (S600) after 30 minutes of irradiation (365 nm) as a function of UV light intensity .....	34
Figure 2.9 Dynamic time sweep of 1 wt% MAX1 at pH 7.4 (50 mM BTP, 150 mM NaCl) at 37 °C (6 rad/s, 0.2 % strain) showing minimal increase in storage modulus ( $G'$ ) upon irradiation, 3 hrs after gelation was triggered.....	35
Figure 2.10 (a) Dynamic time sweep experiment showing increase in storage modulus ( $G'$ ) upon photopolymerization of a pre-formed 1wt% M1NA hydrogel formed at pH 7.4 (50mM BTP, 150mM NaCl, 0.025wt% Irgacure 2959) and 37 °C. (b) Dynamic time sweep experiment showing shear recovery and photopolymerization of pre-formed 1wt% M1NA hydrogels at 37 °C and pH 7.4 (50mM BTP, 150mM NaCl, 0.025wt% Irgacure 2959) monitored as a function of time. ....	37
Figure 2.11 (a) Proposed mechanism of folding and self-assembly leading to hydrogelation and subsequent photopolymerization. X = structure of the photopolymerizable lysine-diene [K(DE)]. (b) Sequence of the photopolymerizable $\beta$ -hairpin peptide (MLD) and its control peptide (M2K).....	39
Figure 2.12 Schematic representation showing design of MLD for efficient polymerization of the $\beta$ -hairpins in the self-assembled state irrespective of the hairpin arrangement along the axis of a given fibril. ....	42
Figure 2.13 (a) CD spectroscopy of 150 $\mu$ M MLD solution at pH 7.4 (50 mM BTP, 150 mM NaCl) showing $[\theta]_{216}$ as a function of temperature. (b) Wavelength spectra of 150 $\mu$ M MLD solution at pH 7.4 showing transition from random coil at 5 °C to $\beta$ -sheet at 37 °C. ....	44

Figure 2.14 (a) Wavelength scans of 0.1wt% MLD showing time dependent decrease in intensity at 245 nm upon photopolymerization. Inset: Magnified view showing the decrease in intensity at 245 nm with polymerization time. (b) UV absorption spectra of self-assembled 0.1wt% MLD at pH 7.4 (50mM BTP, 150mM NaCl) showing decrease in absorption intensity at 257 nm upon photopolymerization with time (0-30 hrs).....	45
Figure 2.15 (a) Normalized photopolymerization profile of 0.1 wt% MLD obtained via CD and UV as a function of irradiation time. (b) Wavelength scans of 1wt% MLD peptide self-assembled at pH 7.4 (50mM BTP, 150mM NaCl, 0.025wt% Irgacure 2959) and 37 °C before and after 5 minutes of photoirradiation at 365 nm.....	47
Figure 2.16 (a) Dynamic time sweep experiment showing about 2.5 fold increase in storage modulus ( $G'$ ) upon photopolymerization of pre-formed 1wt% MLD hydrogel at pH 7.4 (50mM BTP, 150mM NaCl, 0.025wt% Irgacure 2959) and 37 °C (b) Dynamic frequency sweep measurement showing the storage ( $G'$ ) and loss ( $G''$ ) modulus values as a function of angular frequency .....	49
Figure 2.17 Dynamic time sweep experiment showing shear-thinning, recovery and subsequent photopolymerization of pre-fomed 1wt% MLD hydrogel at pH 7.4 (50mM BTP, 150mM NaCl, 0.025wt% Irgacure 2959) and 37 °C. ....	51
Figure 2.18 Dynamic time sweep experiment showing shear-thinning followed by immediate photopolymerization of pre-fomed 1wt% MLD hydrogels at pH 7.4 (50mM BTP, 150mM NaCl, 0.025wt% Irgacure 2959) and 37 °C. ....	52
Figure 2.19 Schematic depicting interfibrillar crosslinking of entanglements following triggered folding and self-assembly.....	55
Figure 2.20 (a) Side and top view of MKA peptide showing lysine position 19 along the $\beta$ -hairpin (b) Side and top view of MKA2 peptide showing lysine position 15 along the $\beta$ -hairpin (c) Structure of Fmoc-N $\epsilon$ -acryloyl-L-lysine-OH employed in synthesis of MKA (d) Sequence of MKA and MKA2 peptide where <b>K(A)</b> is the N $\epsilon$ -acryloyl-L-lysine .....	56
Figure 2.21 Schematic depicting design of $\beta$ -hairpin peptides that favor Interfibrillar crosslinking following self-assembly .....	57

Figure 2.22 CD wavelength spectra of (a) 1 wt% MKA and (b) 1 wt% MKA2 before and after photopolymerization at pH 7.4 and 37 °C.....	58
Figure 2.23 Kinetics of $\beta$ -sheet formation of 1 wt% MKA and MKA2 at pH 7.4 and 37 °C as a function of time .....	60
Figure 2.24 Dynamic time sweep experiments showing increase in mechanical rigidity of pre-formed (a) 1 wt% MKA and (b) 1 wt% MKA2 hydrogels at pH 7.4 and 37 °C upon photoirradiation .....	61
Figure 2.25 Oscillatory shear rheology of 1wt% MKA hydrogels at pH 7.4 (50mM BTP, 150mM NaCl, 0.025wt% Irgacure 2959) and 37 °C.....	62
Figure 2.26 Oscillatory shear rheology of 1wt% MKA hydrogels at pH 7.4 (50mM BTP, 150mM NaCl, 0.025wt% Irgacure 2959) and 37 °C.....	64
Figure 2.27 (a) SANS data of 1 wt% MKA hydrogel at pH 7.4 (50 mM BTP, 150 mM NaCl, 0.025 wt% Irgacure 2959) and 37 °C before and after photopolymerization. (b) TEM micrograph of diluted 1 wt% MKA hydrogel at pH 7.4 and 37 °C.....	65
Figure 2.28 Dynamic time sweep experiments of 1 wt% MKA at pH 7.4 and 37 °C. (a) Time dependent gelation and subsequent polymerization data (shown separately for clarity) (b) Time dependent gelation and subsequent polymerization (all data sets).....	68
Figure 2.29 Peptide concentration dependent mechanical properties of MKA hydrogels before and after photopolymerization.....	69
Figure 3.1 (a) Dynamic frequency sweep and (b) Dynamic strain sweep measurements of photocrosslinked 1 wt% MKA hydrogels at pH 7.4 and 37 °C .....	84
Figure 3.2 Schematic depicting covalent crosslinks formed in the hybrid hydrogel upon photopolymerization.....	85
Figure 3.3 Synthesis of Divinylbenzyl-PEG (PEGDVB) .....	86
Figure 3.4 Mechanical properties of photopolymerized 1 wt% MKA and 10 wt% PEGDVB hybrid hydrogels at pH 7.4 and 37 °C .....	87
Figure 3.5 Dynamic time sweep experiment showing shear-thinning, recovery and subsequent photopolymerization of pre-formed hydrogels of 1 wt% MKA with varying concentrations of PEGDVB.....	89

Figure 3.6 Dynamic frequency sweep of 1 wt% MKA hydrogels with varying concentrations of PEGDVB after photopolymerization .....	90
Figure 3.7 Dynamic time sweep experiment showing shear-thinning followed by immediate photopolymerization of pre-formed hydrogels of 1 wt% MKA with varying concentrations of PEGDVB.....	91
Figure 3.8 Dynamic frequency sweep of 1 wt% MKA hydrogels with varying concentrations of PEGDVB after photopolymerization .....	92
Figure 3.9 Dynamic time sweep experiment of 1 wt% MKA hydrogels with 10 wt% PEGDVB showing effect of photopolymerization time on the mechanical properties of the resultant hydrogels .....	93
Figure 3.10 (a) Stress-strain curve of 1 wt% MKA hydrogel at pH 7.4 (b) Stress-strain curves of polymerized hybrid hydrogels and the single network MKA hydrogel at pH 7.4 (c) Compressive moduli of hydrogels as a function of PEGDVB concentration.....	95
Figure 3.11 (a) Swelling ratio and (b) Equilibrium water content (%) of MKA hydrogels as a function of PEGDVB concentration.....	97
Figure 3.12 Laser scanning confocal microscopy (LSCM) images of a Live/Dead cellular viability assay of C3H10t1/2 (30,000 cells/cm <sup>2</sup> ) incubated on surface of (a) photocrosslinked 1 wt% MKA hydrogel (b) polymerized 10 wt% PEGDVB hydrogel (c) photocrosslinked hybrid hydrogel [1 wt% MKA + 10 wt% PEGDVB] and (d) TCTP control surface after 24 hours. Live cells fluoresce green and dead cells fluoresce red. Scale bar = 100 $\mu$ m.....	98
Figure 3.13 A schematic showing preparation of (a) sequential and (b) simultaneous IPN.....	102
Figure 3.14 Schematic representation of fabrication of MAX1-PEGDA sequential IPN hydrogels. ....	107
Figure 3.15 Swelling ratio and equilibrium water content values of single network and IPN hydrogels.....	108
Figure 3.16 Compressive modulus of single network and IPN hydrogels as determined by compressive tests.....	109

Figure 3.17 Typical appearance of single network PEGDA and IPN hydrogels. PEGDA hydrogels: (a) 5 wt% PEGDA (b) 10 wt% PEGDA (c) 15 wt% PEGDA. IPN hydrogels: (d) 1 wt% MAX1 + 5 wt% PEGDA (e) 1 wt% MAX1 + 10 wt% PEGDA (f) 1 wt% MAX1 + 15 wt% PEGDA .....	110
Figure 3.18 Fracture stress and strain properties of single network PEGDA and IPN hydrogels.....	111
Figure 4.1 (a) Proposed mechanism of folding and self-assembly of EMAX2 leading to hydrogelation. Several EMAX2 molecules are colored red in the fibril to highlight the three-stranded sheet conformation of EMAX2 in the folded and assembled state as well as bilayer formation. (b) Structure and sequence of EMAX2.....	126
Figure 4.2 (a) CD spectroscopy of 150 $\mu$ M EMAX2 solution at pH 9.0 (125 mM borate, 10 mM NaCl) showing $[\theta]_{216}$ as a function of temperature. (Inset) Wavelength spectra of 150 $\mu$ M EMAX2 solution at pH 9.0 showing transition from random coil at 10 $^{\circ}$ C ( $\blacklozenge$ ) to $\beta$ -sheet at 37 $^{\circ}$ C ( $\Delta$ ). (b) $[\theta]_{216}$ measured as a function of time (150 $\mu$ M EMAX2, pH 9.0, 37 $^{\circ}$ C) .....	134
Figure 4.3 (a) Dynamic time sweep of 1 wt % EMAX2 at pH 9 (125 mM borate, 10 mM NaCl) showing the evolution of storage modulus ( $G'$ ) as a function of time at 37 $^{\circ}$ C [ $\blacktriangle$ ] or 50 $^{\circ}$ C [ $\bullet$ ]. (b) Dynamic time sweep of 1 wt % EMAX2 at pH 9 showing the change in storage modulus upon increasing the temperature from 37 to 50 $^{\circ}$ C after 60 min of gelation at 37 $^{\circ}$ C. Dynamic frequency sweep of 1 wt % EMAX2 at pH 9 (125 mM borate, 10 mM NaCl) at (c) 37 $^{\circ}$ C and (d) 50 $^{\circ}$ C.....	138
Figure 4.4 Fourier transform infrared spectroscopy of 1 wt % EMAX2 at pH 9.0 showing $\beta$ -sheet structure at 37 $^{\circ}$ C.....	139
Figure 4.5. (a) Dynamic strain sweep of 1 wt % EMAX2 hydrogel formed at pH 9.0, 37 $^{\circ}$ C. (b) Shear-thinning and recovery profile of 1 wt % EMAX2 hydrogel at pH 9.0, 37 $^{\circ}$ C. ....	140
Figure 4.6 (a) SANS data of 0.5 wt % EMAX2 hydrogel at pH 9.0 (125 mM Borate, 10 mM NaCl in $D_2O$ ) collected at 22 $^{\circ}$ C after 2 h of gelation at 37 $^{\circ}$ C. (b) TEM micrograph of 1 wt% EMAX2 at pH 9.0 (125 mM Borate, 10 mM NaCl), 37 $^{\circ}$ C.....	141

Figure 4.7 (a) $[\theta]_{216}$ is measured as a function of NaCl concentration for 2 wt % EMAX2 preparations at pH 7.4 (50 mM BTP) at 37 °C. (b) TEM micrograph of 1 wt% EMAX2 hydrogel formed at pH 7.4 (50 mM BTP, 150 mM NaCl), 37 °C. ....	143
Figure 4.8 $[\theta]_{216}$ measured as a function of time for 2 wt % EMAX2 at pH 7.4 (DMEM) at 37 °C. ....	144
Figure 4.9 (a) Dynamic time sweep of 2 wt % EMAX2 at pH 9.0 (125 mM Borate, 10 mM NaCl) [ $\blacktriangle$ ] and pH 7.4 (DMEM) [ $\triangle$ ] monitoring $G'$ at 37 °C as a function of time. (b) Shear-thinning and recovery profile of 2 wt % EMAX2 hydrogel at pH 7.4 (DMEM) and 37 °C. ....	145
Figure 4.10 Cellular viability of C3H10t1/2 mesenchymal stem cells after 24 h cultured on (a) 2 wt % EMAX2 hydrogel; (b) TCTP control. ....	147
Figure 4.11 LSCM images of C3H10t1/2 mesenchymal stem cells on the surface of 2 wt % EMAX2 hydrogel after 24 h. Green fluorescence shows Actin where blue fluorescence shows nuclear staining for reference. ....	148
Figure 4.12 Structure and sequence of MAX1 and EMAX2 .....	150
Figure 4.13 CD spectroscopy of 150 $\mu$ M solutions of MAX1 and EMAX2 showing (a) temperature dependent $\beta$ -sheet formation at pH 9.0 and (b) pH dependent $\beta$ -sheet formation at 40 °C monitored at 216 nm. ....	152
Figure 4.14 Kinetics of $\beta$ -sheet formation monitored by measuring $[\theta]_{216}$ as a function of time (150 $\mu$ M MAX1 and EMAX2 solution at pH 9, 37 °C) .....	153
Figure 4.15 Mechanical properties of 1 wt% MAX1 and EMAX2 at pH 9.0 and 37 °C .....	154
Figure 4.16 Fourier transform infrared spectroscopy of (a) 1 wt% MAX1 and (b) 1 wt% EMAX2 at pH 9.0 showing $\beta$ -sheet structure at 37 °C .....	155
Figure 4.17 Shear-thinning and recovery profile of 1 wt% MAX1 and EMAX2 hydrogels at pH 9 and 37 °C.....	156

Figure 4.18 CD spectroscopy of showing salt concentration dependent $\beta$ -sheet formation of 2 wt% MAX1 and EMAX2 solutions at pH 7.4 and 37 °C .....	159
Figure 4.19 Dynamic (a) time and (b) frequency sweep of 2 wt% MAX1 and EMAX2 hydrogels at pH 7.4 (DMEM) and 37 °C.....	160
Figure 5.1 Structure of a typical $\beta$ -turn.....	180
Figure 5.2. Sequence of Three-stranded peptide (EMAX2) showing the two turn regions.....	181
Figure 5.3 Temperature dependent $\beta$ -sheet formation of EMAX 150 $\mu$ M peptides at pH 9.0 (125 mM Borate, 10 mM NaCl).....	183
Figure 5.4. CD spectroscopy of turn sequence peptides (a) Temperature dependent $\beta$ -sheet formation monitored by plotting $[\theta]_{216}$ as a function of temperature (b) pH dependent $\beta$ -sheet formation monitored by measuring $[\theta]_{216}$ as a function of pH (50 mM buffer, 10 mM NaCl) at 40 °C .....	185
Figure 5.5 Fourier transform spectroscopy of 1 wt% EMAX peptides at pH 9 showing $\beta$ -sheet structure at 50 °C.....	186
Figure 5.6 Dynamic time sweep experiment of 1 wt% EMAX peptides at pH 9 and 50 °C.....	187
Figure 6.1 (a) CD spectra and (b) Bulk material properties of 2 wt% MAX1 hydrogels formed with DMEM at 37 °C.....	199
Figure 6.2 Dynamic frequency sweep of 2 wt% MAX1 hydrogels incubated under cell culture conditions for 24 and 48 hrs.....	200
Figure 6.3 Sodium bicarbonate concentration dependent kinetics of self-assembly and hydrogelation of MAX1 at pH 7.4 (50mM BTP, 150 mM NaCl) and 37 °C (a) 0.25 wt% MAX1 (b) 2 wt% MAX1 .....	203
Figure 6.4 Effect of NaCl on the kinetics of self-assembly and hydrogelation of 2 wt% MAX1 hydrogels at pH 7.4 (50mM BTP) in presence of 44 mM NaHCO <sub>3</sub> and 37 °C .....	204
Figure 6.5 Nanoscale morphology of MAX1 hydrogels prepared at pH 7.4 in (a) absence and (b) presence of 44 mM NaHCO <sub>3</sub> .....	205

Figure 6.6 Proposed interaction of bicarbonate anion with lysine side chain .....	206
Figure 6.7 Mechanical properties of 2 wt% MAX1 hydrogels at pH 7.4 and 37 °C based on incubation conditions.....	208
Figure 6.8 Mechanical properties of 2 wt% MAX1 hydrogels at pH 7.4 and 37 °C (a) G' as a function of sodium bicarbonate concentration (b) Effect of CO <sub>2</sub> on rigidity of hydrogels with saturated concentration of sodium bicarbonate.....	210

## ABSTRACT

Self-assembly of *de novo* designed peptides is a promising approach towards fabrication of functional materials. Hydrogels are one such class of materials, which are highly hydrated and mechanically rigid, and show potential as scaffolds for tissue engineering and drug delivery applications. Schneider and Pochan labs have developed a strategy to fabricate three-dimensional scaffolds for biomedical applications employing self-assembling  $\beta$ -hairpin peptides. These 20 amino acid peptides can be triggered to fold and self-assemble in response to environmental cues such as pH and ionic strength, which then leads to formation of a physically crosslinked mechanically rigid hydrogel. A hallmark of these hydrogels is that they can be syringe delivered to a target site with spatial and temporal resolution. This property has been investigated towards development of injectable hydrogels for therapeutic and cellular delivery.

An important criterion for development of scaffolds for tissue engineering applications is that the mechanical properties of the engineered scaffold should be similar to the mechanical properties of the native tissue to restore normal function. A limitation of many physically crosslinked hydrogels is that they are mechanically weak. A potential approach to enhancing the mechanical properties of these hydrogels includes formation of covalent crosslinks through chemical modification of the

peptide sequence. This thesis specifically focuses on molecular level design of stimuli responsive self-assembling peptides to fabricate hydrogels with enhanced mechanical properties. In particular, two avenues were investigated to construct mechanically rigid hydrogels. First, the  $\beta$ -hairpin peptides were covalently modified with photopolymerizable groups at specific positions to allow covalent crosslinking of the hydrogel network. In addition, peptide-polymer hydrogel constructs were prepared using self-assembling peptides and bifunctional polymers to create interpenetrating network hydrogels with enhanced mechanical properties. The material rigidity of the interpenetrating networks could be modulated depending upon the method of its preparation. Second, self-assembling, three-stranded antiparallel  $\beta$ -sheets were designed. These peptides exhibited faster kinetics of self-assembly and formed mechanically more rigid hydrogels than their  $\beta$ -hairpin counterpart. The mechanical properties of the gels formed by the three-stranded peptides were further modulated by varying the hydrophobicity of the turn region residues.

The results described in this thesis demonstrate that peptide-based hydrogel scaffolds with tailored mechanical properties can be constructed through molecular level design. These hydrogel materials show potential for use as load bearing substitutes for tissue engineering applications.

## Chapter 1

# MOLECULAR DESIGN OF BETA-HAIRPIN PEPTIDES FOR MATERIAL CONSTRUCTION

### 1.0 Introduction

Proteins have evolved to fold, and in some cases self-assemble, into a vast array of beautiful structures, in large part, to facilitate function. Their smaller cousins, peptides are attractive building blocks for the construction of functional self-assembled materials owing to their smaller sequence length, ease of synthesis and purification, and a continuing advancement in the understanding of their folding and assembly propensities. The organization of peptides into ordered structures is guided by the formation of interactions such as hydrogen bonds, electrostatic interactions, hydrophobic contacts and aromatic interactions.<sup>1</sup> The amide-containing backbone of peptides can facilitate the formation of H-bonds, amino acids that contain polar side chains can participate in the formation of electrostatic interactions such as salt bridges, cysteine residues can form disulfide linkages, histidine, tryptophan, phenylalanine and tyrosine side chains can promote aromatic interactions, and hydrophobic side chains can facilitate van der Waals contact formation. Even extremely small peptides (< 3 residues) can assemble into impressive structures using a combination of these interactions.<sup>2-4</sup>

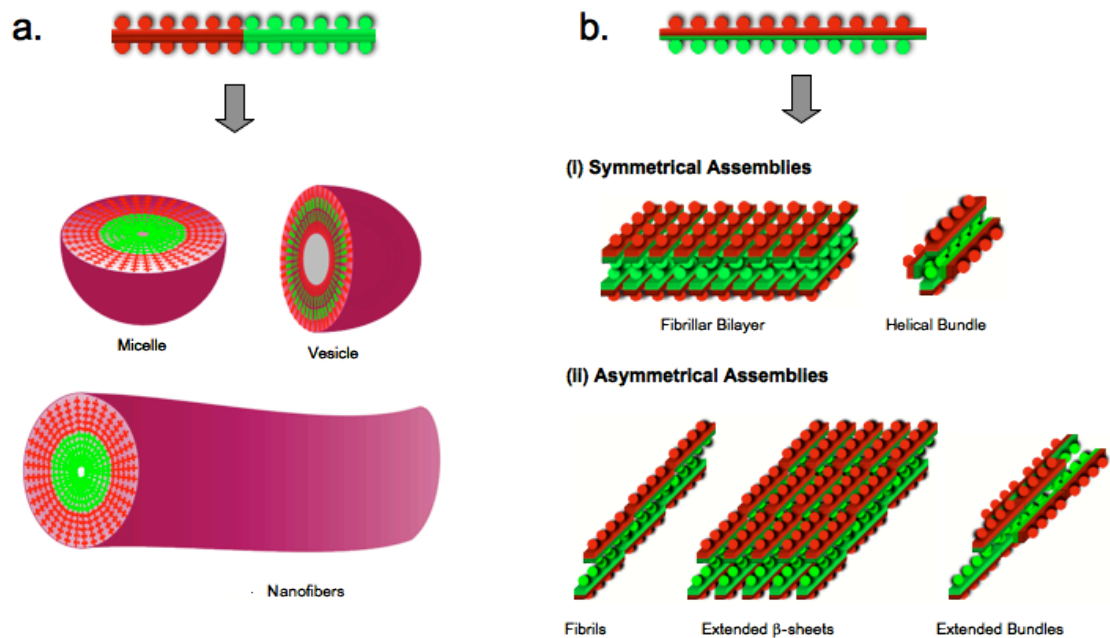


**Figure 1.1 Self-assembled structures derived from peptide amphiphiles (red: hydrophilic, green: hydrophobic) (a) Diblock amphiphile (b) Facial amphiphile**

A straight-forward design strategy that can be used to construct peptides capable of self-assembling into a large number of structures is to simply segregate amino acids along the peptide backbone with respect to their propensity to engage in a particular interaction. For example, amphiphilic peptides contain both hydrophobic and hydrophilic side chains that are segregated from each other. In the simplest of examples, segregation comes in two flavors. First, hydrophilic (A) and hydrophobic (B) residues can be segregated spatially along the length of the peptide sequence (-

$[A]_n-[B]_n$ ) resulting in diblock amphiphiles, Figure 1.1. In a slightly more complex arrangement, residues are segregated spatially with respect to distinct faces of a folded peptide structure, Figure 1.1b. For example, a sequence of alternating hydrophilic and hydrophobic residues ( $-[ABABAB]_n$ )<sup>5</sup> that adopts an extended conformation would have opposing hydrophilic and hydrophobic faces. Peptides having sequences such as ( $-[BAABBAA]_n$ )<sup>6</sup> can adopt facially amphiphilic helical structures that assemble into helical bundles. In aqueous solution, irrespective of the type of segregation, peptide assembly is largely driven by the desolvation and self-association of the hydrophobic portions of the peptide; this process is normally non-specific with respect to the structural outcome of the self-assembly event. However, hydrophilic moieties can be used to design specific polar interactions that can help dictate the formation of a given structure over possible alternatives.

Although not a comprehensive list, common structures resulting from the self-assembly of diblock amphiphiles include micelles<sup>7,8</sup>, vesicles<sup>9</sup> and nanofibers<sup>10</sup>, Figure 1.1a. Facial amphiphiles such as  $\beta$ -strands and  $\beta$ -hairpins often form fibrillar bilayers<sup>11,12</sup> and higher order laminates<sup>13,14</sup>, extended fibrils and extended  $\beta$ -sheets<sup>15</sup>. In addition, linear and cyclic peptides have been designed to assemble into tubes<sup>16</sup>,<sup>17</sup> and other peptides designed to assemble at surfaces<sup>18-20</sup>. Helical facial amphiphiles typically form discrete helical bundles or extended bundles<sup>21,22</sup>, Figure 1.1b.

## 1.1 *De Novo* Designed Self-Assembling $\beta$ -hairpins

Schneider and Pochan have designed peptides, which in response to distinct external stimuli, fold into facially amphiphilic  $\beta$ -hairpins and subsequently self-assemble to form self-supporting, rigid hydrogels. This mechanism allows material formation to take place with temporal resolution. The parent sequence, MAX1, is a 20-amino acid peptide comprised of two  $\beta$ -strands with alternating high  $\beta$ -sheet propensity valine and lysine residues. These strands are connected by a tetrapeptide (-V<sup>D</sup>PPT-) sequence designed to adopt a type II' turn structure (Figure 1.2).<sup>11</sup>

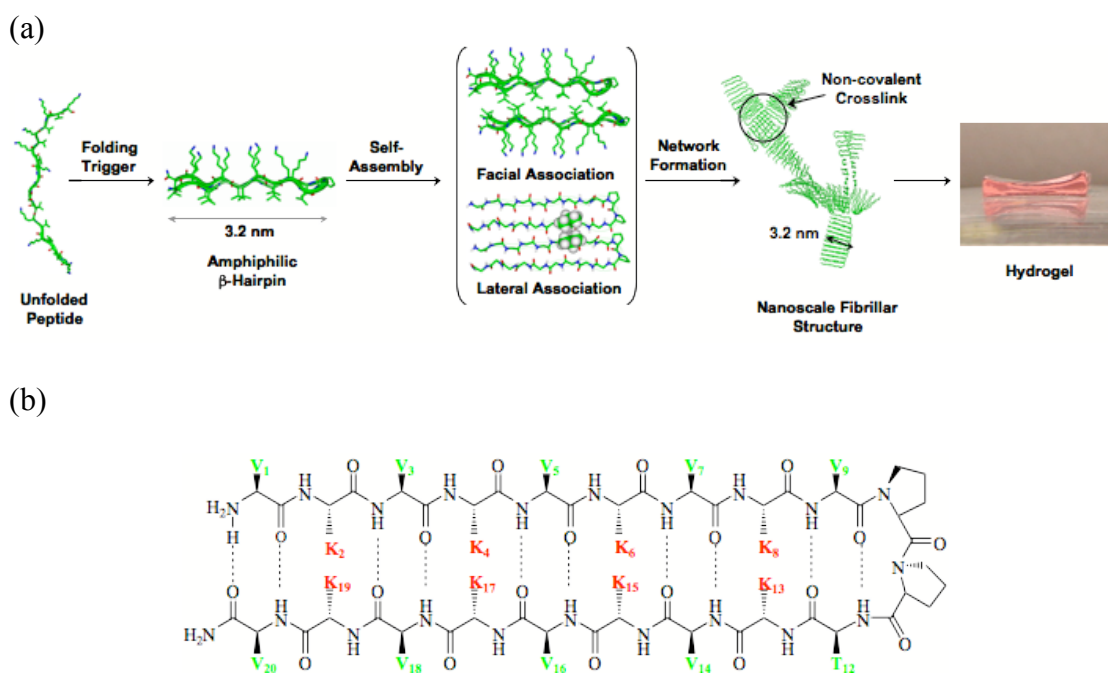


**Figure 1.2 (a) Environmentally triggered folding, self-assembly, and non-covalent fibril crosslinking leading to hydrogelation. (b)  $\beta$ -hairpin structure of MAX 1 comprised of two  $\beta$ -strands of alternating valine (green) and lysine (red) residues connected via a type II'  $\beta$ -turn**

Under acidic conditions, the protonated lysines prevent the peptide from folding and thus self-assembling. Intramolecular folding and consequent self-assembly however can be triggered by either neutralizing the charge by increasing the pH of low ionic strength solutions to 9<sup>11</sup> or by screening the positively charged lysines by the addition of salt at physiological pH<sup>23</sup>. For large part, folding is governed by the electrostatic interactions of the hydrophilic face of the hairpin, the formation of intramolecular van der waals contacts between side chains, deshielding of hydrophobic side chains from water and formation of intramolecular H-bonds between carbonyl and amide moieties of the peptide backbone, Figure 1.3a. In the folded state, amphiphilic MAX1 hairpins, where one face of the hairpin is valine rich and the other face is lysine rich, undergo both facial and lateral association. Facial association occurs when the hydrophobic faces of the self-assembling hairpins collapse to form a bilayer-like structure. Lateral association occurs via the formation of intermolecular H-bonds and side chain-side chain hydrophobic contacts between assembling hairpins, Figure 1.3b. Self-assembly via these mechanisms results in the formation of a non-covalently cross-linked network of short fibrils rich in  $\beta$ -sheet structure, resulting in mechanically rigid hydrogel (Figure 1.2a). Structural characterization using TEM and SANS<sup>24</sup> indicate that the gel is composed of monodispersed fibrils with an average width of  $\sim 3$  nm. This value corresponds to the width of the folded  $\beta$ -hairpin in the self-assembled state and provides support for the proposed self-assembly mechanism (Figure 1.2a). Fibrils are physically cross-linked by interfibril junctions and simple entanglements of fibrils. In the self-assembled state, fibrils are composed of a bilayer

of intermolecularly hydrogen-bonded hairpins directed by the ordered packing of hydrophobic faces of individual hairpins. However, because of the topologically smooth surface of hydrophobic face of each hairpin, facial mispacking also occurs providing nucleation sites for nascent fibril growth in different three-dimensional directions creating branched junctions (Figure 1.2a).

In addition to these interfibril junctions, fibrils can also entangle providing additional physical crosslinks. The number of fibril junctions and entanglements formed during the self-assembly process affects the mechanical rigidity of the hydrogels. When the kinetics of self-assembly is increased, more crosslinks are formed and the resulting gels are more mechanically rigid. Conversely, slow self-assembly kinetics affords less rigid gels with fewer crosslinks. For example, since the rate of self-assembly is concentration dependent,<sup>25</sup> peptide concentration can be varied to modulate the kinetics of self-assembly and ultimate mechanical rigidity of the resulting hydrogel.

In addition to altering the kinetics of self-assembly of MAX1 to prepare gels of differing mechanical properties, the amino acid sequence can also be altered. For example, each of the factors outlined in Figure 1.3 that influence hairpin folding and self-assembly can be modulated by amino acid substitutions to fine-tune the mechanical properties of the gels.

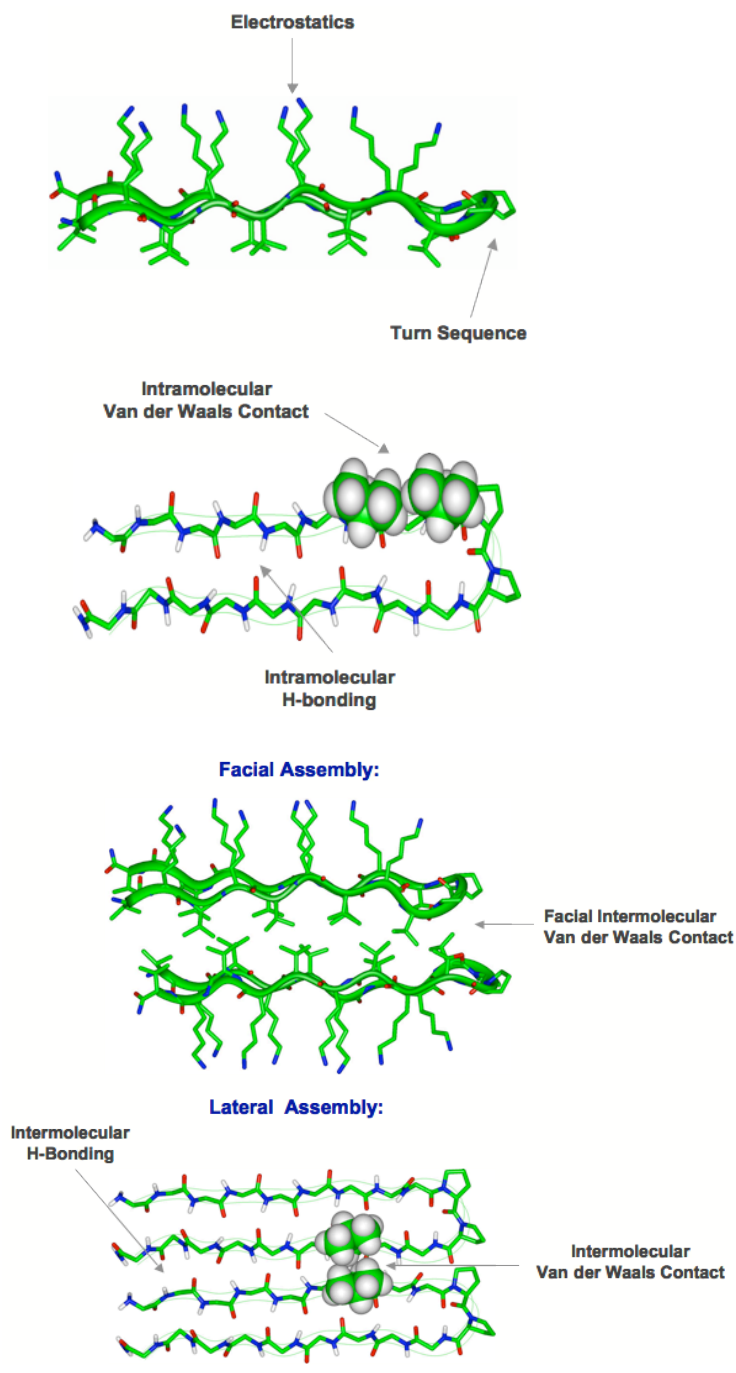


Figure 1.3 Factors affecting (a) folding and (b) self-assembly of  $\beta$ -hairpin peptides

### 1.1.1 Amino Acid Substitutions at the Hydrophilic Face

Under acidic conditions, the lysine side chains in MAX1 are protonated, which prevents the peptide from folding and thus self-assembling. Unfolded MAX1 is highly soluble; solutions up to ~ 4 wt % display rheological properties similar to water. Intramolecular folding and self-assembly is triggered by relieving the charge-charge repulsions with an increase in the pH to 9<sup>11</sup> or through screening the charged lysines with the addition of salt at physiological conditions<sup>23</sup>. In addition, peptide folding and self-assembly is reversible by altering the pH promoting deprotonation and reprotonation of the lysine side chains in low ionic salt solutions.<sup>11</sup> Since folding and self-assembly of MAX1 is dependent upon decreasing the electrostatic repulsions of the lysine side-chains, reducing the charge density on the hydrophilic face by amino acid substitution results in faster folding and self-assembly kinetics at pH 9. More importantly, lowering the positive charge density on the hydrophilic face allows gelation at lower pH values, which is relevant for cell-based applications. For example, replacing the lysine at position 15 with glutamic acid lowers the overall charge state by 2 (e.g. at pH 7.4 the overall charge of MAX1 is +9 from eight lysine residues and one terminal amine, the K15E peptide is +7). The resultant peptide, MAX8 (K15E) forms more rigid hydrogels than MAX1 at pH 7.4 with faster gelation kinetics.<sup>26</sup> In addition, this amino acid substitution has little effect on the nanoscale morphology of the fibrils formed as compared to MAX1, i.e. both gels showed an average fibril width of ~ 3 nm.<sup>26</sup> This was important to assess because peptides of similar secondary structure but differing in amino acid composition and sequence have

been reported to assemble into morphologically distinct structures such as laminating fibrils<sup>1, 27</sup>, ribbons and tapes<sup>13</sup> and tubes<sup>9, 17</sup>; each morphology having distinct bulk material properties. Comprehensive study of MAX8 gels suggest that rational modification of the net charge on the hydrophilic face can be used to control hydrogelation kinetics and thus the mechanical properties of the gel.<sup>26</sup>

### **1.1.2 Amino Acid Substitution at the Hydrophobic Face**

MAX1 also undergoes heat-induced hydrogelation. At temperatures below  $\sim 20^{\circ}\text{C}$  under low ionic strength solution conditions, MAX1 remains unfolded. Upon raising the temperature, hydrophobic side chains are desolvated and the peptide folds and self-assembles to bury its hydrophobic surfaces from water. Modulating the hydrophobic character of the amphiphilic  $\beta$ -hairpin can be employed to control the temperature at which peptide folding and self-assembly is triggered. For example, valines were substituted with threonine to afford modified MAX1 variants, MAX2 (V16T) and MAX3 (V16T, V7T).<sup>28</sup> Threonine is isostructural with valine but less hydrophobic, therefore reducing the overall hydrophobicity of the valine-rich face. The exact temperature at which folding and self-assembly was triggered ( $T_{\text{gel}}$ ) increased with a decrease in hydrophobic character of the amphiphilic peptide (MAX3 > MAX2 > MAX1). Interestingly, MAX3 exhibited thermoreversible self-assembly affording a gel whose properties were highly influenced by environmental temperature. Circular dichroism and oscillatory rheology indicate that MAX3 remains unfolded and its solution is of low viscosity at low temperatures ( $5^{\circ}\text{C}$ ) but folds and

self-assembles at higher temperatures (75 °C) to form a rigid self-supporting hydrogel. Subsequent temperature cycles showed that the conformational change and phase transitions were completely reversible. This indicated that formation of intra- and intermolecular hydrophobic interactions between the valine residues is a key factor in promoting folding and self-assembly to form physical irreversible cross-linked networks (Figure 1.3b).<sup>28</sup>

Furthermore, Haines et al. incorporated a charged residue on the hydrophobic face, which disrupted hydrophobic interactions and thus inhibited folding and self-assembly of the  $\beta$ -hairpin peptide.<sup>29</sup> Incorporating charged residue(s) in a sequence to prevent self-assembly/aggregation is referred to as “negative design” or “gate keeping”. This has been found in naturally occurring proteins, such as the S6 protein from *Thermus thermophilus*. Replacement of the gate keeping charged residues with hydrophobic residues affords a mutant S6-Alz, which is capable of self-assembling into a tetramer.<sup>30</sup> To take advantage of this “negative design” concept, MAX7CNB was designed in which a cysteine with a negatively charged photosensitive group on its side chain was substituted for a valine in MAX1 (Figure 1.4). As expected, this charged bulky residue inhibited the folding and self-assembly process. However, upon photocleavage, a moderately hydrophobic thiol is generated, allowing folding and self-assembly to proceed affording a rigid hydrogel. This novel design affords a peptide whose hydrogelation can be triggered upon UV illumination.<sup>29</sup>

### 1.1.3 Importance of Hydrogen Bonding and Hydrophobic Contacts

In addition to hydrophobic and electrostatic interactions, peptide self-assembly is also directed by the formation of a network of H-bonds (between the amide NH and C=O moieties). A common technique employed to analyze the formation of hydrogen bonds in self-assembled  $\beta$ -sheet networks is Fourier transform infrared spectroscopy (FT-IR). The amide I' band arising primarily from the backbone carbonyl stretch mode is sensitive to peptide secondary structure.<sup>31</sup> In the case of a self-assembling  $\beta$ -hairpin, under unfolded conditions, the peptide in random coil conformation displays a broad amide I' band centered around  $1644\text{ cm}^{-1}$ . Following folding and self-assembly, the amide I' band shifts to form a well-defined peak at  $1615\text{ cm}^{-1}$ , strongly suggesting formation of a self-assembled  $\beta$ -sheet rich structure.<sup>11</sup>,<sup>32</sup> A weaker band  $1680\text{ cm}^{-1}$  is also observed, often associated with an anti-parallel  $\beta$ -sheet arrangement.<sup>33</sup> According to our proposed mechanism, MAX1 would be expected to fold into a symmetrical  $\beta$ -hairpin where all of the *intramolecular* H-bond donors (NH) and acceptors (C=O) are satisfied. However, monomeric hairpins contain unfulfilled acceptors and donors at the  $\beta$ -strand edges that can participate in intermolecular H-bond formation with other hairpins during self-assembly. Ultimately, folding and self-assembly results in the formation of a network of intra- and intermolecular H-bonds along the long axis of fibrils that constitute the gel. We have found that disrupting the ability of peptides to form either intra- or intermolecular

H-bonds grossly influences fibril formation and consequent hydrogel mechanical properties.

Further studies indicate that lateral self-assembly is also governed by intermolecular hydrophobic contacts between the residue side chains of neighboring hairpins (Figure 1.3). In MAX1, the valine residues are placed at H-bonding positions and lysines at the non H-bonding positions within the primary sequence of each strand. According to Wouters and Curmi,<sup>34</sup> valine residues prefer to adopt a *trans*  $\chi_1$  side chain rotamer when contained within  $\beta$ -sheet structures. Therefore, a large portion of MAX1 valine side chains should adopt *trans* dihedral angles, directing their isopropyl side chains away from the center of the hairpin and extending them towards the valine side chains of neighboring hairpins. Thus, the formation of valine-based lateral hydrophobic contacts should drive self-assembly and contribute to the rigidity of the hydrogel. This was confirmed with an inverse design of MAX1. This peptide, MAX4, has the same number of residues and a similar turn region as MAX1, but contains  $\beta$ -strand sequences with valine residues at non H-bonded positions and lysine residues at H-bonded positions (exactly opposite of MAX1). MAX4 should be largely incapable of forming valine-derived lateral intermolecular contacts. In fact, MAX4 not only exhibited slower kinetics of folding and self-assembly but also formed a less rigid hydrogel than MAX1. In addition, structural characterization of MAX4 revealed formation of higher order assemblies unlike MAX1.<sup>35</sup> This indicated that valines at H-bonded positions are also important to achieve well-defined fibril morphology and a mechanically rigid hydrogel.

### 1.1.4 Importance of Turn Region Residues

Turn regions in proteins and peptides are an important class of structures that strongly influence both structure and function. One such turn type is the  $\beta$  or reverse turn, in which at its location in a peptide sequence results in reversal of the overall direction of the polypeptide chain.<sup>36</sup> A  $\beta$ -turn is typically composed of a four residue sequence (denoted as the  $i$  to  $i+3$  residues) that connects two secondary structural elements, and may play a significant role in initiating folding and in stabilizing tertiary structures. Different types of  $\beta$ -turns have been identified and classified according to the main chain dihedral angles ( $\Phi, \Psi$ ) that their  $i + 1$  and  $i + 2$  residues adopt. Each turn type influences  $\beta$ -sheet properties such as  $\beta$ -sheet twist, stability, folding nucleation rate and the hydrogen-bonding registry.<sup>37</sup> Systematic studies indicate that  $\beta$ -turn type and the propensity of the residues occupying turn positions to adopt dihedral angles consistent with  $\beta$ -turn structure influences the formation and stability of  $\beta$ -hairpins.<sup>38-40</sup> MAX1 contains a tetrapeptide sequence (-V<sup>D</sup>P<sup>L</sup>PT-), that has high propensity to adopt a type II'  $\beta$ -turn due, in part, to the chirality of the <sup>D</sup>prolyl residue at the  $i + 1$  position (Figure 1.2). Valine, a  $\beta$ -branched residue, was placed at the  $i$  position (V<sub>9</sub>) of the turn to enforce a *trans*-prolyl amide bond geometry at the succeeding ( $i + 1$ ) position. A threonine residue was placed at the  $i + 3$  position of the turn region since it has a high propensity to occupy this position in type II' turns of hairpins in naturally occurring proteins.<sup>41</sup> Threonine can form a stabilizing side chain-main chain H-bond between its alcoholic proton and the

carbonyl oxygen of the  $i$ th residue of the turn. A control peptide [(VK)<sub>4</sub>] i.e. without the turn region, under folding conditions (pH 9.0), failed to form a hydrogel at ambient temperature. This demonstrates that the turn region is necessary for the folding and self-assembly of MAX1 leading to hydrogelation.<sup>11</sup>

In addition, the stereochemistry of the turn residues is also important in directing the self-assembly process. Lamm et al. investigated this by replacing the <sup>D</sup>proline at the  $i+1$  position in the turn with the stereoisomer and naturally occurring amino acid <sup>L</sup>proline (-V<sup>L</sup>P<sup>L</sup>PT-). This peptide (<sup>L</sup>P<sup>L</sup>P) was unable to intramolecularly fold but still capable of self-assembly into  $\beta$ -sheet rich structure.<sup>32</sup> Unlike MAX1 that folds into a  $\beta$ -hairpin and subsequently self-assembles to form monodispersed well-defined fibrils,<sup>23, 24</sup> <sup>L</sup>P<sup>L</sup>P adopts an extended  $\beta$ -strand conformation (Figure 1.1.4) and assembles into H-bonded fibrils exhibiting a highly laminated, non-twisted morphology.<sup>32</sup>

## **1.2 Functional Materials from Self-Assembling $\beta$ -Hairpins**

### **1.2.1 Mimics of Extracellular Matrix**

When fabricating hydrogels for tissue engineering applications, several general material and biological requirements have to be considered. The scaffold should be self-supporting and mechanically rigid in the presence of cells, porous to allow diffusion of nutrients and waste, cytocompatible and biocompatible. Rheological measurements indicated that MAX1 forms mechanically rigid hydrogels on addition

of cell culture media (DMEM). MAX1 hydrogel surfaces not only proved to be non-toxic towards NIH 3T3 fibroblasts but also allowed facile cell attachment both in the presence and absence of serum. In addition, cells can proliferate on the gel surface with minimal effect on the rheological properties of the scaffold.<sup>42</sup> MAX8 is also cytocompatible towards a broad range of mammalian cells including fibroblasts, stem cells, chondrocytes and pre-osteoblasts. In addition, MAX8's fast assembly kinetics allows homogenous three-dimensional incorporation of cells when gelation is triggered in the presence of cells. Homogenous encapsulation is significant since cell density plays an important role in modulating the behavior of delivered cells.<sup>26, 43</sup>

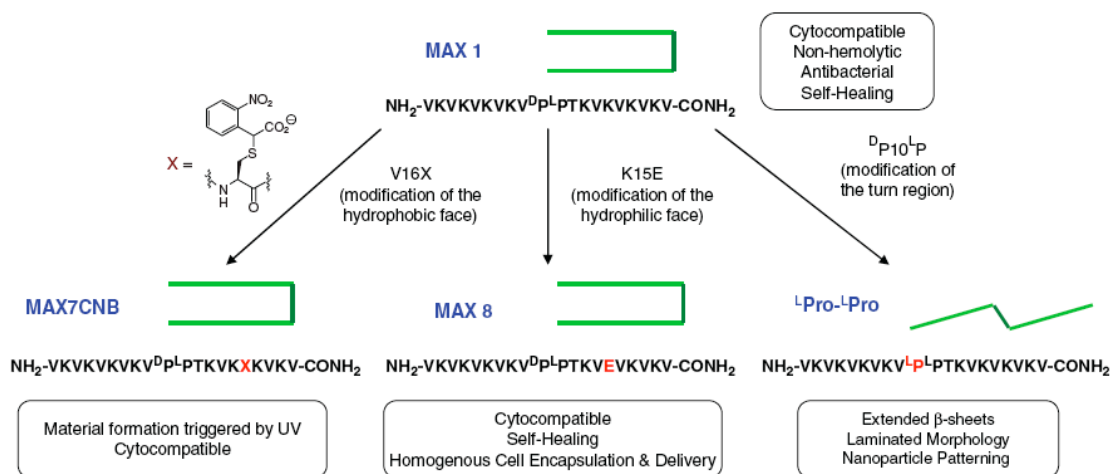


**Figure 1.4 Structure-based design of MAX1. Modifications to the hydrophilic, hydrophobic, and turn regions to create new peptides with tailored properties.**

### 1.2.2 Injectable Delivery

Both MAX1 and MAX8 hydrogels shear thin when a significant stress is applied to the material. However, when the application of shear stress is stopped, the gels immediately self-heal. This shear thinning/self-healing behavior allows delivery of the gels through syringes to targeted sites. Depressing the syringe barrel provides sufficient shear stress to convert the mechanically rigid gel into a viscous gel that flows. After the flowing gel leaves the tip of the needle it immediately recovers forming a gel with near quantitative recovery of its original storage modulus. When MAX8 gels are impregnated with cells, this mechanism can be used to deliver cells to wound sites with spatial resolution. Cells remain viable during encapsulation and the shear-thin delivery process and gel-cell constructs stay localized at the site of introduction. These properties make these gels useful for delivery of cells to targeted biological sites in tissue-regeneration efforts.<sup>26</sup>

### 1.2.3 Antibacterial Activity

Among several important considerations for implantation of a biomaterial, a main concern is the introduction of infection. The surface of MAX1 hydrogels exhibit inherent antibacterial activity. In experiments, MAX1 hydrogel surfaces were challenged with bacterial solutions ranging in concentrations from  $2 \times 10^3$  colony forming units (CFUs)/dm<sup>2</sup> to  $2 \times 10^9$  CFUs/dm<sup>2</sup>, to demonstrate its broad-spectrum antibacterial activity. Results showed that the hydrogel surface was active against Gram-positive (*Staphylococcus epidermidis*, *Staphylococcus aureus*, and

*Streptococcus pyogenes*) and Gram-negative (*Klebsiella pneumoniae* and *Escherichia coli*) bacteria, all prevalent in hospital settings. Live-dead assays employing laser scanning confocal microscopy showed that bacteria are killed when they engaged the surface. In addition, the surface of MAX1 hydrogels was also shown to cause inner and outer membrane disruption in experiments that monitor the release of  $\beta$ -galactosidase from the cytoplasm of lactose permease-deficient *E. coli* ML-35. This data suggested a mechanism of antibacterial action that involved membrane disruption leading to cell death upon cellular contact with the gel surface. Although the hydrogel surface exhibited bactericidal activity, co-culture experiments indicated that the hydrogel surfaces show selective toxicity to bacterial versus mammalian cells. Additionally, gel surfaces were nonhemolytic toward human erythrocytes, which maintained healthy morphologies when in contact with the surface. These material attributes make MAX1 gels attractive candidates for use in tissue regeneration, even in nonsterile environments.<sup>44</sup>

## **1.2 Thesis Objective**

The properties of peptide-based materials discussed so far demonstrate their potential for nanotechnological and biomedical applications. In addition, continuing research is providing insight into the factors that direct the self-assembly process of peptides leading to targeted structures with specific functions. These physically crosslinked gels, although displaying useful properties, are mechanically weak compared to covalently crosslinked hydrogels. Therefore, similar to polymer-

based hydrogels, covalent cross-linking of self-assembled peptides may provide the ability to enhance the mechanical properties of peptide-based hydrogels.

The objective of this thesis work is to design self-assembling peptides that can be covalently crosslinked following hydrogelation to enhance the mechanical rigidity of the resultant hydrogels. The central idea is to retain the shear recovery ability of the hydrogels and yet be able to polymerize the gel after delivery. This would be beneficial for developing injectable biomaterials that can be photocrosslinked following syringe delivery to enhance the mechanical properties of the hydrogel at the tissue site. Towards this objective, Chapter 2 discusses the designs of  $\beta$ -hairpin peptides functionalized with photoactive groups at specific positions to allow covalent crosslinking of the hydrogel network. Here it is demonstrated that the location of the polymerizable moiety in the  $\beta$ -hairpin peptide can be used to manipulate the mechanical properties of the hydrogels upon polymerization. In Chapter 3, the study is further extended towards the preparation of polymerizable composite hydrogels employing self-assembling peptides and bifunctional polymers. Apart from fabricating mechanically robust hydrogels, it is shown that the material rigidity of these crosslinked composite gels varies depending upon the method of its preparation. Chapter 4 discusses an alternative approach of employing designed self-assembling, three-stranded antiparallel  $\beta$ -sheets to construct mechanically rigid hydrogels than their  $\beta$ -hairpin counterpart. Here, chemical crosslinking is not employed and peptide design is solely used to manipulate gel properties. In addition,

the effect of the turn region residues on the mechanical properties of the gels formed by the three-stranded peptides is presented in Chapter 5. An additional study is discussed in Chapter 6 where the role of cell culture conditions in enhancing the mechanical properties of self-assembled  $\beta$ -hairpin peptide hydrogels is investigated. In conclusion, the results and lessons learnt from this work are summarized in Chapter 7

## References

1. Rajagopal, K.; Schneider, J. P., Self-assembling peptides and proteins for nanotechnological applications. *Current Opinion in Structural Biology* **2004**, 14, (4), 480-486.
2. Yang, Z.; Xu, B., Supramolecular hydrogels based on biofunctional nanofibers of self-assembled small molecules. *Journal of Materials Chemistry* **2007**, 17, (23), 2385-2393.
3. Gazit, E., Self-assembled peptide nanostructures: the design of molecular building blocks and their technological utilization. *Chemical Society Reviews* **2007**, 36, (8), 1263-1269.
4. Mart, R. J.; Osborne, R. D.; Stevens, M. M.; Ulijn, R. V., Peptide-based stimuli-responsive biomaterials. *Soft Matter* **2006**, 2, (10), 822-835.
5. Brack, A.; Orgel, L. E., [beta] structures of alternating polypeptides and their possible prebiotic significance. *Nature* **1975**, 256, (5516), 383-387.
6. Raleigh, D. P.; Betz, S. F.; DeGrado, W. F., A de Novo Designed Protein Mimics the Native State of Natural Proteins. *J. Am. Chem. Soc.* **1995**, 117, (28), 7558-7559.
7. Gore, T.; Dori, Y.; Talmon, Y.; Tirrell, M.; Bianco-Peled, H., Self-Assembly of Model Collagen Peptide Amphiphiles. *Langmuir* **2001**, 17, (17), 5352-5360.
8. Koga, T.; Higuchi, M.; Kinoshita, T.; Higashi, N., Controlled Self-Assembly of Amphiphilic Oligopeptides into Shape-Specific Nanoarchitectures. *Chemistry - A European Journal* **2006**, 12, (5), 1360-1367.
9. von Maltzahn, G.; Vauthey, S.; Santoso, S.; Zhang, S., Positively Charged Surfactant-like Peptides Self-assemble into Nanostructures. *Langmuir* **2003**, 19, (10), 4332-4337.
10. Hartgerink, J. D.; Beniash, E.; Stupp, S. I., Peptide-amphiphile nanofibers: A versatile scaffold for the preparation of self-assembling materials. *Proceedings of the National Academy of Sciences of the United States of America* **2002**, 99, (8), 5133-5138.
11. Schneider, J. P.; Pochan, D. J.; Ozbas, B.; Rajagopal, K.; Pakstis, L.; Kretsinger, J., Responsive hydrogels from the intramolecular folding and self-assembly of a designed peptide. *Journal of the American Chemical Society* **2002**, 124, (50), 15030-15037.
12. Dong, H.; Paramonov, S. E.; Aulisa, L.; Bakota, E. L.; Hartgerink, J. D., Self-Assembly of Multidomain Peptides: Balancing Molecular Frustration Controls Conformation and Nanostructure. *Journal of the American Chemical Society* **2007**.
13. Aggeli, A.; Nyrkova, I. A.; Bell, M.; Harding, R.; Carrick, L.; McLeish, T. C. B.; Semenov, A. N.; Boden, N., Hierarchical self-assembly of chiral rod-like molecules as a model for peptide beta-sheet tapes, ribbons, fibrils, and fibers. *Proceedings of the National Academy of Sciences of the United States of America* **2001**, 98, (21), 11857-11862.

14. Ramachandran, S.; Trehwella, J.; Tseng, Y.; Yu, Y. B., Coassembling peptide-based biomaterials: Effects of pairing equal and unequal chain length oligopeptides. *Chemistry of Materials* **2006**, 18, (26), 6157-6162.
15. Yokoi, H.; Kinoshita, T.; Zhang, S., Dynamic reassembly of peptide RADA16 nanofiber scaffold. *Proceedings of the National Academy of Sciences* **2005**, 102, (24), 8414-8419.
16. Dennis T. Bong, M. R. G., Self-Assembling Cyclic Peptide Cylinders as Nuclei for Crystal Engineering. *Angewandte Chemie International Edition* **2001**, 40, (11), 2163-2166.
17. Lu, K.; Jacob, J.; Thiyagarajan, P.; Conticello, V. P.; Lynn, D. G., Exploiting Amyloid Fibril Lamination for Nanotube Self-Assembly. *J. Am. Chem. Soc.* **2003**, 125, (21), 6391-6393.
18. Powers, P. T.; Sung I. Y.; Lieber, M. C.; Kelly, J. W., Ordered Langmuir-Blodgett Films of Amphiphilic beta-Hairpin Peptides Imaged by Atomic Force Microscopy. *Angewandte Chemie International Edition* **2002**, 41, (1), 127-130.
19. Xu, G.; Wang, W.; Groves, J. T.; Hecht, M. H., Self-assembled monolayers from a designed combinatorial library of de novo beta -sheet proteins. *Proceedings of the National Academy of Sciences* **2001**, 98, (7), 3652-3657.
20. Rapaport, H.; Kjaer, K.; Jensen, T. R.; Leiserowitz, L.; Tirrell, D. A., Two-dimensional order in beta-sheet peptide monolayers. *Journal of the American Chemical Society* **2000**, 122, (50), 12523-12529.
21. Woolfson, D. N., The design of coiled-coil structures and assemblies. In *Fibrous Proteins: Coiled-Coils, Collagen and Elastomers*, 2005; Vol. 70, pp 79-+.
22. Zimenkov, Y.; Dublin, S. N.; Ni, R.; Tu, R. S.; Breedveld, V.; Apkarian, R. P.; Conticello, V. P., Rational Design of a Reversible pH-Responsive Switch for Peptide Self-Assembly. *J. Am. Chem. Soc.* **2006**, 128, (21), 6770-6771.
23. Ozbas, B.; Kretsinger, J.; Rajagopal, K.; Schneider, J. P.; Pochan, D. J., Salt-triggered peptide folding and consequent self-assembly into hydrogels with tunable modulus. *Macromolecules* **2004**, 37, (19), 7331-7337.
24. Ozbas, B.; Rajagopal, K.; Schneider, J. P.; Pochan, D. J., Semiflexible chain networks formed via self-assembly of beta-hairpin molecules. *Physical Review Letters* **2004**, 93, (26).
25. Veerman, C.; Rajagopal, K.; Palla, C. S.; Pochan, D. J.; Schneider, J. P.; Furst, E. M., Gelation kinetics of beta-hairpin peptide hydrogel networks. *Macromolecules* **2006**, 39, (19), 6608-6614.
26. Haines-Butterick, L.; Rajagopal, K.; Branco, M.; Salick, D.; Rughani, R.; Pilarz, M.; Lamm, M. S.; Pochan, D. J.; Schneider, J. P., Controlling hydrogelation kinetics by peptide design for three-dimensional encapsulation and injectable delivery of cells. *Proc. Natl. Acad. Sci. U. S. A.* **2007**, 104, (19), 7791-7796.
27. Lopez de la Paz, M.; Goldie, K.; Zurdo, J.; Lacroix, E.; Dobson, C. M.; Hoenger, A.; Serrano, L., De novo designed peptide-based amyloid fibrils. *Proceedings of the National Academy of Sciences* **2002**, 99, (25), 16052-16057.

28. Pochan, D. J.; Schneider, J. P.; Kretsinger, J.; Ozbas, B.; Rajagopal, K.; Haines, L., Thermally reversible hydrogels via intramolecular folding and consequent self-assembly of a de Novo designed peptide. *Journal of the American Chemical Society* **2003**, 125, (39), 11802-11803.
29. Haines, L. A.; Rajagopal, K.; Ozbas, B.; Salick, D. A.; Pochan, D. J.; Schneider, J. P., Light-activated hydrogel formation via the triggered folding and self-assembly of a designed peptide. *Journal of the American Chemical Society* **2005**, 127, (48), 17025-17029.
30. Thirumalai, D.; Klimov, D.; Dima, R., Emerging ideas on the molecular basis of protein and peptide aggregation. *Current Opinion in Structural Biology* **2003**, 13, (2), 146-159.
31. Decatur, S. M., Elucidation of Residue-Level Structure and Dynamics of Polypeptides via Isotope-Edited Infrared Spectroscopy. *Acc. Chem. Res.* **2006**, 39, (3), 169-175.
32. Lamm, M. S.; Rajagopal, K.; Schneider, J. P.; Pochan, D. J., Laminated morphology of nontwisting beta-sheet fibrils constructed via peptide self-assembly. *Journal of the American Chemical Society* **2005**, 127, (47), 16692-16700.
33. Surewicz, W. K.; Mantsch, H. H.; Chapman, D., Determination of protein secondary structure by Fourier transform infrared spectroscopy: A critical assessment. *Biochemistry* **1993**, 32, (2), 389-394.
34. Wouters, M. A.; Curmi, P. M. G., An Analysis of Side-Chain Interactions and Pair Correlations within Antiparallel Beta-Sheets - the Differences between Backbone Hydrogen-Bonded and Non-Hydrogen-Bonded Residue Pairs. *Proteins-Structure Function and Genetics* **1995**, 22, (2), 119-131.
35. Rajagopal, K.; Ozbas, B.; Pochan, D. J.; Schneider, J. P., Probing the importance of lateral hydrophobic association in self-assembling peptide hydrogelators. *European Biophysics Journal with Biophysics Letters* **2006**, 35, (2), 162-169.
36. Karle, I.; Gopi, H. N.; Balaram, P., Supramolecular Chemistry And Self-assembly Special Feature: Infinite pleated beta -sheet formed by the beta -hairpin Boc-beta -Phe-beta -Phe-D-Pro-Gly-beta -Phe-beta -Phe-OMe. *Proceedings of the National Academy of Sciences* **2002**, 99, (8), 5160-5164.
37. Gibbs, A. C.; Bjorndahl, T. C.; Hodges, R. S.; Wishart, D. S., Probing the Structural Determinants of Type II' beta-Turn Formation in Peptides and Proteins. *J. Am. Chem. Soc.* **2002**, 124, (7), 1203-1213.
38. Stanger, H. E.; Gellman, S. H., Rules for Antiparallel beta -Sheet Design: D-Pro-Gly Is Superior to L-Asn-Gly for beta-Hairpin Nucleation. *J. Am. Chem. Soc.* **1998**, 120, (17), 4236-4237.
39. Espinosa, J. F.; Syud, F. A.; Gellman, S. H., Analysis of the factors that stabilize a designed two-stranded antiparallel beta -sheet. *Protein Sci.* **2002**, 11, (6), 1492-1505.
40. de Alba, E.; Rico, M.; Jimenez, M. A., The turn sequence directs beta-strand alignment in designed beta- hairpins. *Protein Sci* **1999**, 8, (11), 2234-2244.

41. Hutchinson, E. G.; Thornton, J. M., A Revised Set of Potentials for Beta-Turn Formation in Proteins. *Protein Science* **1994**, 3, (12), 2207-2216.
42. Kretsinger, J. K.; Haines, L. A.; Ozbas, B.; Pochan, D. J.; Schneider, J. P., Cytocompatibility of self-assembled beta-hairpin peptide hydrogel surfaces. *Biomaterials* **2005**, 26, (25), 5177-5186.
43. Dvir-Ginzberg, M.; Gamlieli-Bonshtein, I.; Agbaria, R.; Cohen, S., Liver Tissue Engineering within Alginate Scaffolds: Effects of Cell-Seeding Density on Hepatocyte Viability, Morphology, and Function. *Tissue Engineering* **2003**, 9, (4), 757-766.
44. Salick, D. A.; Kretsinger, J. K.; Pochan, D. J.; Schneider, J. P., Inherent Antibacterial Activity of a Peptide-Based b-Hairpin Hydrogel. *J. Am. Chem. Soc.* **2007**, 129, (47), 14793-14799.

## Chapter 2

### ENHANCING THE MECHANICAL PROPERTIES OF DESIGNED SELF-ASSEMBLING BETA-HAIRPIN PEPTIDES VIA PHOTOPOLYMERIZATION

#### 2.0 Introduction

The development of three-dimensional scaffolds that have suitable architecture as well as mechanical properties that mimic the natural extracellular matrix has been a challenge to material scientists. Synthetic hydrogels are attractive candidates for this purpose due to their high water content, porous nature and mechanical rigidity.<sup>1-6</sup> Since the choice of material is very critical, a variety of natural and synthetic polymers are continuously being developed as hydrogel precursors for tissue engineering applications.<sup>7-9</sup> For example, a polymeric hydrogel fabricated using a mold can be implanted into a liver<sup>10, 11</sup>, cartilage<sup>12, 13</sup> or a bone<sup>14, 15</sup> defect to aid in tissue repair. However, this approach is invasive in nature. Alternatively, hydrogelation can be induced *in vivo* through sol-gel phase transition of the injected polymer solution<sup>16, 17</sup>. Here, gelation occurs as a result of environmental differences between the polymeric solution and the *in vivo* conditions. In addition, *in situ* hydrogelation of polymer solutions can also be achieved either via chemical crosslinking of the polymers<sup>18, 19</sup> or photocrosslinking the polymer(s) in presence of a photoinitiator<sup>20, 21</sup> upon delivery. These materials, which can be introduced as liquids

at the site of interest using a syringe, form a gel upon crosslinking. Minimal invasive delivery using a syringe allows the gel forming solution to fill an irregularly shaped cavity. In particular, the photopolymerization strategy provides an advantage of control over the hydrogelation process with spatial and temporal resolution within a confined site, therefore allowing manipulation of the gelation time and thus the ultimate mechanical properties. The precursors are typically prepared by functionalizing an existing polymer or its variant with functional groups capable of undergoing photoinitiated crosslinking reactions.<sup>21-23</sup> This has led to development of light-derived hydrogels for various applications such as drug delivery<sup>24-28</sup>, wound healing<sup>29, 30</sup>, tissue engineering<sup>31, 32</sup> and fabrication of contact lenses<sup>33, 34</sup>. Although promising, a potential limitation of polymers introduced at the target site as a solution is their leakage into the neighboring tissues. This may warrant the development of injectable hydrogels that can be easily dispensed and remain confined at the site of delivery.

Recent developments have shown that bio-inspired and *de novo* designed peptides can be employed to fabricate hydrogels for biomedical applications. In particular, amphiphilic  $\beta$ -hairpin peptide sequences have been designed that have the ability to fold and self-assemble into  $\beta$ -sheet-rich hydrogels in response to changes in pH, temperature, ionic strength, light or metal ions.<sup>2, 4, 35-40</sup> Such peptides can be modified at the molecular level, which not only provides control over the rate of self-assembly but also the bulk material properties of the resultant hydrogels.<sup>41</sup> In addition, these physically crosslinked  $\beta$ -sheet rich hydrogels can be syringe delivered to a

target site with spatial and temporal resolution. Here, the low viscosity gel instantaneously recovers a significant amount of its original material rigidity thus preventing leakage to the area surrounding the injection site. This property has been investigated towards development of injectable hydrogels for macromolecular and cell<sup>41</sup> delivery, which may aid in tissue regeneration efforts.

An important criterion to develop tissue replacements is that the engineered scaffold should have similar mechanical properties as that of the native tissue being replaced. However, peptide-based hydrogels prepared via self-assembly are moderately rigid owing to their non-covalently cross-linked network. Therefore, similar to polymer-based hydrogels, covalent cross-linking of self-assembled peptides may provide the ability to enhance the mechanical properties of peptide-based hydrogels. To achieve this, MAX1 peptide can be modified at three possible sites to permit covalent crosslinking namely, the N-terminus, the hydrophobic face or the solvent exposed hydrophilic face, Figure 2.1. The objective of this project is to fabricate  $\beta$ -hairpin peptide hydrogels that can be syringe delivered and subsequently photocrosslinked to enhance the rigidity of the hydrogels at the delivery site. In this chapter, self-assembly and mechanical properties of MAX1 and its photocrosslinkable derivatives prepared by functionalization of the N-terminus and hydrophilic face are discussed.

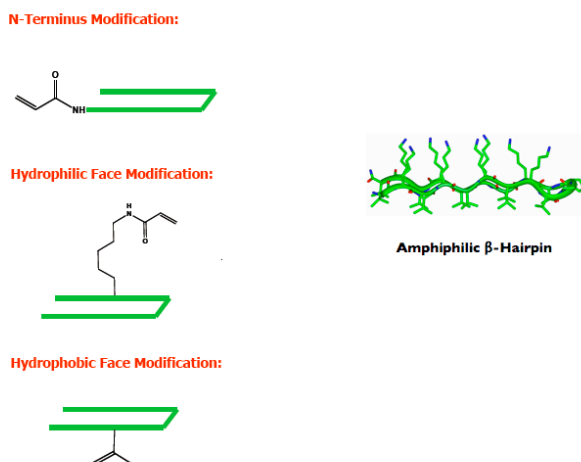


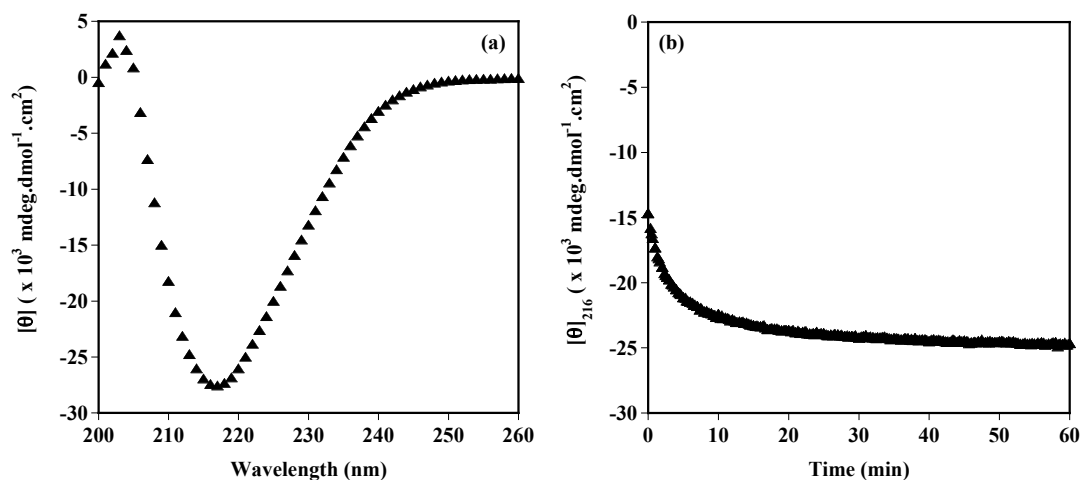
**Figure 2.1 Possible modifications of the amphiphilic MAX1  $\beta$ -hairpin**

## **2.1 Folding, Self-Assembly and Hydrogelation of MAX1 at Physiologically Relevant Conditions**

The MAX1 peptide undergoes a sol-gel phase transition in response to an increase in temperature leading to the formation of a self-supporting hydrogel. In aqueous solutions at low temperatures ( $\sim 10$  °C) in pH 7.4 buffer (50 mM BTP, 150 mM NaCl), MAX1 remains unfolded due to the electrostatic repulsion between the protonated lysine side chains. In addition, the hydrophobic side chains are also well solvated at low temperatures. Raising the temperature to 37 °C results in desolvation of the hydrophobes and most likely promotes the hydrophobic effect, which is necessary to overcome the electrostatic repulsions. As a result, the peptide folds into an amphiphilic  $\beta$ -hairpin and subsequently self-assembles to form a self-supporting

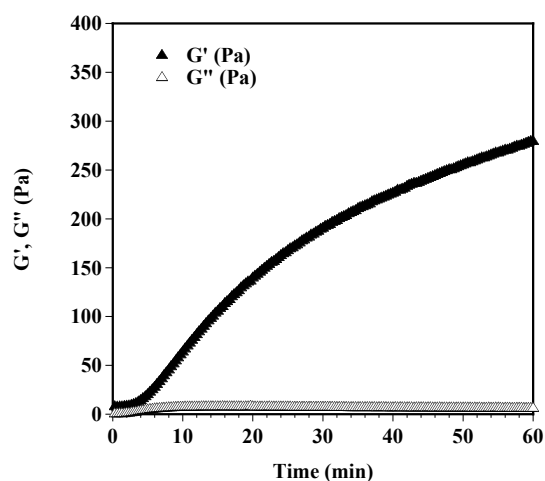
hydrogel. As discussed in Chapter 1, the self-assembly event comprises of facial hydrophobic interactions as well as lateral intermolecular hydrogen bonding of the folded hairpins.

Figure 2.2(a) shows a circular dichroism wavelength spectrum of 1 wt% MAX1 obtained at pH 7.4 (50 mM BTP, 150 mM NaCl) at 37 °C where the mean residual ellipticity  $[\theta]$  is plotted as a function of wavelength. The data shows that MAX1 forms a  $\beta$ -sheet secondary structure as indicated by a minimum at 216 nm. The rate at which  $\beta$ -sheet is formed can be monitored by measuring the change in mean residual ellipticity at 216 nm  $[\theta]_{216}$  as a function of time. Figure 2.2(b) shows that MAX1 forms  $\beta$ -sheet structure under these conditions within an hour.



**Figure 2.2 (a) Circular dichroism wavelength spectrum of a 1 wt% MAX1 hydrogel at pH 7.4 (50 mM BTP, 150 mM NaCl) and 37 °C after a 1hr gelation time. (b)  $[\theta]_{216}$  measured as a function of time (1 wt% MAX1, pH 7.4, 37 °C).**

The data in Figure 2.3 shows oscillatory rheology measurements of 1 wt% MAX1 at pH 7.4 (50 mM BTP, 150 mM NaCl). A dynamic time sweep experiment is shown in which the storage modulus ( $G'$ , a material's elastic response to applied strain, which is indicative of its rigidity) and loss modulus ( $G''$ , a material's viscous response to applied strain) are measured as a function of time. In this experiment, an aqueous solution of 1 wt% MAX1 in pH 7.4 at room temperature ( $\sim 20$  °C) was directly loaded onto the rheometer pre-equilibrated at 37 °C to trigger hydrogelation. The data shows that the 1 wt% MAX1 hydrogel acquires a storage modulus of about 300 Pa after 60 min of gelation time. Gels formed by MAX1 at pH 7.4 are much weaker than gels formed at pH 9.0 as shown previously.<sup>55</sup> Thus for applications that necessitate use at pH 7.4, enhancing the material rigidity may be necessary.



**Figure 2.3 Dynamic time sweep measurement of 1 wt% MAX1 at pH 7.4 (50 mM BTP, 150 mM NaCl) at 37 °C. [6 rad/s, 0.2% strain]**

## 2.2 N-Terminus Modification of MAX1

The free N-terminal amine of resin bound MAX1 peptide was functionalized using acryloyl chloride to give M1NA peptide, Figure 2.4. As a result, M1NA peptide has an overall charge of +8 (eight lysines) as compared to MAX1, which has an overall charge of +9 (eight lysines and one free N-terminus). Previous studies in our lab have shown that reducing the overall charge state of the peptide results in faster kinetics of self-assembly leading to formation of a more rigid hydrogel.<sup>41</sup>

### 2.2.1 Design of N-Acryloyl MAX1 (M1NA)

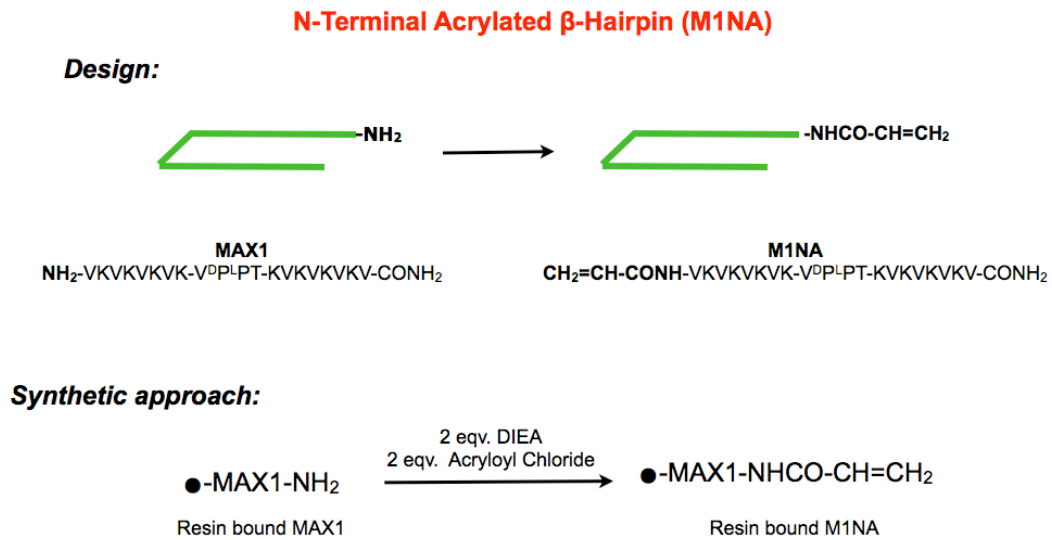


**Figure 2.4 Design and synthesis of M1NA peptide**

## 2.2.2 Folding, Self-Assembly and Hydrogelation

Figure 2.5(a) shows that 1 wt% M1NA at 37 °C in pH 7.4 buffer (50 mM BTP, 150 mM NaCl) has  $\beta$ -sheet secondary structure similar to MAX1 as assessed by CD spectroscopy. However, as shown in Figure 2.5(b), M1NA exhibits faster kinetics of folding and self-assembly than MAX1. The majority of  $\beta$ -sheet formation occurs within first 2 minutes with minimal changes thereafter.

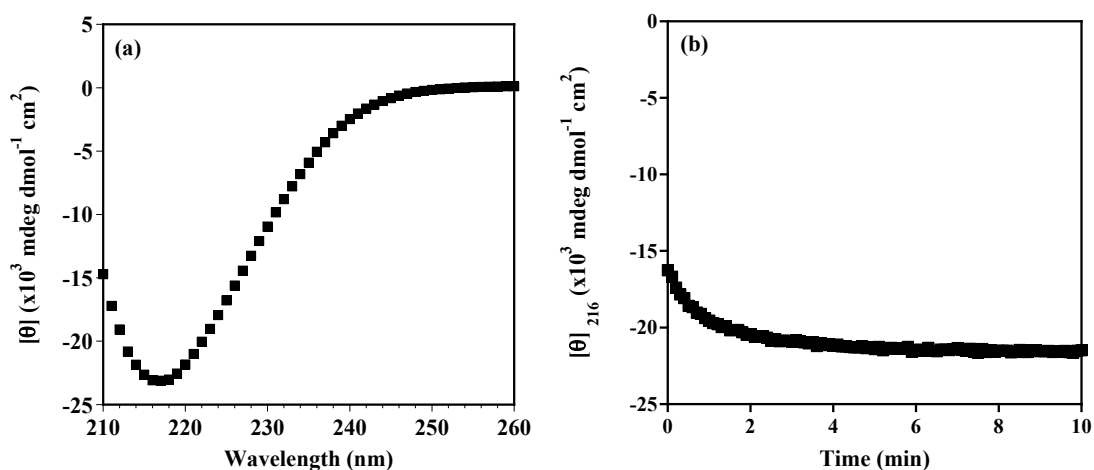


**Figure 2.5 (a) Circular dichroism wavelength spectrum of a 1 wt% M1NA hydrogel at pH 7.4 (50 mM BTP, 150 mM NaCl) and 37 °C after a 1hr gelation time. (b)  $[\theta]_{216}$  measured as a function of time (1 wt% M1NA, pH 7.4, 37 °C).**

The data in Figure 2.6 shows oscillatory rheology measurements of 1 wt% M1NA at pH 7.4 (50 mM BTP, 150 mM NaCl). In this experiment, an aqueous

solution of 1 wt% M1NA in pH 7.4 at room temperature ( $\sim 20\text{ }^{\circ}\text{C}$ ) was directly loaded onto the rheometer pre-equilibrated at  $37\text{ }^{\circ}\text{C}$  to trigger hydrogelation. Since the kinetics of folding and self-assembly is faster than MAX1, a more rigid hydrogel would be expected. The data shows that 1 wt% M1NA hydrogel acquires a storage modulus of about  $2800 \pm 100\text{ Pa}$  after 60 min of gelation time. Figure 2.6(b) shows a dynamic frequency sweep experiment in which the storage and loss modulus are measured as a function of angular frequency. The data shows that the storage modulus is insensitive to a range of frequency suggesting that the hydrogel network is comprised of permanent crosslinks.

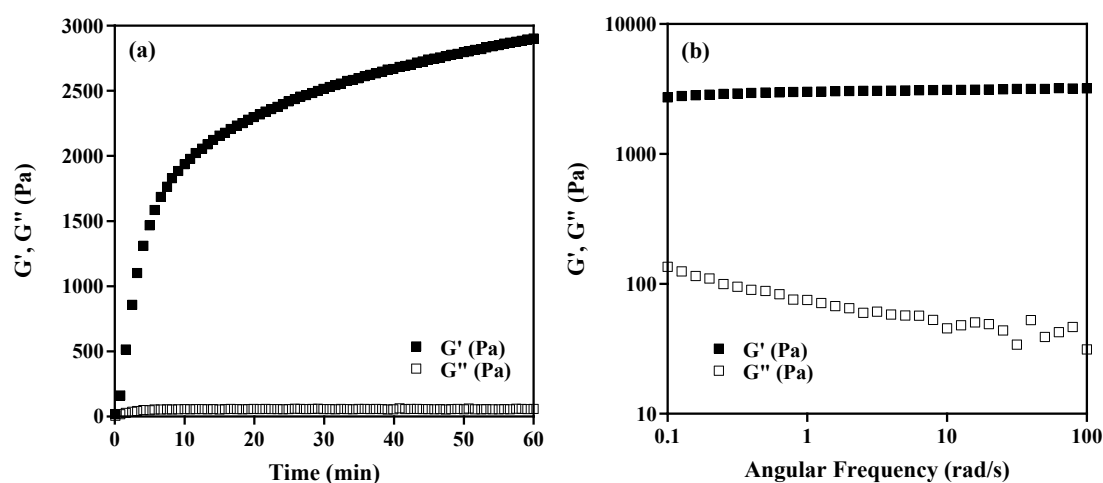


**Figure 2.6 Rheological measurements of 1 wt% M1NA at pH 7.4 (50 mM BTP, 150 mM NaCl) and  $37\text{ }^{\circ}\text{C}$ . (a) Dynamic time sweep experiment showing evolution of storage modulus ( $G'$ ) as a function of time (b) Dynamic frequency sweep measurement showing the storage ( $G'$ ) and loss ( $G''$ ) modulus values as a function of angular frequency.**

### 2.2.3 Optimization of Photopolymerization Parameters

For the photopolymerization studies, Irgacure 2959 (2-hydroxy-1-[4-(hydroxyethoxy)phenyl]-2-methyl-1-propanone), a sparingly water soluble photoinitiator, was employed. Studies by Anseth et al. show that photoinitiation performed in the presence of 0.1 wt% concentration of Irgacure 2959 is non-cytotoxic to cells.<sup>42</sup> However, major concern with photopolymerization strategies is an increase in local temperature during the irradiation process, which can affect the material properties of these thermally triggered  $\beta$ -hairpin peptide hydrogels. In addition, it is important to ensure that any changes in the material rigidity of the photopolymerizable hydrogels occurs due to formation of covalent crosslinks only. Figure 2.8 shows data obtained from a rheological experiments performed with a temperature sensitive standard viscosity oil instead of a self-assembled peptide hydrogel to determine the UV intensity at which minimal change in temperature and viscosity is observed upon irradiation. Viscosity is inversely proportional to temperature, thus as the temperature of the standard oil increases, the viscosity will decrease. The increase in temperature was measured using a thermocouple and the viscosity was measured rheologically. The data shows that a UV intensity of 10% (365 nm) that corresponds to about 16 mW/cm<sup>2</sup>, incurred a minimal rise in temperature ( $\sim 2$  °C) at the sample position after 30 min of irradiation. Similar UV intensities have been employed for fabrication of hydrogels via photopolymerization for biomedical applications,<sup>42</sup> and will be applied to these self-assembled photopolymerizable gels throughout this study.

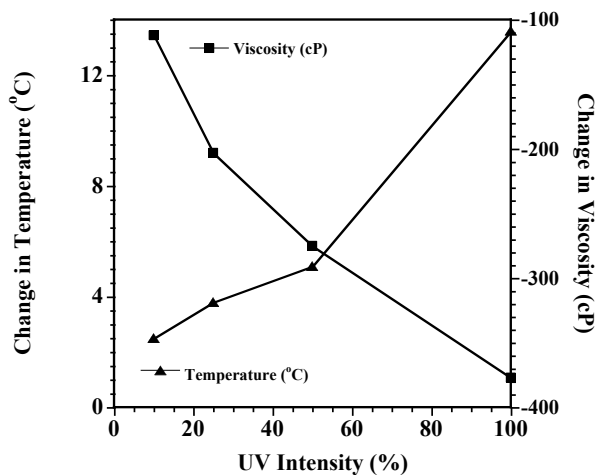


**Figure 2.8 Changes in temperature and viscosity of standard viscosity oil (S600) after 30 minutes of irradiation (365 nm) as a function of UV light intensity**

#### 2.2.4 Effect of Irradiation on Mechanical Properties of MAX1 Hydrogel

More importantly, rheological measurement of a temperature responsive non-photopolymerizable MAX1 hydrogel shows that the UV irradiation (10% intensity) had minimal affect on the material rigidity, Figure 2.9. Here, the 1 wt% MAX1 at pH 7.4 (50 mM BTP, 150 mM NaCl) is first allowed to form a gel by increasing the temperature of the peptide solution to 37 °C. After 3 hrs of gelation, the resultant hydrogel achieves an apparent equilibrium storage modulus of about 400 Pa. At that time, the hydrogel is irradiated with UV light for 15 min as indicated by the arrow in the figure. The data in Figure 2.9 shows that UV irradiation had minimal

effect on the rigidity of MAX1 hydrogel. The gradual increase in  $G'$  is normally observed as part of the aging process. Therefore, it can be assumed that the minimal increase in local temperature due to the UV irradiation does not affect the material properties of temperature responsive hydrogels. Thus, any increase in  $G'$  observed for the acrylated peptide should be due to the installation of chemical crosslinks into the network and not simply local changes in temperature.

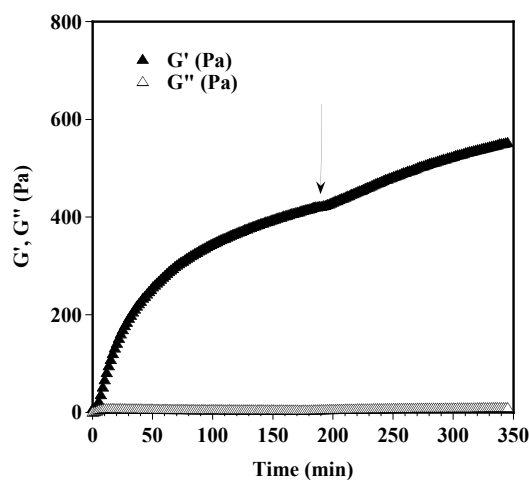


**Figure 2.9 Dynamic time sweep of 1 wt% MAX1 at pH 7.4 (50 mM BTP, 150 mM NaCl) at 37 °C (6 rad/s, 0.2 % strain) showing minimal increase in storage modulus ( $G'$ ) upon irradiation, 3 hrs after gelation was triggered.**

### **2.2.5 Increase in Mechanical Properties of Hydrogels upon Photopolymerization**

To form M1NA hydrogels, the peptide is first dissolved in a solution containing Iracacure 2959 and then an equal volume of pH 7.4 buffer is added to give

a 1 wt% M1NA peptide solution in pH 7.4 (50 mM BTP, 150 mM NaCl) buffer with 0.025 wt% Irgacure 2959. This peptide solution is then loaded onto the rheometer pre-equilibrated at 37 °C to trigger gelation. The low concentration of 0.025 wt% Irgacure 2959 is used to limit any interference with the process of peptide self-assembly and subsequent hydrogelation. Figure 2.10(a) shows the gelation kinetics of 1 wt% M1NA at pH 7.4 and 37 °C in presence of 0.025wt% Irgacure 2959. The hydrogel achieves an average storage modulus of  $3100 \pm 100$  Pa after 3 hrs of gelation time. After which time, the peptide is irradiated with UV light (365 nm) for 15 min. An instantaneous increase in storage modulus is observed at this point. Thereafter, the photocrosslinked hydrogel achieves an equilibrium storage modulus of  $5000 \pm 100$  Pa, a 1.6 fold increase in rigidity. This experiment demonstrates that self-assembled M1NA hydrogels can be successfully photocrosslinked to enhance hydrogel rigidity.

Unphotocrosslinked M1NA hydrogels may exhibit shear recovery behavior. Here, the application of shear strain to the hydrogel can lead to disruption of some of the non-covalent crosslinks that constitute the network. This transforms the self-supporting hydrogel into a fluid-like low viscosity gel. Upon removal of the shear strain, the non-covalent crosslinks reform, allowing the gel to recover its mechanical rigidity. This unique feature of the M1NA hydrogel allows it to be delivered using a syringe to a secondary site in a minimally invasive manner with spatial and temporal resolution.

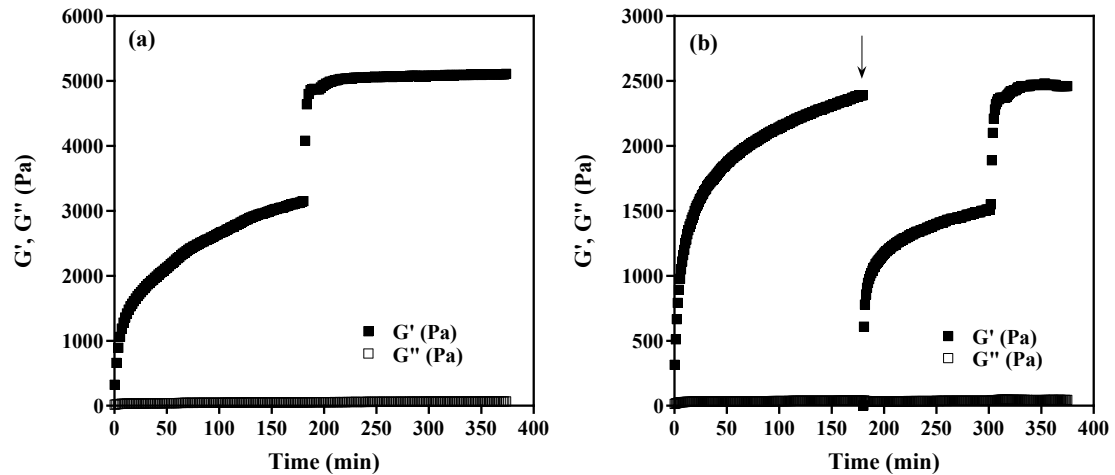


**Figure 2.10 (a) Dynamic time sweep experiment showing increase in storage modulus ( $G'$ ) upon photopolymerization of a pre-formed 1wt% M1NA hydrogel formed at pH 7.4 (50mM BTP, 150mM NaCl, 0.025wt% Irgacure 2959) and 37 °C. (b) Dynamic time sweep experiment showing shear recovery and photopolymerization of pre-formed 1wt% M1NA hydrogels at 37 °C and pH 7.4 (50mM BTP, 150mM NaCl, 0.025wt% Irgacure 2959) monitored as a function of time.**

The shear-thin and recovery properties of M1NA were investigated using oscillatory shear rheology. In this experiment, the 1 wt% M1NA at pH 7.4 solution is first allowed to gel for 3 hrs at 37 °C after which a 1000% strain is applied (denoted by an arrow in Figure 2.10b) for 30 seconds to severely disrupt the network. Thereafter, the strain is reduced to 0.2% and the gel is allowed to recover for 2 hrs. At this point, the hydrogel is irradiated for 15 min and then allowed to achieve an apparent equilibrium modulus for about an hour. As shown in Figure 2.10(b), 1 wt% M1NA hydrogel achieves a storage modulus of  $2700 \pm 300$  Pa after 3 hrs of gelation. However, following application of 1000% strain and followed by 2 hrs of recovery time, the hydrogel recovered only 67% of its original material rigidity, ( $1800 \pm 350$

Pa). Although, UV irradiation at this point resulted in a 1.6 fold increase, the final hydrogel rigidity was only equivalent to the storage modulus of the hydrogel following the initial 3 hrs of gelation. Although, M1NA hydrogels are mechanically more rigid than MAX1 hydrogels under identical conditions, they lack the ability to recover quantitatively following application of high strain.

### **2.3 Hydrophilic Face Modification of MAX1**

MAX1 undergoes folding and subsequently self-assembly in response to temperature to form  $\beta$ -sheet-rich fibrils, which display solvent exposed lysine side-chains. The  $\epsilon$ -amine of the lysine side chains can be selectively modified with different photopolymerizable groups, which can be photocrosslinked following self-assembly to enhance the mechanical rigidity of the peptide hydrogels. In this section, two distinct modifications of MAX1 hairpin are presented to achieve either intrafibrillar or interfibrillar crosslinking of the self-assembled peptide fibrils to enhance the material rigidity.

#### **2.3.1 Intrafibrillar Crosslinking via Polymerization of Lysine-Dienes**

Recent reports have shown that short peptide sequences that self-assemble can be employed as a template to intramolecularly crosslink  $\beta$ -sheet-rich secondary structures via photopolymerization in the crystalline state<sup>47</sup> as well as fibrils in solution<sup>48</sup>. This approach has been shown to impart additional stability to the self-assembled  $\beta$ -sheet-rich fibrils against denaturation.<sup>43</sup>

We sought to develop a photoreactive  $\beta$ -hairpin peptide (MLD) that would polymerize in a controlled manner following ordered self-assembly and hydrogelation (Figure 2.11). This hydrogel system is designed to undergo intrafibrillar crosslinking upon UV irradiation to further modulate the material rigidity.

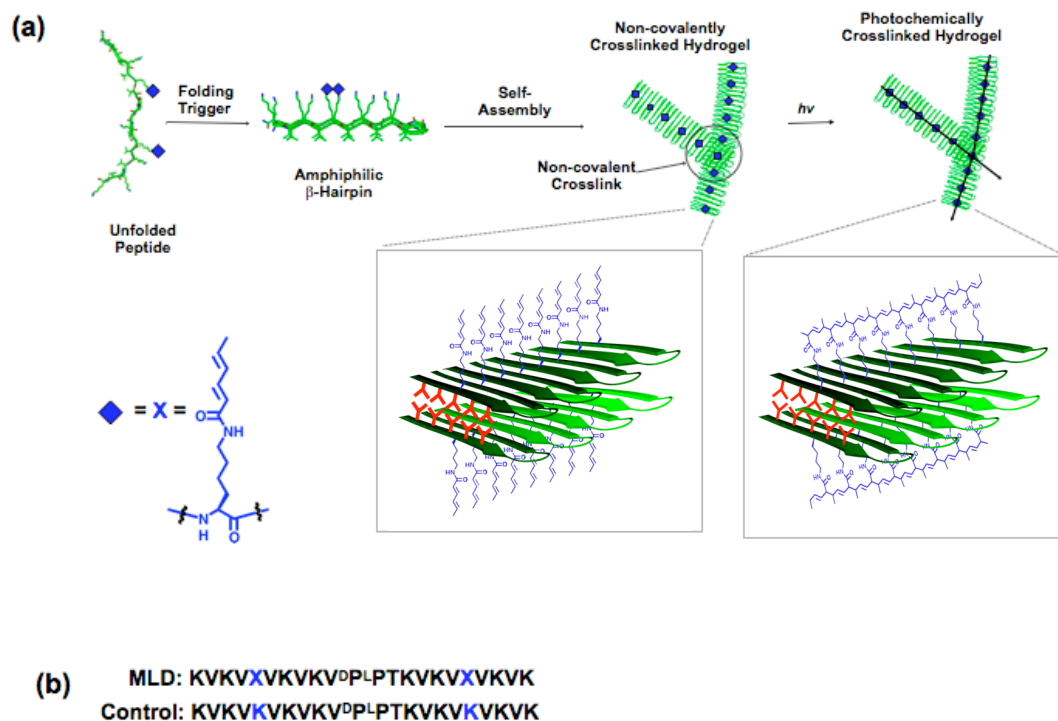


**Figure 2.11 (a) Proposed mechanism of folding and self-assembly leading to hydrogelation and subsequent photopolymerization. X = structure of the photopolymerizable lysine-diene [K(DE)]. (b) Sequence of the photopolymerizable  $\beta$ -hairpin peptide (MLD) and its control peptide (M2K)**

Similar to MAX1, MLD is designed to intramolecularly fold and subsequently self-assemble in response to increase in temperature, to form an extensive network of  $\beta$ -sheet-rich fibrils leading to hydrogelation. This mechanism allows covalent cross-linking of solvent exposed photoreactive groups along the well-defined fibrils to modulate the material rigidity, Figure 2.11.

### 2.3.1.1 Peptide Design

Peptide strands in self-assembled  $\beta$ -sheets typically align about 4.8 Å (0.48 nm) apart depending upon the peptide sequence.<sup>44</sup> Therefore, to successfully photocrosslink the fibrils in the self-assembled state, the photopolymerizable group should not only be able to traverse across this distance but also maintain this separation throughout the photocrosslinking reaction without distorting the peptide secondary structure. In this regard, 1,3-diynes<sup>45</sup> and 1,3-dienes<sup>46, 47</sup> are beneficial since they are known to undergo successful topochemical polymerization when aligned at a distance of 4.9-5.1 Å in the crystalline state and maintain this distance throughout the photopolymerization process. One such diene is sorbic acid which not only polymerizes while maintaining the separation but also yields an isolated trans double bond<sup>48</sup> unlike the diacetylenes, which form a conjugated system that can further react. Therefore, a lysine derivative of sorbic acid or the lysine-diene [K(DE)], was prepared by conjugating the N-hydroxy succinimide ester of sorbic acid to the  $\epsilon$ -

amine of the Fmoc-Lys-OH,<sup>43, 49</sup> which was employed in the synthesis of the MLD peptide.

The exact alignment or arrangement of the laterally assembled  $\beta$ -hairpins along the long axis of a given fibril is not currently known, i.e, whether the turn regions of the  $\beta$ -hairpins are on the same side or alternating sides of the fibril or mixed. To achieve efficient crosslinking along the fibrils in self-assembled state, it is essential that the photopolymerizable lysine-dienes [K(DE)] be displayed along the center of the fibril. This is not possible with MAX1 since it contains four pairs of lysines and thus the lysine dienes cannot be displayed centrally along the hydrophilic face. Therefore, a pair of lysines was added to the termini of MAX1 sequence to give a 22-amino acid peptide (MLD), Figure 2.11(b) and 2.12. MLD is specifically formulated to display 5 pairs of lysines on the solvent exposed hydrophilic face in the folded state, in which the third or the central pair of lysines (i.e. at positions 5 and 18) is substituted with a pair of lysine-dienes [K(DE)]. Therefore the lysine-dienes are displayed along the center of the self-assembled fibril irrespective of the exact alignment of the hairpins along the long axis of the fibril. This should favor polymerization of the dienes along the  $\beta$ -sheet rich fibrils in the self-assembled state upon UV irradiation, Figure 2.12. A control peptide [M2K, Figure 2.10(b)] was prepared in which the lysine-dienes were replaced with lysines.

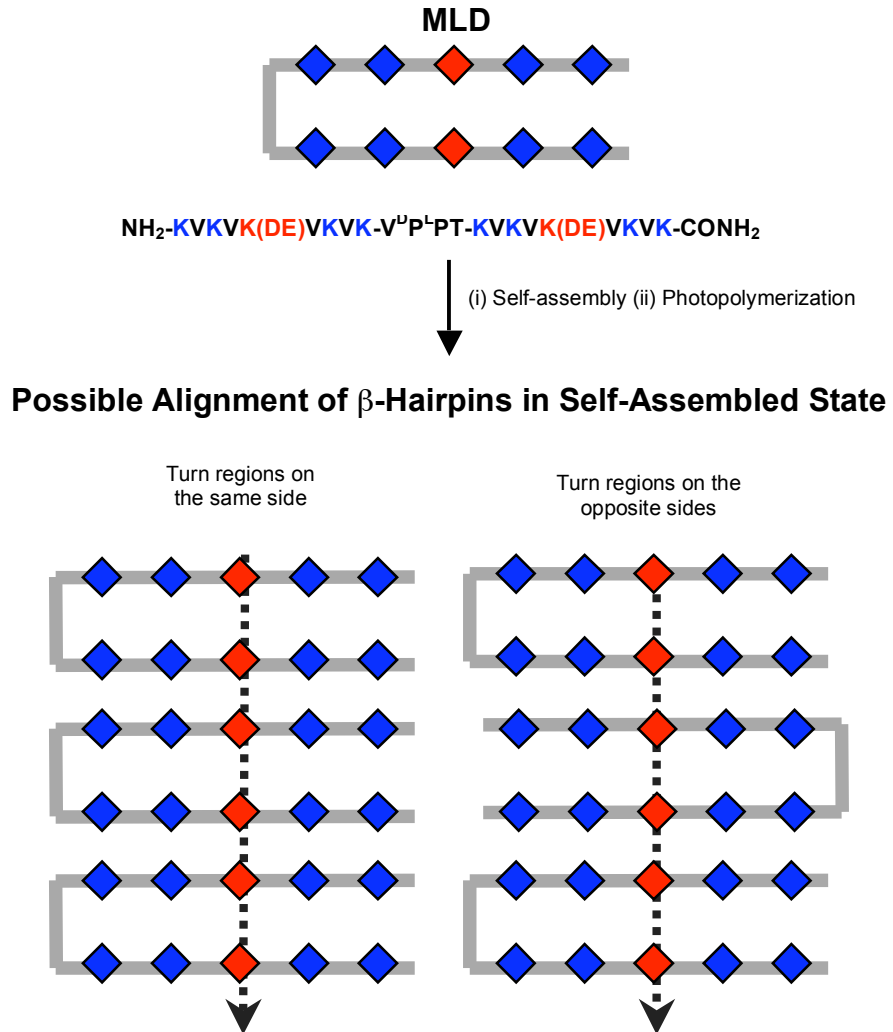


**Figure 2.12 Schematic representation showing design of MLD for efficient polymerization of the  $\beta$ -hairpins in the self-assembled state irrespective of the hairpin arrangement along the axis of a given fibril.**

### 2.3.1.2 Folding, Self-Assembly and Photopolymerization of Peptide Solutions

MLD is designed to undergo triggered folding and self-assembly to promote  $\beta$ -sheet formation in response to temperature. At pH 7.4, it is likely that all

the lysines remain protonated, making peptide folding and self-assembly difficult even at higher temperatures. However, increasing the ionic strength (NaCl) of buffer solutions should screen the charged lysines making thermally-triggered folding possible. Circular dichroism (CD) spectroscopy was used to assess the potential of MLD and M2K to fold and self-assemble at physiological relevant conditions (pH 7.4, 150 mM NaCl). Figure 2.13(a) shows the extent of  $\beta$ -sheet formation [ $\theta_{218}$ ] for 150  $\mu$ M solutions of MLD and M2K peptides as a function of temperature. The control peptide, M2K, exhibits minimal  $\beta$ -sheet formation under these conditions, even at higher temperatures. According to the model of folding and self-assembly, the electrostatic repulsions due to the eleven positively charged amines (10 lysines and 1 N-terminus) of M2K must be overcome for the peptide to fold and subsequently self-assemble at pH 7.4. However, a physiologically relevant ionic strength of 150 mM NaCl may not be sufficient to screen the electrostatic repulsions to allow folding to occur.<sup>50</sup> The data shows that MLD begins to fold and self-assemble at approximately 15 °C and the majority of  $\beta$ -sheet transformation is complete by 40 °C. The overall charge state of MLD is +9 whereas that of M2K is +11. Therefore, MLD has fewer charged lysines that need to be screened for folding and self-assembly to occur under identical conditions. This is also in agreement with similarly designed lysine-rich  $\beta$ -hairpins in which a glutamic acid substitution favored folding and self-assembly to occur at a lower temperature.<sup>41</sup> In addition, the hydrophobic dienes may also promote folding and self-assembly via the hydrophobic effect.

Temperature dependent conformational changes in the secondary structure of MLD can also be illustrated by CD as a function of wavelength. Figure 2.13(b) shows a wavelength spectrum of MLD at 5 °C in pH 7.4 buffer of high ionic strength (150 mM NaCl), indicative of a random coil structure. Upon increasing the temperature to 37 °C, the wavelength spectrum not only displays a minimum centered at about 218 nm, which is indicative of  $\beta$ -sheet secondary structure, but also a maximum centered at about 249 nm. The maximum around 249 nm probably arises due to the absorption of the diene chromophores in a chiral environment following self-assembly.<sup>51, 52</sup>

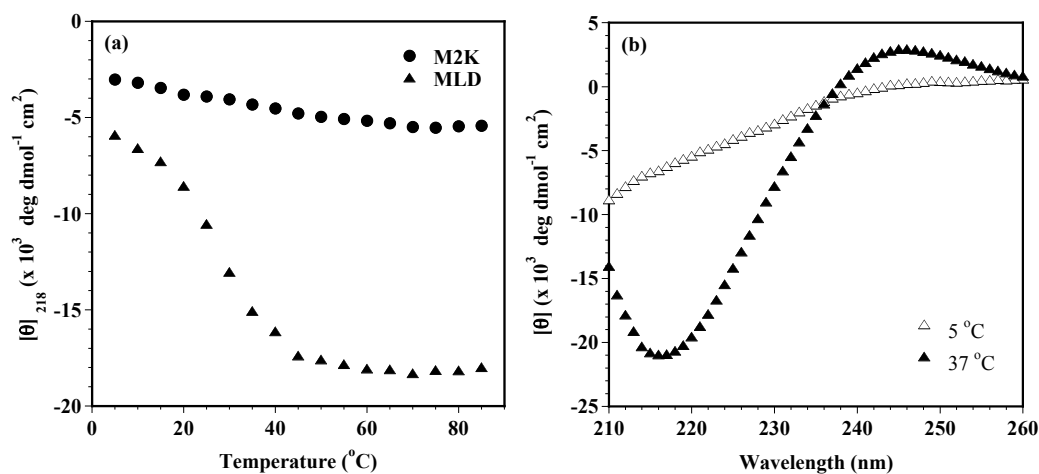


**Figure 2.13 (a) CD spectroscopy of 150  $\mu\text{M}$  MLD solution at pH 7.4 (50 mM BTP, 150 mM NaCl) showing  $[\theta]_{216}$  as a function of temperature. (b) Wavelength spectra of 150 mM MLD solution at pH 7.4 showing transition from random coil at 5  $^{\circ}\text{C}$  to  $\beta$ -sheet at 37  $^{\circ}\text{C}$ .**

### 2.3.1.3 Monitoring Photopolymerization of Self-Assembled Peptide using CD and UV Spectroscopy

MLD is designed to self-assemble into  $\beta$ -sheet-rich fibrils, which can undergo intrafibrillar polymerization upon UV irradiation. Figure 2.14(a) shows wavelength spectra as a function of photopolymerization of self-assembled 0.1 wt% (300  $\mu$ M) MLD peptide in pH 7.4 buffer (150 mM NaCl) [ $\Delta$ ].

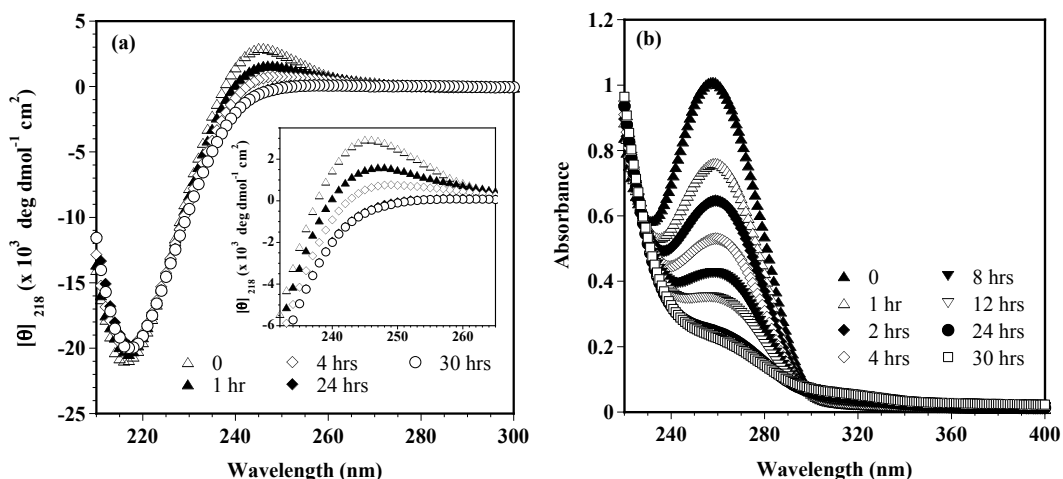


**Figure 2.14 (a) Wavelength scans of 0.1wt% MLD showing time dependent decrease in intensity at 245 nm upon photopolymerization. Inset: Magnified view showing the decrease in intensity at 245 nm with polymerization time. (b) UV absorption spectra of self-assembled 0.1wt% MLD at pH 7.4 (50mM BTP, 150mM NaCl) showing decrease in absorption intensity at 257 nm upon photopolymerization with time (0-30 hrs).**

Before photopolymerization, the spectrum is similar to Figure 2.13(b), a minimum at 218 nm and a maximum at 245 nm are observed. The blue shift in diene absorption

from 249 nm to 245 nm is primarily due to the higher concentration of MLD employed in this experiment.<sup>53, 54</sup> Upon UV irradiation, the intensity of the CD signal at 245 nm decreases with time due to the photoreaction. More importantly, the photopolymerization reaction barely distorts the  $\beta$ -sheet secondary structure as observed by a minimal change in intensity at 218 nm. This suggests that the gross structure of the preformed  $\beta$ -sheet rich fibril network is not disrupted when crosslinked.

Sorbate chromophores have been shown to exhibit a broad UV absorption at 260 nm in the crystalline state that disappears upon UV irradiation (in absence of a photoinitiator) over time due to a photoreaction.<sup>48</sup> This was also observed in the case of MLD. Figure 2.14(b) shows an absorption spectrum of self-assembled 0.1 wt% (300  $\mu$ M) MLD peptide in pH 7.4 buffer (150 mM NaCl) prior to irradiation, ( $\blacktriangle$ ). Here, MLD displays an absorption band centered around 258 nm due to the conjugated dienes on the self-assembled  $\beta$ -hairpins. As expected, upon irradiation, the absorption intensity at 258 nm progressively decreases with time.

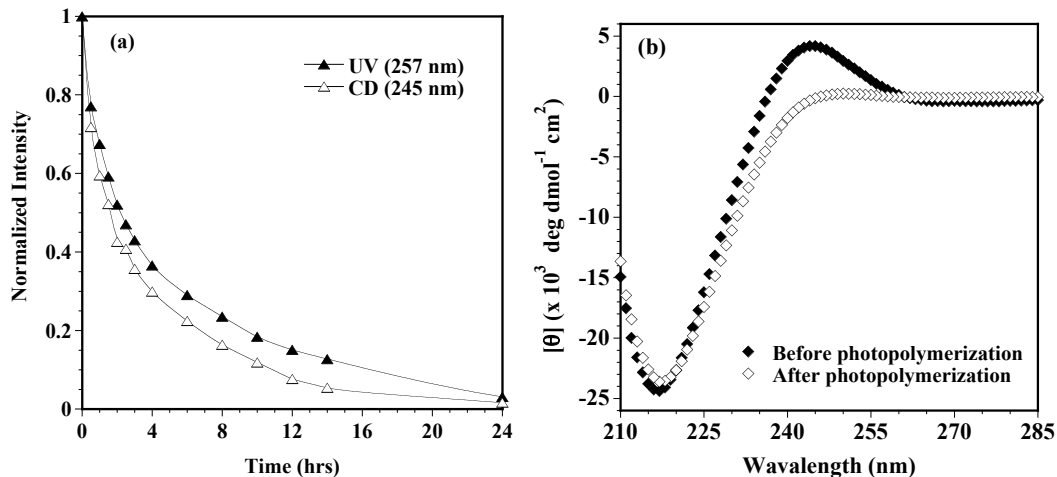


**Figure 2.15 (a) Normalized photopolymerization profile of 0.1 wt% MLD obtained via CD and UV as a function of irradiation time. (b) Wavelength scans of 1wt% MLD peptide self-assembled at pH 7.4 (50mM BTP, 150mM NaCl, 0.025wt% Irgacure 2959) and 37 °C before and after 5 minutes of photoirradiation at 365 nm.**

Time dependent polymerization of the dienes in self-assembled MLD was monitored using both UV and CD spectroscopy and therefore their polymerization profiles can be compared as a function of time. Figure 2.15(a) shows a plot of normalized intensity with photopolymerization time. The data indicates that the polymerization profile of MLD with time using both the techniques is very similar. The use of CD spectroscopy to monitor the photocrosslinking reaction would be particularly beneficial when an aromatic photoinitiator such as Irgacure 2959 is used to accelerate the polymerization reaction, which would otherwise interfere with the UV absorption spectra. This is demonstrated using 1wt% MLD peptide in the presence of Irgacure 2959 at pH 7.4 and 37 °C. At this concentration, MLD can be thermally-

triggered to fold and self-assemble to form a self-supporting hydrogel. Figure 2.15(b) shows a wavelength spectrum of 1 wt% MLD peptide hydrogel formed in presence of 0.025 wt% Irgacure 2959 at pH 7.4 (150 mM NaCl) and 37 °C displaying a minimum at 218 nm and a maximum at 245 nm. Following irradiation for 5 min, the peak intensity at 245 nm again diminishes whereas the minima at 218 nm remains undistorted, thus maintaining the  $\beta$ -sheet secondary structure. This data indicates that MLD polymerizes efficiently even at gel forming concentrations.

#### **2.3.1.4 Mechanical Properties of Photopolymerized Hydrogels**

The bulk material properties of MLD hydrogels formed at pH 7.4 in response to increase in temperature were assessed using oscillatory shear rheology similar to the M1NA peptide. The data in Figure 2.16(a) shows the gelation kinetics of 1 wt% MLD at pH 7.4 (150 mM NaCl) and 37 °C in presence of 0.025wt% Irgacure 2959. Here, the hydrogel is first formed by increasing the temperature from about 20 °C (RT) to 37 °C and then irradiated with UV light. When gelation is triggered at 37 °C, MLD forms a moderately rigid hydrogel with an average storage modulus of  $220 \pm 50$  Pa after 3 hrs. Control experiments show that MLD forms moderately rigid hydrogels within 3 hrs of gelation with no significant increase in  $G'$  over longer times. After which time, the gel is irradiated for 15 min at 365 nm ( $\sim 16$  mW/cm<sup>2</sup>). An instantaneous increase in material rigidity ( $G'$ ) is observed over time, and achieves an average equilibrium storage modulus of  $500 \pm 75$  Pa over a 1 hr period. This

experiment demonstrates that self-assembled MLD hydrogels can be successfully photocrosslinked to yield an average 2.5 fold increase in material rigidity. Dynamic frequency sweep measurements of MLD hydrogels before and after UV irradiation show that the  $G'$  values are an order of magnitude higher than  $G''$ , and that  $G'$  is insensitive to a range of frequency indicating formation of permanent crosslinks, Figure 2.16(b).

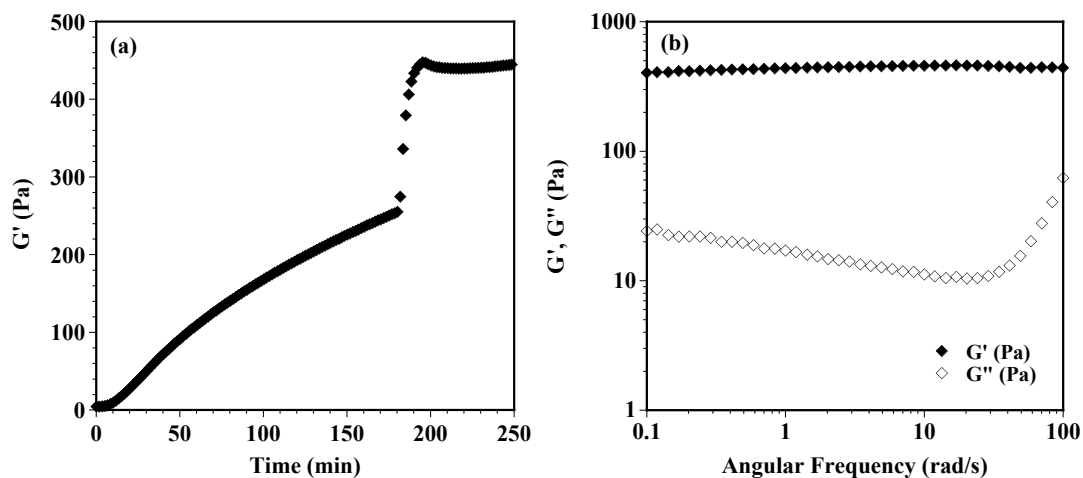


**Figure 2.16 (a) Dynamic time sweep experiment showing about 2.5 fold increase in storage modulus ( $G'$ ) upon photopolymerization of pre-formed 1wt% MLD hydrogel at pH 7.4 (50mM BTP, 150mM NaCl, 0.025wt% Irgacure 2959) and 37 °C (b) Dynamic frequency sweep measurement showing the storage ( $G'$ ) and loss ( $G''$ ) modulus values as a function of angular frequency**

### 2.3.1.5 Shear Recovery and Subsequent Photopolymerization of Hydrogels

Similar to the M1NA peptide, the ability of MLD hydrogels to shear recover and then polymerize upon irradiation was also probed. As shown in Figure 2.17, in part (i) of this experiment, a 1 wt% MLD hydrogel is formed at pH 7.4 (150 mM NaCl) by increasing the temperature to 37 °C. After 3 hrs of gelation ( $G' = 200 \pm 40$  Pa) [part (ii)], a 1000 % strain is applied for 30 sec to shear thin the material, which severely disrupts the hydrogel network. After which time, part (iii), the applied strain is decreased to 0.2 % and the gel is allowed to recover for a period of 2 hrs. The gel recovers quantitatively within an hour with further increase in  $G'$  over time. Following recovery for 2 hrs ( $G' = 240 \pm 30$  Pa), the hydrogel is irradiated (part iv) for 15 min at 365 nm ( $\sim 16$  mW/cm<sup>2</sup>), which causes the  $G'$  to increase rapidly over time. After which time, the photocrosslinked hydrogel achieves an equilibrium storage modulus of  $590 \pm 30$  Pa over a period of about 3 hrs. Although the sample was irradiated for 15 min, no substantial increase in  $G'$  is observed after 10 min of exposure indicating that the photocrosslinking reaction is most likely complete.

For practical applications, the 2 hr recovery period following the shear-thinning event may not be feasible. To overcome this limitation, the shear recovery process was shortened to better simulate applications where photocrosslinking is initiated directly after syringe delivery. This was accomplished by eliminating the 2 hr recovery period from the experiment. For this experiment [Figure 2.18], parts (i) and (ii) were performed exactly as described for Figure 2.17. However, in part (iii), where

the high strain is reduced to 0.2 %, the recovering hydrogel is irradiated for 15 min (365 nm,  $\sim 16 \text{ mW/cm}^2$ ) and then allowed to achieve equilibration storage modulus. Even though the shear-thinned hydrogel was not allowed to recover completely, MLD hydrogel still achieved  $\sim 2.5$  fold increase in rigidity following UV irradiation. This experiment demonstrates that the full recovery of the shear-thinned material is not necessary for photocrosslinking to occur. In addition, this observation provides insight into the nature of the fibrillar network during the shear process.

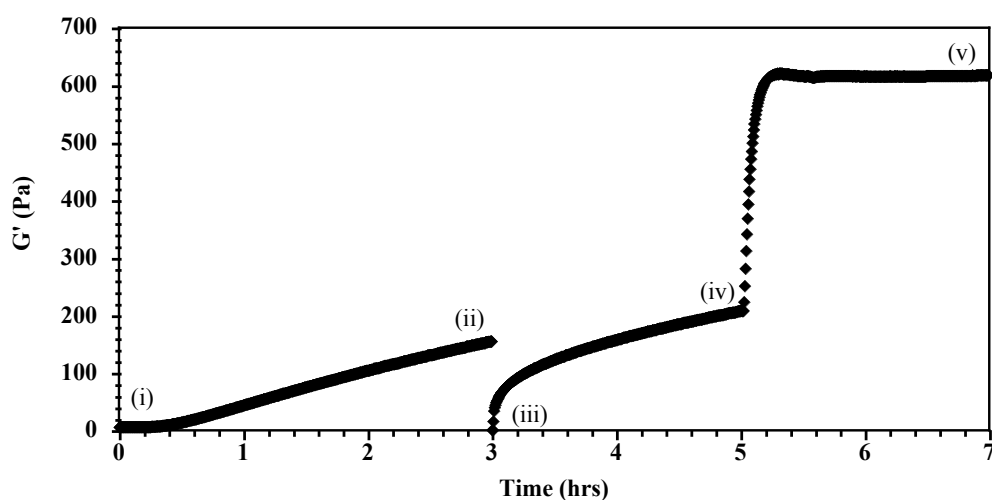


**Figure 2.17** Dynamic time sweep experiment showing shear-thinning, recovery and subsequent photopolymerization of pre-formed 1wt% MLD hydrogel at pH 7.4 (50mM BTP, 150mM NaCl, 0.025wt% Irgacure 2959) and 37 °C.

The fact that MLD hydrogels achieve ~ 2.5 fold increase in rigidity upon irradiation during or after the shear process suggests that the fibrillar network may not be completely disrupted during the shear-thinning process. If shear-thinning did completely disrupt the network then the intrafibrillar polymerization should have been limited to shorter fibrils and thus form weaker gels. Collectively, these results demonstrate that MLD hydrogels show potential as syringe deliverable scaffolds because they can be shear-thin delivered, and recover their original mechanical rigidity. In addition, the rigidity can be further modulated via photopolymerization following delivery to the target site.

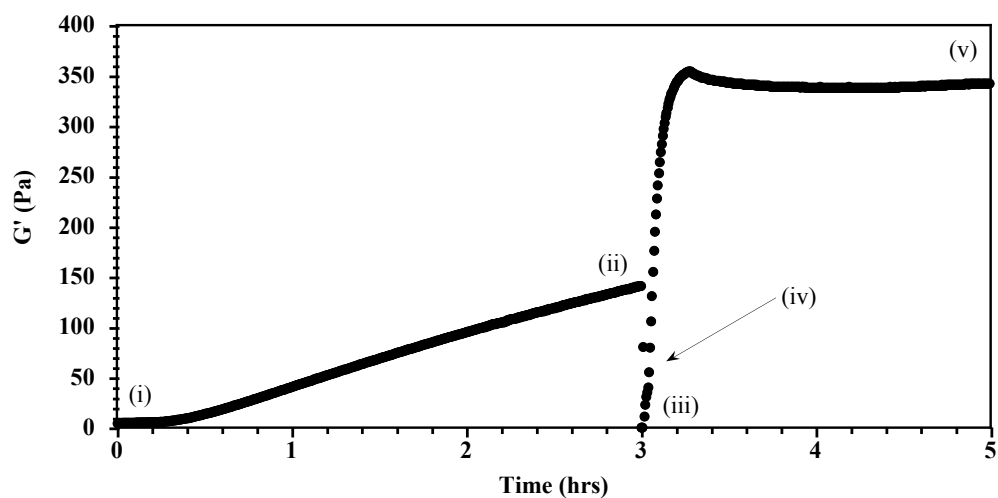


**Figure 2.18** Dynamic time sweep experiment showing shear-thinning followed by immediate photopolymerization of pre-formed 1wt% MLD hydrogels at pH 7.4 (50mM BTP, 150mM NaCl, 0.025wt% Irgacure 2959) and 37 °C.

### 2.3.1.6 Conclusions

Our strategy to fabricate hydrogels involves triggered folding and subsequently self-assembly of  $\beta$ -hairpin peptides. We have shown earlier that  $\beta$ -hairpin peptides can be designed to undergo triggered hydrogelation in response to changes in pH, temperature, ionic strength and light. Results from this study demonstrate that additional functionality can also be introduced into  $\beta$ -hairpins to modulate the ultimate material properties. We achieved this by incorporating a pair of lysine-dienes into the  $\beta$ -hairpins such that following self-assembly; the photopolymerizable dienes are displayed along the center of the  $\beta$ -sheet rich fibril. CD can be employed to monitor the polymerization of these chiral dienes in the self-assembled state even at gel forming concentrations in presence of an initiator. Upon irradiation, intrafibrillar crosslinking results in  $\sim 2.5$  fold increase in the mechanical rigidity of the hydrogel. In addition, the physically crosslinked hydrogels exhibit shear recovery, which allows the delivery of pre-formed gel to the target in a controlled fashion prior to irradiation. The injectable hydrogel can be irradiated after or during shear-thin recovery without significantly affecting the increase in rigidity ( $\sim 2.5$  fold). These attributes of MLD hydrogels would enable the modulation of the material properties via photopolymerization at the tissue site post shear recovery. This demonstrates that structure based design of  $\beta$ -hairpins can be employed to create functional materials with predictable material properties for biomedical applications.

### 2.3.2 Interfibrillar Crosslinking via Polymerization of N $\epsilon$ -Acryloyl-L-Lysine

MAX1 is designed to fold into an amphiphilic  $\beta$ -hairpin in response to environmental stimuli such as temperature, pH or ionic strength. The folded  $\beta$ -hairpin rapidly self-assembles into an extended network of  $\beta$ -sheet-rich fibrils resulting in formation of a mechanically rigid hydrogel. In the self-assembled state, fibrils are composed of a bilayer of intermolecularly hydrogen-bonded hairpins directed by the packing of hydrophobic faces of individual hairpins. However, because of the topologically smooth surface of the hydrophobic face of each hairpin, facial mispacking occurs. This provides nucleation sites for nascent fibril growth in different three-dimensional directions creating branched junctions. In addition to these interfibril junctions, fibrils can also become entangled. This provides additional physical cross-links. The number of fibril junctions and entanglements formed during the self-assembly process affects the mechanical rigidity of the hydrogels. This section discusses design of a  $\beta$ -hairpin peptide that specifically favors interfibrillar covalent crosslinking of the non-permanent entanglements formed during the self-assembly process, to further enhance the mechanical rigidity of the hydrogels, Figure 2.19.

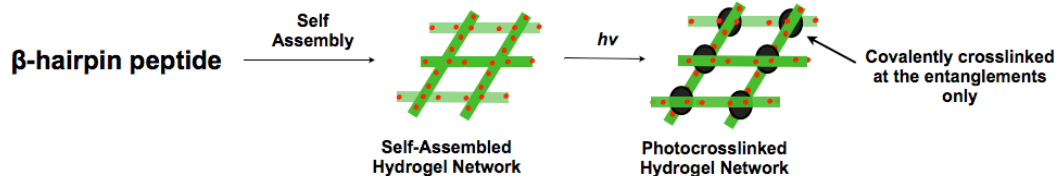


**Figure 2.19 Schematic depicting interfibrillar crosslinking of entanglements following triggered folding and self-assembly**

### 2.3.2.1 Peptide Design

To design a photopolymerizable  $\beta$ -hairpin peptide that would allow efficient interfibrillar crosslinking only as opposed to crosslinking along the long axis of the fibril as was the case for the MLD peptide, two criteria need to be satisfied. First, it is required to functionalize an appropriate lysine residue along the hydrophilic face of the  $\beta$ -hairpin that will only allow efficient interfibrillar covalent crosslinking upon UV irradiation. Second, an appropriate short photopolymerizable group must be selected that would favor interfibrillar crosslinking only. Towards this objective, MKA, a  $\beta$ -hairpin peptide with an  $N\epsilon$ -acryloyl-L-lysine at position 19 was designed, Figure 2.20. Lysine at position 19 on the  $\beta$ -hairpin is chosen to display the photopolymerizable group on the flexible side chain of the residue at the edge of the  $\beta$ -hairpin. The  $N\epsilon$ -acryloyl-L-lysine at position 19 will disfavor any intrafibrillar crosslinking reaction since the acryloyl group is too short to react with another acrylate along the long axis of the same fibril as shown in Figure 2.21.

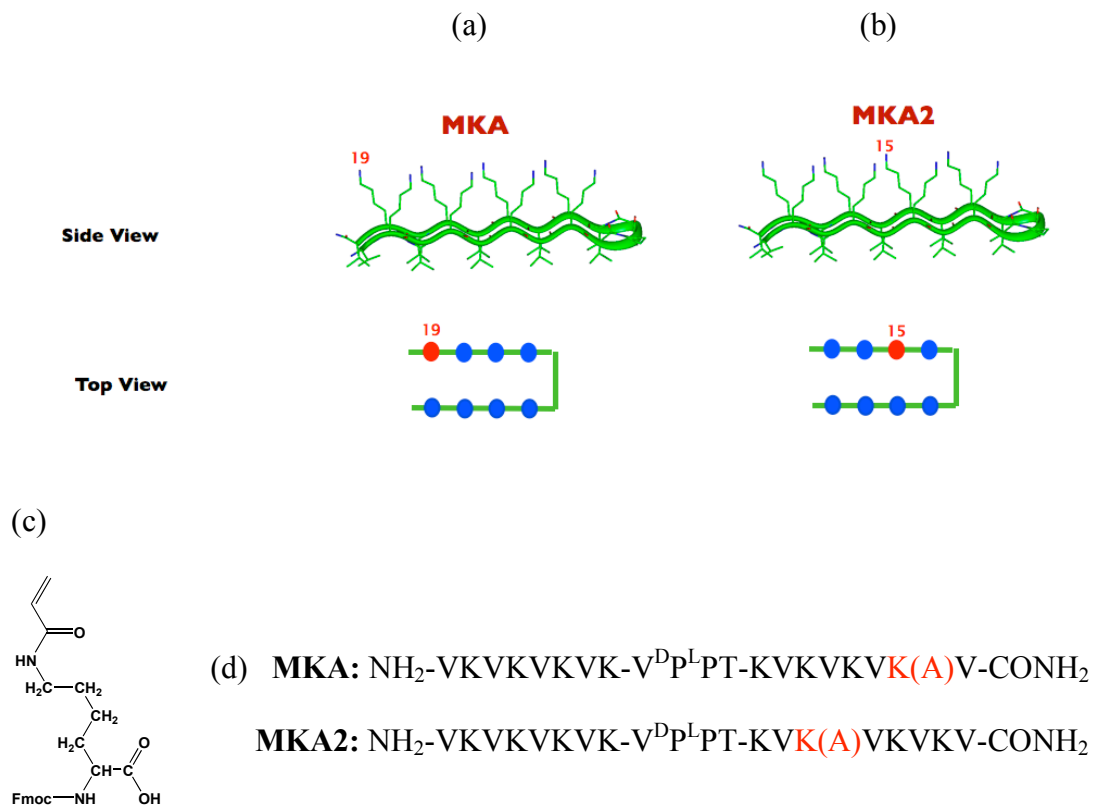


**Figure 2.20** (a) Side and top view of MKA peptide showing lysine position 19 along the  $\beta$ -hairpin (b) Side and top view of MKA2 peptide showing lysine position 15 along the  $\beta$ -hairpin (c) Structure of Fmoc-N $\epsilon$ -acryloyl-L-lysine-OH employed in synthesis of MKA (d) Sequence of MKA and MKA2 peptide where **K(A)** is the N $\epsilon$ -acryloyl-L-lysine

The positional dependence of the acryloyl group was investigated by designing a second peptide, MKA2. MKA2 incorporates the N $\epsilon$ -acryloyl-L-lysine at an interior position 15, Figure 2.20. Here, the N $\epsilon$ -acryloyl-L-lysine is sterically hindered by the neighbouring lysines side-chains and therefore should be less accessible for the

crosslinking reaction. However, MKA2 will still favor interfibrillar crosslinking only as shown in Figure 2.21.

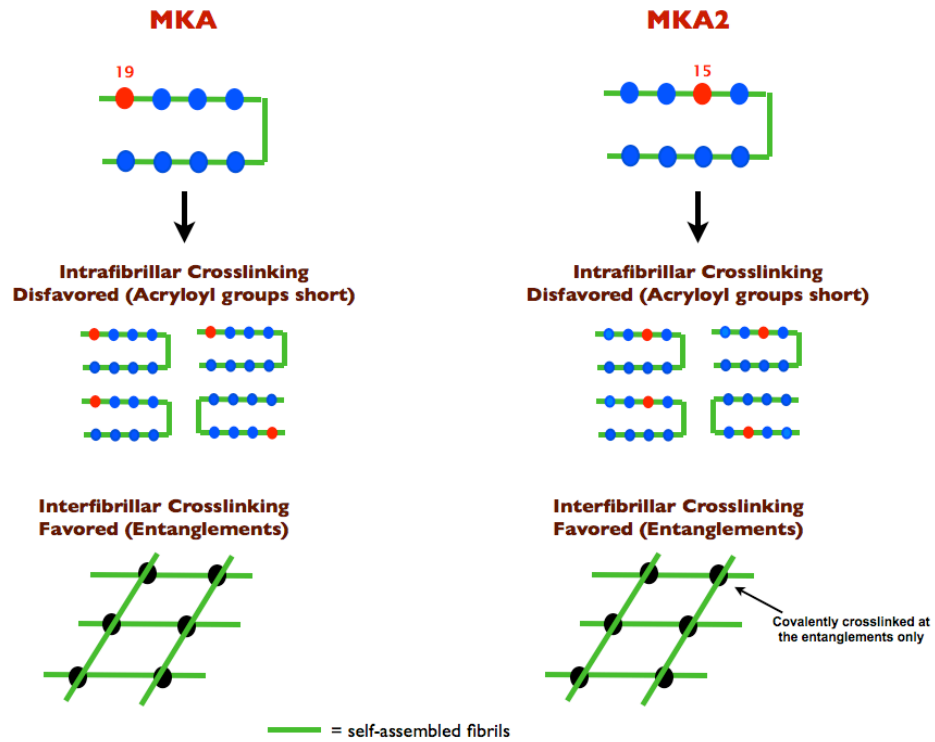


**Figure 2.21 Schematic depicting design of  $\beta$ -hairpin peptides that favor Interfibrillar crosslinking following self-assembly**

### 2.3.2.2 Effect of Photopolymerization on $\beta$ -Sheet Structure of Peptide Hydrogels

Figure 2.22 shows CD wavelength spectra of 1 wt% MKA and MKA2 peptide at pH 7.4 (50 mM BTP, 150 mM NaCl, 0.025wt% Irgacure 2959) at 37 °C. The data shows that both MKA and MKA2 form  $\beta$ -sheet secondary structure as indicated by a minimum at 216 nm. In addition, upon UV irradiation, there is no gross distortion in the  $\beta$ -sheet structure of these peptides. The rate of  $\beta$ -sheet formation can be measured by measuring the mean residual ellipticity  $[\theta]$  at 216 nm as a function of time. Figure 2.23 shows the kinetics of  $\beta$ -sheet formation for 1 wt% MKA and MKA2 at pH 7.4 (50 mM BTP, 150 mM NaCl, 0.025 wt% Irgacure 2959) and 37 °C.

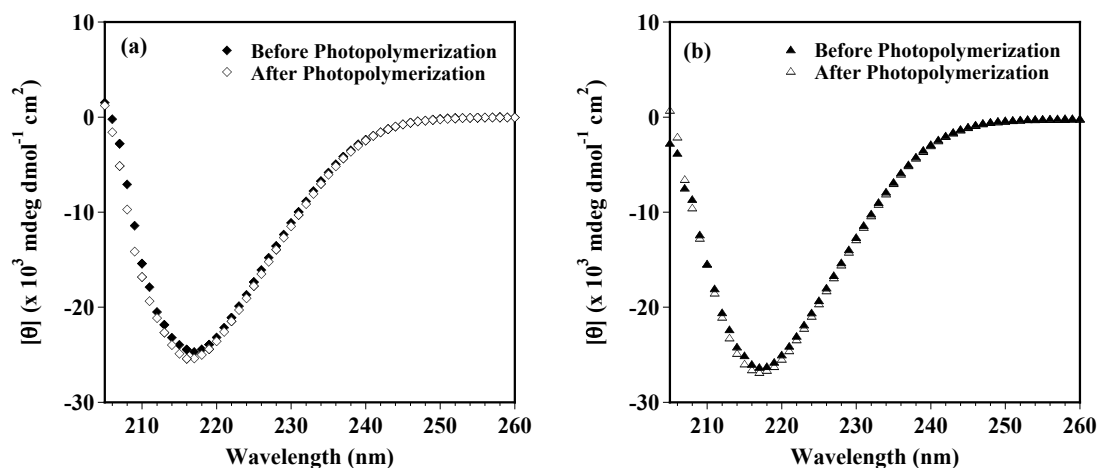


**Figure 2.22** CD wavelength spectra of (a) 1 wt% MKA and (b) 1 wt% MKA2 before and after photopolymerization at pH 7.4 and 37 °C.

The data shows that both MKA and MKA2 peptide exhibit rapid kinetics of  $\beta$ -sheet formation. The majority of the  $\beta$ -sheet is formed within first 2 min with no significant increase thereafter.

### **2.3.2.3 Mechanical Properties of Photopolymerized Hydrogels**

The mechanical properties of MKA and MKA2 were assessed by oscillatory rheology as shown in Figure 2.24. In this experiment, a 1 wt% peptide solution at pH 7.4 (50 mM BTP, 150 mM NaCl, 0.025 wt% Irgacure 2959) at about 20 °C is directly loaded onto the rheometer pre-equilibrated at 37 °C to trigger hydrogelation. After 3 hrs of gelation time, the hydrogels are irradiated with UV light for 15 min to initiate the polymerization reaction. After which time, the crosslinked gels are allowed to equilibrate over time. In Figure 2.24, panel (a) shows that MKA achieves an average storage modulus value of  $2000 \pm 100$  Pa after 3 hrs of gelation time. Upon irradiation, an instantaneous increase in the storage moduli is observed, which then equilibrates to an average storage modulus of  $4800 \pm 100$  Pa. This data shows that MKA hydrogels exhibit about 2.4 fold increase in rigidity due to the covalent crosslinks formed at the entanglements. Similarly, MKA2 hydrogels (panel b) first achieve an average storage modulus of  $2700 \pm 100$  Pa upon gelation. However, upon UV irradiation, these hydrogels exhibit only a 1.27 fold increase in rigidity measuring  $3500 \pm 100$  Pa.

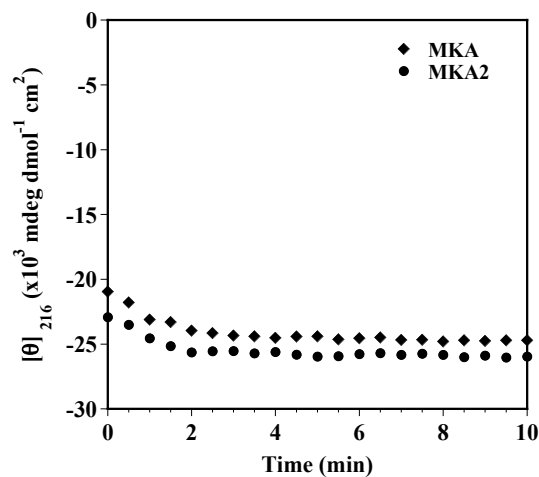


**Figure 2.23 Kinetics of  $\beta$ -sheet formation of 1 wt% MKA and MKA2 at pH 7.4 and 37 °C as a function of time**

Collectively, the results from Figure 2.24 indicate that MKA peptide, which has a N $\epsilon$ -acryloyl-L-lysine at the edge of the  $\beta$ -hairpin (position 19) exhibits better polymerization efficiency and thus results in greater fold increase in rigidity. However, MKA2 that has an N $\epsilon$ -acryloyl-L-lysine in the interior (position 15), is possibly less accessible and thus results in lower fold increase in rigidity.

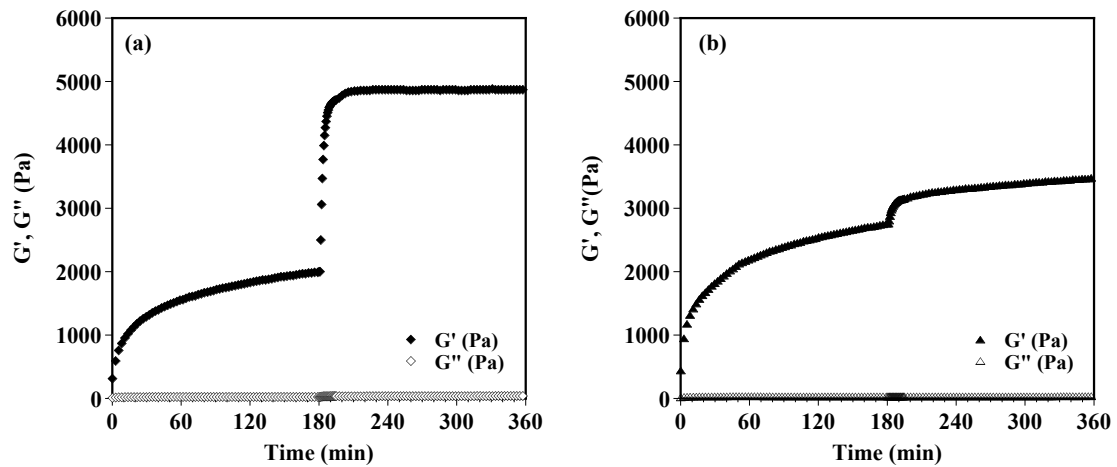


**Figure 2.24 Dynamic time sweep experiments showing increase in mechanical rigidity of pre-formed (a) 1 wt% MKA and (b) 1 wt% MKA2 hydrogels at pH 7.4 and 37 °C upon photoirradiation**

### 2.3.2.4 Shear Recovery and Subsequent Photopolymerization of Hydrogels

The ability of MKA hydrogels to exhibit shear recovery and subsequent polymerization to yield mechanically more rigid hydrogels was investigated using oscillatory dynamic time sweeps experiments. As shown in Figure 2.25, in part (i) of this experiment, a MKA hydrogel is formed at pH 7.4 (50 mM BTP, 150 mM NaCl, 0.025 wt% Irgacure 2959) by increasing the temperature to 37 °C. After 3 hrs of gelation ( $G' = 2250 \pm 150$  Pa) [part (ii)], a 1000 % strain is applied for 30 sec to shear thin the material, which severely disrupts the hydrogel network. After which time, part (iii), the applied strain is decreased to 0.2 % and the gel is allowed to recover over a period of time. The gel recovers about 92% of its original mechanical rigidity in a period of 2 hrs. Following recovery ( $G' = 2100 \pm 100$  Pa), the hydrogel is irradiated

(part iv) for 15 min at 365 nm ( $\sim 16 \text{ mW/cm}^2$ ), after which the  $G'$  increases rapidly over time. Although the sample is irradiated for 15 min, no substantial increase in  $G'$  is observed after 10 min of exposure indicating that the photocrosslinking reaction was almost complete after this point. After 1 hr, the crosslink hydrogel achieves an equilibrium storage modulus of  $4600 \pm 200 \text{ Pa}$ , a 2.2 fold increase in mechanical rigidity. This data shows that MKA hydrogel show promise as an injectable biomaterial because it can be shear-thin delivered. In addition, the rigidity of the gel can be further modulated via photopolymerization following delivery to the target site.

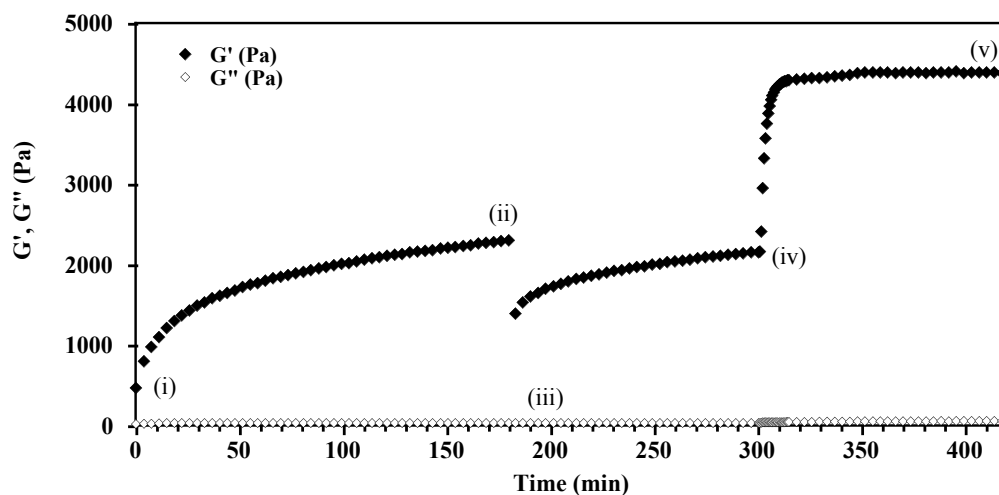


**Figure 2.25** Dynamic time sweep experiment showing shear-thinning, recovery and subsequent photopolymerization of pre-formed 1wt% MKA hydrogel at pH 7.4 (50mM BTP, 150mM NaCl, 0.025wt% Irgacure 2959) and 37 °C.

For use of MKA hydrogels as tissue engineering scaffold, the 2 hr recovery period after shear-thinning may not be practically feasible. Therefore, the syringe delivery and subsequent polymerization process was modified for use of MKA hydrogels as injectable materials in a clinical setting. As shown in Figure 2.26, the MKA solution (part i) is allowed to form a gel for 3 hrs (part ii), achieving an average storage modulus of  $2100 \pm 100$  Pa. At this point, a 1000% strain is applied for 30 sec to shear thin the hydrogel as evident by instantaneous decrease in the storage modulus. After the shear-thinning event, the strain is then decreased to 0.2% (part iii). Thirty seconds after the strain is decreased to 0.2% strain, the material is irradiated for 15 min as the network is recovering (part iv). After 15 min of irradiation and subsequent equilibration, the irradiated hydrogel achieves a storage modulus value of  $3600 \pm 100$  Pa, which corresponds to about 1.7 fold increase in rigidity. This is lower than what was observed in the previous experiment (Figure 2.25) where the shear-recovered hydrogel achieved a 2.2 fold increase in rigidity upon irradiation. These results suggest that some entanglements may be disrupted during the application of high strain, and therefore fewer entanglements can participate in the crosslinking reaction leading to a 1.7 fold increase in rigidity only.

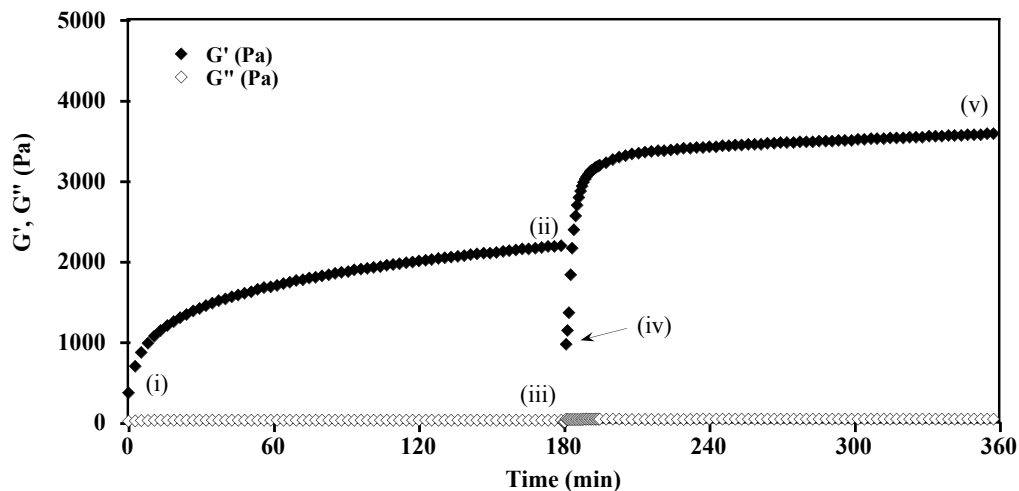


**Figure 2.26** Dynamic time sweep experiment showing shear-thinning followed by immediate photopolymerization of pre-formed 1wt% MKA hydrogels at pH 7.4 (50mM BTP, 150mM NaCl, 0.025wt% Irgacure 2959) and 37 °C.

### 2.3.2.5 Nanoscale Structure Analysis

Small angle neutron scattering (SANS) experiments were employed to investigate the nanoscale structure of MKA fibrils formed during hydrogelation. In addition, any change in the network structure of the hydrogels as a result of photocrosslinking reaction of the entanglements was also probed. SANS data collected on 1 wt % MKA gels formed at pH 7.4 (50 mM BTP, 150 mM NaCl, 0.025 wt% Irgacure) and 37 °C is shown in Figure 2.27(a) where the scattering intensity is plotted as function of the scattering vector. Upon irradiation, minimal change in the scattering intensity is observed indicating that the irradiation process does not induce any substantial changes to the network structure. This data suggests that the enhancement

in storage modulus observed as a result of irradiation stems from covalent crosslinking of the non-permanent entanglements without causing any gross changes to the network. Transmission electron microscopy (TEM) experiments show that MKA gel is composed of monodispersed fibrils similar to MAX1,<sup>55</sup> which measure about 3 nm in width, Figure 2.27(b). TEM of crosslinked MKA hydrogels was not performed since it would be practically impossible to distinguish between covalent and non-covalent entanglements.

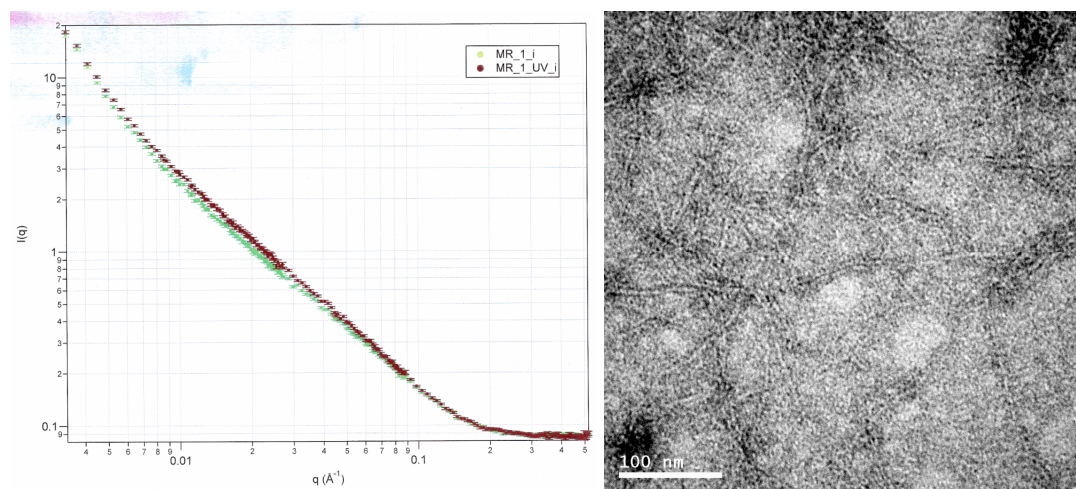


**Figure 2.27 (a) SANS data of 1 wt% MKA hydrogel at pH 7.4 (50 mM BTP, 150 mM NaCl, 0.025 wt% Irgacure 2959) and 37 °C before and after photopolymerization. (Data by Monica Branco) (b) TEM micrograph of diluted 1 wt% MKA hydrogel at pH 7.4 and 37 °C. (Image taken by Radhika Nagarkar)**

### **2.3.2.6 Effect of Gelation Time on Mechanical Properties of Photopolymerized Hydrogels**

Hydrogels prepared via folding and self-assembly of  $\beta$ -hairpin peptides exhibit an increase in storage modulus at a constant rate even after about 1 hr of gelation. This feature, normally referred to as the “aging” process, leads to an increase in storage modulus value over time. One hypothesis is that the fibrils constituting the hydrogel network may be undergoing a reorganization process, which leads to an increase in the material rigidity. The interfibril junctions and entanglements that are believed to impart rigidity to the hydrogel might be playing a role in this process. Since the entanglements are non-permanent and the fibrils may be able to slide over each other, the reorganization process may include rearrangement or formation of more entanglements. The MKA peptide was specifically designed to covalently crosslink the entanglements and thus may be beneficial to understand this behavior. Oscillatory rheology experiments employing the MKA peptide were performed to gain some insight into this mechanism on a shorter time scale. Figure 2.28 shows time sweep experiments of 1wt% MKA gels prepared at pH 7.4 (50 mM BTP, 150 mM NaCl, 0.025 wt% Irgacure 2959) and 37 °C. The results are presented in Table 1. In this study, an aqueous solution of MKA peptide is triggered to form a hydrogel for a specified amount of time, after which the resultant hydrogel is irradiated for 15 min at 365 nm and then allowed to equilibrate over time. Here, independent 1 wt% MKA solutions were allowed to form a gel for either 15, 30, 60 or 180 min prior to irradiation. As expected, prior to irradiation, the storage modulus of the MKA

hydrogels is proportional to the gelation time. Also, the absolute magnitude of increase in storage moduli due to the crosslinking reaction increases with initial gelation time. This is expected if more entanglements are being formed during the aging process. As initial gelation time increases, more entanglements are formed that can be ultimately crosslinked, see Table 2.1. However, after irradiation and equilibration, all the gel samples exhibit an average 2.4 fold increase in storage modulus irrespective of gelation time. This suggests that the efficiency of photocrosslinking remains constant irrespective of the number of entanglement sites available to be chemically crosslinked. Importantly, once the entanglements are covalently locked into their respective positions, the reorganization of fibrils is inhibited. This is evident in Figure 2.28. After photolysis, the value of  $G'$  remains constant indicating that the “aging” process has been inhibited. Overall, this suggests that the “aging” process observed prior to photolysis is at least, partly due to the reorganization of fibrils leading to more entanglements.

#### **2.3.2.7 Peptide Concentration Dependent Mechanical Rigidity of Hydrogels**

Previous studies have shown that varying the peptide concentration can modulate the mechanical properties of self-assembled  $\beta$ -hairpin peptide hydrogels. Higher peptide concentrations exhibit faster kinetics of folding and self-assembly leading to formation of more rigid hydrogels. Figure 2.29 shows peptide concentration dependent gelation kinetics of MKA hydrogels at pH 7.4 and 37 °C. After 3 hrs of

gelation time, the resultant gels were then photoirradiated to enhance the mechanical rigidity of the hydrogels. The results are presented in Table 2.2.

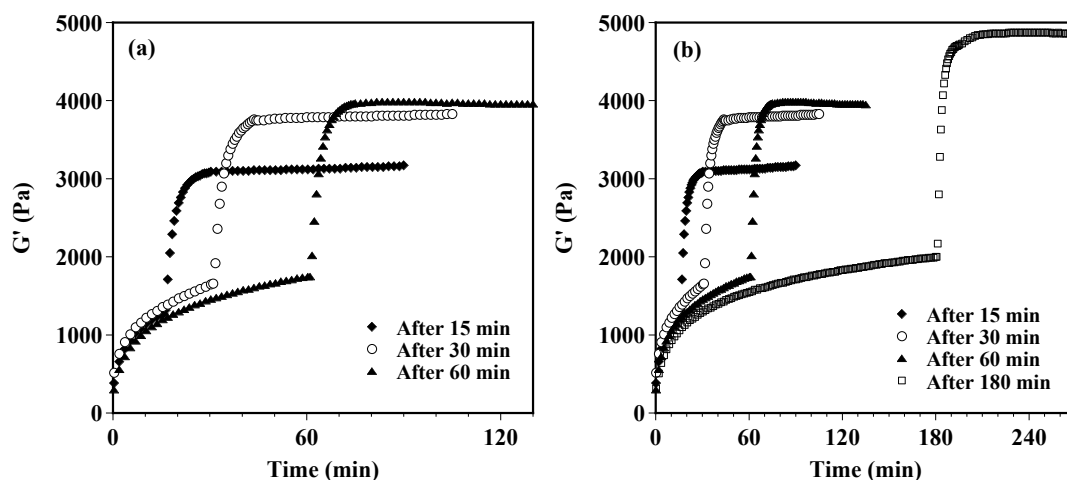


**Figure 2.28 Dynamic time sweep experiments of 1 wt% MKA at pH 7.4 and 37 °C. (a) Time dependent gelation and subsequent polymerization data (shown separately for clarity) (b) Time dependent gelation and subsequent polymerization (all data sets).**

<b>Gelation Time (min)</b>	<b>15</b>	<b>30</b>	<b>60</b>	<b>180</b>
<b><math>G'</math> (Pa)</b>	1200 $\pm$ 100	1575 $\pm$ 100	1770 $\pm$ 50	2000 $\pm$ 100
<b><math>G'</math> after <math>h\nu</math> (Pa)</b>	3200 $\pm$ 50	3700 $\pm$ 150	4000 $\pm$ 150	4800 $\pm$ 100
<b>Increase in <math>G'</math> (Pa)</b>	2000	2125	2230	2800
<b>Fold Increase</b>	2.6	2.35	2.26	2.4

**Table 2.1 Dynamic time sweep experiment data of 1 wt% MKA hydrogels showing physical gelation time dependent increase in storage modulus upon photopolymerization**

The results show that the rigidity of MKA hydrogels increased with an increase in peptide concentration. In addition, upon polymerization, the gel samples exhibit an

average of 2.5 fold increase in storage modulus. Also, the magnitude of increase in storage modulus increased with peptide concentration. This study demonstrates that varying the peptide concentration employed to fabricate the hydrogel can further modulate the rigidity of the photocrosslinked MKA hydrogels.

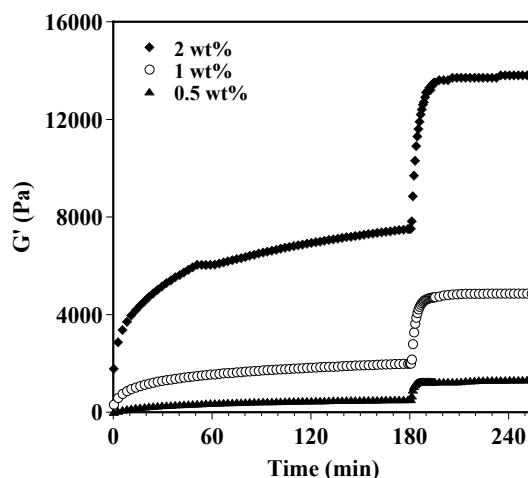


**Figure 2.29 Peptide concentration dependent mechanical properties of MKA hydrogels before and after photopolymerization**

**Table 2.2 Concentration dependent mechanical rigidity of MKA hydrogels before and after photopolymerization at pH 7.4 and 37 °C**

<b>MKA Concentration</b>	<b>0.5 wt%</b>	<b>1 wt%</b>	<b>2 wt%</b>
<b>G' (Pa)</b>	520 ± 30	2000 ± 100	7175 ± 1050
<b>G' after <math>h\nu</math> (Pa)</b>	1350 ± 175	4800 ± 100	13200 ± 1750
<b>Increase in G' (Pa)</b>	830	2800	6025
<b>Fold Increase</b>	2.6	2.4	1.85

### 2.3.2.8 Conclusions

Our strategy to fabricate hydrogels involves triggered folding and subsequently self-assembly of  $\beta$ -hairpin peptides. Results from this study demonstrate that additional functionality can be introduced into  $\beta$ -hairpins at selective positions or sites to direct the mode of crosslinking and modulate the ultimate material properties. We achieved this by incorporating an N $\epsilon$ -acryloyl-L-lysine at position 19 in the MAX1  $\beta$ -hairpin such that following self-assembly the fibrils can be covalently crosslinked interfibrillarly via photopolymerization. Upon irradiation, interfibrillar crosslinking results in  $\sim 2.5$  fold increase in mechanical rigidity. In addition, the physically crosslinked hydrogels exhibit shear recovery, which allows the delivery of pre-formed gel to the target in a controlled fashion prior to irradiation. The injectable hydrogel can be irradiated after recovery without significantly affecting the increase in rigidity ( $\sim 2.5$  fold). However, if the sheared hydrogel is irradiated during the recovery, the enhancement in storage modulus is lower ( $\sim 1.7$  fold) due to insufficient number of entanglements. This suggests that the shearing process probably disrupts the entanglements, which reform during the recovery period to regain the original rigidity. This demonstrates that structure based design of  $\beta$ -hairpins can be employed to create functional materials with predictable material properties for biomedical applications. In addition, more structural information about the physically crosslinked hydrogel network can be obtained through such designs.

### 2.3.3 Experimental Section

**Materials.** Rink amide resin was purchased from Polymer Laboratories. Trifluoroacetic acid (TFA), Triisopropylsilane (TIPS), Diisopropylethylamine (DIEA) and Acryloyl chloride were purchased from Acros. Appropriately side-chain-protected Fmoc-amino acids were obtained from Novabiochem. 1-H-Benzotriazolium-1-[bis(Dimethylamino)Methylene]-5-Chloro-Hexafluorophosphate-(1-), 3-Oxide (HCTU) was purchased from Peptide International. Bis-Tris Propane (BTP) was purchased from Sigma. Photoinitiator Irgacure 2959 (I2959) was a generous gift from Ciba Specialty Chemicals and used as received. MilliQ (Millipore) with a resistivity of 18.2 M $\Omega$ .cm was used for all experiments and is referred to as “water” in this paper. Fmoc-Lys(DE)-OH<sup>43</sup> and Fmoc-N $\epsilon$ -acryloyl-L-lysine<sup>56</sup> were synthesized according to published procedures.

**Peptide Synthesis and Purification.** Peptides were prepared on Rink amide resin via automated Fmoc peptide synthesis employing an ABI 433A peptide synthesizer and HCTU activation.<sup>57</sup> The resulting dry resin-bound peptides were cleaved and side-chain-deprotected using a cocktail of TFA/TIPS (90:10) for 2 hrs under nitrogen. The resin was filtered and peptide precipitated from the filtrate using cold diethyl ether. Crude peptide was subsequently purified by Reverse Phase-HPLC (Waters 600 series) using a semi-preparative Vydac C18 peptide/protein column. HPLC solvents consisted of solvent A (0.1% TFA in water) and solvent B (90% acetonitrile, 10% water, and

0.1% TFA). All the peptides were purified at 40 °C employing isocratic conditions of 0 % B for 2 minutes followed by a linear gradient of 0 to 25% B in 17 minutes and an additional linear gradient of 10 to 100% B in 150 minutes. Using this gradient, pure M2K, MLD, MKA and MKA2 eluted at 28, 35, 34 and 34 minutes respectively. MS (ESI), M2K:  $m/z$ : 1244 [(M+2H)<sup>2+</sup>], calcd 1244.5, MLD:  $m/z$ : 1337.7 [(M+2H)<sup>2+</sup>] calcd 1337.2, MKA:  $m/z$ : 1142.4 [(M+2H)<sup>2+</sup>] calcd 1142.7, MKA2:  $m/z$ : 1142.6 [(M+2H)<sup>2+</sup>] calcd 1142.7 The resulting peptide solutions were frozen with liquid nitrogen and lyophilized to afford pure peptides. The purity of the peptide was established using Electrospray ionization mass spectrometry and analytical HPLC.

**Circular Dichroism Studies.** CD spectra were collected on a Jasco model J-810 spectropolarimeter. A 1 mM peptide stock was prepared by dissolving the appropriate amount of purified peptide in water. UV-Vis spectroscopy was employed to determine the concentration of the peptide stock [M2K ( $\epsilon_{220} = 20350 \text{ cm}^{-1} \text{ M}^{-1}$ ), MLD ( $\epsilon_{258} = 24080 \text{ cm}^{-1} \text{ M}^{-1}$ )<sup>58</sup>, MKA and MKA2 ( $\epsilon_{220} = 15750 \text{ cm}^{-1} \text{ M}^{-1}$ )]. This 1 mM peptide stock was diluted to afford a 300  $\mu\text{M}$  peptide final stock solution, which was used to prepare all of the CD samples. For each CD sample, 300  $\mu\text{M}$  stock of the peptide was mixed with an equal volume of pH 7.4 buffer (100 mM BTP, 300 mM NaCl to afford a final concentration of 150  $\mu\text{M}$  peptide solution at pH 7.4 buffer (50 mM BTP, 150 mM NaCl). Mean residue ellipticity  $[\theta]$  was calculated from the equation  $[\theta] = (\theta_{\text{obs}}/10lc)/r$ , where  $\theta_{\text{obs}}$  is the measured ellipticity in millidegrees,  $l$  is the length of the cell (centimeters),  $c$  is the molar concentration, and  $r$  is the number of residues.

Four separate CD experiments were performed on individual samples of the peptides. (i) Mean residual ellipticity  $[\theta]$  at 218 nm was measured as a function of temperature using a step size of 5 °C and an equilibration time of 10 minutes. (ii) A wavelength spectrum from 260 to 210 nm was obtained in a 0.1 cm path length quartz cell at 5 °C and 37 °C to assess the secondary structure of the peptides. (iii) Wavelength scans of 0.1 wt% MLD at pH 7.4 (50 mM BTP, 150 mM NaCl) and 37 °C were first recorded in a 0.1 cm pathlength quartz cell to ensure complete  $\beta$ -sheet transformation. Thereafter, the self-assembled peptide sample was irradiated (365 nm) and the wavelength spectra were recorded at the indicated times to monitor the progress of the photoreaction. (iv) 1 wt% peptide was allowed to self-assemble at pH 7.4 (50 mM BTP, 150 mM NaCl, 37 °C, 0.02 wt% Irgacure 2959) in a 0.01 mm pathlength cell. Thereafter, wavelength scans of the peptide before and after 5 min of irradiation were recorded. No changes in wavelength spectrum were observed at longer irradiation times. A UV lamp (spectroline Model xx-15A, 365 nm, 6 mW/cm<sup>2</sup>) was placed 4 cm above the sample during the irradiation process.

**UV-vis Spectroscopy.** Absorption spectra were collected on a HP 8453 UV-visible spectrophotometer. MLD (0.1 wt%) samples prepared for CD analysis [part (iii)] were used for this study. After recording the wavelength spectra on CD, a UV absorption spectrum was recorded for each indicated time point.

**Oscillatory Shear Rheology.** Rheological measurements were performed on Anton Paar-Physica MCR 500 rheometer with a quartz glass plate fixture (Anton Paar, Advanced UV system, UV cell) to allow UV irradiation. A 25 mm parallel plate geometry and 0.5 mm gap distance was employed for all experiments. Omnicure (EXFO) series 1000 spot curing system (Model S1000, 100W Hg Arc, Wavelength 320-500nm) was used as a UV source. The light power (10% laser intensity) at the sample position was  $\sim 16 \text{ mW/cm}^2$  as measured by a radiometer (Apprise Technologies, Chromaline, UV Minder with peak response at 370 nm). The distance between the UV source and the sample was 4 cm.

The peptide was first dissolved in a solution of Irgacure 2959 (0.05 wt%) to obtain a concentration that is twice the final peptide concentration in the gel. Then, an equal amount of pH 7.4 buffer (100mM BTP, 300mM NaCl) was added to the peptide stock solution, mixed gently and immediately loaded onto the rheometer plate equilibrated to 37 °C. After the sample was loaded and the parallel plate lowered, standard low-viscosity mineral oil was used to insulate the sides of the parallel plate in order to prevent evaporation. Control experiments have shown that the mineral oil had no effect on the rheological measurements. Gelation was observed by monitoring the evolution of the storage modulus ( $G'$ ) with time, in a dynamic time sweep experiment performed at an angular frequency of 6 rad/s and strain of 0.2 %. Storage moduli values ( $G'$ ) obtained are reported with standard deviation values in parentheses obtained from experiments performed in triplicate. Frequency sweep experiments were performed by varying the frequency from 0.1-100 rad/s at a constant strain of 0.2

%. The frequency sweep experiment verified that all time sweep experiments were performed within the linear viscoelastic regime.

Shear-thin and recovery experiments were performed by first allowing gels to form for 3 hours in a dynamic time sweep experiment (6 rad/s and 0.2% strain) and subsequently subjecting the gel to a shear-thinning and recovery cycle. The shear-thinning and recovery cycle consisted of application of 1000 % strain at 6 rad/s for 30 sec followed by a 2 hour recovery period at a constant 0.2 % strain at 6 rad/s angular frequency. A 1000% strain for 30 sec was employed to ensure complete disruption of the hydrogel network.

Photopolymerization experiments were performed by irradiating the peptide hydrogel for 15 min ( $\sim 16 \text{ mW/cm}^2$ , 365 nm) at specified times depending upon the experiment. Control experiments were performed with standard viscosity oil (S600) to observe the change in viscosity at variable UV light intensities with respect to increase in temperature. The temperature was simultaneously recorded using a thermocouple in contact with the quartz UV plate during irradiation of the S600 oil.

## References:

1. Lee, K. Y.; Mooney, D. J., Hydrogels for tissue engineering. *Chemical Reviews* **2001**, 101, (7), 1869-1879.
2. Rughani, R. V.; Schneider, J. P., Molecular Design of b-Hairpin Peptides for Material Construction. *MRS Bulletin* **2008**, 33, (5), 530-535.
3. Mart, R. J.; Osborne, R. D.; Stevens, M. M.; Ulijn, R. V., Peptide-based stimuli-responsive biomaterials. *Soft Matter* **2006**, 2, (10), 822-835.
4. Xu, C. Y.; Kopecek, J., Self-assembling hydrogels. *Polymer Bulletin* **2007**, 58, (1), 53-63.
5. Peppas, N. A.; Hilt, J. Z.; Khademhosseini, A.; Langer, R., Hydrogels in biology and medicine: from molecular principles to bionanotechnology. *Advanced Materials (Weinheim, Germany)* **2006**, 18, (11), 1345-1360.
6. Fabrizio Gelain, A. H. S. Z., Designer Self-Assembling Peptide Scaffolds for 3-D Tissue Cell Cultures and Regenerative Medicine. *Macromolecular Bioscience* **2007**, 7, (5), 544-551.
7. Chow, D.; Nunalee, M. L.; Lim, D. W.; Simnick, A. J.; Chilkoti, A., Peptide-based biopolymers in biomedicine and biotechnology. *Materials Science and Engineering: R: Reports* **2008**, 62, (4), 125-155.
8. Benjamin Le Droumaguet, K. V., Click Chemistry: A Powerful Tool to Create Polymer-Based Macromolecular Chimeras. *Macromolecular Rapid Communications* **2008**, 29, (12-13), 1073-1089.
9. Van Tomme, S. R.; Storm, G.; Hennink, W. E., In situ gelling hydrogels for pharmaceutical and biomedical applications. *International Journal of Pharmaceutics* **2008**, 355, (1-2), 1-18.
10. Bruns, H.; Kneser, U.; Holzhuter, S.; Roth, B.; Kluth, J.; Kaufmann, P. M.; Kluth, D.; Fiegel, H. C., Injectable Liver: A Novel Approach Using Fibrin Gel as a Matrix for Culture and Intrahepatic Transplantation of Hepatocytes. *Tissue Engineering* **2005**, 11, (11-12), 1718-1726.
11. Hammond, J. S.; Beckingham, I. J.; Shakesheff, K. M., Scaffolds for liver tissue engineering. *Expert Review of Medical Devices* **2006**, 3, (1), 21-27.
12. Freed, L. E.; Marquis, J. C.; Nohria, A.; Emmanuel, J.; Mikos, A. G.; Langer, R., Neocartilage formation in vitro and in vivo using cells cultured on synthetic biodegradable polymers. *Journal of Biomedical Materials Research* **1993**, 27, (1), 11-23.
13. Bryant, S. J.; Durand, K. L.; Anseth, K. S., Manipulations in hydrogel chemistry control photoencapsulated chondrocyte behavior and their extracellular matrix production. *Journal of Biomedical Materials Research Part A* **2003**, 67A, (4), 1430-1436.
14. Holland, T. A.; Bodde, E. W. H.; Baggett, L. S.; Tabata, Y.; Mikos, A. G.; Jansen, J. A., Osteochondral repair in the rabbit model utilizing bilayered, degradable oligo(poly(ethylene glycol) fumarate) hydrogel scaffolds. *Journal of Biomedical Materials Research Part A* **2005**, 75A, (1), 156-167.

15. Simmons, C. A.; Alsberg, E.; Hsiong, S.; Kim, W. J.; Mooney, D. J., Dual growth factor delivery and controlled scaffold degradation enhance in vivo bone formation by transplanted bone marrow stromal cells. *Bone* **2004**, 35, (2), 562-569.
16. Yu, L.; Ding, J., Injectable hydrogels as unique biomedical materials. *Chemical Society Reviews* **2008**, 37, (8), 1473-1481.
17. Bos, G. W.; Jacobs, J. J. L.; Koten, J. W.; Van Tomme, S.; Veldhuis, T.; van Nostrum, C. F.; Den Otter, W.; Hennink, W. E., In situ crosslinked biodegradable hydrogels loaded with IL-2 are effective tools for local IL-2 therapy. *European Journal of Pharmaceutical Sciences* **2004**, 21, (4), 561-567.
18. Balakrishnan, B.; Mohanty, M.; Umashankar, P. R.; Jayakrishnan, A., Evaluation of an in situ forming hydrogel wound dressing based on oxidized alginate and gelatin. *Biomaterials* **2005**, 26, (32), 6335-6342.
19. Grinstaff, M. W., Designing hydrogel adhesives for corneal wound repair. *Biomaterials* **2007**, 28, (35), 5205-5214.
20. Sontjens, S. H. M.; Nettles, D. L.; Carnahan, M. A.; Setton, L. A.; Grinstaff, M. W., Biodendrimer-Based Hydrogel Scaffolds for Cartilage Tissue Repair. *Biomacromolecules* **2006**, 7, (1), 310-316.
21. Ifkovits, J. L.; Burdick, J. A., Review: Photopolymerizable and Degradable Biomaterials for Tissue Engineering Applications. *Tissue Engineering* **2007**, 13, (10), 2369-2385.
22. van de Wetering, P.; Metters, A. T.; Schoenmakers, R. G.; Hubbell, J. A., Poly(ethylene glycol) hydrogels formed by conjugate addition with controllable swelling, degradation, and release of pharmaceutically active proteins. *Journal of Controlled Release* **2005**, 102, (3), 619-627.
23. Rydholm, A. E.; Bowman, C. N.; Anseth, K. S., Degradable thiol-acrylate photopolymers: polymerization and degradation behavior of an in situ forming biomaterial. *Biomaterials* **2005**, 26, (22), 4495-4506.
24. Weiner, A. A.; Bock, E. A.; Gipson, M. E.; Shastri, V. P., Photocrosslinked anhydride systems for long-term protein release. *Biomaterials* **2008**, 29, (15), 2400-2407.
25. Quick, D. J.; Anseth, K. S., DNA delivery from photocrosslinked PEG hydrogels: encapsulation efficiency, release profiles, and DNA quality. *Journal of Controlled Release* **2004**, 96, (2), 341-351.
26. Ward, J. H.; Peppas, N. A., Preparation of controlled release systems by free-radical UV polymerizations in the presence of a drug. *Journal of Controlled Release* **2001**, 71, (2), 183-192.
27. An, Y.; Hubbell, J. A., Intraarterial protein delivery via intinally-adherent bilayer hydrogels. *Journal of Controlled Release* **2000**, 64, (1-3), 205-215.
28. Quaglia, F., Bioinspired tissue engineering: The great promise of protein delivery technologies. *International Journal of Pharmaceutics* **2008**, 364, (2), 281-297.

29. Leach, J. B.; Bivens, K. A.; Collins, C. N.; Schmidt, C. E., Development of photocrosslinkable hyaluronic acid-polyethylene glycol-peptide composite hydrogels for soft tissue engineering. *Journal of Biomedical Materials Research Part A* **2004**, 70A, (1), 74-82.
30. West, J. Å.; Hubbell, J. Å., Separation of the arterial wall from blood contact using hydrogel barriers reduces intimal thickening after balloon injury in the rat: The roles of medial and luminal factors in arterial healing. *Proceedings of the National Academy of Sciences of the United States of America* **1996**, 93, (23), 13188-13193.
31. Baroli, B., Photopolymerization of biomaterials: issues and potentialities in drug delivery, tissue engineering, and cell encapsulation applications. *Journal of Chemical Technology & Biotechnology* **2006**, 81, 491-499.
32. Nguyen, K. T.; West, J. L., Photopolymerizable hydrogels for tissue engineering applications. *Biomaterials* **2002**, 23, (22), 4307-4314.
33. Venkatesh, S.; Sizemore, S. P.; Byrne, M. E., Biomimetic hydrogels for enhanced loading and extended release of ocular therapeutics. *Biomaterials* **2007**, 28, (4), 717-724.
34. Winterton, L. C.; Lally, J. M.; Sentell, K. B.; Chapoy, L. L., The elution of poly (vinyl alcohol) from a contact lens: The realization of a time release moisturizing agent/artificial tear. *Journal of Biomedical Materials Research Part B: Applied Biomaterials* **2007**, 80B, (2), 424-432.
35. Zhang, S. G., Fabrication of novel biomaterials through molecular self-assembly. *Nature Biotechnology* **2003**, 21, (10), 1171-1178.
36. Ramachandran, S.; Trewhella, J.; Tseng, Y.; Yu, Y. B., Coassembling peptide-based biomaterials: Effects of pairing equal and unequal chain length oligopeptides. *Chemistry of Materials* **2006**, 18, (26), 6157-6162.
37. Lamm, M. S.; Rajagopal, K.; Schneider, J. P.; Pochan, D. J., Laminated morphology of nontwisting beta-sheet fibrils constructed via peptide self-assembly. *Journal of the American Chemical Society* **2005**, 127, (47), 16692-16700.
38. Yang, Z.; Xu, B., Supramolecular hydrogels based on biofunctional nanofibers of self-assembled small molecules. *Journal of Materials Chemistry* **2007**, 17, (23), 2385-2393.
39. Hartgerink, J. D.; Beniash, E.; Stupp, S. I., Supramolecular Chemistry And Self-assembly Special Feature: Peptide-amphiphile nanofibers: A versatile scaffold for the preparation of self-assembling materials. *Proceedings of the National Academy of Sciences* **2002**, 99, (8), 5133-5138.
40. Collier, J. H.; Hu, B. H.; Ruberti, J. W.; Zhang, J.; Shum, P.; Thompson, D. H.; Messersmith, P. B., Thermally and photochemically triggered self-assembly of peptide hydrogels. *Journal of the American Chemical Society* **2001**, 123, (38), 9463-9464.
41. Haines-Butterick, L.; Rajagopal, K.; Branco, M.; Salick, D.; Rughani, R.; Pilarz, M.; Lamm, M. S.; Pochan, D. J.; Schneider, J. P., Controlling hydrogelation

- kinetics by peptide design for three-dimensional encapsulation and injectable delivery of cells. *Proc. Natl. Acad. Sci. U. S. A.* **2007**, 104, (19), 7791-7796.
42. Bryant, S. J.; Nuttelman, C. R.; Anseth, K. S., Cytocompatibility of UV and visible light photoinitiating systems on cultured NIH/3T3 fibroblasts in vitro. *Journal of Biomaterials Science, Polymer Edition* **2000**, 11, 439-457.
  43. Mori, T.; Yasutake, S.; Inoue, H.; Minagawa, K.; Tanaka, M.; Niidome, T.; Katayama, Y., "Threading" of beta-Sheet Peptides via Radical Polymerization. *Biomacromolecules* **2007**, 8, (2), 318-321.
  44. Pauling, L.; Corey, R. B., Configurations of Polypeptide Chains with Favored Orientations around Single Bonds - 2 New Pleated Sheets. *Proceedings of the National Academy of Sciences of the United States of America* **1951**, 37, (11), 729-740.
  45. Mori, T.; Shimoyama, K.; Fukawa, Y.; Minagawa, K.; Tanaka, M., Parallel & beta;-sheet as a Novel Template for Polymerization of Diacetylene. *Chemistry Letters* **2005**, 34, (1), 116-117.
  46. Matsumoto, A.; Sada, K.; Tashiro, K.; Miyata, M.; Tsubouchi, T.; Tanaka, T.; Odani, T.; Nagahama, S.; Tanaka, T.; Inoue, K.; Saragai, S.; Nakamoto, S., Reaction Principles and Crystal Structure Design for the Topochemical Polymerization of 1,3-Dienes. *Angewandte Chemie International Edition* **2002**, 41, (14), 2502-2505.
  47. Matsumoto, A., Reactions of 1,3-Diene Compounds in the Crystalline State. In *Organic Solid State Reactions*, 2005; pp 263-305.
  48. Tieke, B., Solid state polymerization of butadienes. Polymerization of long chain derivatives of sorbic and muconic acid. *Colloid & Polymer Science* **1985**, 263, (12), 965-972.
  49. Sheradsky, T.; Silcoff, E., Synthesis of (2R,5R)-2-Amino-5-Hydroxyhexanoic Acid by Intramolecular Cycloaddition. *Molecules* **1998**, 3, (3), 80-87.
  50. Caplan, M. R.; Moore, P. N.; Zhang, S.; Kamm, R. D.; Lauffenburger, D. A., Self-Assembly of a b-Sheet Protein Governed by Relief of Electrostatic Repulsion Relative to van der Waals Attraction. *Biomacromolecules* **2000**, 1, (4), 627-631.
  51. Jager, M.; Dendle, M.; Fuller, A. A.; Kelly, J. W., A cross-strand Trp-Trp pair stabilizes the hPin1 WW domain at the expense of function. *Protein Science* **2007**, 16, (10), 2306-2313.
  52. Cochran, A. G.; Skelton, N. J.; Starovasnik, M. A., Tryptophan zippers: Stable, monomeric b-hairpins. *Proceedings of the National Academy of Sciences of the United States of America* **2001**, 98, (10), 5578-5583.
  53. Prins, L. J.; Thalacker, C.; Wörthner, F.; Timmerman, P.; Reinhoudt, D. N., Chiral exciton coupling of merocyanine dyes within a well defined hydrogen-bonded assembly. *Proceedings of the National Academy of Sciences of the United States of America* **2001**, 98, (18), 10042-10045.
  54. Yagai, S.; Higashi, M.; Karatsu, T.; Kitamura, A., Tunable interchromophore electronic interaction of a merocyanine dye in hydrogen-bonded supramolecular

- assemblies scaffolded by bismelamine receptors. *Chemical Communications* **2006**, (14), 1500-1502.
55. Ozbas, B.; Kretsinger, J.; Rajagopal, K.; Schneider, J. P.; Pochan, D. J., Salt-triggered peptide folding and consequent self-assembly into hydrogels with tunable modulus. *Macromolecules* **2004**, 37, (19), 7331-7337.
  56. Gerardo, B.; Mirit, C.-O.; Daniel, R., Fast and versatile microwave-assisted intramolecular Heck reaction in peptide macrocyclization using microwave energy. *Peptide Science* **2006**, 84, (3), 274-282.
  57. Nagarkar, R. P.; Schneider, J. P., Synthesis and Primary Characterization of Self-Assembled Peptide-based hydrogels. In *Nanostructure Design, Methods and Protocols*, Gazit, E.; Nussinov, R., Eds. Humana Press: 2008; pp 61-77.
  58. de Villiers, M. M.; Bergh, J. J., Comparing HPLC and UV Spectrophotometric Analysis Methods for Determining the Stability of Sorbic Acid in Nonionic Creams Containing Lactic Acid. *Drug Development and Industrial Pharmacy* **2000**, 26, (5), 539 - 547.

## Chapter 3

### FABRICATING MECHANICALLY ROBUST PEPTIDE-POLYMER HYDROGELS VIA PHOTOPOLYMERIZATION

#### 3.0 Introduction

Various strategies are currently being pursued towards the construction and development of robust three-dimensional matrices for tissue engineering applications. Hydrogels are promising candidates for this purpose due to their biocompatibility, mechanical rigidity and highly hydrated three-dimensional structure. A variety of natural as well as synthetic polymers have been developed as precursors, which can undergo physical or chemical crosslinking reactions to form mechanically rigid hydrogels. In addition, peptide sequences have also been designed to assemble into a physically crosslinked fibrillar networks, leading to hydrogelation in response to changes in environmental cues.<sup>1</sup> Although several promising strategies for fabricating hydrogels with diverse material properties have been discovered, the challenge to construct scaffolds that mimic the mechanical properties of natural tissues still exists.

The extracellular matrix (ECM) in tissues, is a complex hydrated structure primarily composed of a physically and chemically crosslinked network of different biopolymers that provide a wide range of biochemical cues and mechanical support for its function. Since the organization of ECM components is unique to each tissue

type, it is crucial that the engineered substitute mimics the structural and functional properties of the natural tissue.<sup>2</sup> A promising approach to construct ECM mimics is by the preparation of hybrid hydrogels. One way to create hybrid gels includes copolymerization of two different network-forming components where both the networks are covalently crosslinked with each other. Another approach includes fabrication of interpenetrating networks where two independent networks are physically interlocked with each other but not chemically crosslinked. Both of these approaches can be employed to fabricate mechanically rigid hydrogels. This chapter discusses the design and characterization of self-assembled  $\beta$ -hairpin peptides for the fabrication of both hybrid peptide-polymer networks and interpenetrating polymer networks with enhanced mechanical properties for use as potential artificial tissues.

### **3.1 Construction of Mechanically Rigid Hydrogels via the Formation of Crosslinked Network of Peptide and Divinylbenzyl PEG**

Schneider and Pochan labs have developed a family of self-assembling  $\beta$ -hairpin peptides that fold and self-assemble in response to external stimuli to form self-supporting hydrogels. These highly hydrated hydrogels are not only mechanically rigid but are also non-cytotoxic to mesenchymal stem cells. In addition, the physically crosslinked hydrogels exhibit shear recovery properties and therefore have the potential to be used as injectable biomaterials. All the above characteristics make the self-assembled hydrogels attractive candidates for tissue engineering applications.

Although the resultant hydrogels are mechanically rigid, the physically crosslinked nature of these gels renders them soft and thus allow them to yield at lower strains. This is demonstrated using oscillatory rheology experiments performed with 1 wt% MKA hydrogels. MKA is a photopolymerizable peptide with an N $\epsilon$ -acryloyl-L-lysine at position 19. This allows interfibrillar polymerization of the fibrils following self-assembly to enhance the mechanical properties of the hydrogel.

Figure 3.1(a) shows a dynamic frequency sweep measurement of 1 wt% MKA hydrogels at pH 7.4 (50 mM BTP, 150 mM NaCl) and 37 °C following UV irradiation. The data shows that the storage modulus ( $G'$ ) of MKA hydrogels is insensitive to a range of frequencies, indicating the presence of permanent crosslinks. Figure 3.1(b) shows a dynamic strain sweep measurement of the same MKA hydrogel following the dynamic frequency sweep. In this experiment, the storage and loss modulus are measured as function of increasing strain. The data shows that the storage modulus is linear until  $\sim$  4-5 % strain, but decreases significantly at higher strain values.

We were interested in developing a composite hydrogel with MKA that can be syringe delivered and subsequently polymerized to enhance the mechanical properties. In particular, the primary interest was to fabricate a hydrogel that can withstand higher strain than the single network  $\beta$ -hairpin peptide hydrogels.

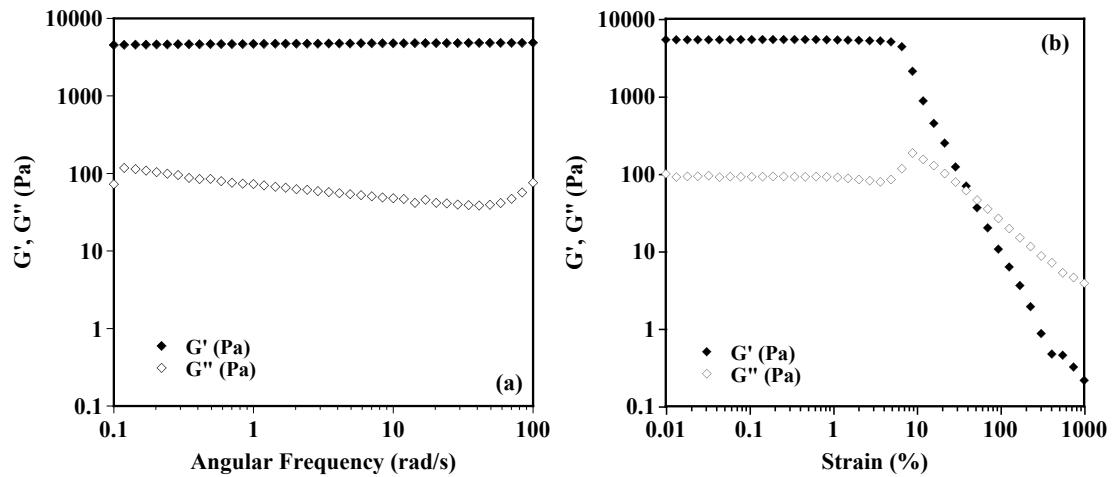


**Figure 3.1 (a) Dynamic frequency sweep and (b) Dynamic strain sweep measurements of photocrosslinked 1 wt% MKA hydrogels at pH 7.4 and 37 °C**

### 3.1.1 Design and Fabrication Strategy of Peptide-Polymer Hydrogels

Bifunctional PEG polymers have been extensively used to fabricate a variety of hydrogel materials via photopolymerization. Here, the material properties of the hydrogels can be manipulated depending upon the molecular weight of the photoreactive polymer. For example, short bifunctional PEG (~ 500-700 Mw) forms mechanically rigid yet brittle hydrogels due to higher crosslink density of the hydrogel network. However, longer bifunctional PEG (~8000-10000 Mw) forms relatively less rigid but more malleable hydrogels at the same polymer concentration due to lower crosslink density of the hydrogel network. Knowing this, we chose to construct a hybrid hydrogel by incorporating a polymerizable bifunctional PEG (Mw 10000) into the MKA hydrogel, which can be subsequently photocrosslinked. Photopolymerizing

the hybrid hydrogel will lead to formation of (1) interfibrillar crosslinking of MKA fibrils, (2) crosslinking between the MKA fibrils & bifunctional PEG and (3) possible intermolecular crosslinking between the bifunctional PEG, Figure 3.2. Collectively, these events should not only provide a more malleable hydrogel due to the covalently crosslinked high molecular weight PEG but also enhance the mechanical properties due to formation of more covalent crosslinks.

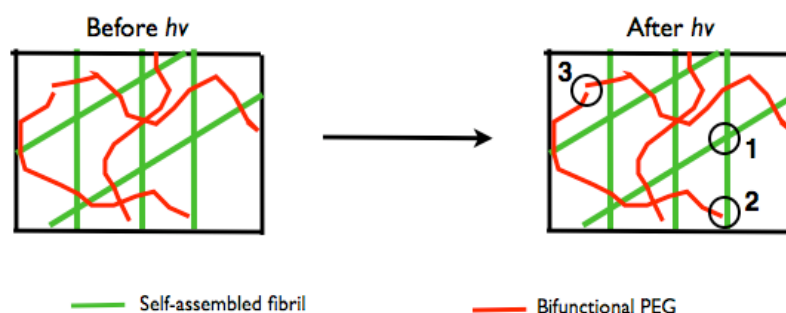


**Figure 3.2 Schematic depicting covalent crosslinks formed in the hybrid hydrogel upon photopolymerization**

### 3.1.2 Synthesis of Divinylbenzyl PEG (PEGDVB)

The bifunctional PEG was synthesized by modifying a published protocol.<sup>3,4</sup> As shown in Figure 3.3, PEG is reacted with 4-vinylbenzyl chloride under basic conditions in toluene at 60 °C for 3 days to form dibenzylvinyl-PEG (PEGDVB) in 60% yield. The extent of functionalization was calculated to be 92-100% using a previously published <sup>1</sup>H-NMR method.<sup>5</sup>

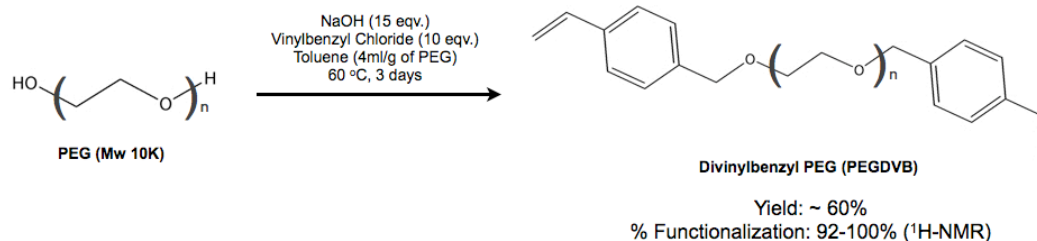


**Figure 3.3 Synthesis of Divinylbenzyl-PEG (PEGDVB)**

### 3.1.3 Mechanical Properties of Single Network Hydrogels

For this study, hydrogels containing 1 wt% MKA and 2.5 wt%, 5 wt% or 10 wt% PEGDVB in pH 7.4 buffer (50 mM BTP, 150 mM NaCl, 0.025 wt% Irgacure 2959) were employed. However, it is important to first analyze the mechanical properties of the single component networks before fabricating the hybrid hydrogels. Figure 3.4 shows the mechanical properties of single network hydrogels of 1wt% MKA and 10 wt% PEGDVB, each at pH 7.4 and 37 °C upon polymerization. Aqueous solution of 1 wt% MKA at pH 7.4 (50 mM BTP, 150 mM NaCl, 0.025wt% Irgacure 2959) is triggered to form a physically crosslinked hydrogel by increasing the temperature of the peptide solution to 37 °C. After 3 hrs of gelation, the hydrogel is irradiated for 15 min (365 nm, 16 mW/cm<sup>2</sup>) to form the covalent crosslinks and then allowed to equilibrate over time. MKA hydrogel was irradiated for 15 min only because no significant change in rigidity is observed after 10 minutes of irradiation. The 10 wt% PEGDVB at pH 7.4 (50 mM BTP, 150 mM NaCl, 0.025wt% Irgacure

2959) and 37 °C does not form a physical gel under these conditions and therefore was irradiated for 30 min after a time sweep of 10 min to form a covalently crosslinked hydrogel. A 30 min irradiation time is also used for polymerization of the hybrid hydrogels. The data shows that 1 wt% MKA achieves a storage modulus of  $4800 \pm 100$  Pa following photopolymerization whereas 10 wt% PEGDA achieves a storage modulus of  $2600 \pm 250$  Pa. Lower concentrations (2.5 and 5 wt%) of PEGDVB solutions did not form a hydrogel upon UV irradiation.

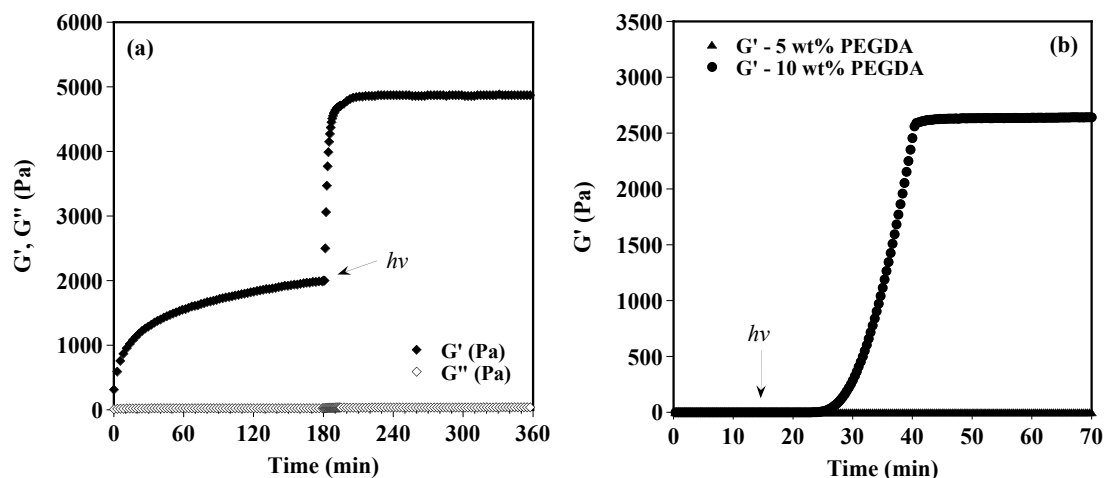


**Figure 3.4 Mechanical properties of photopolymerized 1 wt% MKA and 10 wt% PEGDVB hybrid hydrogels at pH 7.4 and 37 °C**

### 3.1.4 Shear Recovery and Polymerization of Pre-formed Hydrogels

Towards our goal, the utility of hybrid hydrogels as potential injectable scaffolds with controlled mechanical properties was demonstrated using oscillatory

dynamic time sweep experiments. For every experiment, an aqueous solution of MKA is mixed with an equal volume of PEGDVB in pH 7.4 buffer at room temperature. Thereafter, physical gelation of the MKA gel is triggered by loading the peptide-polymer solution at pH 7.4 (50 mM BTP, 150 mM NaCl, 0.025 wt% Irgacure 2959) onto the rheometer pre-equilibrated at 37 °C, Figure 3.5 [part (i)]. After 3 hours gelation time [part (ii)], a 1000% strain is applied for 30 sec to disrupt the hydrogel network as observed by instantaneous decrease in the storage modulus. Thereafter the strain is lowered to 0.2% [part (iii)], allowing the network to recover for 2 hrs. At the end of recovery period [part (iv)], the hydrogel is irradiated [365 nm, 16 mW/cm<sup>2</sup>] for 30 min to covalently crosslink the peptide-polymer networks, and allow enough time to achieve an equilibrium storage modulus, [part (v)].

For these experiments, hybrid hydrogels containing 1 wt% MKA and 2.5, 5 or 10 wt% PEGDVB were investigated. In all cases, the rigidity of the hydrogels at the end of first 3 hrs [part (ii)] was similar to the rigidity of 1 wt% MKA hydrogel alone. This suggests that PEGDVB does not grossly affect the gelation of MKA. In addition, all the samples exhibit about 90% recovery following removal of high strain [part (iv)]. Following irradiation, the hybrid hydrogels exhibit PEGDVB concentration dependent increase in storage modulus ranging from 9900 to 20300 Pa, Figure 3.5. The storage moduli values shown in Figure 3.5 were extracted at 6 rad/s from the dynamic frequency sweep measurements (Figure 3.6) performed after the dynamic time sweep. Collectively, the data from Figure 3.5 shows that the polymerized hybrid hydrogels exhibit a non-additive enhancement in the mechanical properties compared

to the covalently crosslinked single network hydrogels of MKA and PEGDVB. Here, the storage moduli of the crosslinked hybrid hydrogels are not only greater than the storage moduli of the individual hydrogel networks but also greater than the sum of the storage moduli of the individual networks.

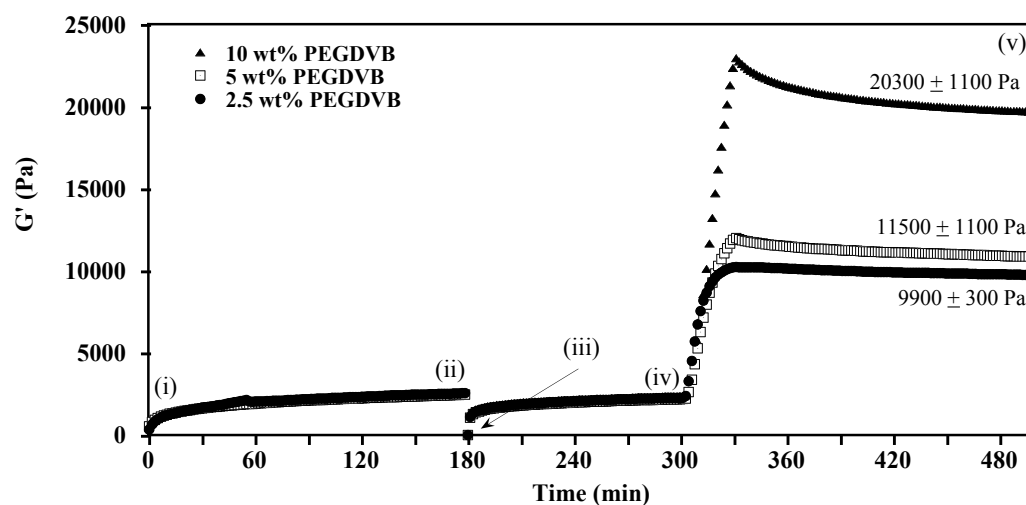


**Figure 3.5 Dynamic time sweep experiment showing shear-thinning, recovery and subsequent photopolymerization of pre-formed hydrogels of 1 wt% MKA with varying concentrations of PEGDVB.**

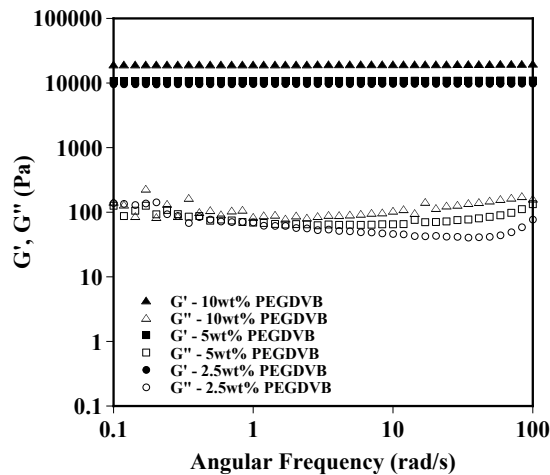


**Figure 3.6 Dynamic frequency sweep of 1 wt% MKA hydrogels with varying concentrations of PEGDVB after photopolymerization**

These results demonstrate that the hybrid hydrogels show promise as syringe deliverable scaffolds because they are shear-thinning and recover their mechanical properties. Importantly, the rigidity of the shear-thinned hydrogel can be further modulated via photopolymerization at the target site.

For practical applications, the 2 hr recovery period following the shear-thinning event be too long of a time to wait before photopolymerizing the system. To overcome this limitation, the shear recovery process was shortened by eliminating the 2 hr recovery period from the experiment. For this experiment [Figure 3.7], parts (i) and (ii) were performed exactly as described for Figure 3.5 with the 1000% strain applied for 300 sec. After cessation of shear [part (iii)], by reducing the strain back to 0.2 %, the recovering hydrogel is irradiated for 30 min instantaneously (365 nm, ~ 16

mW/cm<sup>2</sup>) and then allowed to achieve equilibration storage modulus. For this set of experiments, a high strain is applied for 300 sec as compared to 30 sec in previous data to simulate syringe delivery. Even though the shear-thinned hydrogel is not allowed to recover completely, polymerized hybrid hydrogels still achieved similar moduli values as obtained for the experiments shown in Figure 3.5. The storage moduli values were extracted from the dynamic frequency sweep measurements (Figure 3.8) at 6 rad/s, which is performed after the dynamic time sweep experiment.

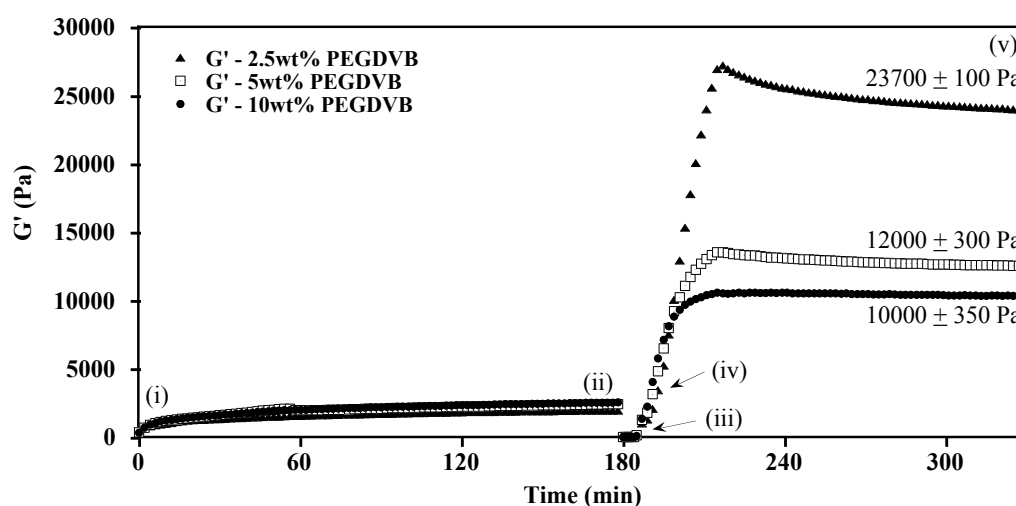


**Figure 3.7 Dynamic time sweep experiment showing shear-thinning followed by immediate photopolymerization of pre-formed hydrogels of 1 wt% MKA with varying concentrations of PEGDVB.**

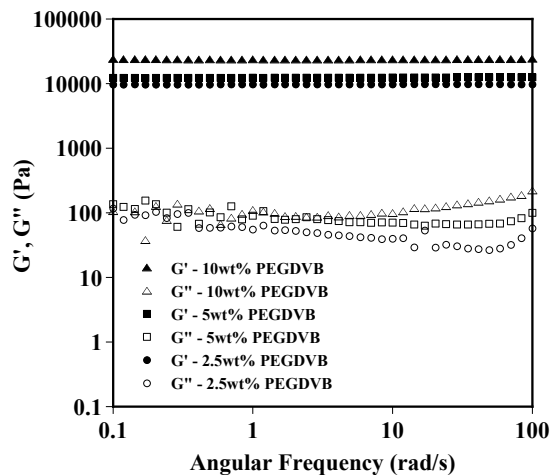


**Figure 3.8 Dynamic frequency sweep of 1 wt% MKA hydrogels with varying concentrations of PEGDVB after photopolymerization**

In Figures 3.5 and 3.7, the polymerized hybrid hydrogel with 10 wt% PEGDVB exhibits small decrease in storage modulus over time after 30 min of irradiation. This can possibly be due to the increase in local temperature as a result of the polymerization reaction since polymerization of vinyl groups is an exothermic reaction. This decrease in the modulus after irradiation is a PEGDVB concentration dependent effect. For example, polymerized hybrid hydrogel containing 2.5 wt% PEGDVB achieves an apparent equilibrium modulus with little decrease following irradiation. Thus, higher concentration of PEGDVB produces more heat and this effect is exaggerated. Figure 3.9 shows that the hybrid hydrogel irradiated for 60 min achieves an apparent equilibrium storage modulus value of  $37000 \pm 1200$  Pa. This

data suggests that after 30 min, the reaction is incomplete. However, this irradiation time can be varied to tune the final material rigidity.

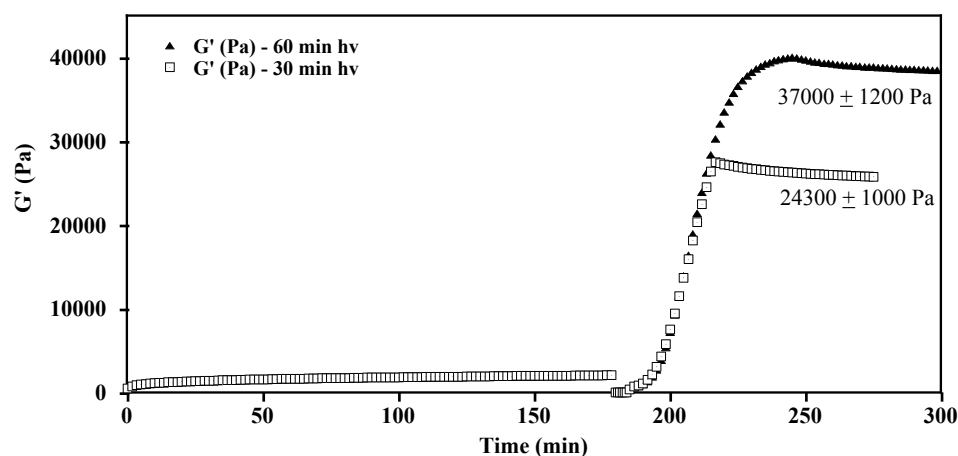


**Figure 3.9 Dynamic time sweep experiment of 1 wt% MKA hydrogels with 10 wt% PEGDVB showing effect of photopolymerization time on the mechanical properties of the resultant hydrogels**

The hybrid hydrogels were primarily designed to impart more resilience to strain as compared to the MKA hydrogel alone. However, strain sweep measurements performed on an oscillatory rheometer were inconclusive due to the slippage of the rheometer-measuring tool during the analysis. Therefore, the mechanical properties of the hydrogels were investigated via compression tests on a dynamic mechanical analyzer (DMA).

### 3.1.5 Compression Analysis of Photopolymerized Hydrogels

Figure 3.10(a) shows the stress-strain profile of a photocrosslinked 1 wt% MKA hydrogel in absence of PEGDVB at pH 7.4 (50 mM BTP, 150 mM NaCl) fabricated prior to analysis. The data shows that the MKA hydrogel shows a linear increase in stress up to 5% strain. After which, the hydrogel begins to yield gradually at higher strains (> 10% strain). As a comparison, Figure 3.10(b) shows the stress-strain profiles of the photocrosslinked MKA and hybrid hydrogels. Hydrogels prepared from PEGDVB only were not included as part of the study because they were too weak for compression analysis. The data shows that all the hybrid hydrogels can withstand at least 30% strain, which is significantly higher than the MKA hydrogel alone. The compressive moduli of the hydrogels can be calculated from the linear region (between 0-5%) of the stress-strain curves shown in Figure 3.10(b). The plot in Figure 3.10(c) shows the compressive moduli of the hybrid hydrogels as a function of PEGDVB concentration. The data shows that there is a synergistic increase in the compressive modulus of the crosslinked hydrogels with increase in PEGDVB concentration. For example, the compressive modulus of crosslinked 1 wt% MKA hydrogel is about 12700 Pa whereas the calculated compressive modulus of 10 wt% PEGDVB is about 7800 Pa (assuming  $E' = 3G'$  where  $G'$  from Figure 3.4 is 2600 Pa). However, the compressive moduli of the crosslinked hybrid hydrogel of 1 wt% MKA and 10 wt% PEGDVB is 54700 Pa. The compressive modulus of this hybrid hydrogel is not only greater than the compressive moduli of the individual hydrogel

networks but also greater than the sum of the compressive moduli of the individual networks.

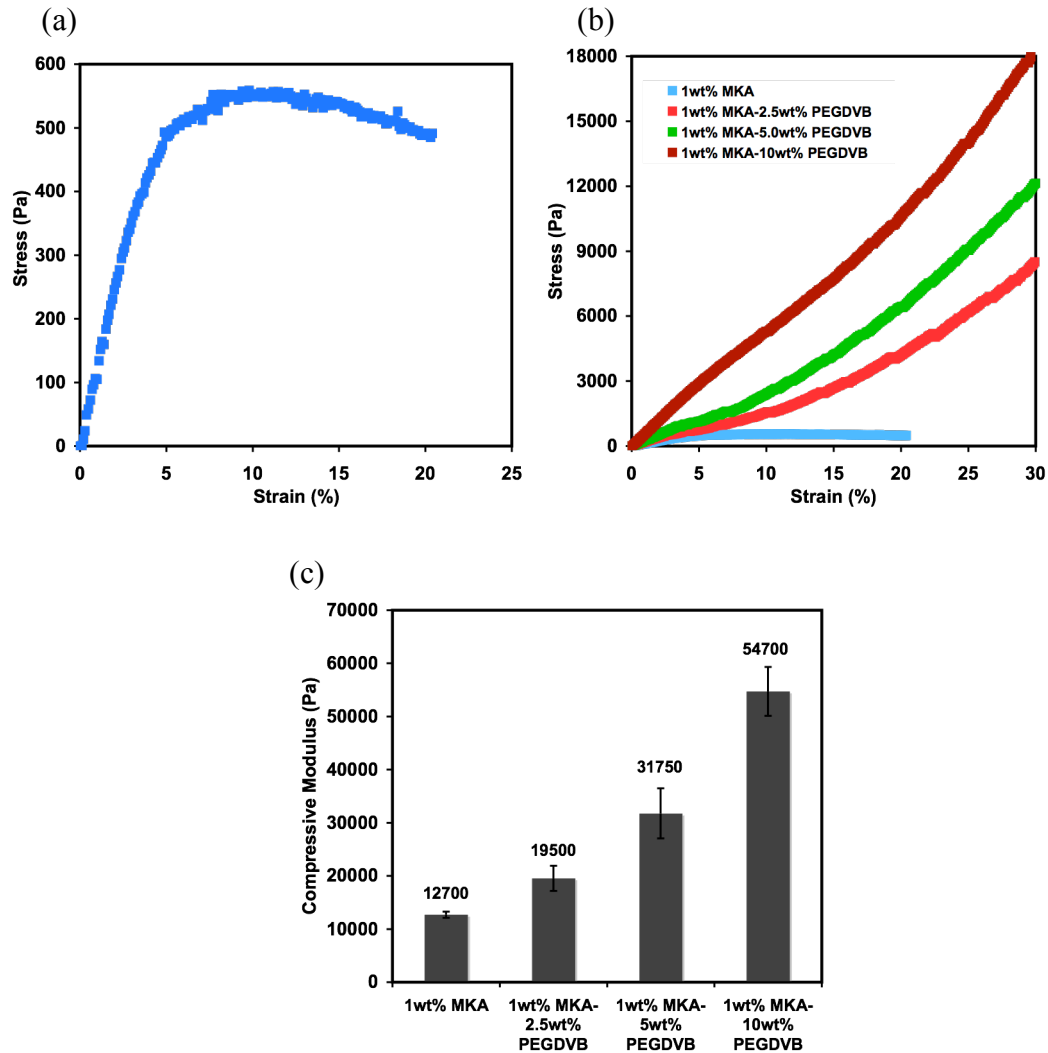


**Figure 3.10 (a) Stress-strain curve of 1 wt% MKA hydrogel at pH 7.4 (b) Stress-strain curves of polymerized hybrid hydrogels and the single network MKA hydrogel at pH 7.4 (c) Compressive moduli of hydrogels as a function of PEGDVB concentration**

The results from the compression tests indicate that copolymerization of PEGDVB and MKA networks not only enhanced the resistance to strain but also the mechanical properties of the resultant hydrogels. In addition, varying the PEGDVB concentration provides the ability to modulate the ultimate mechanical rigidity of these hydrogels.

Generally, polymeric hydrogels swell when soaked in water or buffer solutions depending upon the molecular weight of the polymer and the crosslinking density. The higher the cross-linking density, higher the modulus and lower the swelling. Swelling in turn influences the water content of the hydrogels. Higher swelling indicates more water intake and therefore results in higher water content. The extent of swelling of injectable hydrogel materials is of significance in two ways. First, the mechanical properties of the hydrogels are related to its swelling properties, i.e more swelling results in a decrease in mechanical properties. Second, it will be beneficial to limit the swelling of the injected scaffold to retain its size and shape *in vivo*.

To determine the swelling ratio of a hydrogel, it is soaked in solvent of interest, either buffer or water, and the mass gain of the hydrogel is determined as a function of time. The swelling ratio of a hydrogel is calculated as the ratio of the mass of the soaked hydrogel to the mass of original hydrogel. Equilibrium water content is the ratio of weight of lyophilized hydrogel (solids) to the weight of fully swollen hydrogel. As shown in Figure 3.11, all the hydrogels in this study exhibit minimal swelling and high equilibrium water content of greater than 94%. Minimal swelling

ratio indicates that the mechanical properties of the hybrid hydrogels should not change significantly when placed in a highly hydrated environment such as a tissue.

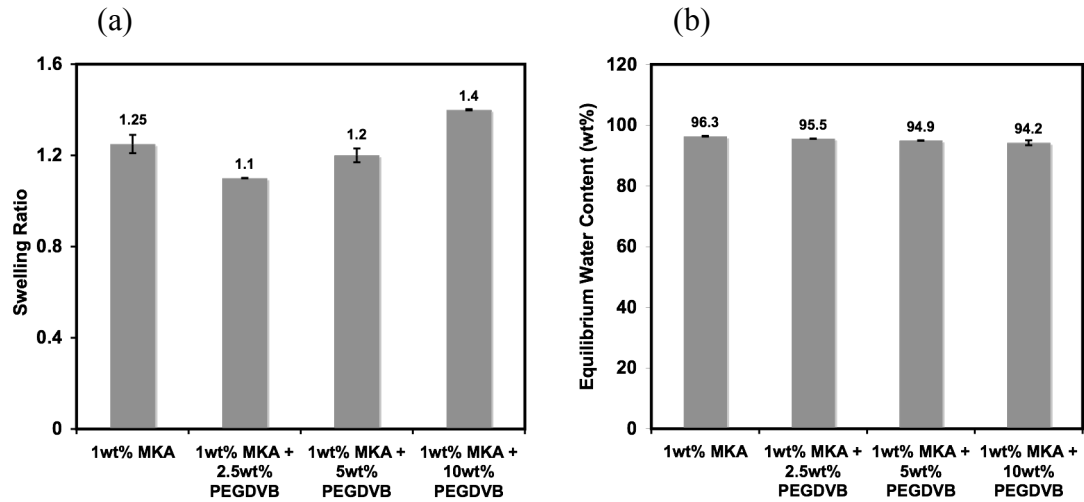


**Figure 3.11 (a) Swelling ratio and (b) Equilibrium water content (%) of MKA hydrogels as a function of PEGDVB concentration**

### 3.1.6 Cytocompatibility of Hydrogel Surfaces

Compatibility of the hydrogel surface toward mammalian cells was assessed. Figure 3.12 shows a live/dead assay where C3H10t1/2 mesenchymal stem cells were seeded onto the pre-formed gel surfaces (i.e. after hydrogelation, photopolymerization and equilibration with DMEM at pH 7.4). This cell line was chosen because they are very sensitive to their environment and provides a rigorous assessment of the hydrogel surface with respect to cell viability. Cells were cultured in the presence of serum on the hydrogel surface for 24 h, which is sufficient time to

allow cells to adhere and adopt healthy morphologies through formation of actin stress fibers.<sup>7</sup>

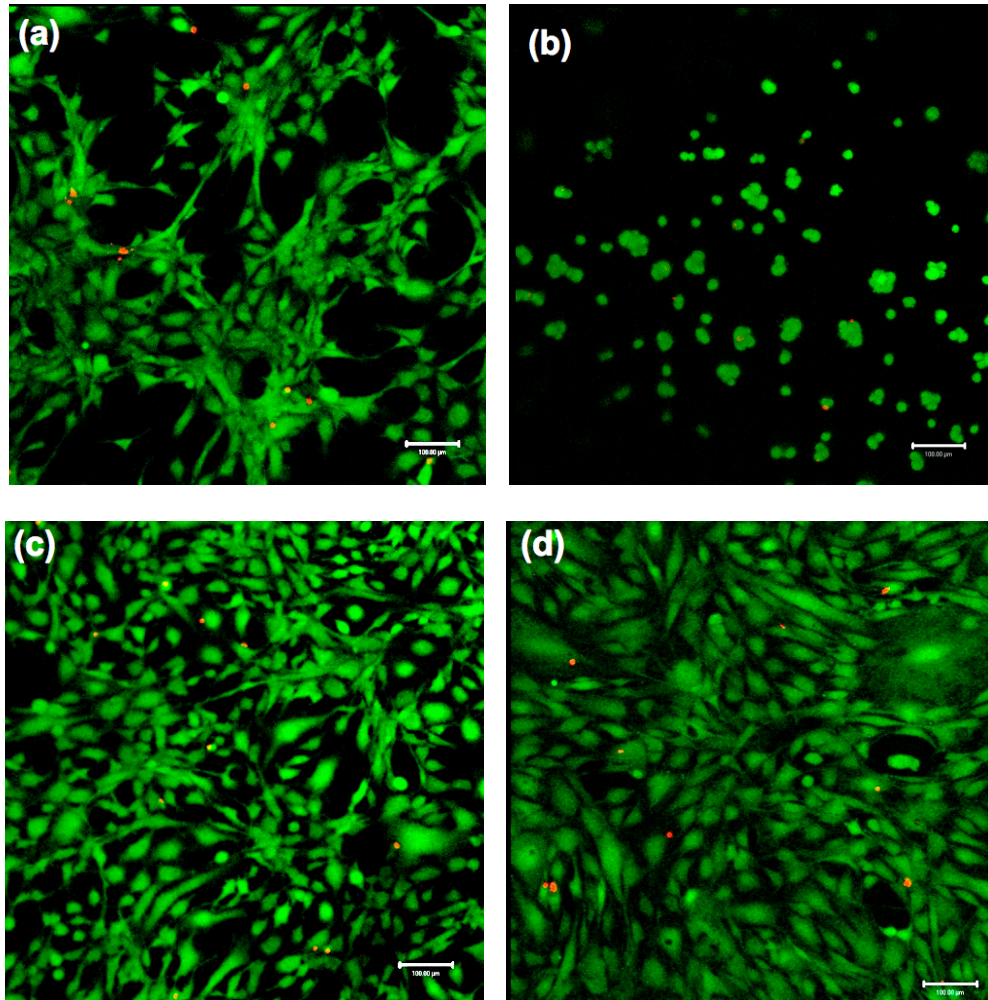


**Figure 3.12** Laser scanning confocal microscopy (LSCM) images of a Live/Dead cellular viability assay of C3H10t1/2 (30,000 cells/cm<sup>2</sup>) incubated on surface of (a) photocrosslinked 1 wt% MKA hydrogel (b) polymerized 10 wt% PEGDVB hydrogel (c) photocrosslinked hybrid hydrogel [1 wt% MKA + 10 wt% PEGDVB] and (d) TCTP control surface after 24 hours. Live cells fluoresce green and dead cells fluoresce red. Scale bar = 100 μm. Data obtained by Chomdao Sinthuvanich

Figure 3.12 (a-c) shows a laser scanning confocal microscopy (LSCM) image of cells cultured on the surface of (a) photocrosslinked 1 wt % MKA hydrogels (b) photocrosslinked 10 wt% PEGDVB hydrogels and (c) photocrosslinked hybrid hydrogels (1 wt% MKA + 10 wt% PEGDVB) after fluorescent dyes have been added that specifically dye living cells (green) and dead cells (red). Also, shown for comparisons are cells that have been cultured onto a tissue culture treated polystyrene (TCTP) control surface under identical conditions [Figure 3.12(d)]. The figure shows that all hydrogel surfaces are non-cytotoxic to C3H10t1/2 cells. However, the cells cultured on the 10 wt% PEGDVB hydrogel surface do not spread and are more round-like. This is expected because PEG is a known non-protein fouling polymer and therefore, few serum proteins can coat the surface of the gel to aid cell attachment. Also, there is no cell binding motifs on the polymer itself to promote cell adherence.

### **3.1.7 Potential Advantage of MKA-based Hybrid Hydrogels over Polymer Hydrogels for Tissue Engineering Applications**

Polymer based hydrogels have been widely used for various tissue engineering applications. A polymeric hydrogel can be fabricated using a mold and then be implanted into a defect to aid in tissue repair. However, this approach is invasive. Alternatively, hydrogelation of polymeric solutions can be induced *in vivo* by either taking advantage of the environmental differences between the polymeric solution and *in vivo* conditions or by chemical or photocrosslinking the polymer solution upon delivery. Although this strategy is less invasive, a potential problem

with this approach is the leakage of the polymer solution into the neighboring tissues. With respect to MKA-PEGDVB hybrid hydrogels, hydrogel formation can be triggered in the presence of PEGDVB, which can then be delivered via syringe to the tissue site with spatial and temporal resolution to fill up the irregularly shaped cavity without any leakage into the neighboring tissues. Thereafter, the syringe-delivered hydrogel can be irradiated to enhance its mechanical properties at the tissue site. In addition, due to the rapid gelation kinetics of MKA, homeogenous encapsulation of cells, growth factors and proteins into the hydrogel may be possible, which can further aid in tissue regeneration efforts.

### **3.1.8 Conclusions**

In this section, we have presented a strategy to fabricate hybrid hydrogels wherein a bifunctional PEG (PEGDVB) is encapsulated into a photopolymerizable self-assembled peptide (MKA) hydrogel. Encapsulation of the PEGDVB does not affect the rigidity of the resulting MKA hydrogel as compared to MKA hydrogel alone. Furthermore, these hybrid hydrogels can be syringe delivered and then polymerized to afford mechanically rigid hydrogels. Varying the concentration of PEGDVB incorporated into the hydrogel during the gelation process provides the ability to modulate the ultimate rigidity of the hybrid hydrogels. Above all, the hybrid hydrogels exhibit higher resistance to applied strain compared to MKA hydrogel.

### 3.2 Construction of Interpenetrating Network Hydrogels of Self-Assembled Peptide and Polymerized PEG-Diacrylate Network

Recent developments have shown that hydrogels with high mechanical strength can be prepared by fabricating an interpenetrating network (IPN).<sup>8, 9</sup> Interpenetrating networks (IPN) are a unique blend of crosslinked polymers in which two independently crosslinked networks are interlocked with one another.<sup>9</sup> The IPNs are regarded as alloys of polymer networks and are often prepared to combine the key attributes of each of the components in network form.

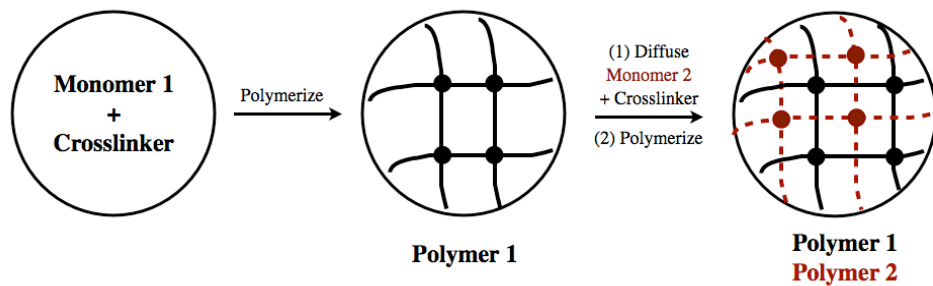
There are two types of IPNs, which are primarily distinguished on the basis of their method of preparation, Figure 3.13:

(1) *Sequential Interpenetrating Network*: This is a two-step method of fabrication that begins with the synthesis of a crosslinked polymer I from monomer I. This is followed by the diffusion of monomer II plus initiator into polymer I and then polymerization is initiated *in situ*.

(2) *Simultaneous Interpenetrating Network*: The monomers (I and II) plus activators of both networks are mixed together and crosslinked via independent non-interfering modes.

If one of the two components is a linear polymer (uncrosslinked), a semi-IPN is obtained. A homo-IPN is obtained if the same monomer or polymer is used to synthesize both the networks.

(a) Sequential IPN



(b) Simultaneous IPN

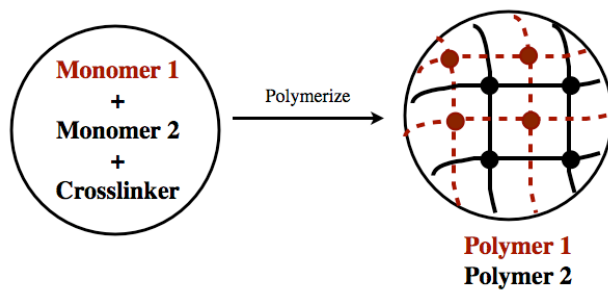


**Figure 3.13** A schematic showing preparation of (a) sequential and (b) simultaneous IPN

### 3.2.1 Interpenetrating Network Hydrogels

Polymeric IPN hydrogels have been synthesized via both simultaneous and sequential methods. The resultant hydrogels exhibit enhanced mechanical properties, which may be due to additional physical entanglements and network interactions between the two distinct polymer networks compared to its individually crosslinked networks. A few examples of each type of IPN and their compressive moduli values are listed in Table 3.1. In particular, IPN hydrogels prepared via sequential polymerization have yielded mechanically robust hydrogels with potential for use as artificial tissues<sup>10</sup>, load bearing tissue substitutes<sup>11</sup> and drug delivery matrices<sup>12</sup>.

Gong et al. first reported “Double-Networks” or sequential IPN hydrogels that exhibit a nonlinear enhancement in mechanical properties as characterized by compression tests.<sup>10</sup> These IPN hydrogels contain about 50-90% water and exhibit high fracture stress up to 40 times compared to its individual components. This discovery has led to development of artificial tissues especially for load-bearing structures. Gong et al.’s most promising IPN hydrogel is comprised of a primary network of densely crosslinked poly(2-acrylamido-2-methylpropanesulfonic acid) (PAMPS) interpenetrated with a more flexible, loosely crosslinked, neutral network of polyacrylamide (PAAm).

#	Components Employed	Range of Compressive Moduli Achieved	Potential Applications	Reference
<b>Sequential IPN</b>				
1	(1) PEGDA (2) Acrylic acid	1.0-19.0 MPa	Artificial tissues (cornea, cartilage)	Myung et al. <sup>13, 14</sup>
2	(1) PAMPS (2) Acrylamide	0.4-0.9 MPa	Artificial cartilage	Azuma et al. <sup>15</sup>
3	(1) Methacrylated Hyaluronic acid (2) N,N-dimethylcrylamide	0.39-0.5 MPa	Spinal disc substitutes	Weng et al. <sup>16</sup>
<b>Simultaneous IPN</b>				
1	(1) PEG-dimethacrylate (2) Chitosan & Glutaraldehyde	0.06-0.8 MPa	Drug delivery Wound dressing	Lee et al. <sup>17</sup>
<b>Semi-IPN</b>				
1	(1) Methacrylated Hyaluronic acid (2) Collagen	~ 0.01-0.8 MPa	Tissue Engineering	Brigham et al. <sup>18</sup>
2	(1) Silk fibroin (2) Acrylamide	0.16-0.19 MPa	Drug delivery matrix	Mandal et al. <sup>19</sup>

**Table 3.1 Literature examples of different types of IPNs and their compressive moduli**

Here, the individual networks of PAMPS and PAAm are mechanically distinct, that is the former is stiff and brittle and the latter is soft and ductile. Their combined IPN hydrogel however is stiff yet not brittle, ductile yet not soft. Recent studies have revealed that the loosely crosslinked PAAm network plays an important

role in enhancing the compressive properties of the IPNs possibly by effectively dissipating the applied stress. This was supported by the fact that IPN hydrogels with a loosely crosslinked PAAm network exhibits the most significant increase in the fracture stress. However, upon increasing the crosslink density of the PAAm network (second network) leads to a substantial decrease in fracture stress of the IPN gel.

In general, IPNs are prepared using either long chain polymers and or monomers that form extended networks following polymerization. While much work has been done with synthetic and natural polymers, there have not been any reports of IPN hydrogels prepared with self-assembling peptides as one of the network forming components. This is of particular interest since self-assembling peptides have been employed to fabricate mechanically rigid hydrogels for tissue engineering<sup>20</sup> and drug delivery<sup>21</sup> applications.

### **3.2.2 Design and Fabrication of Peptide-Polymer IPN Hydrogels**

Herein, we present the first example of an IPN hydrogel fabricated using a self-assembling  $\beta$ -hairpin peptide (MAX1) and PEG-diacrylate (PEGDA, Mw 700), Figure 3.14. MAX1, previously described in Chapter 1, is first triggered to fold and self-assemble to form a physically crosslinked hydrogel (first network) in response to an increase in pH to 9. The second network is subsequently formed by photocrosslinking PEGDA in presence of the pre-formed MAX1 network. We demonstrate that the concentration of PEGDA can be manipulated to modulate the mechanical properties of the IPN hydrogels. In all, this combination presents a

complementary binary system with a cytocompatible peptide network (soft) and a chemically crosslinked hydrolyzable PEGDA network (rigid). The advantage of employing a self-assembling system to fabricate the first network is that the network structure can be easily manipulated. For example, crosslink density and therefore its pore size can be modulated by simply modulating the peptide concentration and/or folding and assembly kinetics as discussed earlier. Altered pore size should influence the interpenetration of the second network and thus the resultant material properties. This approach could provide new avenues to take advantage of self-assembling materials with controlled material properties and nanostructures as the first network to dictate the ultimate material properties of the IPNs, promoting its use for biomedical and material based applications.

Employed in this IPN to form the first network is a MAX 1 hydrogel, see Chapter 1 for the peptide sequence. The self-assembled hydrogel is comprised of well-defined  $\beta$ -sheet-rich fibrils that extend throughout the network.<sup>22</sup> The number of physical crosslinks, i.e. entanglements and interfibril junctions, that are formed during the self-assembly process govern the ultimate material properties of the hydrogel, Figure 3.14 (a) and (b). The second network is synthesized using PEGDA, which is first diffused into the peptide-based hydrogel and subsequently photopolymerized to form a mechanically rigid IPN hydrogel. All the hydrogels in this study exhibit minimal swelling and high equilibrium water content of greater than 80%, Figure 3.15. Minimal swelling ratio indicates that the mechanical properties of the IPN hydrogels should not change significantly in a highly hydrated environment since the mechanical



hydrogels than the sum of the pure peptide and PEGDA control hydrogels. As expected, the compressive moduli of the IPN hydrogels increase with an increase in PEGDA concentration.

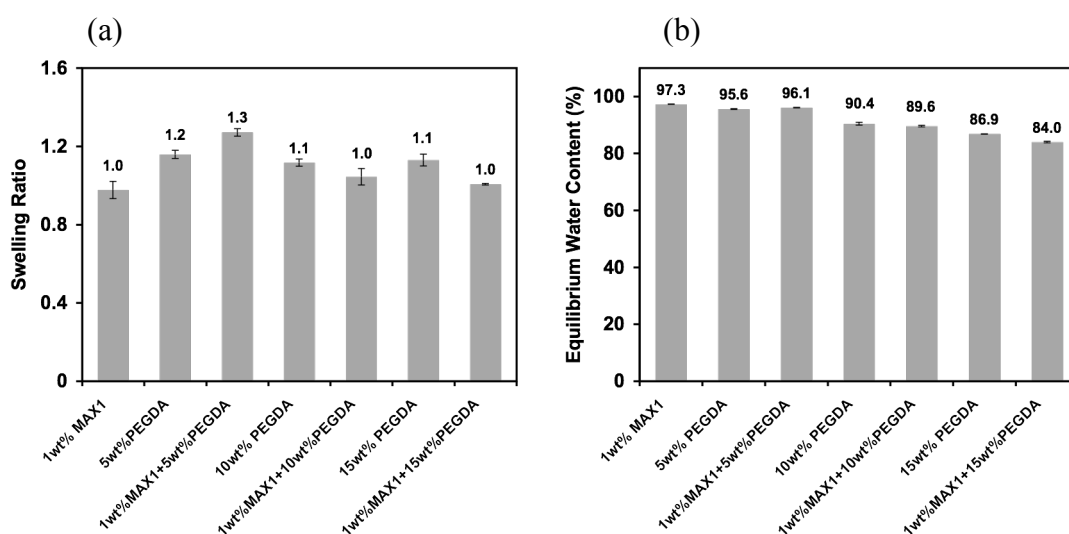


**Figure 3.15 Swelling ratio and equilibrium water content values of single network and IPN hydrogels**

An interesting observation is that presence of 1wt% MAX1 as the primary network in the IPN hydrogels resulted in a synergistic increase in the compressive moduli compared to the corresponding pure PEGDA hydrogels respectively. The significant increase in compressive moduli of the IPN hydrogels may stem from its binary structure, as well as can originate from the inter-chain interactions at the entanglements of the IPN networks. Additionally, the MAX1 fibrillar hydrogel network may reduce the heterogeneity of the PEGDA polymerization event reducing

phase separation of the diffused PEGDA monomers compared to the polymerization of pure PEGDA solution. As shown in Figure 3.17, the IPN gels are relatively more transparent as compared to the single network PEGDA, which show phase separation with an increase in polymer concentration of the hydrogel. Phase separation or turbidity in crosslinked polymer hydrogels arises due to heterogenous polymerization of the monomers employed to form the gel, which inherently leads to formation of more brittle hydrogels.<sup>24, 25</sup> Hydrogels with a homogeneous network are mechanically more rigid than the ones with a heterogeneous network.<sup>24</sup>

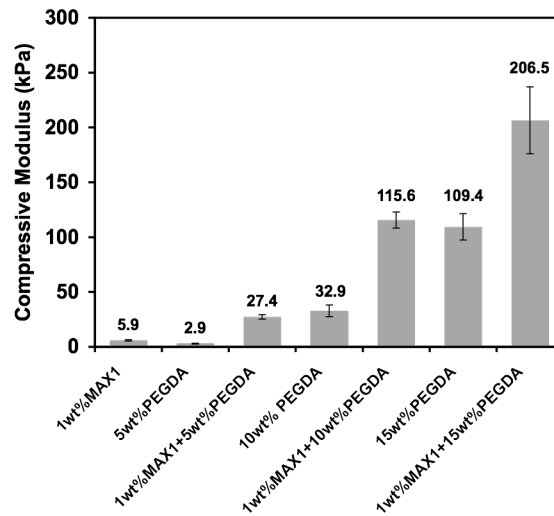


**Figure 3.16 Compressive modulus of single network and IPN hydrogels as determined by compressive tests.**

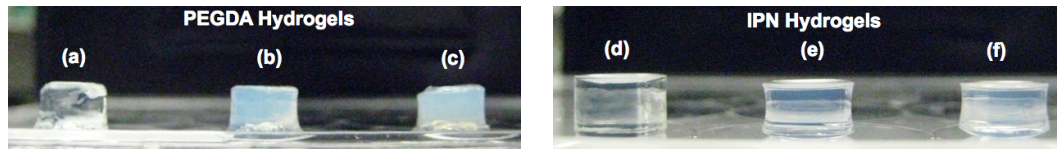


**Figure 3.17 Typical appearance of single network PEGDA and IPN hydrogels. PEGDA hydrogels: (a) 5 wt% PEGDA (b) 10 wt% PEGDA (c) 15 wt% PEGDA. IPN hydrogels: (d) 1 wt% MAX1 + 5 wt% PEGDA (e) 1 wt% MAX1 + 10 wt% PEGDA (f) 1 wt% MAX1 + 15 wt% PEGDA**

Furthermore, the mechanical properties of the hydrogels under applied strain were investigated to determine the ultimate fracture stress and strain values. The fracture stress point is identified as the stress value prior to uniform breakage of the hydrogel (maximum stress measured). The corresponding strain value at this maximum stress was identified as the fracture strain point. As shown in Figure 3.18a, the fracture stress values of the IPN hydrogels with increasing PEGDA concentration are significantly higher than the corresponding pure MAX1 and PEGDA hydrogels. High deviation with PEGDA hydrogels ( $> 5\text{wt}\%$ ) arises due to the heterogeneous polymerization of the PEGDA monomers in solution. Similarly, as shown in Figure 3.18b, the fracture strain values for the IPN hydrogels were significantly higher compared to that of the peptide hydrogel, but little to moderately higher as compared to that of pure PEGDA hydrogels. A significant increase in fracture strain value is observed for the IPN hydrogels with 10 wt% and 15 wt% PEGDA. These results indicate that the crosslink density of the PEGDA network also plays an important role in enhancing the mechanical properties of the IPN hydrogels.

Based on the stress-strain profile, the physically crosslinked MAX 1 hydrogel has a low fracture stress and strain value whereas the PEGDA hydrogels are more elastic and ductile than MAX 1 hydrogel. Interestingly, the IPN hydrogels prepared with 1wt% MAX 1 and 5-15 wt% PEGDA exhibit higher fracture stress and strain values compared to the control hydrogels. Therefore in addition to the binary structure of the IPNs, the inter-chain entanglements may also be contributing to the properties of the IPN hydrogels, which may be further strengthened due to H-bonding between the  $\epsilon$ -amine of lysine side chains and the carbonyl oxygen and/or ether oxygen of PEGDA chains. Myung et al. have shown that inter-chain H-bonding in a PEGDA-containing sequential IPN enhances the compressive moduli of the resultant IPN hydrogels and may also be responsible for the enhancement in the fracture properties.<sup>13</sup>

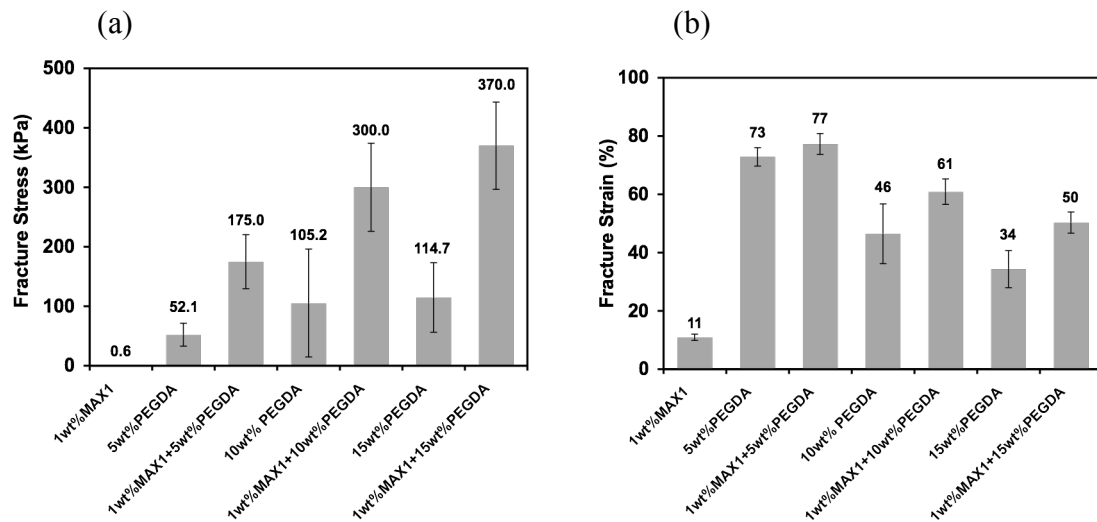


**Figure 3.18 Fracture stress and strain properties of single network PEGDA and IPN hydrogels**

Alternatively, as observed for Osada and Gong's work on another IPN system,<sup>10</sup> the physically crosslinked MAX1 fibrils may also be acting as long chains at higher strain values (> 10%) following disruption of entanglements in the peptide network (e.g long non-entangled  $\beta$ -fibrils), thereby potentially dissipating the applied stress and preventing crack formation which can lead to higher fracture stress and strain values. Additional experiments with varying concentrations of MAX1 need to be performed at different pH conditions to gain further insight into the mechanism(s) responsible for the enhanced mechanical properties of these MAX1-PEGDA IPN hydrogel systems.

Collectively, the greater compressive moduli and higher fracture stress and strain values of the MAX1 based IPN hydrogels as a function of PEGDA concentration suggest that this approach may be beneficial in preparation of mechanically robust hydrogels for tissue engineering applications.

### **3.2.4 Conclusion**

We have developed peptide-PEGDA based dual-network hydrogels by a two-step process. The IPN hydrogels, with more than 80% water, not only exhibit significantly higher compressive moduli but also exhibit higher fracture stress and strain values than the corresponding control hydrogels. The mechanical properties of the IPNs are related to the concentration of PEGDA employed to synthesize the second network. This study demonstrates that dual-network hydrogels can be prepared

to achieve mechanically robust IPN hydrogel scaffolds that may have potential for biomedical applications especially as load bearing substitutes. Future studies could investigate the effect of peptide concentration on IPN mechanical properties.

### 3.3 Experimental Section

**Materials:** Polyethylene glycol (PEG, Mw 10000), 4-vinylbenzylchloride, Polyethylene glycol diacrylate (PEGDA, Mw 700) and Boric acid were purchased from Sigma and used as received. Photoinitiator Irgacure 2959 (I2959) was a generous gift from Ciba Specialty Chemicals and used as received. MAX 1 peptide was synthesized and purified as reported earlier.<sup>26,27</sup>

#### Synthesis of DivinylbenzylPEG (PEGDVB)

PEG Mw 10000 (10gm, 2 mmol) and sodium hydroxide pellets (1.2 gm, 30 mmol) in 40 ml of toluene (4 ml toluene/gm of PEG) in a round bottom flask equipped with a reflux condenser were gently heated to 60 °C till the PEG dissolved. After which, the heating source was removed and 4-vinylbenzyl chloride (2.8 ml, 20 mmol) was added dropwise via syringe. Two minutes after addition of 4-vinylbenzyl chloride is complete, the reaction was gently refluxed to 60 °C for 3 days. During this time, a white precipitate is formed (NaCl). The reaction was then filtered through kieselguhr to remove white solid. The filtrate was rotavaped completely and then redissolved in sufficient water. The aqueous solution was then extracted with dichloromethane (3X). The organic layer was separated and dried over anhydrous sodium sulfate. Thereafter, organic extract was rotavaped to about ¼ of the volume. To this, diethyl ether was added gently while swirling till the solution turns hazy and small particles appear. At this point, the suspension was left in the refrigerator to allow complete precipitation of the product overnight. The product was collected by filtration, washed with ether and

allowed to dry. The product was stored at 8 °C till use. The product was confirmed by NMR and the extent of functionalization was calculated according to the reported formula.<sup>5</sup> PEGDVB Mw 10000, ~ 6 gm (92% functionalized). <sup>1</sup>H-NMR (CDCl<sub>3</sub>): 3.6 ppm (493.08 H, PEG), 4.6 ppm (s, 2H, CH<sub>2</sub>=CH-Ph-CH<sub>2</sub>-O-), 5.25 ppm and 5.75 ppm (d, 2H, CH<sub>2</sub>=CH-Ph-CH<sub>2</sub>-), 6.7 ppm (dd, 1H, CH<sub>2</sub>=CH-Ph-), 7.3 ppm and 7.4 ppm (2 d, 4H, aromatic H).

**Oscillatory Shear Rheology.** Rheological measurements were performed on Anton Paar-Physica MCR 500 rheometer with a quartz glass plate fixture (Anton Paar, Advanced UV system, UV cell) to allow UV irradiation. A 25 mm parallel plate geometry and 0.5 mm gap distance was employed for all experiments. Omnicure (EXFO) series 1000 spot curing system (Model S1000, 100W Hg Arc, Wavelength 320-500nm) was used as a UV source. The light power (10% laser intensity) at the sample position was ~ 16 mW/cm<sup>2</sup> as measured by a radiometer (Apprise Technologies, Chromaline, UV Minder with peak response at 370 nm). The distance between the UV source and the sample was 4 cm.

The peptide was first dissolved in a solution of Irgacure 2959 (0.05 wt%) to obtain a concentration that is twice the final peptide concentration in the gel. Similarly, PEGDVB was first dissolved in pH 7.4 buffer (100mM BTP, 300mM NaCl) to obtain a concentration that is twice the final PEGDVB concentration in the gel. Then, an equal amount of PEGDVB in pH 7.4 buffer (100mM BTP, 300mM NaCl) was added to the peptide stock solution, mixed gently and immediately loaded

onto the rheometer plate equilibrated to 37 °C. After the sample was loaded and the parallel plate lowered, standard low-viscosity mineral oil was used to insulate the sides of the parallel plate in order to prevent evaporation. Control experiments have shown that the mineral oil had no effect on the rheological measurements. Gelation was observed by monitoring the evolution of the storage modulus ( $G'$ ) with time, in a dynamic time sweep experiment performed at an angular frequency of 6 rad/s and strain of 0.2 %.

Shear-thin and recovery experiments were performed by first allowing gels to form for 3 hours in a dynamic time sweep experiment (6 rad/s and 0.2% strain) and subsequently subjecting the gel to a shear-thinning and recovery cycle. The shear-thinning and recovery cycle consisted of application of 1000 % strain at 6 rad/s for 30 sec or 300 sec followed by a recovery period at a constant 0.2 % strain at 6 rad/s angular frequency. A 1000% strain was employed to ensure complete disruption of the hydrogel network. Frequency sweep experiments were performed by varying the frequency from 0.1-100 rad/s at a constant strain of 0.2 %.

Photopolymerization experiments were performed by irradiating the hydrogels for 30 min or more min ( $\sim 16 \text{ mW/cm}^2$ , 365 nm) at specified times depending upon the experiment. Control experiments were performed with standard viscosity oil (S200) to observe the change in viscosity at variable UV light intensities with respect to increase in temperature. The temperature was simultaneously recorded using a thermocouple in contact with the quartz UV plate during irradiation of the S200 oil.

**Preparation of the Interpenetrating Network (IPN) Hydrogels:** A two-step network formation approach was employed to fabricate the IPN hydrogels. The first network of the IPN gel was constructed using 1wt% MAX 1 peptide. Here, MAX 1 was first dissolved in water containing 0.1wt% Irgacure 2959 to give a 2 wt% peptide solution. Then, an equal amount of pH 9 buffer (250 mM Borate, 20 mM NaCl) was added to the peptide solution. The resulting 1 wt% MAX 1 solution (200  $\mu$ L) at pH 9 (125 mM Borate, 10 mM NaCl, 0.05 wt% Irgacure 2959) was transferred into a cell culture transwell insert and allowed to form a hydrogel for 4 hours at room temperature. Thereafter, 600  $\mu$ L of PEGDA stock in pH 9 buffer (125 mM Borate, 10 mM NaCl) containing 0.05 wt % Irgacure was added on top of the gel and allowed to diffuse into the MAX 1 hydrogel for 12 hours. After which, the supernatant was removed and the hydrogel was irradiated for 30 min at 365 nm (xx-15, 6 mW/cm<sup>2</sup>), to synthesize the PEGDA network in presence of the first network.

**Preparation of the Single Network Hydrogels:**

*MAX 1 Hydrogels:* MAX 1 hydrogels were prepared in a similar manner as described above. Thereafter, only pH 9 buffer (125 mM Borate, 10 mM NaCl, 0.05 wt % Irgacure) was added on top of the gel and allowed to diffuse into the gel for 12 hours. Thereafter, the gels were treated in the same manner as the IPN hydrogels.

*PEGDA Hydrogels:* Appropriate amount of PEGDA was first mixed with water containing 0.1wt% Irgacure. Then, an equal amount of pH 9 buffer (250 mM Borate, 20 mM NaCl) was added to give PEGDA solution of desired concentration. The

resulting PEGDA solution (200  $\mu\text{L}$ ) was transferred into a cell culture transwell insert and irradiated for 30 min at 365 nm.

**Swelling Ratio:** The hydrogel samples were prepared as described above. The hydrogels were then transferred into a pre-weighed vial and the wet weight of the hydrogels was measured. Following incubation in pH 7.4 buffer (50 mM BTP, 150 mM NaCl) or pH 9 buffer (125 mM Borate, 10 mM NaCl) at room temperature for 24 hrs, the swelling ratio was determined by comparing the change in weight of hydrogel before and after incubation

$$S.R = \left( \frac{W_t - W_o}{W_o} \right)$$

$W_t$  = Weight of hydrogel after 24 hrs,  $W_o$  = Weight of hydrogel before incubation

**Equilibrium Water Content:** Hydrogels were immersed in 600  $\mu\text{L}$  of pH 7.4 buffer (50 mM BTP, 150 mM NaCl) or pH 9 buffer (125 mM Borate, 10 mM NaCl) and allowed to equilibrate for 24 hours. Excess liquid was carefully removed and the equilibrated hydrogels were weighed. The hydrogels were then lyophilized twice to ensure complete removal of water and then weighed again. Percent water content was determined by using the following equation:

$$\%EWC = 100 \times \left( \frac{W_t - W_d}{W_t} \right)$$

$W_t$  = Weight of hydrogel after equilibration,  $W_d$  = Weight of hydrogel after lyophilization

**Mechanical Characterization:** The mechanical properties of the pre-soaked hydrogels were characterized by compressive stress-strain measurements using an RSA III Rheometrics System Analyzer (TA Instruments) in parallel-plate configuration. The cylindrical hydrogel samples approximately 6 mm in diameter and 4 mm in height were placed on the lower plate and compressed by the upper plate at a strain rate of 6%/min until failure. The hydrogels were pre-conditioned to a 10% strain prior to analysis to prevent slippage and maintain efficient contact with the upper plate during the experiment. The compressive modulus was determined from the linear slope of the stress-strain curve over the strain range of 0.3-4%. Fracture stress and strain values from the compression test were determined from the peak of the stress-strain curve.

### **Cell Viability Assay**

PEGDVB was dissolved in 100 mM BTP 300 mM NaCl pH 7.4 resulting in 20 wt% PEGDVB solution. Lyophilized MKA peptide was dissolved in water containing 0.5mg/ml Irgacure 2959 resulting in a soluble 2 wt% peptide solution. Equal amount of peptide and polymer solution were mixed and 200  $\mu$ l was transferred to a

borosilicate plate. Control hydrogel surfaces, 1wt% MKA and 10wt% PEGDVB, were also prepared under identical conditions. After incubating for 4 hours at 37 °C, the hydrogels were exposed to 6 mW/cm<sup>2</sup> of UV light (365 nm) for 30 minutes. The hydrogels were then incubated for another 30 minutes to complete the polymerization reaction. Thereafter, 400 µl of growth media (90% DMEM supplemented with 25 mM HEPES, 10% FBS, 5mM L-glutamine, and 50 ug/ml Gentamicin) was added on to the hydrogel surfaces and allowed to incubate overnight at 37 °C, 5% CO<sub>2</sub>. To assess cytotoxicity of hydrogel, C3H10t1/2 cells were first cultured on tissue culture treated polystyrene (TCTP) plates in growth media (DMEM) then trypsinized, and counted using a hemacytometer. The resulting cell suspension was plated at 30,000 cells/cm<sup>2</sup> on control TCTP culture plate, MKA, PEGDVB and MKA-PEGDVB hybrid hydrogel surfaces. Cell viability was assessed using a Live/Dead assay after 24 hours of incubation. A stock solution containing both 1 µM calcein AM and 2 µM ethidium homodimer in DMEM with 25mM HEPES were prepared according to the Live-Dead assay (Molecular Probes # L3224) package instructions. After gently washing each surface with DMEM with 25mM HEPES, 200 ul of dye stock solution was added to each well. Samples were imaged using a Zeiss 510 laser scanning confocal microscope at a magnification of 10X.

## References:

1. Rughani, R. V.; Schneider, J. P., Molecular Design of b-Hairpin Peptides for Material Construction. *MRS Bulletin* **2008**, 33, (5), 530-535.
2. Kumar, C., *Tissue, Cell and Organ Engineering, Nanotechnologies for the Life Sciences*. Wiley-VCH: 2006; Vol. 9, p 519.
3. Bogdan, M.; Corneliu, C.; Amar, Z.; Jean-Pierre, M., New adhesives prepared from vinyl benzyl chloride copolymerization. *Journal of Applied Polymer Science* **1998**, 67, (6), 1151-1156.
4. Gabor, E.; Joseph, P. K., Ideal tetrafunctional amphiphilic PEG/PDMS conetworks by a dual-purpose extender/crosslinker. I. Synthesis. *Journal of Polymer Science Part A: Polymer Chemistry* **2005**, 43, (20), 4953-4964.
5. Gregory, M. C.; Orion, D. H.; David, S. S.; Jeffrey, A. H., A sensitivity study of the key parameters in the interfacial photopolymerization of poly(ethylene glycol) diacrylate upon porcine islets. *Biotechnology and Bioengineering* **1998**, 57, (6), 655-665.
6. Macosko, C. W., *Rheology Principles, Measurements and Applications*. Wiley-VCH, Inc.: 1994; p 550.
7. Haines, L. A.; Rajagopal, K.; Ozbas, B.; Salick, D. A.; Pochan, D. J.; Schneider, J. P., Light-activated hydrogel formation via the triggered folding and self-assembly of a designed peptide. *Journal of the American Chemical Society* **2005**, 127, (48), 17025-17029.
8. David Myung; Dale Waters; Meredith Wiseman; Pierre-Emile Duhamel; Frank, J. N. C. N. T. C. W., Progress in the development of interpenetrating polymer network hydrogels. *Polymers for Advanced Technologies* **2008**, 19, (6), 647-657.
9. Kostanski, L. K.; Huang, R. X.; Filipe, C. D. M.; Ghosh, R., Interpenetrating Polymer Networks as a Route to Tunable Multi-responsive Biomaterials: Development of Novel Concepts. *Journal of Biomaterials Science-Polymer Edition* **2009**, 20, (3), 271-297.
10. J.P. Gong; Y. Katsuyama; T. Kurokawa; Osada, Y., Double-Network Hydrogels with Extremely High Mechanical Strength. *Advanced Materials* **2003**, 15, (14), 1155-1158.
11. Darwis, D.; Stasica, P.; Razzak, M. T.; Rosiak, J. M., Characterization of poly(vinyl alcohol) hydrogel for prosthetic intervertebral disc nucleus. *Radiation Physics and Chemistry* **2002**, 63, (3-6), 539-542.
12. Chivukula, P.; Dusek, K.; Wang, D.; Duskov-Smrckov, M.; Kopeckov, P.; Kopecek, J., Synthesis and characterization of novel aromatic azo bond-containing pH-sensitive and hydrolytically cleavable IPN hydrogels. *Biomaterials* **2006**, 27, (7), 1140-1151.
13. Myung, D.; Koh, W.; Ko, J.; Hu, Y.; Carrasco, M.; Noolandi, J.; Ta, C. N.; Frank, C. W., Biomimetic strain hardening in interpenetrating polymer network hydrogels. *Polymer* **2007**, 48, (18), 5376-5387.

14. Myung, D.; Koh, W.; Bakri, A.; Zhang, F.; Marshall, A.; Ko, J.; Noolandi, J.; Carrasco, M.; Cochran, J.; Frank, C.; Ta, C., Design and fabrication of an artificial cornea based on a photolithographically patterned hydrogel construct. *Biomedical Microdevices* **2007**, 9, (6), 911-922.
15. Chinatsu, A.; Kazunori, Y.; Yoshie, T.; Hiroko, T.; Fuminori, K.; Atsushi, N.; Yong Mei, C.; Jian Ping, G.; Yoshihito, O., Biodegradation of high-toughness double network hydrogels as potential materials for artificial cartilage. *Journal of Biomedical Materials Research Part A* **2007**, 81A, (2), 373-380.
16. Weng, L.; Gouldstone, A.; Wu, Y.; Chen, W., Mechanically strong double network photocrosslinked hydrogels from N,N-dimethylacrylamide and glycidyl methacrylated hyaluronan. *Biomaterials* **2008**, 29, (14), 2153-2163.
17. Lee, S. J.; Kim, S. S.; Lee, Y. M., Interpenetrating polymer network hydrogels based on poly(ethylene glycol) macromer and chitosan. *Carbohydrate Polymers* **2000**, 41, (2), 197-205.
18. Brigham, M. D.; Bick, A.; Lo, E.; Bendali, A.; Burdick, J. A.; Khademhosseini, A., Mechanically Robust and Bioadhesive Collagen and Photocrosslinkable Hyaluronic Acid Semi-Interpenetrating Networks. *Tissue Engineering Part A* 0, (0).
19. Mandal, B. B.; Kapoor, S.; Kundu, S. C., Silk fibroin/polyacrylamide semi-interpenetrating network hydrogels for controlled drug release. *Biomaterials* **2009**, 30, (14), 2826-2836.
20. Haines-Butterick, L.; Rajagopal, K.; Branco, M.; Salick, D.; Rughani, R.; Pilarz, M.; Lamm, M. S.; Pochan, D. J.; Schneider, J. P., Controlling hydrogelation kinetics by peptide design for three-dimensional encapsulation and injectable delivery of cells. *Proc. Natl. Acad. Sci. U. S. A.* **2007**, 104, (19), 7791-7796.
21. Branco, M. C.; Pochan, D. J.; Wagner, N. J.; Schneider, J. P., Macromolecular diffusion and release from self-assembled [beta]-hairpin peptide hydrogels. *Biomaterials* **2009**, 30, (7), 1339-1347.
22. Ozbas, B.; Rajagopal, K.; Schneider, J. P.; Pochan, D. J., Semiflexible chain networks formed via self-assembly of beta-hairpin molecules. *Physical Review Letters* **2004**, 93, (26).
23. Park, Y. D.; Tirelli, N.; Hubbell, J. A., Photopolymerized hyaluronic acid-based hydrogels and interpenetrating networks. *Biomaterials* **2003**, 24, (6), 893-900.
24. Sakai, T.; Matsunaga, T.; Yamamoto, Y.; Ito, C.; Yoshida, R.; Suzuki, S.; Sasaki, N.; Shibayama, M.; Chung, U.-i., Design and Fabrication of a High-Strength Hydrogel with Ideally Homogeneous Network Structure from Tetrahedron-like Macromonomers. *Macromolecules* **2008**, 41, (14), 5379-5384.
25. Shibayama, M., Universality and Specificity of Polymer Gels Viewed by Scattering Methods. *Bulletin of the Chemical Society of Japan* **2006**, 79, (12), 1799-1819.
26. Nagarkar, R. P.; Schneider, J. P., Synthesis and Primary Characterization of Self-Assembled Peptide-based hydrogels. In *Nanostructure Design, Methods and Protocols*, Gazit, E.; Nussinov, R., Eds. Humana Press: 2008; pp 61-77.

27. Schneider, J. P.; Pochan, D. J.; Ozbas, B.; Rajagopal, K.; Pakstis, L.; Kretsinger, J., Responsive hydrogels from the intramolecular folding and self-assembly of a designed peptide. *Journal of the American Chemical Society* **2002**, 124, (50), 15030-15037.

## Chapter 4

### DESIGN AND CHARACTERIZATION OF SELF-ASSEMBLING THREE-STRANDED BETA-SHEET PEPTIDES

#### 4.0 Introduction

Protein assembly resulting in the formation of amyloid fibrils, assemblies rich in cross  $\beta$ -sheet structure, is normally thought of as a deleterious event associated with disease. However, amyloid formation is also involved in a diverse array of normal biological functions such as cell adhesion<sup>1</sup>, melanin synthesis<sup>2</sup>, insect defense mechanisms<sup>3</sup> and modulation of water surface tension by fungi and bacteria<sup>4, 5</sup>. Recent studies have identified functional amyloid in bacteria<sup>6, 7</sup>, fungi<sup>8, 9</sup>, invertebrates<sup>3, 10</sup> and humans<sup>2, 11, 12</sup>. For example, bacteria such as *Escherichia coli* and *Salmonella spp.* produce amyloid fibers known as curli, to create a proteinaceous matrix that enables surface attachment and colonization.<sup>13, 14</sup> In humans, amyloid fibers composed of the protein Pmel17 play an important role in the biosynthesis of melanin by serving as a template to direct the polymerization of reactive melanin precursors.<sup>2, 11</sup> These findings indicate that Nature has evolved to take advantage of large, proteinaceous fibrillar assemblies to elicit function. Chemists have shown that self-assembling peptides can be used to prepare synthetic materials composed of fibrils that contain

cross  $\beta$ -sheet quaternary structure. Concern can be raised regarding the utility of these materials in biological applications based on their structural resemblance to amyloid at nanometer length scales. However, paralleling the recent realization that amyloid can be beneficially functional in both prokaryotes and eukaryotes,  $\beta$ -sheet rich materials have found use in biological applications. For example, peptide-based hydrogels have been designed as extracellular matrix substitutes<sup>15</sup>, cell culturing platforms<sup>16, 17</sup> and cell delivery vehicles<sup>18</sup>.

Various secondary structural motifs such as  $\alpha$ -helices<sup>19, 20</sup>, single  $\beta$ -strands<sup>16, 21-28</sup> and  $\beta$ -hairpins<sup>18, 29-33</sup> have been used to construct materials. Strand and hairpin building blocks consist of only one or two  $\beta$ -strands respectively, and are capable of undergoing ordered assembly leading to well-defined fibril morphologies. The fact that these peptides self-assemble in an orderly fashion, in contrast to non-specifically aggregating, can be partially rationalized considering that only a moderate entropic penalty is paid to organize a limited number of strands per monomer during assembly. In contrast, many proteins involved in amyloid formation typically contain sheets comprised of multiple strands.<sup>34, 35</sup> Recent high resolution structural analysis of crystalline amyloid indicate that proteins comprised of multistrand sheets can also undergo ordered assembly; this is quite impressive given the entropic demands of ordering a larger number of strands during assembly.<sup>36</sup> With respect to biomimetic materials design, very little is known concerning the preparation of self-assembled fibrillar materials from multi-stranded precursors.<sup>37, 38</sup> In this chapter, we explore the

feasibility of using *de novo* designed multi-stranded  $\beta$ -sheets for the fabrication of self-assembled hydrogels.

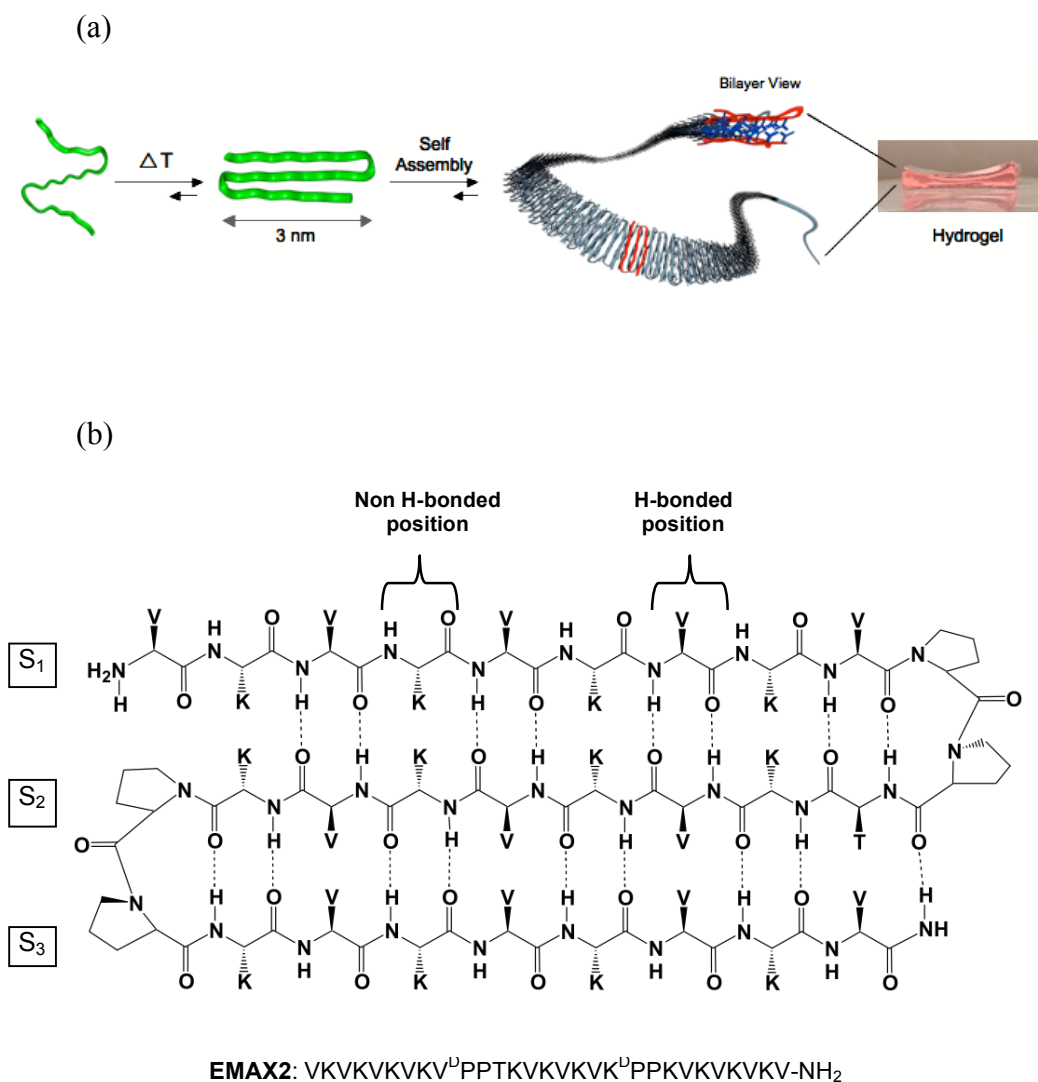


**Figure 4.1 (a) Proposed mechanism of folding and self-assembly of EMAX2 leading to hydrogelation. Several EMAX2 molecules are colored red in the fibril to highlight the three-stranded sheet conformation of EMAX2 in the folded and assembled state as well as bilayer formation. (b) Structure and sequence of EMAX2.**

To our knowledge, there are no reports of  $\beta$ -sheet peptides containing more than two-strands that undergo ordered self-assembly to afford a mechanically rigid hydrogel.

The design of a three-stranded  $\beta$ -sheet (EMAX2) that undergoes triggered self-assembly to form networks of well-ordered  $\beta$ -sheet rich fibrils that constitute a mechanically rigid, yet injectable, non-cytotoxic hydrogel is presented. The properties of this material are consistent with the recent appreciation that natural occurring amyloid can be functionally beneficial.

#### **4.1 Design of a Three-Stranded Self-Assembling Peptide**

EMAX2 is designed to undergo a thermally-induced intramolecular folding event to afford a three-stranded  $\beta$ -sheet that subsequently self-assembles to form an extensive network of fibrils leading to hydrogelation, Figure 4.1(a). This mechanism allows material formation to take place with temporal resolution since EMAX2 is designed to self-assemble into a gel only when folded into the sheet conformation.

The primary sequence of EMAX2 contains 29 amino acids [Figure 4.1(b)], 12 of which are lysine residues and 12 of which are valine residues. As will be shown, when dissolved in appropriate aqueous buffer solutions at temperatures below  $\sim 20$  °C, the peptide remains unfolded. Mainly, this is due to electrostatic

repulsion between the protonated lysine side chains and the ability of water to solvate the hydrophobic valine side chains at low temperatures<sup>39</sup>. However, increasing the temperature favors the desolvation of hydrophobic side chains and leads to EMAX2 folding and self-assembly, (Figure 4.1), leading to a hydrogel network where the valine side chains are shielded from water. In this folding and self-assembly mechanism, the free energy gained in shielding the hydrophobic portions of EMAX2 from water outweighs the electrostatic repulsions, mainly between lysine side chains, that must be overcome for the peptide to fold. In the folded state, EMAX2 is designed to self-assemble in a facial manner to form a bilayer burying its hydrophobic valine residues. The folded peptide is also designed to assemble laterally forming a network of hydrogen bonds that defines the long axis of a given fibril.

Because EMAX2 must both fold and self-assemble for hydrogelation to occur, its design utilized both established criteria developed for *de novo* designed, non-assembling model sheets to impart efficient folding of EMAX2 as well as a structural consideration of naturally occurring proteins that assemble into amyloid. Although most of the monomeric model sheet systems reported contain design elements that disfavor self-assembly, important design criteria can be gleaned from these studies that can be applied to an assembling system.  $\beta$ -strand length, the propensity of individual strand residues to adopt  $\beta$ -dihedral angles, the turn type connecting the strands, and the propensities of the residues in the turn region to adopt turn structure strongly influences the stability of the folded sheet relative to any unfolded conformations.

EMAX2 contains three strands ( $S_1$ ,  $S_2$  and  $S_3$ ) comprised of 8, 6, and 7 residues respectively. Hecht *et al.* identified six-stranded  $\beta$ -sheets from a combinatorial library that self-assemble into monolayers.<sup>37, 40, 41</sup> A three-stranded sheet, as opposed to a sheet containing more strands, was employed in our design since it is the simplest of multi-strand sheets and design criteria exists in the literature for model, monomeric three-stranded sheets.<sup>42-47</sup> For these model systems, the number of residues contained within each strand varies from two to six (excluding the  $i^{\text{th}}$  residue of the turn region). In general, increasing the number of residues in a strand corresponds to an increase in overall sheet stability. However, increasing the number of strand residues beyond 6 in many model systems has diminishing returns with respect to the stability of the folded monomer.<sup>48</sup> In contrast, the number of residues contained in the strand regions of amyloid-forming proteins ranges from 2 to 32, with the median number of residues per strand being 7. We derived these statistics by assessing a limited number of proteins known to form amyloid whose pre-assembled structures are well-defined, namely transthyretin<sup>49</sup>,  $\alpha$ 1-antitrypsin<sup>50</sup>, AcP<sup>51</sup>, kappa I Bre<sup>52</sup>, Human Cystatin C<sup>53</sup>, OspA<sup>54</sup>, anti-thrombin<sup>55</sup> and Sup 35<sup>56</sup>. The structures of these proteins suggest that longer strands may have a greater propensity to self-assemble. Recent studies investigating the kinetics of polyglutamine assembly support this assertion<sup>57</sup>. Each strand of EMAX2 contains a sufficient number of residues to facilitate the formation of a stable sheet capable of ordered self-assembly.

Statistical analysis of the protein data bank shows that  $\beta$ -strand regions of proteins contain a disproportional amount of  $\beta$ -branched residues (valine, isoleucine

and threonine). The hydrophobic side chains of these residues prefer to adopt  $\chi_1$  rotamers that influence main chain dihedral angles and form inter-residue van der Waal interactions that stabilize  $\beta$ -sheet secondary structure. These residues have been used extensively in the design of monomeric sheets and are also found in many amyloid structures. EMAX2 contains  $\beta$ -strands composed of an alternating sequence of valine and lysine residues, high and moderately high propensity  $\beta$ -sheet residues, respectively.<sup>58</sup> The alternating pattern imparts amphiphilicity to the sheet that should promote self-assembly.<sup>41, 59</sup>

The relative positioning of the valine residues within each strand of EMAX2 is important not only to define the amphiphilic nature of the sheet but also to promote intermolecular association of EMAX2 along the sheet edges.<sup>40</sup> In general,  $\beta$ -branched residues prefer to adopt a trans  $\chi_1$  rotamer when contained in  $\beta$ -sheet structure. This defines the orientation of their side chains relative to the protein backbone. In designed monomeric systems,  $\beta$ -branched residues are often incorporated at non H-bonding positions within the strands that define the edges of the sheet. For example, for a three-stranded  $\beta$ -sheet, this would be the first and the third strand. At non-hydrogen bonding positions, the side chains of  $\beta$ -branched residues are projected into the interior of the sheet away from solvent. This facilitates the formation of *intramolecular* van der Waals interactions between side chains of residues on a given face of the sheet and helps define the monomeric structure. However, when  $\beta$ -branched residues are incorporated at hydrogen bonding positions

in edge strands, their side chains are projected away from the edge of the sheet into the solvent. This enables intermolecular interactions to take place between the edge strands of distinct sheets and helps to facilitate self-assembly, Figure 4.1(b).<sup>60</sup> The first strand of EMAX2 ( $S_1$ ) contains valines at hydrogen-bonded positions to foster edge-to-edge inter-sheet interactions. However, in the third strand ( $S_3$ ), the valines had to be incorporated at non-hydrogen bonded positions to maintain strand registry and sheet amphiphilicity.

The  $\beta$ -turn regions of EMAX2 were designed to ensure main chain reversal at distinct locations, define the strand registry and strand trajectory.<sup>61</sup> Although type I and type II  $\beta$ -turns are found most commonly in proteins, it is their mirror image turns, type I' and II' turns, that dominate in sheet-rich structures. These turns have a right-handed twist, with a larger twist angle for type I' relative to the flatter type II' turns.<sup>62-64</sup> Type II' turns were designed to connect the strands of EMAX2, rather than type I', to limit sheet twist and favor the formation of ideal intra and intermolecular hydrogen bonds. Strands  $S_1$ - $S_2$  and  $S_2$ - $S_3$  are connected by the tetrapeptide sequences,  $-V^D P^L P T-$  and  $-K^D P^L P K-$  respectively. Both turns contain a central  $^D P^L P$  dipeptide unit at the  $i+1$  and  $i+2$  positions. Structure-based studies have shown that incorporating D-stereoisomers at the  $i+1$  position enforces dihedral angles consistent with both type I' and II' turn formation.<sup>65</sup> However, NMR and X-ray crystallographic studies have shown that when  $^L$ Pro accompanies  $^D$ Pro at the  $i+2$  position, a type II' turn is strongly favored.<sup>65, 66</sup> Valine was incorporated at the  $i$  position of the first turn to enforce a trans-prolyl amide bond geometry at the  $i+1$

position to facilitate turn formation<sup>67,68</sup> as well as to maintain the amphiphilicity of the sheet. A threonine residue was included at the  $i+3$  position based on its high propensity to occupy this position in type II' turns found in naturally occurring proteins.<sup>69</sup> Threonine can form a stabilizing side chain-main chain hydrogen bond between its alcoholic proton and the carbonyl oxygen of the  $i^{\text{th}}$  residue of the turn. In addition, the threonine residue also preserves the amphiphilic nature of the three-stranded sheet. In the second  $\beta$ -turn (-K<sup>D</sup>PPK-), lysine residues were included at the  $i^{\text{th}}$  and  $i+3$  positions. Although, statistical analysis of  $\beta$ -turn residues in proteins has shown that lysine has only a moderate propensity to occupy these positions,<sup>70</sup> they were included to maintain the strand registry and hydrophilic facial amphiphilicity in that region of the sheet.

On folding, the sequential organization of the residues in the  $\beta$ -strands of EMAX2 is designed to impart amphiphilicity to the faces of the three-stranded  $\beta$ -sheet. The amphiphilic nature of the folded peptide should favor facial association resulting in the burial of the valine-rich face to form a bilayer-like structure with the lysine-rich face solvent exposed.<sup>71</sup> Concurrently, the unfulfilled H-bond donors and acceptors along the  $\beta$ -strand edges of the folded  $\beta$ -sheet should promote lateral intermolecular H-bond formation with other folded  $\beta$ -sheets.<sup>41</sup> This model predicts that folding and self-assembly leads to the formation of a fibrillar network where each fibril consists of a bilayer of H-bonded EMAX2 peptides.<sup>72-77</sup> Although folding and

self-assembly are discussed as separate events, it is likely that these events have linked equilibria.<sup>71</sup> For example, folding could take place at the surface of a growing fibril.

## **4.2 Folding, Self-assembly and Bulk Material Properties of a *De Novo* Designed Three-Stranded $\beta$ -sheet Hydrogel**

### **4.2.1 Temperature Triggered Folding and Self-Assembly**

EMAX2 is designed to undergo triggered folding and self-assembly to promote hydrogel formation in response to an increase in temperature. Circular Dichroism (CD) spectroscopy was used to assess the folded state of EMAX2 as a function of temperature. The inset in Figure 4.2(a) shows a wavelength spectrum of EMAX2 at 10 °C in pH 9.0 buffer of low ionic strength (10 mM NaCl). The minimum at 198 nm is indicative of random coil structure and indicates that EMAX2 is unfolded. Under these conditions, a majority of the lysine side chains are protonated and EMAX2 remains unfolded to minimize electrostatic repulsion. In addition, water can better solvate the hydrophobic side chains of the valine residues at this low temperature than at higher temperatures.<sup>78, 79</sup> However, when the temperature is increased to 37 °C, the wavelength spectrum shows that EMAX2 adopts  $\beta$ -sheet rich structure as indicated by formation of a clear minimum at 216 nm and a maximum at 196 nm.<sup>29</sup> Raising the temperature most likely promotes the hydrophobic effect and results in desolvation of the valine side chains.<sup>78, 79</sup> In response, EMAX2 folds and

self-assembles to shield these side chains from water. The temperature at which this transition takes place was determined by monitoring the mean residual ellipticity at 216 nm as a function of temperature. The data in Figure 4.2(a) show that EMAX2 begins to fold and assemble at approximately 20 °C. The CD data was collected using 150  $\mu$ M solutions of EMAX2 to facilitate spectroscopic measurements. At this low concentration, EMAX2 is incapable of forming a rigid hydrogel but still folds and self-assembles to form sheet-rich assemblies.

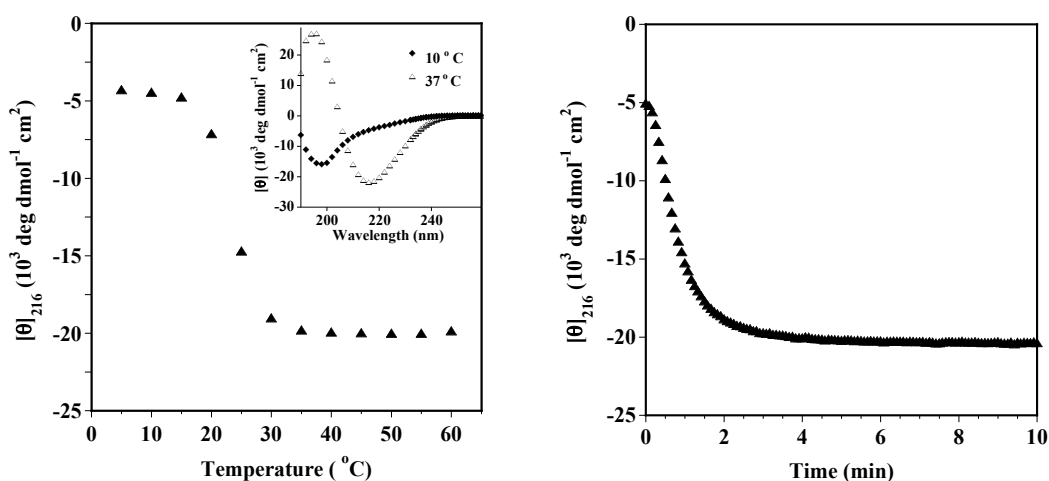


**Figure 4.2 (a) CD spectroscopy of 150  $\mu$ M EMAX2 solution at pH 9.0 (125 mM borate, 10 mM NaCl) showing  $[\theta]_{216}$  as a function of temperature. (Inset) Wavelength spectra of 150  $\mu$ M EMAX2 solution at pH 9.0 showing transition from random coil at 10 °C ( $\blacklozenge$ ) to  $\beta$ -sheet at 37 °C ( $\triangle$ ). (b)  $[\theta]_{216}$  measured as a function of time (150  $\mu$ M EMAX2, pH 9.0, 37 °C).**

The rate at which EMAX2 folds and assembles was assessed by measuring the onset of  $[\theta]_{216}$  at 37 °C as a function of time as shown in Figure 4.2(b). This temperature was chosen based on the data in Figure 4.2(a) that shows that EMAX2 is capable of complete folding and self-assembly at this temperature. The majority of  $\beta$ -sheet formation occurs within the first 2 minutes with minimal changes after 4 minutes suggesting that at higher peptide concentrations, temperature triggered gelation should be fairly rapid.<sup>80</sup>

#### 4.2.2 Temperature Triggered Hydrogelation

Higher concentrations of EMAX2 than those used for spectroscopic measurements in Figure 4.2 are capable of undergoing triggered folding and self-assembly leading to hydrogel formation. The data in Figure 4.3(a) shows oscillatory shear rheological measurements of 1 wt% (2.12 mM) EMAX2 at pH 9.0 (10 mM NaCl). A dynamic time sweep experiment is shown in which the evolution of the storage modulus ( $G'$ , a material's elastic response to strain, which is indicative of its rigidity) is monitored as a function of time. Here, hydrogelation is triggered by increasing the temperature from 5 °C to either 37 °C or 50 °C. When gelation is triggered at 37 °C, EMAX2 forms a self-supporting gel (~1000 Pa) within about 10 minutes that further stiffens with time. After 60 minutes, the EMAX2 hydrogel reaches an apparent equilibrium storage modulus of  $1750 \pm 200$  Pa. When gelation is triggered at 50 °C, EMAX2 folds and assembles much more quickly producing a

substantially more rigid material. After 10 minutes, a  $G'$  of about 3000 Pa is realized with the gel stiffening further with time ( $G' = 4700 \pm 500$  Pa at 60 minutes). The increase in gelation kinetics may be due to an increase in the rate of desolvation of hydrophobes at higher temperatures. It is clear from the data in Figure 4.3(a) that more rigid hydrogels are formed at higher triggering temperatures. This could be due to morphological differences in the fibrillar networks formed at different temperatures. For example, more physical crosslinks in the network may be formed when the gel is formed at the higher temperature. Alternatively, the overall morphologies of the gels formed at different temperatures could be similar but intermolecular interactions that are temperature-dependent and help define the network, such as hydrophobic interactions, could be enhanced resulting in the higher modulus. These possibilities were investigated by performing an experiment where a 1 wt% EMAX2 gel was first formed at 37 °C and then the temperature increased to 50 °C. If  $G'$  increases to the magnitude of that of a gel initially formed at 50 °C, this would suggest that intermolecular temperature-dependent interactions are being enhanced at higher temperatures. The data in Figure 4.3(b) shows that when the temperature is increased from 37 °C to 50 °C, an intermediate increase in  $G'$  is realized. This suggests that when gels are initially formed at higher temperatures, changes in network morphology and temperature-dependent interactions may be contributing to the higher storage modulus. At any rate, control over fabrication of gels with varying rigidities could prove to be beneficial in tissue regenerative applications where material stiffness influences cell behavior.<sup>81</sup> Frequency sweep measurements of EMAX2 hydrogels

formed at 37 °C and 50 °C show that the  $G'$  values are an order of magnitude higher than  $G''$  (the loss modulus,  $G''$ , a material's viscous response to strain) and that  $G'$  is insensitive to frequency, [Figure 4.3(c) and 4.3(d)].

Fourier transform infrared spectroscopy (FT-IR) was used to investigate the secondary structure of EMAX2 in the self-assembled, gelled state. Figure 4 shows an FTIR spectrum of 1 wt% EMAX2 hydrogel formed at 37 °C. The amide I' band is centered at  $1615\text{ cm}^{-1}$ , indicative of  $\beta$ -sheet structure.<sup>29, 74, 82, 83</sup> A weaker band at  $1680\text{ cm}^{-1}$  is also observed often associated with an anti-parallel  $\beta$ -sheet arrangement.<sup>83, 84</sup> Taken together, the rheological and FTIR data show that EMAX2 forms visco-elastic hydrogels composed of self-assembled  $\beta$ -sheets.

Hydrogels formed by self-assembly do not contain covalent crosslinks, which are often needed to form hydrogels from traditional synthetic polymers.<sup>85-89</sup> As such, self-assembled gels may exhibit shear-recovery behavior. Here, the application of shear stress to the hydrogel can result in the disruption of some of the physical crosslinks that define the gel network. This converts the mechanically rigid gel into a low viscosity gel capable of flow. However, when the shear stress is removed, the physical crosslinks reform and the gel recovers its mechanical rigidity. Figure 4.5(a) shows dynamic strain sweep data for a 1 wt% EMAX2 hydrogel formed at 37 °C (pH 9, 10 mM NaCl). Here,  $G'$  and  $G''$  are monitored as a function of increasing strain and the material yields at an applied strain of ~15 %. However, upon the removal of applied strain, the disrupted hydrogel recovers its mechanical rigidity over time.

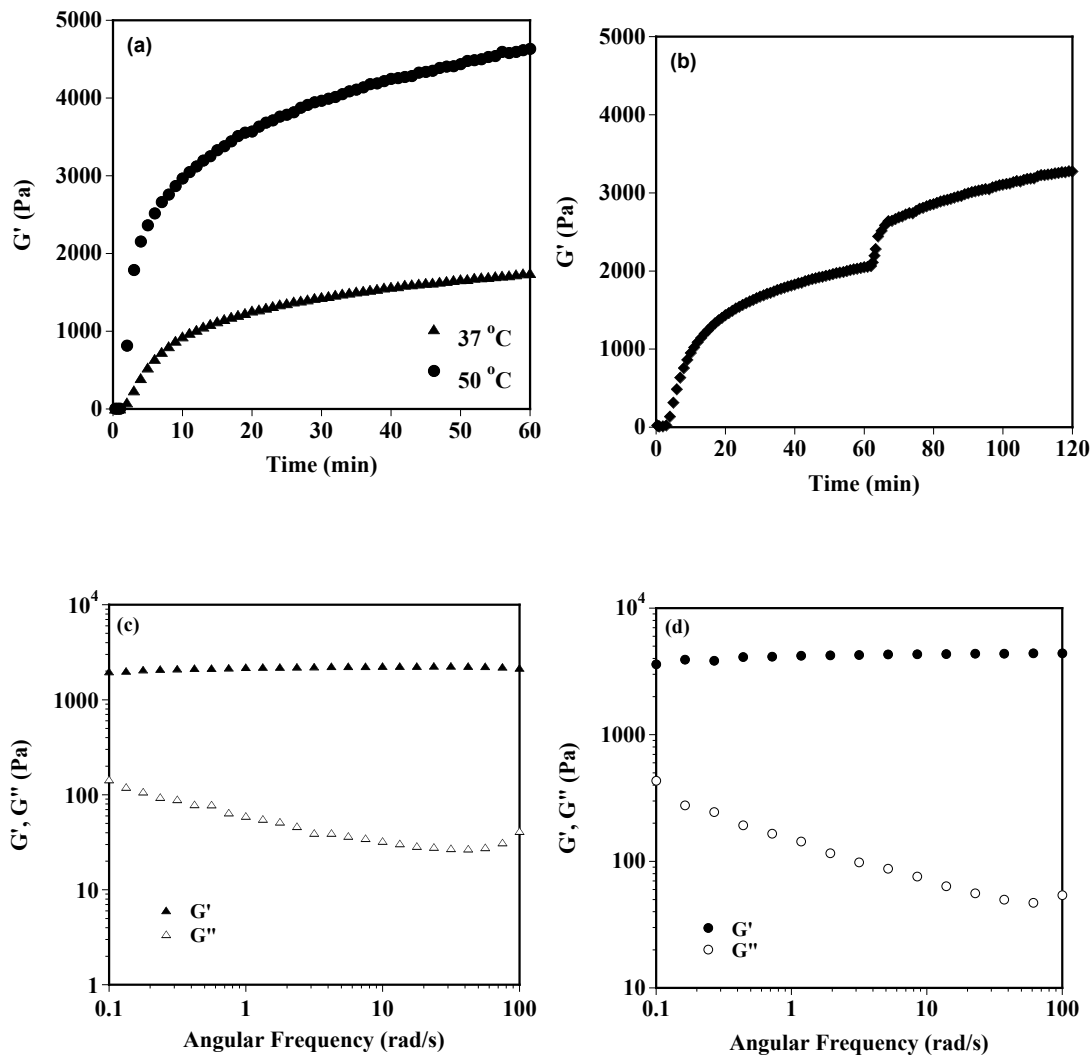


**Figure 4.3 (a)** Dynamic time sweep of 1 wt % EMAX2 at pH 9 (125 mM borate, 10 mM NaCl) showing the evolution of storage modulus ( $G'$ ) as a function of time at 37 °C [▲] or 50 °C [●]. **(b)** Dynamic time sweep of 1 wt % EMAX2 at pH 9 showing the change in storage modulus upon increasing the temperature from 37 to 50 °C after 60 min of gelation at 37 °C. Dynamic frequency sweep of 1 wt % EMAX2 at pH 9 (125 mM borate, 10 mM NaCl) at **(c)** 37 °C and **(d)** 50 °C.

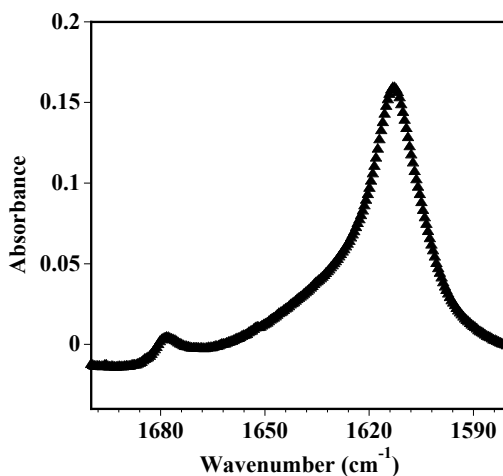


**Figure 4.4 Fourier transform infrared spectroscopy of 1 wt % EMAX2 at pH 9.0 showing  $\beta$ -sheet structure at 37 °C.**

Figure 4.5(b) shows a time sweep experiment where a EMAX2 hydrogel is initially formed at 37 °C. After 60 minutes, 1000% strain is applied to the gel for three minutes (arrow in figure) to shear thin the material as evident by an instantaneous decrease in  $G'$ . After shear-thinning, the strain is decreased to 0.2 % and the recovery of  $G'$  is measured as a function of time. The data shows that EMAX2 recovers its mechanical rigidity via a rapid phase of recovery, wherein around 50 % of its original mechanical rigidity is recovered in the first 25 seconds. This is followed by a slower recovery phase in which the gel quantitatively recovers its original rigidity within an hour. This type of behavior may prove beneficial in the development of injectable hydrogel materials that can be delivered with spatial resolution from a syringe.<sup>18</sup>

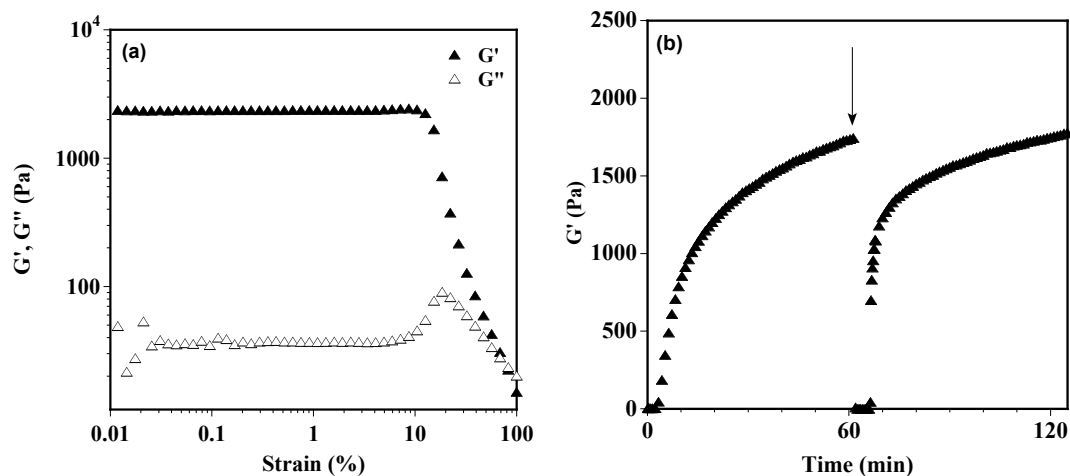


**Figure 4.5. (a) Dynamic strain sweep of 1 wt % EMAX2 hydrogel formed at pH 9.0, 37 °C. (b) Shear-thinning and recovery profile of 1 wt % EMAX2 hydrogel at pH 9.0, 37 °C.**

EMAX2 is designed to fold and self-assemble into fibrils which constitute the hydrogel network. Small Angle Neutron Scattering (SANS) experiments were employed to investigate the nanoscale structure of the fibrils formed during hydrogelation. SANS data collected on 0.5 wt% EMAX2 gels formed at 37 °C is shown in Figure 4.6(a) where the scattering intensity is plotted as function of the scattering vector and fit using a cylindrical form factor.<sup>77</sup> The goodness of fit suggests that EMAX2 assembles into well-defined rod-like fibrils. The inset shows a modified Guinier analysis that was used to calculate the average cross-sectional diameter of the fibrils that constitute the EMAX2 hydrogel network. This analysis provided an average fibril diameter of  $31.0 \pm 1.0 \text{ \AA}$  ( $3.1 \pm 0.1 \text{ nm}$ ), which is in excellent agreement with the computationally measured width of one folded EMAX2 sheet. Transmission

electron microscopy (TEM) was also performed and is consistent with the SANS analysis, Figure 4.6(b).

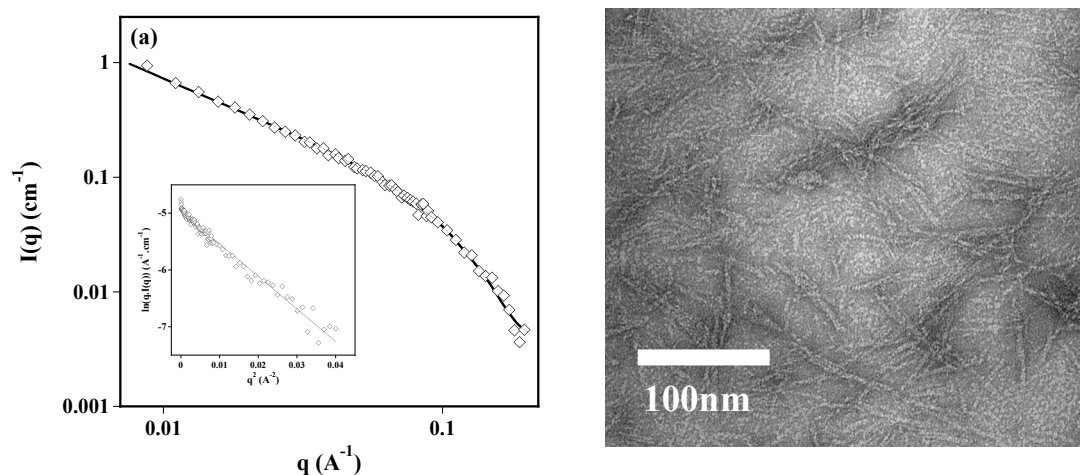


**Figure 4.6 (a) SANS data of 0.5 wt % EMAX2 hydrogel at pH 9.0 (125 mM Borate, 10 mM NaCl in D<sub>2</sub>O) collected at 22 °C after 2 h of gelation at 37 °C. (b) TEM micrograph of 1 wt% EMAX2 at pH 9.0 (125 mM Borate, 10 mM NaCl), 37 °C. (SANS data collected by Tuna Yucel and TEM data collected by Matthew Lamm)**

The spectroscopic, microscopic and scattering experiments suggest that EMAX2 undergoes triggered intramolecular folding and self-assembly to form well-defined  $\beta$ -sheet rich fibrils. The rheological data indicates that the fibrils are non-covalently crosslinked to form a visco-elastic hydrogel capable of shear-recovery at pH 9.

### 4.2.3 Triggered Folding, Self-Assembly and Hydrogelation under Physiologically-relevant Conditions

Although 1 wt% aqueous preparations of EMAX2 are capable of undergoing thermally-induced gelation at pH 9 and low ionic strength (10 mM NaCl), biomedical applications may necessitate that gels be formed at physiological conditions. At pH 9, although most of the lysine side chains are protonated, a small population is deprotonated, limiting the unfavorable electrostatic interactions that must be overcome for folding and self-assembly to occur. At pH 7.4, it is likely that all of the lysine side chains are protonated, making EMAX2 folding and assembly more difficult even at higher temperatures. However, increasing the concentration of NaCl in the buffer solution screens the lysine-derived charge making thermally-triggered folding possible. Figure 4.7(a) monitors the extent of  $\beta$ -sheet formation via CD ( $[\theta_{216}]$ ) as a function of NaCl concentration for 2 wt% (4.24 mM) solutions of EMAX2 at pH 7.4 and 37 °C. At low ionic strength (up to 10 mM NaCl), EMAX2 remains unfolded due to inefficient screening of the positively charged lysines. But, raising the NaCl concentration (> 10 mM NaCl) favors folding and self-assembly of EMAX2 by attenuating the charge repulsion that must be overcome. The data shows that at a concentration of 2 wt%, EMAX2 is capable of folding and assembly at physiological conditions (pH 7.4, 150 mM NaCl, 37 °C). A higher concentration of EMAX2 (2 wt%) was employed for these studies since 1 wt% EMAX2 solutions formed only weak gels under these buffer conditions. TEM micrographs of diluted gel shows that EMAX2 assembles into fibrils that consistently measure 3 nm in width.

This value is consistent with the measurements obtained for 1 wt% EMAX2 hydrogels prepared at pH 9 (10 mM NaCl). Therefore, irrespective of the solution conditions and exact temperature used to trigger gelation, EMAX2 assembles to give fibrils of similar nanoscale structure.

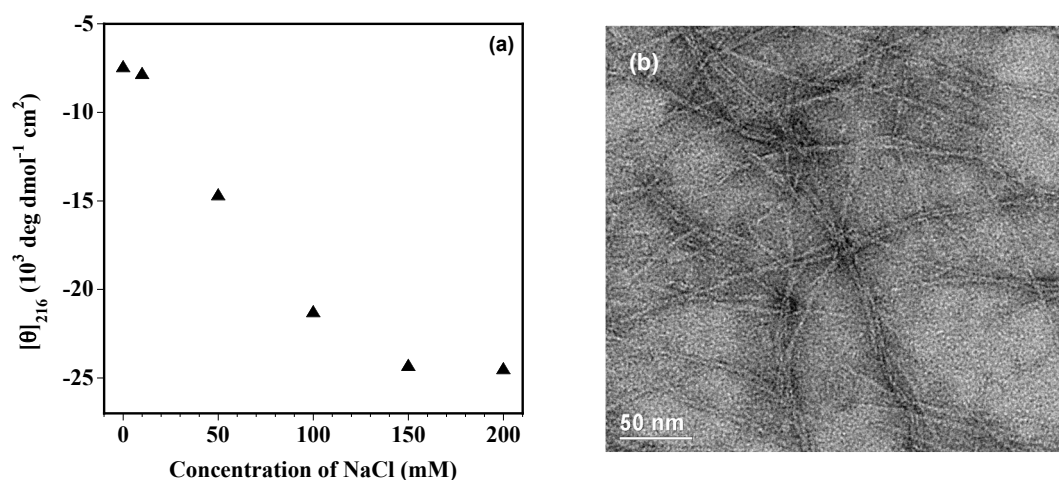


**Figure 4.7 (a)  $[\theta]_{216}$  is measured as a function of NaCl concentration for 2 wt % EMAX2 preparations at pH 7.4 (50 mM BTP) at 37 °C. (b) TEM micrograph of 1 wt% EMAX2 hydrogel formed at pH 7.4 (50 mM BTP, 150 mM NaCl), 37 °C. (TEM data collected by Matthew Lamm)**

To fabricate peptide-based hydrogels for biomedical applications, hydrogelation of EMAX2 can be initiated with cell culture media, such as Dulbecco's Modified Essential Medium (DMEM), which contains about 160 mM mono and divalent salts.<sup>90, 91</sup> Using cell culture media instead of saline facilitates formation of a hydrogel that contains cellular nutrients. The rate at which 2 wt% EMAX2 folds and assembles on addition of the cell culture media was assessed by CD where the onset of

$[\theta]_{216}$  at 37 °C was measured as a function of time, Figure 4.8. The majority of  $\beta$ -sheet formation occurs within the first 3 minutes with minimal changes occurring after 5 minutes suggesting that EMAX2 may undergo rapid hydrogelation under cell culture conditions.

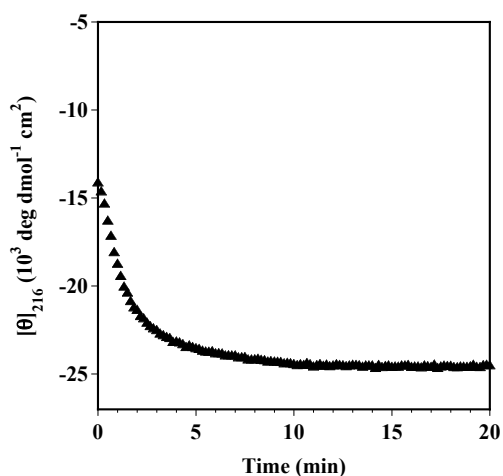


**Figure 4.8**  $[\theta]_{216}$  measured as a function of time for 2 wt % EMAX2 at pH 7.4 (DMEM) at 37 °C.

The kinetics of gelation can also be assessed rheologically. Figure 4.9(a) compares the onset of EMAX2 gelation using DMEM cell culture media versus pH 9 buffer. Two wt% EMAX2 at pH 7.4 (DMEM) is gelled by increasing the temperature from 5 °C to 37 °C. EMAX2 forms a rigid hydrogel ( $\sim 2500$  Pa) within 10 minutes, which further stiffens over time. After 60 minutes, 2 wt% EMAX2 hydrogel acquires a storage modulus of  $8500 \pm 1250$  Pa. In comparison, a 2 wt% solution of EMAX2 was gelled at pH 9 (10 mM NaCl). The data shows that EMAX2 exhibits faster gelation kinetics at pH 9.0 as compared to pH 7.4 (DMEM). For example, 2 wt% EMAX2 at

pH 9.0 forms a rigid hydrogel with a storage modulus ( $G'$ ) of  $\sim 475$  Pa within 1 min after initiating gelation whereas the DMEM sample exhibits a storage modulus ( $G'$ ) of  $\sim 20$  Pa in the same time. Although EMAX2 folds and assembles slower in DMEM cell culture media, the final hydrogel formed is of nearly the same mechanical rigidity [at pH 9,  $G' = 9000 \pm 300$  Pa and at pH 7.4 (DMEM),  $G' = 8500 \pm 1250$  Pa] [Figure 4.9(a)]. Dynamic frequency sweeps of 2 wt% EMAX2 hydrogels (pH 9 and DMEM) also showed that the storage modulus ( $G'$ ) is independent of frequency suggesting formation of rigid non-covalent crosslinks (data not shown).

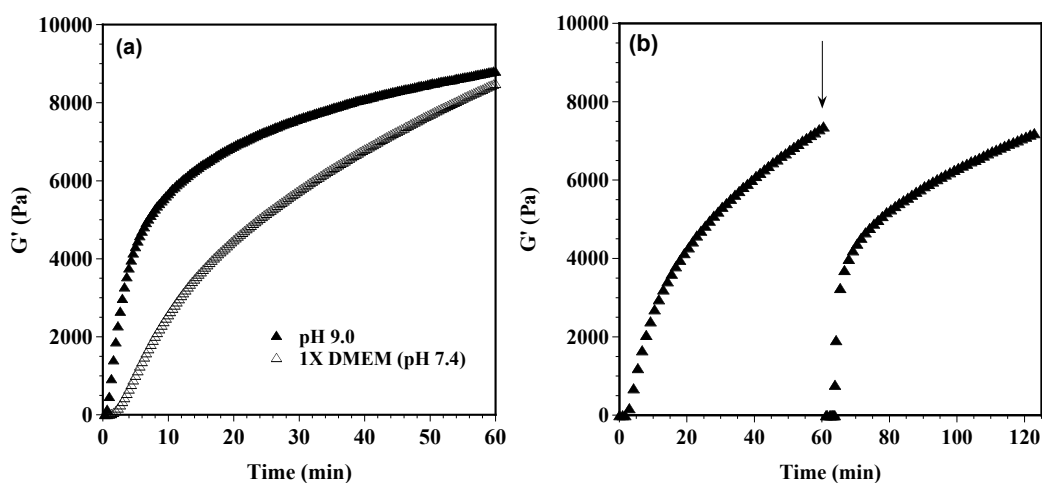


**Figure 4.9 (a) Dynamic time sweep of 2 wt % EMAX2 at pH 9.0 (125 mM Borate, 10 mM NaCl) [▲] and pH 7.4 (DMEM) [△] monitoring  $G'$  at 37 °C as a function of time. (b) Shear-thinning and recovery profile of 2 wt % EMAX2 hydrogel at pH 7.4 (DMEM) and 37 °C.**

As shown earlier, 1 wt% EMAX2 hydrogels formed at pH 9 exhibit shear-recovery behavior. We examined the ability of 2 wt% EMAX2 hydrogels formed via

DMEM to shear-thin and recover. Figure 9(b) shows a time sweep experiment that monitors the initial formation of a EMAX2 hydrogel after the temperature is raised from 5 °C to 37 °C. After 60 minutes of gelation time, a 1000 % strain is applied for 3 min (arrow), which disrupts the network indicated by a sudden decrease in  $G'$ . After which, the applied strain is reduced to 0.2 % and the hydrogel recovery monitored over time. The data show that EMAX2 exhibits a rapid recovery phase wherein about 40% of its original rigidity is recovered within the first 25 seconds. EMAX2 recovers about 90% of its mechanical rigidity within an hour. This data suggests that the EMAX2 hydrogel can be delivered by shear-thinning via syringe to a target site where it recovers the bulk of its mechanical rigidity.

#### **4.2.4 Cytocompatibility of EMAX2 Hydrogels**

Compatibility of the hydrogel surface towards mammalian cells was assessed. Figure 4.10(a) shows a live/dead assay where C3H10t1/2 mesenchymal stem cells were seeded onto the gel following hydrogelation and equilibration with Dulbecco's modified Eagle medium (DMEM) at pH 7.4. This cell line was chosen because they are very sensitive to their environment and provide a rigorous assessment of the hydrogel surface with respect to cell viability. Cells were cultured in the presence of serum on the EMAX2 surface for 24 hrs, which is sufficient time to allow cells to adhere and adopt healthy morphologies through formation of actin stress fibers. Figure 4.10(a) shows a laser scanning confocal microscopy (LSCM) image of

cells cultured on the surface of 2 wt% EMAX2 hydrogels after fluorescent dyes have been added that specifically dye living cells (green) and dead cells (red). Also, shown for comparisons are cells that have been cultured onto a tissue culture treated polystyrene (TCTP) control surface under identical conditions [Figure 4.10(b)].

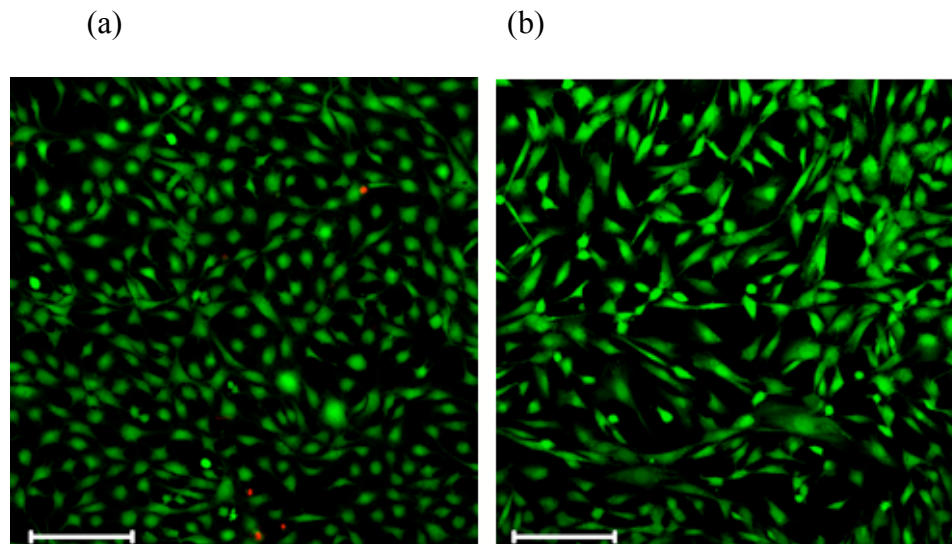


**Figure 4.10 Cellular viability of C3H10t1/2 mesenchymal stem cells after 24 h cultured on (a) 2 wt % EMAX2 hydrogel; (b) TCTP control. LSCM images showing live/dead assays, scale bar is 200  $\mu\text{m}$ . Green = live cells, red = dead cells.  $N = 3$ . (Data collected by Daphne A. Salick)**

These experiments demonstrate that EMAX2 hydrogels are non-cytotoxic to C3H10t1/2 cells. Figure 4.11 shows an image of cells that have been stained with both a DNA-specific fluorescent dye (4', 6-diamidino-2-phenylindole, blue) and a fluorescent dye specific for F-actin (Alexa fluor 488 phalloidin, green). Cells undergoing surface adhesion events form F-actin-containing stress fibers, lamelopodia

and filopodia, which assist in defining the cellular morphology and aid in locomotion.<sup>92</sup> In Figure 4.11, the inset shows a magnified view where the formation of lamellipodia (flattened projections from cells), filopodia (thin extensions from cells) and ruffled cellular membranes are more clearly observed. Ruffled membranes or edges indicate migration of cells as they traverse across the surface of the hydrogel. Collectively, the LSCM data substantiate that EMAX2 hydrogel surfaces are noncytotoxic, support cell adhesion and allow cellular migration.

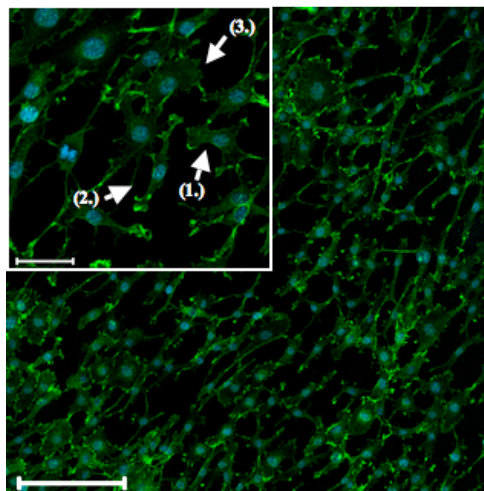


**Figure 4.11 LSCM images of C3H10t1/2 mesenchymal stem cells on the surface of 2 wt % EMAX2 hydrogel after 24 h. Green fluorescence shows Actin where blue fluorescence shows nuclear staining for reference. Scale bar = 200  $\mu\text{m}$ . Inset shows distinct Actin features where arrows show lamellipodium (1) and fillipodium (2). Ruffling of the cellular membrane can be seen as denoted by (3). Scale bar = 50  $\mu\text{m}$ . (Data collected by Daphne A. Salick)**

#### 4.2.5 Conclusions

EMAX2, a three-stranded  $\beta$ -sheet, was designed to undergo thermally triggered folding and self-assembly to afford mechanically rigid hydrogels. The peptide remains unfolded at lower temperatures but folds and self-assembles into  $\beta$ -sheet rich fibrils upon raising the temperature of the aqueous solutions at pH 9.0 or pH 7.4 (150mM NaCl) to form mechanically rigid hydrogels. EMAX2 self-assembles into monodispersed fibrils measuring  $\sim 3$  nm in width, which corresponds to the width of the peptide in its folded state. Oscillatory rheology demonstrates that gelation temperature as well as peptide concentration can be employed to modulate the mechanical properties of the hydrogels. Experiments in which mesenchymal stem cells were cultured on the gel surface for 24 h show that the surface is non-cytotoxic and allows cells to adopt typical morphologies. In addition, EMAX2 gels exhibit shear recovery properties and show promise as injectable biomaterials. This work demonstrates that design principles and structural considerations from both, non-assembling *de novo* designed  $\beta$ -sheets and naturally occurring self-assembling proteins, can be employed as a useful resource to create responsive functional materials.

### 4.3 Comparing the Self-Assembly and Material Properties of a Three-Stranded Peptide (EMAX2) and a $\beta$ -Hairpin Peptide (MAX1)

In the last section, the self-assembly and material properties of EMAX2, a model three-stranded amphiphilic peptide sequence, was presented. Structurally, EMAX2 is an extension of MAX1, a well-characterized self-assembling  $\beta$ -hairpin peptide discussed in chapter 1, Figure 4.12. EMAX2 comprises of an additional turn region (-K<sup>D</sup>P<sup>L</sup>PK-) as well as a  $\beta$ -strand strand ( $S_3$ ) compared to MAX1. The objective of this section is to compare the material properties of MAX1 and EMAX2 due to their respective designs.

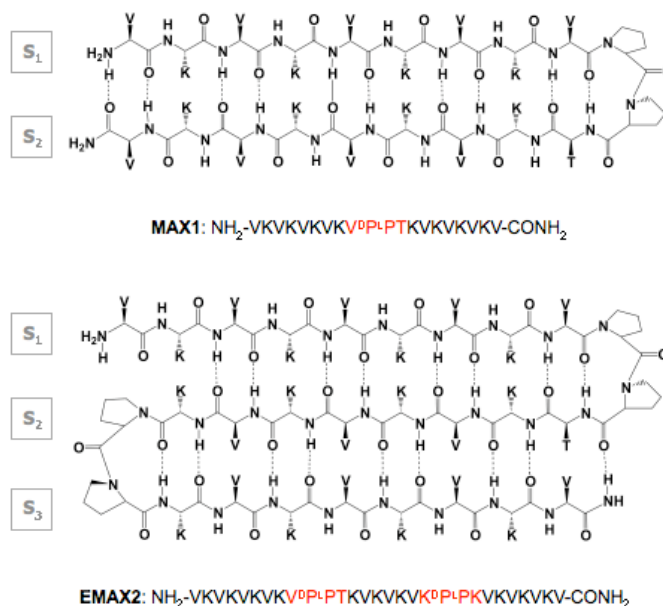


**Figure 4.12 Structure and sequence of MAX1 and EMAX2**

## Results and Discussion

### 4.3.1 Temperature Triggered Folding and Self-Assembly

Circular Dichroism (CD) spectroscopy was used to assess the formation of  $\beta$ -sheet secondary structure of both MAX1 and EMAX2 peptides in pH 9 buffer (125 mM borate, 10 mM NaCl) as a function of temperature. The temperature dependent  $\beta$ -sheet formation is followed by monitoring the mean residual ellipticity at 216 nm, which is indicative of  $\beta$ -sheet structure, as a function of temperature. The data in Figure 4.13(a) shows that both MAX1 and EMAX2 form  $\beta$ -sheet structure with an increase in temperature and exhibit marginally different folding transitions. The EMAX2 peptide exhibits a slightly lower folding transition temperature of  $\sim 25$  °C as compared to  $\sim 30$  °C for MAX1. Similarly, pH dependent  $\beta$ -sheet formation is monitored by measuring the mean residue ellipticity at 216 nm as a function of pH of the peptide solutions. Figure 4.13(b) shows that both MAX1 and EMAX2 form  $\beta$ -sheet structure at pH values greater than 8 at 40 °C. Although EMAX2 has a higher charge state of +13 (12 lysines and 1 N-terminus) compared to +9 for MAX1, there is no difference in its pH dependence. Therefore, at pH 9 solution conditions, the differences in self-assembly behavior of EMAX2 may be arising due to its overall hydrophobicity and thus its temperature dependent hydrophobic interactions. At such low concentrations (150  $\mu$ M), MAX1 and EMAX2 are incapable of forming a hydrogel but still fold and self-assemble to form  $\beta$ -sheet-rich structures.

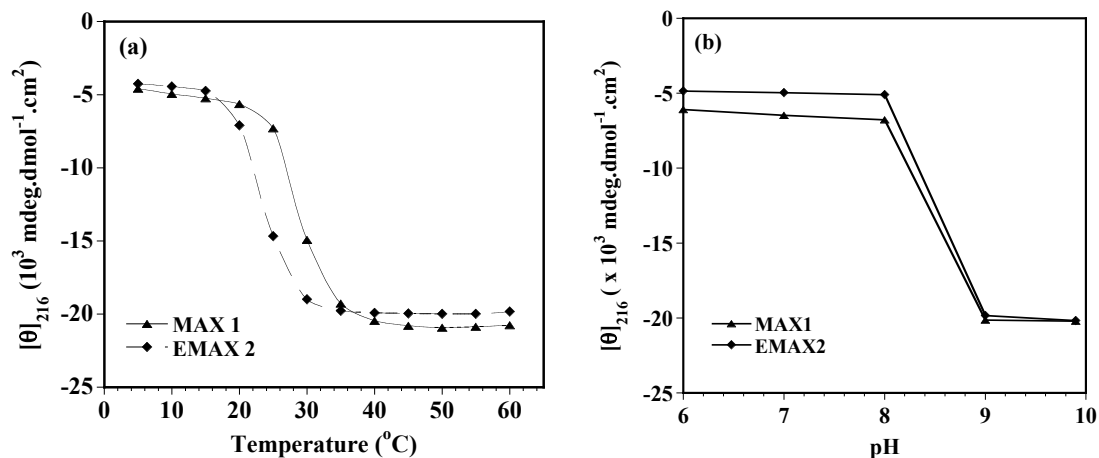


**Figure 4.13** CD spectroscopy of 150  $\mu\text{M}$  solutions of MAX1 and EMAX2 showing (a) temperature dependent  $\beta$ -sheet formation at pH 9.0 and (b) pH dependent  $\beta$ -sheet formation at 40  $^{\circ}\text{C}$  monitored at 216 nm.

Furthermore, the rate of  $\beta$ -sheet formation can be assessed by monitoring change in ellipticity at ( $\theta_{216}$ ) at 37  $^{\circ}\text{C}$  as a function of time, Figure 4.14. This temperature was selected based on data in Figure 4.13(a), which shows that the peptides are capable of achieving complete  $\beta$ -sheet formation at this temperature. As shown in Figure 4.14, EMAX2 exhibits moderately faster kinetics of  $\beta$ -sheet formation than MAX1.

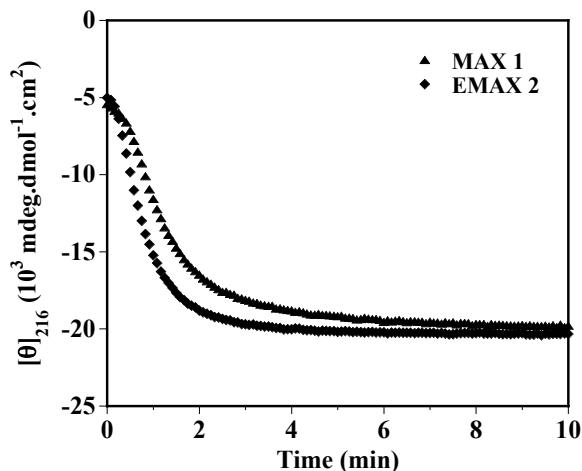


**Figure 4.14 Kinetics of  $\beta$ -sheet formation monitored by measuring  $[\theta]_{216}$  as a function of time (150  $\mu$ M MAX1 and EMAX2 solution at pH 9, 37  $^{\circ}$ C)**

We have previously shown that peptides exhibiting faster kinetics of  $\beta$ -sheet formation yield more rigid hydrogels.<sup>18</sup> Therefore, based on data shown in Figure 4.14, EMAX2 peptide would be expected to form slightly more rigid hydrogels.

### 4.3.2 Temperature Triggered Hydrogelation

Figure 4.15. shows the bulk material rheological properties of 1 wt% peptide hydrogels at pH 9 and 37  $^{\circ}$ C. Figure 4.15(a) shows the kinetics of hydrogel formation monitored by measuring the evolution of storage modulus ( $G'$ ) and loss modulus ( $G''$ ) as a function of time. In this experiment, the temperature of the peptide solutions is increased from 5  $^{\circ}$ C to 37  $^{\circ}$ C in 100 sec to trigger gel formation and then

allowing gel formation to occur for 60 minutes at 37 °C. The data shows that EMAX2 forms a more rigid hydrogel with an apparent equilibrium storage modulus of  $1750 \pm 200$  Pa compared to MAX1, which attains an apparent equilibrium storage modulus of  $1000 \pm 100$  Pa after one hour.

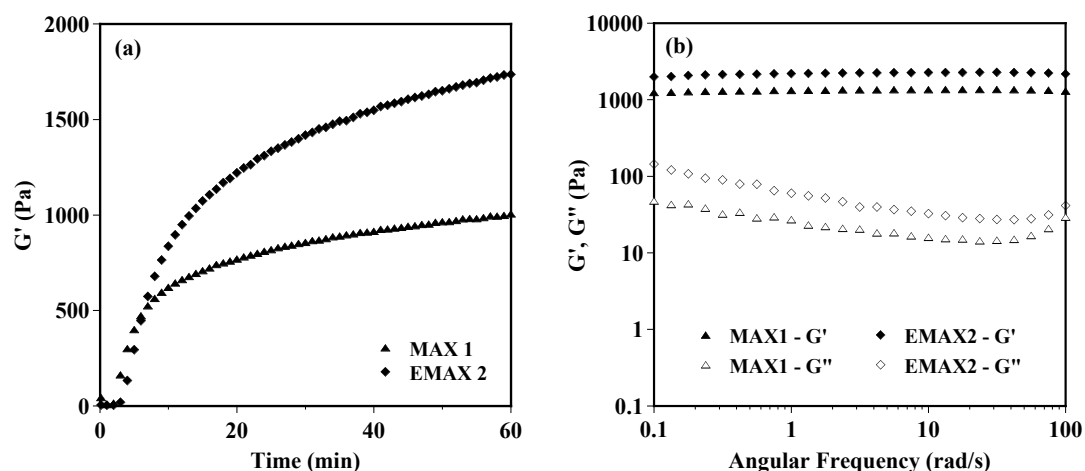


**Figure 4.15 Mechanical properties of 1 wt% MAX1 and EMAX2 at pH 9.0 and 37 °C**

Frequency sweep data [Figure 4.15(b)] of MAX1 and EMAX2 at 37 °C shows that  $G'$  is insensitive to a range of frequencies, which indicates that the gels are formed as a result of permanent cross-links.

The folding and subsequent self-assembly events of the peptides can also be confirmed by FTIR spectroscopy. As shown in Figure 4.16, analysis of the amide I' band of the 1 wt% peptide hydrogels at pH 9, incubated at 37 °C for 10 minutes, shows predominantly  $\beta$ -sheet secondary structure as indicated by the characteristic

peak at  $1615\text{ cm}^{-1}$  and a small shoulder at about  $1680\text{ cm}^{-1}$  (possible indication of an antiparallel  $\beta$ -sheet structure). These characteristic IR bands are observed for both MAX1<sup>29</sup> and EMAX2 since they both form  $\beta$ -sheet secondary structure in the self-assembled state.

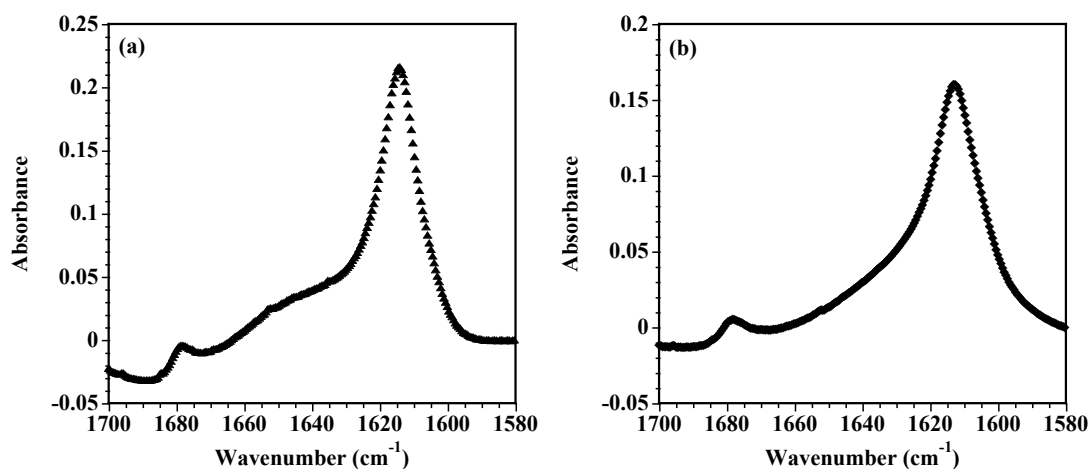


**Figure 4.16** Fourier transform infrared spectroscopy of (a) 1 wt% MAX1 and (b) 1 wt% EMAX2 at pH 9.0 showing  $\beta$ -sheet structure at  $37\text{ }^{\circ}\text{C}$

Both MAX1 and EMAX2 are designed to undergo triggered folding and self-assembly to form physically crosslinked hydrogels, which are capable of shear recovery. Figure 4.17 shows a time sweep experiment where 1wt% peptide hydrogel is initially formed at pH 9 and  $37\text{ }^{\circ}\text{C}$ . After 60 minutes of gelation, 1000% strain is applied to the gel for 3 minutes to shear thin the material as evident by instantaneous decrease in storage modulus. Thereafter, the strain is decreased to 0.2% and the recovery is measured as a function of time. The data in Figure 4.17 shows that both

MAX1 and EMAX2 quantitatively recover their original mechanical rigidity within an hour. Therefore, both MAX1 and EMAX2 show potential as injectable hydrogel materials that can be delivered with spatial resolution from a syringe.

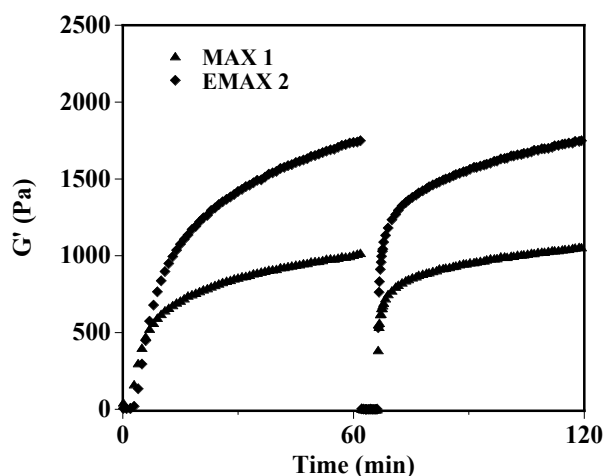


**Figure 4.17 Shear-thinning and recovery profile of 1 wt% MAX1 and EMAX2 hydrogels at pH 9 and 37 °C.**

Transmission Electron Microscopy (TEM) and Small Angle Neutron Scattering (SANS) experiments have been employed to investigate the nanoscale structure of the fibrils formed during hydrogelation of MAX1<sup>77</sup> and EMAX2 (see Figure 4.6) at pH 9 and 37 °C. The analyses provided an average fibril diameter of  $30.9 \pm 0.2 \text{ \AA}$  (3.09 nm) and  $31.0 \pm 1.0 \text{ \AA}$  (3.1 nm) for MAX1 and EMAX2 respectively. These dimensions are in excellent agreement with the computationally measured width of the peptides in the folded state.

### 4.3.3 Peptide Sequence, Hydrophobicity and Material Properties

Previous research with  $\beta$ -hairpin peptides have showed that the material properties of their constitutive gels can be manipulated by making amino acid substitutions to their primary sequence. For example, varying the turn region residues as well as altering the charge state of the peptide can influence gel properties. In this section, the properties of MAX1 were compared with EMAX2, a three-stranded peptide. EMAX2 has an additional  $\beta$ -strand and a second turn region as compared to MAX1. EMAX2 has a total charge state of +13 as compared to +9 for MAX1, but still EMAX2 folds and self-assembles at pH values greater than 8, similar to MAX1. Under identical experimental conditions, EMAX2 exhibits a lower folding temperature transition and faster kinetics of self-assembly resulting in a more mechanically rigid hydrogel. One possible explanation for the lower folding and self-assembly transition temperature may be that EMAX2 is simply more hydrophobic than MAX1. More hydrophobic sequences require less thermal energy to drive the hydrophobic effect. The difference in hydrophobicity between MAX1 and EMAX2 was estimated by theoretically calculating the free energy transfer from octanol to water using Insight II molecular modeling software. The values are shown in Table 4.1 relative to MAX1 and indicate that EMAX2 is indeed more hydrophobic.

<b>Peptide</b>	<b>Number of Residues</b>	<b>Charge State (Lysines + N-Termini)</b>	<b>Hydrophobicity <math>\Delta G</math> kcal/mole (Octanol-Water)</b>	<b>Storage Modulus G' (Pa) 1 wt%, pH 9.0, 37 °C</b>
MAX1	20	+9	0.00	1000 (100)
EMAX2	29	+13	4.86	1750 (200)

**Table 4.1 Differences between MAX1 and EMAX2**

#### **4.3.4 Folding, Self-Assembly and Hydrogelation under Physiologically relevant Conditions**

The use of these hydrogels for potential biomedical applications necessitate that the gels be formed at physiological conditions. Figure 4.18 shows salt concentration dependent  $\beta$ -sheet formation via CD ( $[\theta]_{216}$ ) for 2 wt% MAX1 and 2 wt% EMAX2 solutions at pH 7.4 (50 mM BTP) and 37 °C. It is evident that 2 wt % MAX1 undergoes folding and self-assembly at lower salt concentrations as compared to 2 wt % EMAX2. This may be due to the fact that EMAX2 has more positive charges to be screened and therefore requires higher salt concentrations to efficiently screen the lysine derived charges before folding and self-assembly can occur at pH 7.4. However, both the peptides are fully folded and self-assembled at physiologically

relevant conditions (pH 7.4, 150 mM NaCl, 37 °C). A higher concentration of peptides (2 wt%) was employed since 1 wt% peptide solutions formed weaker gels under these buffer conditions.

Hydrogelation was also initiated using cell culture media [Dulbecco's Modified Essential Medium (DMEM)]. This media contains about 160 mM mono and divalent salts.

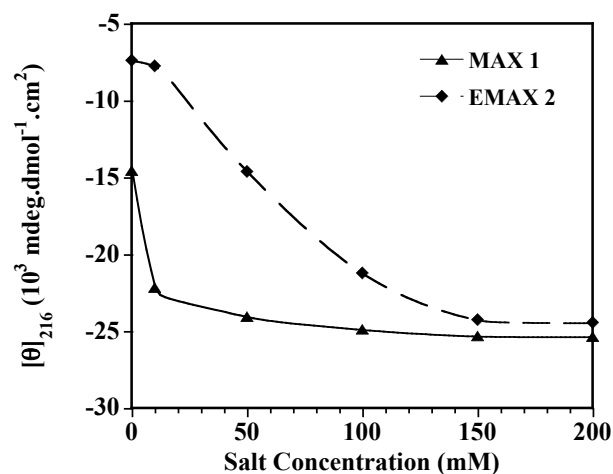


**Figure 4.18 CD spectroscopy of showing salt concentration dependent  $\beta$ -sheet formation of 2 wt% MAX1 and EMAX2 solutions at pH 7.4 and 37 °C**

Figure 4.19(a) compares the onset of hydrogelation of MAX1 and EMAX2 peptide solutions using cell culture media at pH 7.4 and 37 °C. Two wt % peptide solutions at pH 7.4 (DMEM) are gelled by increasing the temperature from 5 °C to 37 °C. After 1 hour of gelation, 2 wt% MAX1 achieves a storage modulus of

6000  $\pm$  1300 Pa whereas 2 wt% EMAX2 achieved a storage modulus of 8500  $\pm$  1250 Pa respectively. Dynamic time sweep experiments of DMEM based hydrogel samples yielded G' values having higher standard deviations. This could be due to the fact that maintaining the buffer capacity of DMEM without a source of carbon dioxide is difficult in these rheological experiments. However, care was taken to perform every experiment with freshly CO<sub>2</sub> incubated DMEM at pH 7.4. Frequency sweep experiments [Figure 4.19(b)] show that the peptides in cell growth media form rigid hydrogels with G' being insensitive to frequency indicating the permanent nature of the crosslinks.

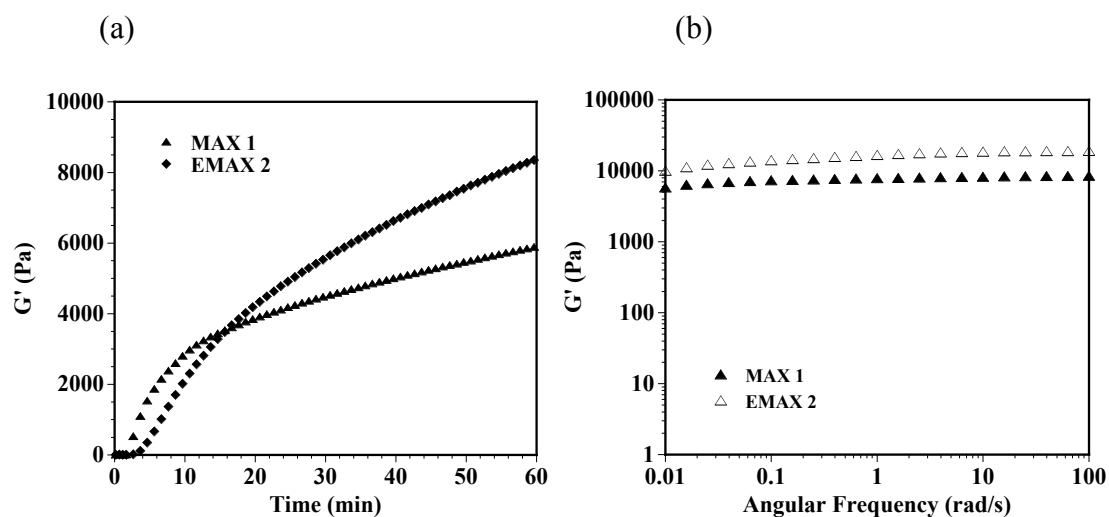


**Figure 4.19 Dynamic (a) time and (b) frequency sweep of 2 wt% MAX1 and EMAX2 hydrogels at pH 7.4 (DMEM) and 37 °C.**

A delayed onset of gelation is observed for the EMAX2 peptide sample compared to MAX1 upon raising the temperature of the peptide solution to 37 °C. This may be due to the small difference in molarity of the peptide samples. Two wt% EMAX2 corresponds to 4.24 mM peptide concentration whereas 2 wt% MAX1 corresponds to 6.14 mM peptide concentration due to the difference in the peptides molecular weight. The lower concentration of EMAX2 may take longer to form a gel. At any rate, 2 wt% EMAX2 forms a more rigid hydrogel than 2 wt% MAX1 over a 1 hour period.

#### **4.4 Conclusions:**

We have designed a three-stranded antiparallel  $\beta$ -sheet peptide that is responsive to increase in pH, increase in ionic strength and cell culture media similar to its parent  $\beta$ -hairpin peptide. EMAX2 exhibits a lower temperature folding transition and faster kinetics of folding and self-assembly and also forms more rigid hydrogels than MAX1. However, both MAX1 and EMAX2 hydrogels can be shear-thinned and recover making them potential candidates as injectable biomaterials. Collectively, addition of third strand connected via a second turn region to MAX1 positively affects the folding, self-assembly and bulk material properties of the resultant hydrogel.

#### 4.5 Experimental Section

**Materials.** Rink amide resin was purchased from Polymer Laboratories. Trifluoroacetic acid (TFA), piperidine, thioanisole, ethanedithiol, and anisole were purchased from Acros. Appropriately side-chain-protected Fmoc-amino acids were obtained from Novabiochem. 1-H-Benzotriazolium-1-[bis(Dimethylamino)Methylene]-5-Chloro-Hexafluorophosphate-(1-),3-Oxide (HCTU) was purchased from Peptide International. D<sub>2</sub>O was purchased from Aldrich. Dulbecco's Modified Eagle's Medium (DMEM), Boric acid and Bis-Tris Propane (BTP) were purchased from Sigma. MilliQ (Millipore) with a resistivity of 18.2 MΩ.cm was used for all experiments and is referred to as "water" in this paper.

**Peptide Synthesis and Purification.** Peptides were prepared on Rink amide resin via automated Fmoc peptide synthesis employing an ABI 433A peptide synthesizer and HCTU activation.<sup>93</sup> The resulting dry resin-bound peptides were cleaved and side-chain-deprotected using a cocktail of TFA/thioanisole/ethanedithiol/anisole (90:5:3:2) for 2 hrs under nitrogen. The resin was filtered and peptide precipitated from the filtrate using cold diethyl ether. Crude peptide was subsequently purified by Reverse Phase-HPLC (Waters 600 series) using a semi-preparative Vydac C18 peptide/protein column. HPLC solvents consisted of solvent **A** (0.1% TFA in water) and solvent **B** (90% acetonitrile, 10% water, and 0.1% TFA). MAX1 and EMAX2 were purified

employing isocratic conditions of 0 % **B** for 2 minutes followed by a linear gradient of 0 to 10% **B** in 5 minutes and an additional linear gradient of 10 to 100% **B** in 90 minutes. The resulting peptide solution was frozen with liquid nitrogen and lyophilized to afford pure peptide. The purity of the peptide was established using Electrospray ionization mass spectrometry and analytical HPLC.

**Circular Dichroism Studies.** CD spectra were collected on a Jasco model J-810 spectropolarimeter. A 1 mM peptide stock of EMAX2 was prepared by dissolving the appropriate amount of purified peptide in water. UV-Vis spectroscopy was employed to determine the concentration of the peptide stock solution using the extinction coefficient ( $\epsilon$ ) of MAX1 at 220 nm [ $\epsilon_{220} = 15750 \text{ cm}^{-1} \text{ M}^{-1}$  (MAX1 peptide)] and EMAX2 at 220 nm [ $\epsilon_{220} = 20350 \text{ cm}^{-1} \text{ M}^{-1}$  (EMAX2 peptide)].  $\epsilon_{220}$  was determined by amino acid analysis. This 1 mM peptide stock was diluted to afford a 300  $\mu\text{M}$  peptide final stock solution, which was used to prepare all of the CD samples. For each CD sample, 300  $\mu\text{M}$  stock of peptide was mixed with an equal volume of pH 9.0 buffer (250 mM Borate, 20 mM NaCl) to afford a final concentration of 150  $\mu\text{M}$  peptide solution at pH 9 (125 mM Borate, 10 mM NaCl). A similar procedure was adopted for pH 7.4 studies except that an equal volume of pH 7.4 buffer (100 mM BTP, 300 mM NaCl or 2X DMEM) was used and the final concentration of peptide employed was 2 wt%. Mean residue ellipticity  $[\theta]$  was calculated from the equation  $[\theta] = (\theta_{\text{obs}}/10lc)/r$ , where  $\theta_{\text{obs}}$  is the measured ellipticity in millidegrees,  $l$  is the length of the cell (centimeters),  $c$  is the molar concentration, and  $r$  is the number of residues.

Four separate CD experiments were performed on individual samples of the peptides. Wavelength spectra from 260 to 190 nm were obtained in a 0.1 cm path length quartz cell at 37 °C to assess the secondary structure of MAX1 and EMAX2. Temperature-dependent spectra were recorded by measuring the mean residual ellipticity  $[\theta]$  at 216 nm as a function of temperature using a step size of 5 °C and an equilibration time of 10 minutes. The rate of  $\beta$ -sheet formation was assessed by monitoring  $[\theta]_{216}$  as a function of time at 37 °C. Salt [NaCl]-dependent spectra were collected by measuring  $[\theta]_{216}$  of 2 wt% peptide preparations at pH 7.4 (50 mM BTP) as a function of NaCl concentration. NaCl concentrations ranged from 0-200 mM. A 0.1 mm quartz cell was used for this study and the  $[\theta]_{216}$  values obtained at the end of 30 minutes are reported, enough time for all samples to reach a constant  $[\theta]_{216}$  value.

**Procedure for Hydrogel Preparation.** Generally, basic solutions (low ionic strength) or neutral solutions (high ionic strength) of the peptides will undergo gelation at concentrations of 1 wt% or greater. For example, 300  $\mu$ L of 1 wt% hydrogels can be prepared as follows: To a solution of 3.0 mg of peptide in 150  $\mu$ L of MilliQ water, 150  $\mu$ L of a buffer stock solution (pH 9.0, 250 mM Borate, 20 mM NaCl or pH 7.4, 100 mM BTP, 300 mM NaCl) was added resulting in a 1 wt% solution (pH 9.0, 125 mM borate, 10 mM NaCl or pH 7.4, 50 mM BTP, 150 mM NaCl) of peptide. After minimal pipet mixing, this solution was allowed to stand for 10 minutes (pH 9.0) or 60 minutes (pH 7.4) in a sand bath pre-equilibrated to 37 °C until gelation was complete.

**Infrared Spectroscopy.** IR spectra were collected on a Nicolet Magna-IR 860 spectrometer employing a 30  $\mu\text{M}$  path length zinc-selenide flow cell. Deuterated peptide\* $\text{nDCl}$  was prepared by lyophilizing the TFA salt of MAX1 or EMAX2 once from 0.1 M HCl and twice from  $\text{D}_2\text{O}$ . The samples were prepared by dissolving the deuterated chloride salt of the peptide in  $\text{D}_2\text{O}$  to obtain a 2 wt% solution. To this solution an equal volume of pH 9.0 buffer (250 mM Borate and 20 mM NaCl) in  $\text{D}_2\text{O}$  was added and the contents were gently mixed and incubated on a sand bath at 37  $^\circ\text{C}$ . IR measurements were taken at room temperature. Spectra were collected at 1  $\text{cm}^{-1}$  resolution, and the spectrum recorded was an average of 100 scans.

**Oscillatory Shear Rheology.** Dynamic time, frequency, and strain sweep experiments were performed on a Paar-Physica MCR 500 rheometer with a 25 mm parallel plate geometry and 0.5 mm gap distance. The peptide was first dissolved in ice-cold water to obtain a concentration that is twice the final peptide concentration in the gel. Then, an equal amount of ice-cold buffer pH 9 (250mM Borate, 20mM NaCl) or pH 7.4 (2X DMEM) was added to the peptide stock solution, mixed gently and immediately loaded onto the rheometer plate equilibrated to 5  $^\circ\text{C}$ . After the sample was loaded and the parallel plate lowered, standard low-viscosity mineral oil was used to insulate the sides of the parallel plate in order to prevent evaporation. The temperature was then increased to 37  $^\circ\text{C}$  to initiate folding, assembly and gelation. Control experiments show that the mineral oil has no effect on the rheological measurements. Gelation was

observed by monitoring the evolution of the storage modulus ( $G'$ ) with time, in a dynamic time sweep experiment performed at an angular frequency of 6 rad/s and strain of 0.2 %. Storage moduli values ( $G'$ ) obtained at the end of 1 hr are reported with standard deviation values in parentheses obtained from experiments performed in triplicate. Frequency sweep experiments were performed by varying the frequency from 0.1-100 rad/s at a constant strain of 0.2 % and strain sweep experiments were performed by varying the strain from 0.01 to 100 % at a constant frequency of 6 rad/s. The frequency and strain sweep experiments verified that all time sweep experiments were performed within the linear viscoelastic regime.

Shear-thin and recovery experiments were performed by first allowing gels to form for 1 hr in a dynamic time sweep experiment (6 rad/s and 0.2% strain) and subsequently subjecting the gels to a shear-thinning and recovery cycle. The shear-thinning and recovery cycle consisted of application of 1000 % strain at 6 rad/s for 3 minutes followed by a 1 hour recovery period at a constant 0.2 % strain at 6 rad/s angular frequency.

**Transmission Electron Microscopy.** 1 wt% hydrogels were incubated for at least 24 hours prior to sample preparation. A 2-5  $\mu\text{L}$  aliquot of diluted gel was applied to carbon-coated copper grids. The samples were negatively stained by placing a drop of 2 % (w/v) uranyl acetate aqueous solution on the grid. The excess of the solution was blotted with filter paper, and the sample was subsequently left to dry. Concentrated samples were diluted to 0.1 % (w/v) with deionized water prior to staining. Bright

field images of the fibril nanostructure were taken on a JEOL 2000-FX transmission electron microscope (TEM) at 200 kV accelerating voltage on both a Gatan CCD camera and Kodak negative films.

**Small Angle Neutron Scattering.** SANS experiments were performed on the 30-m instrument on beamline NG3 at the National Center for Neutron Research (NCNR), National Institute of Standards and Technology (NIST), Gaithersburg, MD. The neutron beam was monochromated to a wavelength  $\lambda = 6 \text{ \AA}$  with a velocity selector having a wavelength spread  $\Delta\lambda/\lambda = 0.15$ . The scattered neutrons were detected by a 64 cm x 64 cm two-dimensional detector using two different sample-to-detector distances of 1.3 and 4 m. These configurations allow values of the scattering wavevector,  $q = 4\pi \sin(\theta/2)/\lambda$ , where  $\theta$  is the scattering angle in the range  $0.008 \text{ \AA}^{-1} < q < 0.500 \text{ \AA}^{-1}$ . The resulting data were corrected for background electronic noise, detector inhomogeneity, empty cell scattering, and solvent scattering. The uncertainties of the  $I(q)$  vs  $q$  individual data points are calculated statistically from the number of averaged detector counts. The data was fit to a cylindrical form factor using the following function:<sup>77</sup>

$$I(q) = \frac{\phi}{V_{cyl}} \int_0^{\pi} f^2(q, \alpha) \sin \alpha d\alpha, \text{ where}$$

$$f(q, \alpha) = 2(\rho_{cyl} - \rho_{solv})V_{cyl} \frac{\sin(qH \cos \alpha)}{qH \cos \alpha} \frac{J_1(qr \sin \alpha)}{(qr \sin \alpha)}$$

The form factor for a rod-like particle with a finite cross-sectional diameter is approximated as  $P(q) \sim [\exp(-q^2 R_c^2 / 2)] / q$  where  $R_c$  is the radius of gyration of the cross section. From the modified Guinier analysis,<sup>94</sup> plotted as  $\ln[I(q)q]$  vs  $q^2$ , the radius of the cross section of a rod was determined using  $-slope = R_c^2 / 2$ . The cross section of the rod,  $R$ , was then calculated using  $R = R_c \sqrt{2}$ .

### **Hydrogel Preparation for Cellular Viability and Actin/Nuclear Staining Assays.**

Hydrogels for the cellular viability and actin/nuclear staining assays were prepared in separate wells of 8-well borosilicate confocal plates. For a given well, 75  $\mu\text{L}$  of a EMAX2 peptide stock solution (4 wt%; 18 mg EMAX2 in 450  $\mu\text{L}$  sterile filtered  $\text{H}_2\text{O}$ ) was introduced, followed by the addition of 75  $\mu\text{L}$  of serum-free DMEM to initiate gelation. The resulting 2 wt% hydrogels (150  $\mu\text{L}$  total volume) were allowed to incubate at 37  $^\circ\text{C}$ , 5%  $\text{CO}_2$  for one hour, after which 300  $\mu\text{L}$  of serum-free DMEM was introduced to the surface of each hydrogel and allowed to incubate overnight at 37  $^\circ\text{C}$ , 5%  $\text{CO}_2$ .

**Cell Culture Conditions.** C3H10t1/2 mesenchymal stem cells (ATCC # CCL-226) were cultured using Dulbecco's Modified Eagle's Medium (DMEM, Sigma Aldrich, D6546) supplemented with 10% Fetal Bovine Serum, 5 mM L-Glutamine, 50  $\mu\text{g}/\text{mL}$  Gentamicin at 37  $^\circ\text{C}$  in 5%  $\text{CO}_2$ . Cells were cultured in T75 cell culture flasks. Cells used for both cellular viability assays as well as actin/nuclear staining assays were on

passage number 9. For cell plating, cells were trypsinized and counted using a hemacytometer. The resultant cell suspension was introduced to the hydrogel and borosilicate control surfaces such that a cell loading density of 30,000 cells/cm<sup>2</sup> was achieved. These samples were incubated for 24 hours at 37 °C, 5% CO<sub>2</sub>.

**Cellular Viability Assays of C3H10t1/2 Mesenchymal Stem Cells.** For cellular viability assays, the media above the hydrogel and borosilicate control surfaces was removed and a solution of 1 μM calcein AM and 2 μM ethidium homodimer in DMEM supplemented with 25 mM HEPES (prepared as suggested in the live/dead assay instructions) was introduced. Samples were imaged using a Zeiss 510 laser scanning confocal microscope at a magnification of 10X.

**Actin and Nuclear Staining of C3H10t1/2 Mesenchymal Stem Cells.** For actin and nuclear staining assays, the media above the hydrogel and borosilicate control surfaces was removed. Each respective surface was gently washed three times with Ca/Mg free PBS. To fix the cells, 200 μL of a 4% paraformaldehyde solution in Ca/Mg free PBS was introduced to each well and allowed to incubate for 30 minutes. The samples were again washed three times with Ca/Mg free PBS. To permeabilize the cells to allow for penetration of each dye, 200 μL of a 0.5% Triton-X-100 solution in PBS was introduced to each well for 5 minutes. The cells were again washed three times with PBS and stained with 200 μL of a 143 μM solution of 4', 6-diamino-2-phenylindole (Molecular Probes, D1306) in Ca/Mg free PBS for 20 minutes. Next,

200  $\mu\text{L}$  of a 26.4 nM solution of Alexa fluor 488 phalloidin (Molecular Probes A12379) in Ca/Mg free PBS was introduced and allowed to incubate for 90 minutes. Lastly, the wells were washed three times with Ca/Mg free PBS and stored in the refrigerator until imaging. Cells were imaged using a Zeiss 510 laser scanning multiphoton confocal microscope at a magnification of 10X.

## References

1. Chapman, M. R.; Robinson, L. S.; Pinkner, J. S.; Roth, R.; Heuser, J.; Hammar, M.; Normark, S.; Hultgren, S. J., Role of Escherichia coli Curli Operons in Directing Amyloid Fiber Formation. *Science* **2002**, 295, (5556), 851-855.
2. Fowler, D. M.; Koulov, A. V.; Alory-Jost, C.; Marks, M. S.; Balch, W. E.; Kelly, J. W., Functional Amyloid Formation within Mammalian Tissue. *PLoS Biology* **2006**, 4, (1), e6.
3. Vassiliki, A. I.; Gert, V.; Stavros, J. H., Amyloids protect the silkworm oocyte and embryo. *FEBS letters* **2000**, 479, (3), 141-145.
4. Claessen, D.; Rink, R.; de Jong, W.; Siebring, J.; de Vreugd, P.; Boersma, F. G. H.; Dijkhuizen, L.; Wosten, H. A. B., A novel class of secreted hydrophobic proteins is involved in aerial hyphae formation in *Streptomyces coelicolor* by forming amyloid-like fibrils. *Genes Dev.* **2003**, 17, (14), 1714-1726.
5. Kwan, A. H. Y.; Winefield, R. D.; Sunde, M.; Matthews, J. M.; Haverkamp, R. G.; Templeton, M. D.; Mackay, J. P., Structural basis for rodlet assembly in fungal hydrophobins. *Proc. Natl. Acad. Sci. U. S. A.* **2006**, 103, (10), 3621-3626.
6. Oh, J.; Kim, J.-G.; Jeon, E.; Yoo, C.-H.; Moon, J. S.; Rhee, S.; Hwang, I., Amyloidogenesis of Type III-dependent Harpins from Plant Pathogenic Bacteria. *J. Biol. Chem.* **2007**, 282, (18), 13601-13609.
7. Barnhart, M. M.; Chapman, M. R., Curli Biogenesis and Function. *Annu Rev Microbiol* **2006**, 60, (1), 131-147.
8. Tessier, P. M.; Lindquist, S., Prion recognition elements govern nucleation, strain specificity and species barriers. *Nature* **2007**, 447, (7144), 556-561.
9. Si, K.; Lindquist, S.; Kandel, E. R., A Neuronal Isoform of the *Aplysia* CPEB Has Prion-Like Properties. *Cell* **2003**, 115, (7), 879-891.
10. Podrabsky, J. E.; Carpenter, J. F.; Hand, S. C., Survival of water stress in annual fish embryos: dehydration avoidance and egg envelope amyloid fibers. *Am J Physiol Regul Integr Comp Physiol* **2001**, 280, (1), R123-131.
11. Fowler, D. M.; Koulov, A. V.; Balch, W. E.; Kelly, J. W., Functional amyloid - from bacteria to humans. *Trends Biochem Sci* **2007**, 32, (5), 217-224.
12. Kranenburg, O.; Bouma, B.; Kroon-Batenburg, L. M. J.; Reijerkerk, A.; Wu, Y. P.; Voest, E. E.; Gebbink, M., Tissue-type plasminogen activator is a multiligand cross-beta structure receptor. *Curr. Biol.* **2002**, 12, (21), 1833-1839.
13. Wang, X.; Smith, D. R.; Jones, J. W.; Chapman, M. R., In Vitro Polymerization of a Functional Escherichia coli Amyloid Protein. *J. Biol. Chem.* **2007**, 282, (6), 3713-3719.
14. Hammer, N. D.; Schmidt, J. C.; Chapman, M. R., The curli nucleator protein, CsgB, contains an amyloidogenic domain that directs CsgA polymerization. *Proc. Natl. Acad. Sci. U. S. A.* **2007**, 104, (30), 12494-12499.
15. Holmes, T. C.; de Lacalle, S.; Su, X.; Liu, G.; Rich, A.; Zhang, S., Extensive neurite outgrowth and active synapse formation on self-assembling peptide scaffolds. *Proc. Natl. Acad. Sci. U. S. A.* **2000**, 97, (12), 6728-6733.

16. Fabrizio Gelain, A. H. S. Z., Designer Self-Assembling Peptide Scaffolds for 3-D Tissue Cell Cultures and Regenerative Medicine. *Macromol Biosci* **2007**, 7, (5), 544-551.
17. Haines, L. A.; Rajagopal, K.; Ozbas, B.; Salick, D. A.; Pochan, D. J.; Schneider, J. P., Light-activated hydrogel formation via the triggered folding and self-assembly of a designed peptide. *J. Am. Chem. Soc.* **2005**, 127, (48), 17025-17029.
18. Haines-Butterick, L.; Rajagopal, K.; Branco, M.; Salick, D.; Rughani, R.; Pilarz, M.; Lamm, M. S.; Pochan, D. J.; Schneider, J. P., Controlling hydrogelation kinetics by peptide design for three-dimensional encapsulation and injectable delivery of cells. *Proc. Natl. Acad. Sci. U. S. A.* **2007**, 104, (19), 7791-7796.
19. Smith, A. M.; Banwell, E. F.; Edwards, W. R.; Pandya, M. J.; Woolson, D. N., Engineering increased stability into self-assembled protein fibers. *Adv. Funct. Mater.* **2006**, 16, (8), 1022-1030.
20. Zimenkov, Y.; Dublin, S. N.; Ni, R.; Tu, R. S.; Breedveld, V.; Apkarian, R. P.; Conticello, V. P., Rational Design of a Reversible pH-Responsive Switch for Peptide Self-Assembly. *J. Am. Chem. Soc.* **2006**, 128, (21), 6770-6771.
21. Collier, J. H.; Hu, B. H.; Ruberti, J. W.; Zhang, J.; Shum, P.; Thompson, D. H.; Messersmith, P. B., Thermally and photochemically triggered self-assembly of peptide hydrogels. *J. Am. Chem. Soc.* **2001**, 123, (38), 9463-9464.
22. Ramachandran, S.; Trehwella, J.; Tseng, Y.; Yu, Y. B., Coassembling peptide-based biomaterials: Effects of pairing equal and unequal chain length oligopeptides. *Chem. Mater.* **2006**, 18, (26), 6157-6162.
23. Gupta, M.; Bagaria, A.; Mishra, A.; Mathur, P.; Basu, A.; Ramakumar, S.; Chauhan, V. S., Self-Assembly of a Dipeptide- Containing Conformationally Restricted Dehydrophenylalanine Residue to Form Ordered Nanotubes. *Adv. Mater.* **2007**, 19, (6), 858-861.
24. Reches, M.; Gazit, E., Designed aromatic homo-dipeptides: formation of ordered nanostructures and potential nanotechnological applications. *Phys. Biol.* **2006**, 3, (1), S10-S19.
25. Yan, X.; He, Q.; Wang, K.; Duan, L.; Cui, Y.; Li, J., Transition of Cationic Dipeptide Nanotubes into Vesicles and Oligonucleotide Delivery. *Angew. Chem.* **2007**, 119, (14), 2483-2486.
26. Jayawarna, V.; Ali, M.; Jowitt, T. A.; Miller, A. F.; Saiani, A.; Gough, J. E.; Ulijn, R. V., Nanostructured Hydrogels for Three-Dimensional Cell Culture Through Self-Assembly of Fluorenylmethoxycarbonyl-Dipeptides. *Adv. Mater.* **2006**, 18, (5), 611-614.
27. Yang, Z. M.; Liang, G. L.; Ma, M. L.; Gao, Y.; Xu, B., Conjugates of naphthalene and dipeptides produce molecular hydrogelators with high efficiency of hydrogelation and superhelical nanofibers. *J. Mater. Chem.* **2007**, 17, (9), 850-854.
28. Dong, H.; Paramonov, S. E.; Aulisa, L.; Bakota, E. L.; Hartgerink, J. D., Self-Assembly of Multidomain Peptides: Balancing Molecular Frustration

- Controls Conformation and Nanostructure. *J. Am. Chem. Soc.* **2007**, 129, (41), 12468-12472.
29. Schneider, J. P.; Pochan, D. J.; Ozbas, B.; Rajagopal, K.; Pakstis, L.; Kretsinger, J., Responsive hydrogels from the intramolecular folding and self-assembly of a designed peptide. *J. Am. Chem. Soc.* **2002**, 124, (50), 15030-15037.
  30. Ozbas, B.; Kretsinger, J.; Rajagopal, K.; Schneider, J. P.; Pochan, D. J., Salt-triggered peptide folding and consequent self-assembly into hydrogels with tunable modulus. *Macromolecules* **2004**, 37, (19), 7331-7337.
  31. Pochan, D. J.; Schneider, J. P.; Kretsinger, J.; Ozbas, B.; Rajagopal, K.; Haines, L., Thermally reversible hydrogels via intramolecular folding and consequent self-assembly of a de Novo designed peptide. *J. Am. Chem. Soc.* **2003**, 125, (39), 11802-11803.
  32. Chong Wang; Lixin Huang; Lijun Wang; Yuankai Hong; Sha, Y., One-dimensional self-assembly of a rational designed  $\beta$ -structure peptide. *Biopolymers* **2007**, 86, (1), 23-31.
  33. Lockwood, N. A.; van Tankeren, R.; Mayo, K. H., Aqueous Gel Formation of a Synthetic Peptide Derived from the  $\beta$ -Sheet Domain of Platelet Factor-4. *Biomacromolecules* **2002**, 3, (6), 1225-1232.
  34. Tycko, R., Molecular structure of amyloid fibrils: insights from solid-state NMR. *Q. Rev. Biophys.* **2006**, 39, (1), 1-55.
  35. Nelson, R.; Eisenberg, D., Recent atomic models of amyloid fibril structure. *Curr. Opin. Struct. Biol.* **2006**, 16, (2), 260-265.
  36. Eisenberg, D.; Nelson, R.; Sawaya, M. R.; Balbirnie, M.; Sambashivan, S.; Ivanova, M. I.; Madsen, A. O.; Riek, C., The Structural Biology of Protein Aggregation Diseases: Fundamental Questions and Some Answers. *Acc. Chem. Res.* **2006**, 39, (9), 568-575.
  37. Xu, G.; Wang, W.; Groves, J. T.; Hecht, M. H., Self-assembled monolayers from a designed combinatorial library of de novo  $\beta$ -sheet proteins. *Proc. Natl. Acad. Sci. U. S. A.* **2001**, 98, (7), 3652-3657.
  38. Rapaport, H.; Moller, G.; Knobler, C. M.; Jensen, T. R.; Kjaer, K.; Leiserowitz, L.; Tirrell, D. A., Assembly of Triple-Stranded  $\beta$ -Sheet Peptides at Interfaces. *J. Am. Chem. Soc.* **2002**, 124, (32), 9342-9343.
  39. Privalov, P. L., *Crit. Rev. Biochem. Mol. Biol.* **1990**, 25, 281-305.
  40. Wurth, C.; Kim, W.; Hecht, M. H., Combinatorial Approaches to Probe the Sequence Determinants of Protein Aggregation and Amyloidogenicity. *Protein Peptide Lett* **2006**, 13, 279-286.
  41. Brown, C. L.; Aksay, I. A.; Saville, D. A.; Hecht, M. H., Template-Directed Assembly of a de Novo Designed Protein. *J. Am. Chem. Soc.* **2002**, 124, (24), 6846-6848.
  42. Das, C. R.; Raghothama, S.; Balaram, P., A Designed Three Stranded  $\beta$ -Sheet Peptide as a Multiple  $\beta$ -Hairpin Model. *J. Am. Chem. Soc.* **1998**, 120, (23), 5812-5813.

43. De Alba, E.; Santoro, J.; Rico, M.; Jimenez, M. A., De novo design of a monomeric three-stranded antiparallel  $\beta$ -sheet. *Protein Sci.* **1999**, 8, (4), 854-865.
44. Schenck, H. L.; Gellman, S. H., Use of a Designed Triple-Stranded Antiparallel  $\beta$ -Sheet To Probe  $\beta$ -Sheet Cooperativity in Aqueous Solution. *J. Am. Chem. Soc.* **1998**, 120, (19), 4869-4870.
45. Kortemme, T.; Ramirez-Alvarado, M.; Serrano, L., Design of a 20-amino acid, three-stranded  $\beta$ -sheet protein. *Science* **1998**, 281, (5374), 253-6.
46. Sharman, G. J.; Searle, M. S., Cooperative Interaction between the Three Strands of a Designed Antiparallel  $\beta$ -Sheet. *J. Am. Chem. Soc.* **1998**, 120, (21), 5291-5300.
47. Doig, A. J., A three stranded  $\beta$ -sheet peptide in aqueous solution containing N-methyl amino acids to prevent aggregation. *Chem. Commun.* **1997**, 2153-2154.
48. Stanger, H. E.; Syud, F. A.; Espinosa, J. F.; Giriat, I.; Muir, T.; Gellman, S. H., Length-dependent stability and strand length limits in antiparallel  $\beta$ -sheet secondary structure. *Proc. Natl. Acad. Sci. U. S. A.* **2001**, 98, (21), 12015-12020.
49. Klabunde, T.; Petrassi, H. M.; Oza, V. B.; Raman, P.; Kelly, J. W.; Sacchettini, J. C., Rational design of potent human transthyretin amyloid disease inhibitors. *Nat Struct Mol Biol* **2000**, 7, (4), 312-321.
50. Kim, S.-J.; Woo, J.-R.; Seo, E. J.; Yu, M.-H.; Ryu, S.-E., A 2.1  $\approx$  resolution structure of an uncleaved  $[\alpha]1$ -antitrypsin shows variability of the reactive center and other loops. *J. Mol. Biol.* **2001**, 306, (1), 109-119.
51. Pagano, K.; Ramazzotti, M.; Viglino, P.; Esposito, G.; Degl'Innocenti, D.; Taddei, N.; Corazza, A., NMR solution structure of the acylphosphatase from *Escherichia coli*. *J. Biomol. NMR* **2006**, 36, (3), 199-204.
52. Steinrauf, L. K.; Chiang, M. Y.; Shiuan, D., Molecular Structure of the Amyloid-Forming Protein kappa I Bre. *J Biochem* **1999**, 125, (2), 422-429.
53. Janowski, R.; Kozak, M.; Abrahamson, M.; Grubb, A.; Jaskolski, M., 3D domain-swapped human cystatin C with amyloidlike intermolecular  $\beta$ -sheets. *Proteins* **2005**, 61, (3), 570-578.
54. Makabe, K.; Tereshko, V.; Gawlak, G.; Yan, S.; Koide, S., Atomic-resolution crystal structure of *Borrelia burgdorferi* outer surface protein A via surface engineering. *Protein Sci* **2006**, 15, (8), 1907-1914.
55. Skinner, R.; Abrahams, J.-P.; Whisstock, J. C.; Lesk, A. M.; Carrell, R. W.; Wardell, M. R., The 2.6  $\approx$  structure of antithrombin indicates a conformational change at the heparin binding site. *J. Mol. Biol.* **1997**, 266, (3), 601-609.
56. Kong, C.; Ito, K.; Walsh, M. A.; Wada, M.; Liu, Y.; Kumar, S.; Barford, D.; Nakamura, Y.; Song, H., Crystal Structure and Functional Analysis of the Eukaryotic Class II Release Factor eRF3 from *S. pombe*. *Mol. Cell* **2004**, 14, (2), 233-245.
57. Thakur, A. K.; Wetzel, R., Mutational analysis of the structural organization of polyglutamine aggregates. *Proc. Natl. Acad. Sci. U. S. A.* **2002**, 99, (26), 17014-17019.

58. Wouters, M. A.; Curmi, P. M. G., An Analysis of Side-Chain Interactions and Pair Correlations within Antiparallel Beta-Sheets - the Differences between Backbone Hydrogen-Bonded and Non-Hydrogen-Bonded Residue Pairs. *Proteins-Struct. Funct. Genet.* **1995**, 22, (2), 119-131.
59. Broome, B. M.; Hecht, M. H., Nature disfavors sequences of alternating polar and non-polar amino acids: implications for amyloidogenesis. *J. Biol. Chem.* **2000**, 275, (4), 961-968.
60. Rajagopal, K.; Ozbas, B.; Pochan, D. J.; Schneider, J. P., Probing the importance of lateral hydrophobic association in self-assembling peptide hydrogelators. *Eur Biophys J Biophys Lett* **2006**, 35, (2), 162-169.
61. Choo, D. W.; Schneider, J. P.; Graciani, N. R.; Kelly, J. W., Nucleated Antiparallel  $\beta$ -Sheet That Folds and Undergoes Self-Assembly: A Template Promoted Folding Strategy toward Controlled Molecular Architectures. *Macromolecules* **1996**, 29, (1), 355-366.
62. Mattos, C.; Petsko, G. A.; Karplus, M., Analysis of Two-residue Turns in Proteins. *J. Mol. Biol.* **1994**, 238, (5), 733-747.
63. Sibanda, B. L.; Thornton, J. M., Beta-Hairpin Families in Globular-Proteins. *Nature* **1985**, 316, (6024), 170-174.
64. Yang, A.-S.; Hitz, B.; Honig, B., Free Energy Determinants of Secondary Structure Formation: III.  $[\beta]$ -Turns and their Role in Protein Folding. *J. Mol. Biol.* **1996**, 259, (4), 873-882.
65. Venkatraman, J.; Shankaramma, S. C.; Balaram, P., Design of Folded Peptides. *Chem. Rev.* **2001**, 101, (10), 3131-3152.
66. Nair, C. M.; Vijayan, M.; Venkatachalapathi, Y. V.; Balaram, P., X-Ray Crystal-Structure of Pivaloyl-D-Pro-L-Pro-L-Ala-N-Methylamide - Observation of a Consecutive Beta-Turn Conformation. *J. Chem. Soc. Chem. Comm.* **1979**, (24), 1183-1184.
67. Christoph Grathwohl, K. W. t., The X-Pro peptide bond as an nmr probe for conformational studies of flexible linear peptides. *Biopolymers* **1976**, 15, (10), 2025-2041.
68. Struthers, M. D.; Cheng, R. P.; Imperiali, B., Economy in Protein Design: Evolution of a Metal-Independent  $\beta$ ;  $\beta$ ;  $\alpha$ ; Motif Based on the Zinc Finger Domains. *J. Am. Chem. Soc.* **1996**, 118, (13), 3073-3081.
69. Hutchinson, E. G.; Thornton, J. M., A Revised Set of Potentials for Beta-Turn Formation in Proteins. *Protein Sci.* **1994**, 3, (12), 2207-2216.
70. Guruprasad, K.; Rajkumar, S.,  $\beta$ - and  $\gamma$ -turns in proteins revisited: A new set of amino acid turn-type dependent positional preferences and potentials. *J. Biosciences* **2000**, 25, (2), 143-156.
71. Xiong, H.; Buckwalter, B. L.; Shieh, H. M.; Hecht, M. H., Periodicity of polar and nonpolar amino acids is the major determinant of secondary structure in self-assembling oligomeric peptides. *Proc. Natl. Acad. Sci. U. S. A.* **1995**, 92, (14), 6349-6353.

72. Hecht, M. H., De novo design of beta-sheet proteins. *Proc. Natl. Acad. Sci. U. S. A.* **1994**, 91, (19), 8729-8730.
73. Rughani, R. V.; Schneider, J. P., Molecular Design of b-Hairpin Peptides for Material Construction. *MRS Bull.* **2008**, 33, (5), 530-535.
74. Nagarkar, R. P.; Hule, R. A.; Pochan, D. J.; Schneider, J. P., De Novo Design of Strand-Swapped b-Hairpin Hydrogels. *J. Am. Chem. Soc.* **2008**, 130, (13), 4466-4474.
75. Rajagopal, K.; Schneider, J. P., Self-assembling peptides and proteins for nanotechnological applications. *Curr. Opin. Struc. Biol.* **2004**, 14, (4), 480-486.
76. Yucel, T.; Micklitsch, C. M.; Schneider, J. P.; Pochan, D. J., Direct Observation of Early-Time Hydrogelation in  $\beta$ -Hairpin Peptide Self-Assembly. *Macromolecules* **2008**, 41, (15), 5763-5772.
77. Ozbas, B.; Rajagopal, K.; Schneider, J. P.; Pochan, D. J., Semiflexible chain networks formed via self-assembly of beta-hairpin molecules. *Phys. Rev. Lett.* **2004**, 93, (26).
78. Privalov, P. L.; Griko, Y. V.; Venyaminov, S. Y.; Kutyshenko, V. P., Cold denaturation of myoglobin. *J. Mol. Biol.* **1986**, 190, (3), 487-498.
79. Privalov, P. L.; Makhatadze, G. I., Contribution of Hydration to Protein Folding Thermodynamics : II. The Entropy and Gibbs Energy of Hydration. *J. Mol. Biol.* **1993**, 232, (2), 660-679.
80. Veerman, C.; Rajagopal, K.; Palla, C. S.; Pochan, D. J.; Schneider, J. P.; Furst, E. M., Gelation kinetics of beta-hairpin peptide hydrogel networks. *Macromolecules* **2006**, 39, (19), 6608-6614.
81. Discher, D. E.; Janmey, P.; Wang, Y. L., Tissue cells feel and respond to the stiffness of their substrate. *Science* **2005**, 310, (5751), 1139-1143.
82. Lamm, M. S.; Rajagopal, K.; Schneider, J. P.; Pochan, D. J., Laminated morphology of nontwisting beta-sheet fibrils constructed via peptide self-assembly. *J. Am. Chem. Soc.* **2005**, 127, (47), 16692-16700.
83. Collier, J. H.; Messersmith, P. B., Self-assembling polymer-peptide conjugates: Nanostructural tailoring. *Adv. Mater.* **2004**, 16, (11), 907-910.
84. Surewicz, W. K.; Mantsch, H. H.; Chapman, D., Determination of protein secondary structure by Fourier transform infrared spectroscopy: A critical assessment. *Biochemistry* **1993**, 32, (2), 389-394.
85. Mason, M. N.; Metters, A. T.; Bowman, C. N.; Anseth, K. S., Predicting Controlled-Release Behavior of Degradable PLA-b-PEG-b-PLA Hydrogels. *Macromolecules* **2001**, 34, (13), 4630-4635.
86. Elisseff, J.; Anseth, K.; Langer, R.; Hrkach, J. S., Synthesis and Characterization of Photo-Cross-Linked Polymers Based on Poly(L-LACTIC ACID-CO-L-aspartic acid). *Macromolecules* **1997**, 30, (7), 2182-2184.
87. Hahn, M. S.; Taite, L. J.; Moon, J. J.; Rowland, M. C.; Ruffino, K. A.; West, J. L., Photolithographic patterning of polyethylene glycol hydrogels. *Biomaterials* **2006**, 27, (12), 2519-2524.

88. Mellott, M. B.; Searcy, K.; Pishko, M. V., Release of protein from highly cross-linked hydrogels of poly(ethylene glycol) diacrylate fabricated by UV polymerization. *Biomaterials* **2001**, 22, (9), 929-941.
89. Cruise, G. M.; Scharp, D. S.; Hubbell, J. A., Characterization of permeability and network structure of interfacially photopolymerized poly(ethylene glycol) diacrylate hydrogels. *Biomaterials* **1998**, 19, (14), 1287-1294.
90. Kretsinger, J. K.; Haines, L. A.; Ozbas, B.; Pochan, D. J.; Schneider, J. P., Cytocompatibility of self-assembled ss-hairpin peptide hydrogel surfaces. *Biomaterials* **2005**, 26, (25), 5177-5186.
91. Salick, D. A.; Kretsinger, J. K.; Pochan, D. J.; Schneider, J. P., Inherent Antibacterial Activity of a Peptide-Based b-Hairpin Hydrogel. *J. Am. Chem. Soc.* **2007**, 129, (47), 14793-14799.
92. Mitchison, T. J.; Cramer, L. P., Actin-Based Cell Motility and Cell Locomotion. *Cell* **1996**, 84, (3), 371-379.
93. Nargarkar, R. P.; Schneider, J. P., Synthesis and Primary Characterization of Self-Assembled Peptide-based hydrogels. In *Nanostructure Design, Methods and Protocols*, Gazit, E.; Nussinov, R., Eds. Humana Press: 2008; pp 61-77.
94. Burkoth, T. S.; Benzinger, T. L. S.; Urban, V.; Morgan, D. M.; Gregory, D. M.; Thiyagarajan, P.; Botto, R. E.; Meredith, S. C.; Lynn, D. G., Structure of the b-Amyloid(10-35) Fibril. *J. Am. Chem. Soc.* **2000**, 122, (33), 7883-7889.

## Chapter 5

### ROLE OF TURN SEQUENCE IN MODULATING THE MECHANICAL PROPERTIES OF THREE-STRANDED PEPTIDE HYDROGELS

#### 5.0 Introduction

The  $\beta$ -turn region (-<sup>D</sup>P<sup>L</sup>P-) incorporated into the self-assembling  $\beta$ -hairpin (MAX1) and  $\beta$ -sheet (EMAX2) peptides, has been designed to ensure main chain reversal at distinct locations, define the strand registry and strand trajectory.<sup>1</sup> Previous studies have shown that altering the stereochemistry of the  $i+1$  proline of the turn region from D to L in MAX1, results in a peptide (P5), which was unable to intramolecularly fold but was still capable of self-assembly into  $\beta$ -sheet structure.<sup>2</sup> Unlike MAX1 that folds and self-assembles to form monodispersed fibrils, P5 adopted an extended  $\beta$ -sheet conformation and self-assembled into fibrils exhibiting a highly laminated and non-twisted morphology.<sup>2</sup> Also, a control peptide, (VK)<sub>4</sub> without the turn region failed to form a hydrogel.<sup>3</sup> These studies established that  $\beta$ -hairpin conformation is important for the folding and self-assembly of the peptides that leads to hydrogelation.

In addition, the dissertation work of Karthikan Rajagopal (U.D) demonstrated that different turn sequences and turn types within self-assembling amphiphilic  $\beta$ -hairpins can be employed to alter the mechanical properties of the resultant hydrogels. In this chapter, a series of three-stranded peptides were prepared to investigate the influence of turn sequence on material properties.

## 5.1 Turns in proteins and peptides

Turn regions in proteins and peptides are an important class of structures that strongly influence both structure and function. One such turn type is the  $\beta$ -turn or reverse turn. In this case, the turn causes the polypeptide chain to reverse direction after the location of the turn in the peptide sequence.<sup>4</sup> A  $\beta$ -turn is typically composed of a four-residue sequence (denoted as the  $i$  to  $i + 3$  residues) that connects two secondary structural elements and may play a significant role in initiating folding and in stabilizing tertiary structures. Different types of  $\beta$ -turns have been identified and classified according to the main-chain dihedral angles ( $\Phi, \Psi$ ) that their  $i + 1$  and  $i + 2$  residues adopt. Each turn type influences  $\beta$ -sheet properties such as  $\beta$ -sheet twist, stability, folding nucleation rate, and the hydrogen-bonding registry.<sup>5</sup> Systematic studies indicate that  $\beta$ -turn type and the propensity of the residues occupying the turn positions to adopt dihedral angles consistent with  $\beta$ -turn structure influence the formation and stability of  $\beta$ -hairpins.<sup>6-8</sup> Although, type I and type II turns are most commonly found in proteins, it is their mirror image turns, type I' and II', that dominate sheet-rich structures. Structure based studies have shown that incorporating

D-stereoisomers at the  $i + 1$  position enforces dihedral angles consistent with type I' and type II' turns.<sup>9</sup> Based on these studies, a number of dipeptide sequences have been designed, which when incorporated into peptide sequences form type I' or type II' turns. For example, Gellman et al. showed that <sup>D</sup>Pro-Gly forms a type II' turn, which when incorporated into a 20 amino acid sequence at two locations, cooperatively allows formation of a three-stranded antiparallel  $\beta$ -sheet peptide.<sup>10</sup>

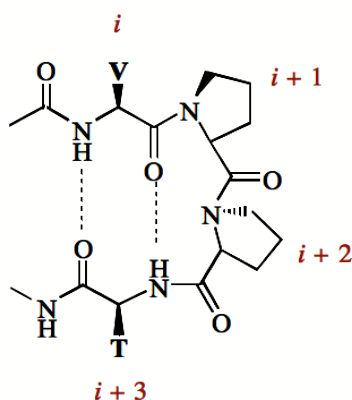


**Figure 5.1 Structure of a typical  $\beta$ -turn**

### 5.2 *De novo* designed $\beta$ -turns

EMAX2 contains two tetrapeptide turn sequences,  $-V^D P^L P T-$  and  $-K^D P^L P K-$  that have high propensity to adopt a type II'  $\beta$ -turn due, in part, to the chirality of the <sup>D</sup>prolyl residue at the  $i + 1$  position. Valine, a  $\beta$ -branched residue, at the  $i$  position ( $V_9$ ) of the first turn, enforces a *trans*-prolyl amide bond geometry at the succeeding ( $i + 1$ ) position. A threonine residue was placed at the  $i + 3$  position of the turn region based on its high propensity to occupy this position in type II' turns of

hairpins of naturally occurring proteins. Threonine can form a stabilizing sidechain-main-chain H-bond between its alcoholic proton and the carbonyl oxygen of the  $i$ th residue of the turn. In the second turn, lysines were included at  $i$  and  $i + 3$  positions to maintain the strand registry and hydrophilic facial amphiphilicity of the  $\beta$ -sheet in folded state.

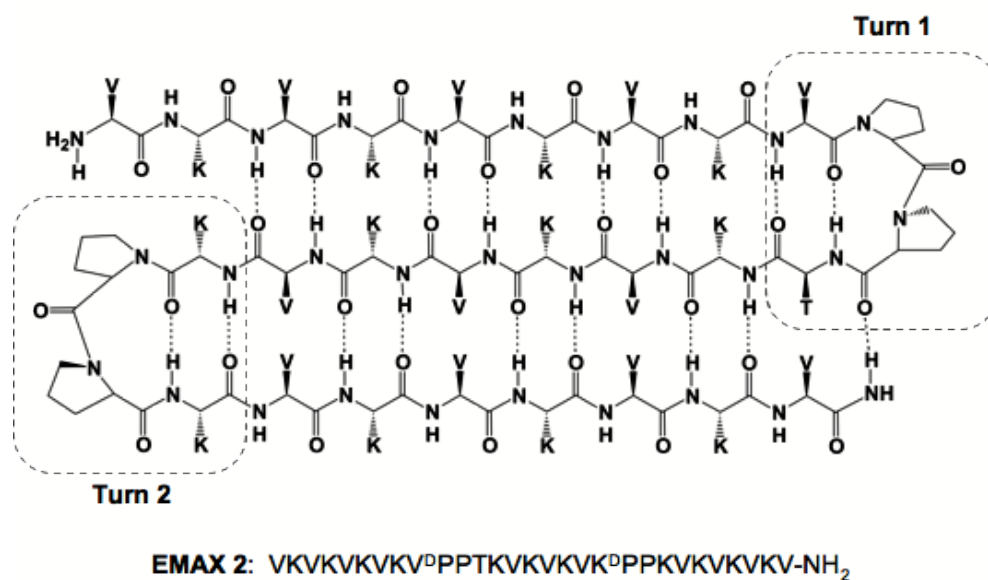


**Figure 5.2.** Sequence of Three-stranded peptide (EMAX2) showing the two turn regions

### 5.3 Turn Sequence dependent Self-Assembly and Hydrogelation

In this chapter, we demonstrate the effect of varying the turn region residues on the folding, self-assembly and hydrogelation properties of three-stranded peptides. Towards this objective, three additional peptides were studied where the central  $i + 1$  and  $i + 2$  residues of each turn were sequentially replaced with <sup>D</sup>PG. This

dipeptide motif is known type II' turn formation, similar to <sup>D</sup>P<sup>L</sup>P. However, <sup>D</sup>PG is less hydrophobic in nature and displays less surface area, which may impact its ability to intermolecularly pack during self-assembly.

### 5.3.1 Design of Turn Sequence Peptides

The peptide sequences and their respective turn region residues are shown in Table 5.1. The EMAX2 peptide as discussed in the previous chapter contains a strong type II' turn nucleator (-X<sup>D</sup>P<sup>L</sup>PX-) at both the turns.

**Table 5.1 Sequences of three-stranded peptides with identical or mixed turn regions**

**Sequence:** VKVKVKVK-XXXX-KVKVKV-YYYY-VKVKVKV-NH<sub>2</sub>

Peptide	Turn 1 (XXXX)	Turn 2 (YYYY)
EMAX 2	-V <sup>D</sup> P <sup>L</sup> PT-	-K <sup>D</sup> P <sup>L</sup> PK-
EMAX 4	-V <sup>D</sup> PGT-	-K <sup>D</sup> P <sup>L</sup> PK-
EMAX 6	-V <sup>D</sup> P <sup>L</sup> PT-	-K <sup>D</sup> PGK-
EMAX 3	-V <sup>D</sup> PGT-	-K <sup>D</sup> PGK-

### 5.3.2 Folding, Self-Assembly and Hydrogelation of EMAX Peptides

The EMAX peptides are designed to undergo temperature triggered folding and self-assembly to form a hydrogel. Figure 5.3 shows the CD wavelength spectra of the EMAX peptides at pH 9.0 (125 mM borate, 10 mM NaCl). At 5 °C, all the EMAX peptides exist in random coil conformation as indicated by a minimum at 198 nm. However, upon raising the temperature to 50 °C, the peptides adopt a β-sheet-rich structure as indicated by minimum at 216 nm and maximum at 196 nm.<sup>3</sup> The

temperature dependent formation of  $\beta$ -sheet structure can be determined by monitoring the mean residual ellipticity at 216 nm as a function of temperature.

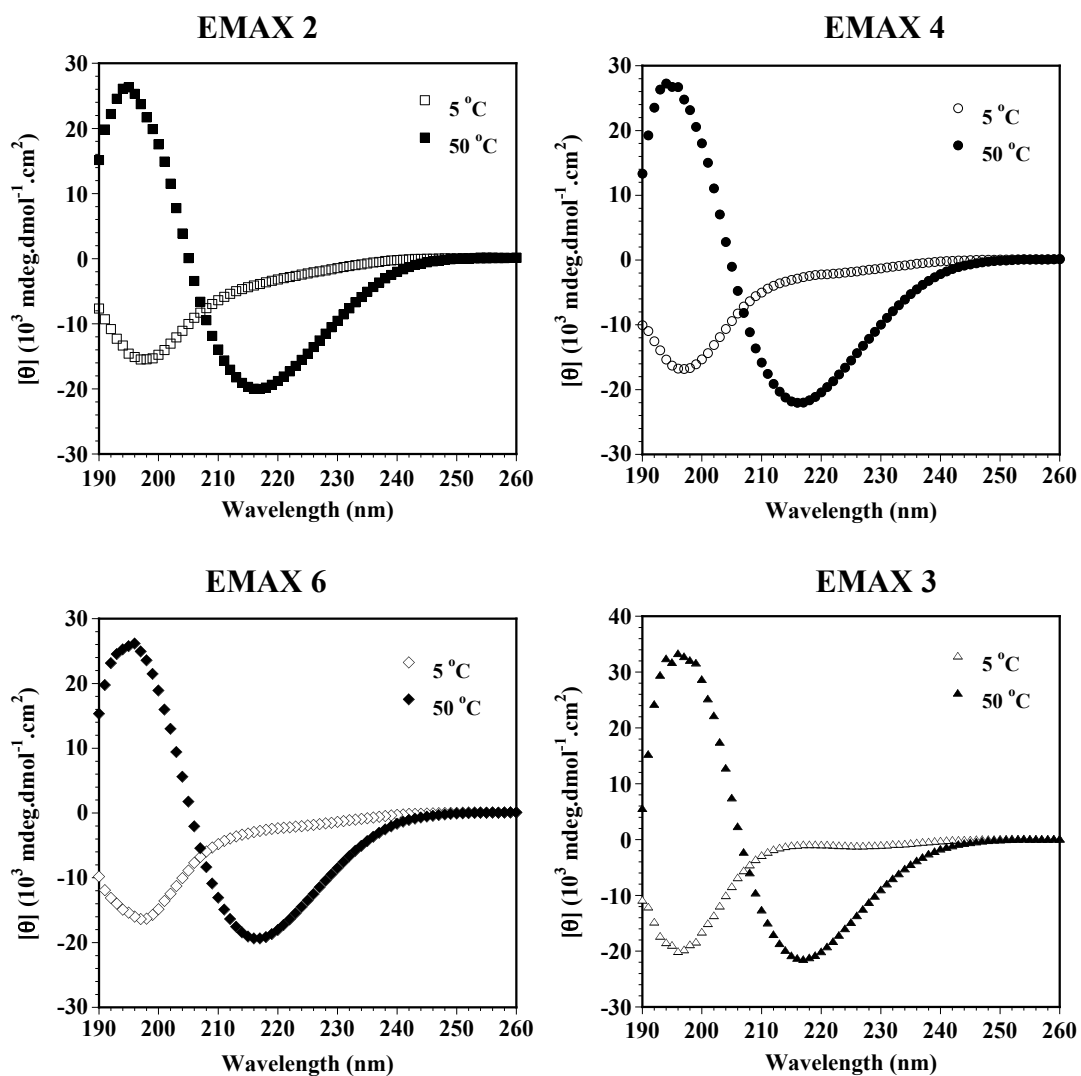


**Figure 5.3** Temperature dependent  $\beta$ -sheet formation of EMAX  $150 \mu\text{M}$  peptides at pH 9.0 (125 mM Borate, 10 mM NaCl)

The data in Figure 5.4(a) shows that the EMAX peptides exhibit the same folding transition irrespective of the turn region residues employed in the respective

sequences. Similar results were observed with  $\beta$ -hairpin peptides with  $^{\text{D}}\text{P}^{\text{L}}\text{P}$ - and  $^{\text{D}}\text{PG}$ - turn region residues as demonstrated in thesis work of Karthikan Rajagopal (U.D). Similarly, pH dependent  $\beta$ -sheet formation was monitored by measuring the mean residual ellipticity at 216 nm as a function of pH. As shown in Figure 5.4(b), the peptides form  $\beta$ -sheet structure at pH values greater than 8. The charge state in all the peptides is the same and thus peptide folding and subsequent self-assembly is disfavored at values of pH 8 or lower due to electrostatic repulsions between the positively charged lysine residues. Collectively, varying the turn region residues in the EMAX2 does not affect its pH dependent nor temperature dependent folding and self-assembly properties.

In Figure 5.4(a), although the peptides are unfolded at 5 °C, small differences in the magnitude of the mean residual ellipticity at 216 nm are observed. Since these peptides differ only in their turn region residues, the differences may be arising due to the contribution of the turn conformations to the CD signal in respective peptide sequences. Under unfolding conditions, the  $^{\text{D}}\text{PG}$  turn is relatively more unstructured due to the presence of the flexible glycine residue than the  $^{\text{D}}\text{P}^{\text{L}}\text{P}$  turn, which is more rigid due to the heterochiral proline residues. Here, EMAX2 with two  $^{\text{D}}\text{P}^{\text{L}}\text{P}$  turn regions exhibits a more negative mean residual ellipticity whereas EMAX3 with two  $^{\text{D}}\text{PG}$  turn regions exhibits less negative mean residual ellipticity at 216 nm under unfolding conditions. EMAX4 and EMAX6 have one  $^{\text{D}}\text{P}^{\text{L}}\text{P}$  and one  $^{\text{D}}\text{PG}$  turn and have mean residual ellipticity values at 216 nm at 5 °C between EMAX2 and EMAX3. The differences in  $[\theta]_{216}$  at 5 °C suggest that peptides that contain the  $^{\text{D}}\text{P}^{\text{L}}\text{P}$

turn sequence may be pre-organized about the turn region even under unfolding solution conditions.

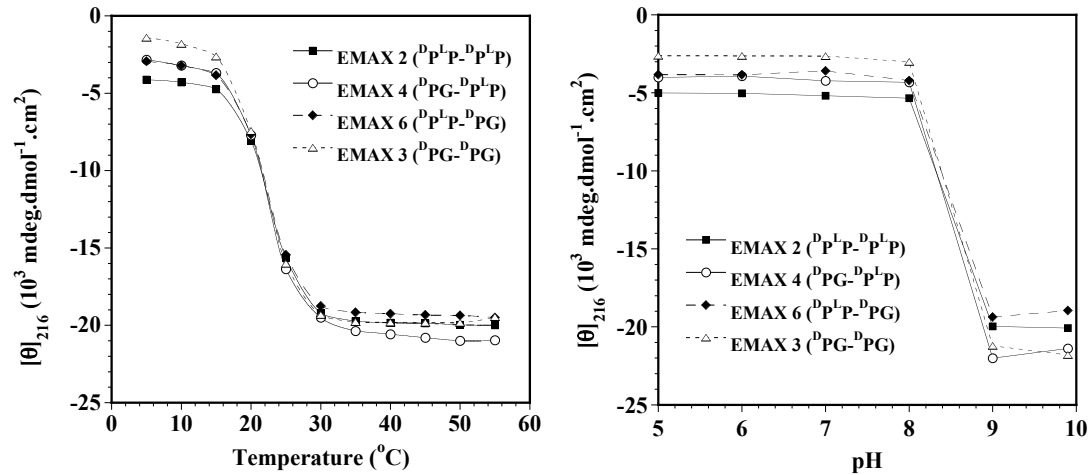


**Figure 5.4.** CD spectroscopy of turn sequence peptides (a) Temperature dependent  $\beta$ -sheet formation monitored by plotting  $[\theta]_{216}$  as a function of temperature (b) pH dependent  $\beta$ -sheet formation monitored by measuring  $[\theta]_{216}$  as a function of pH (50 mM buffer, 10 mM NaCl) at 40 °C

At higher peptide concentrations,  $\beta$ -sheet formation can be monitored by Infrared spectroscopy. Figure 5.5 shows the FTIR spectra in the amide I' region (1700-1580  $\text{cm}^{-1}$ ) for 1wt% peptide gels at pH 9 and 50 °C. The formation of  $\beta$ -sheet structure is indicated by an intense absorption centered at 1615  $\text{cm}^{-1}$ .<sup>2, 11, 12</sup> In addition, a low intensity absorption at about 1680  $\text{cm}^{-1}$  is attributed to the anti-parallel registry of the  $\beta$ -sheet structure.<sup>13</sup>

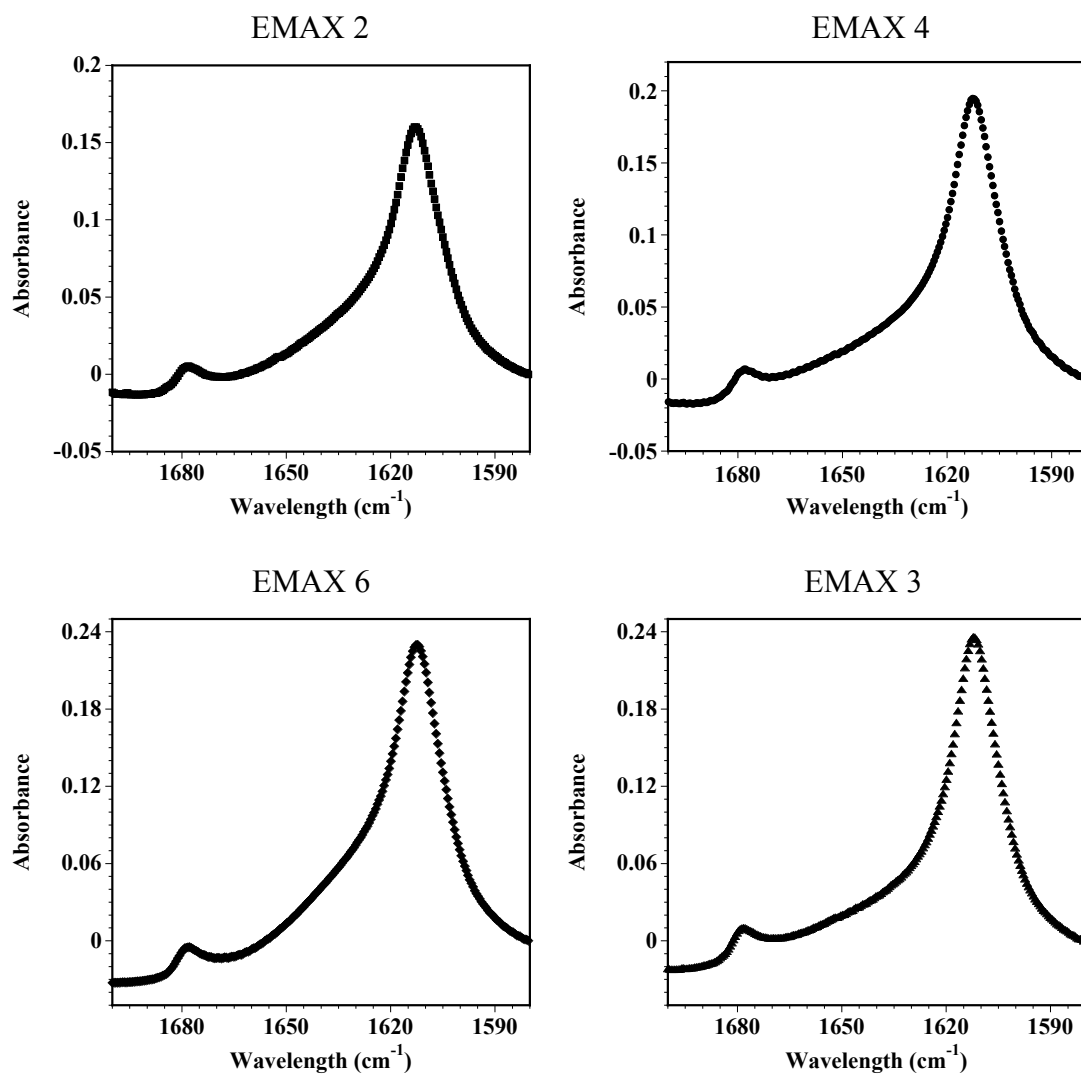


**Figure 5.5** Fourier transform spectroscopy of 1 wt% EMAX peptides at pH 9 showing  $\beta$ -sheet structure at 50 °C.

Figure 5.6 shows the rheological properties of 1 wt% peptide hydrogels at pH 9 (125 mM borate, 10 mM NaCl) and 50 °C. The peptide sample is first loaded onto the rheometer at 5 °C and then the temperature was raised to 50 °C to trigger hydrogelation. The kinetics of hydrogelation was monitored by measuring the increase

in the storage modulus of the peptide samples as a function of time. As shown in Figure 5.6, there is a significant increase in the material stiffness as a result of self-assembly and network formation. This is followed by a gradual increase in the network stiffness with time. At the end of 1 hour, the storage modulus ranged from 1850 pascals to 4700 pascals depending upon the turns regions present in the peptide sequences. The results are summarized in Table 5.2.

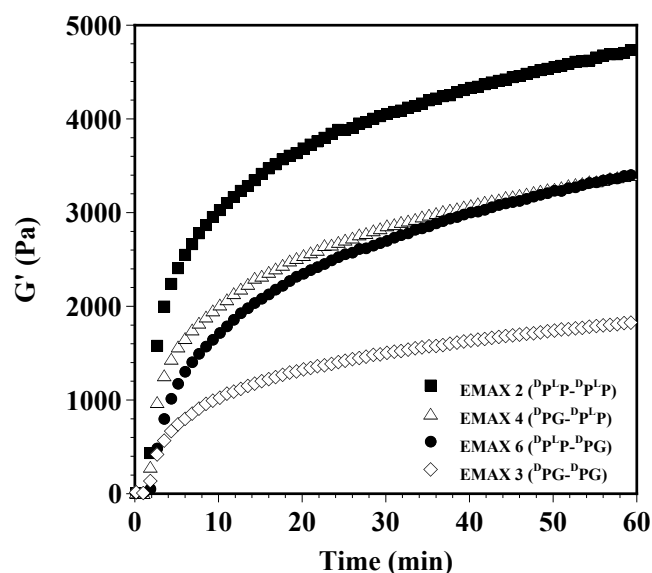


**Figure 5.6** Dynamic time sweep experiment of 1 wt% EMAX peptides at pH 9 and 50 °C.

EMAX 2, the peptide incorporating a  $^{-D}P^L P^{-}$  at both its turns formed the most rigid hydrogels with a storage modulus of around 4700 Pa. However, the EMAX3 peptide, which incorporates a  $^D P G$  at both the turns formed the weakest hydrogel with a storage modulus of about 1850 Pa. The EMAX4 and EMAX6

peptides, each having one <sup>D</sup>P<sup>L</sup>P and one <sup>D</sup>PG turns formed hydrogels with intermediate storage moduli of about 3400 Pa. Both <sup>D</sup>P<sup>L</sup>P and <sup>D</sup>PG are type II' turns with high propensity to form a  $\beta$ -turn and are known to impart stability to the resulting  $\beta$ -sheet structures. The CD and FTIR data is consistent with the high turn propensity of the turns. All four peptides show similar pH dependent folding traits with similar CD wavelength and FTIR spectra. However, gels formed from these peptides EMAX peptides exhibit a wide range of storage modulus values following hydrogelation.

Two main differences exist between the <sup>D</sup>P<sup>L</sup>P and the <sup>D</sup>PG turn. First, their hydrophobic content is different. The hydrophobicity of the turn region residues can contribute to the material stiffness in two possible ways. First, the temperature dependent hydrophobic effect would be more pronounced in more hydrophobic peptides and therefore will allow the peptides to fold and self-assemble at lower temperatures. However, based on data in Figure 5.4, the folding transitions of all the EMAX peptides is the same. Second, in the self-assembled state, peptides having more hydrophobic side chains may form better van der Waals contacts during the self-assembly contributing to the increase in material stiffness. The differences in the hydrophobicity between the EMAX peptides was estimated by theoretically calculating the free energy of transfer from octanol to water for each of the peptide sequences. The values shown in Table 5.2 correlate well with the composition of the turn regions in the peptides. For example, EMAX2 with two <sup>D</sup>P<sup>L</sup>P turns has larger  $\Delta G$  values compared to EMAX3 with two <sup>D</sup>PG turns. Also, EMAX4 and EMAX6 with one turn of each kind have intermediate  $\Delta G$  values. The second difference between the

turns is that the <sup>D</sup>PG display a much smaller surface area than <sup>D</sup>P<sup>L</sup>P. Larger surface areas facilitate intermolecular packing of the molecules during self-assembly.

**Table 5.2 Properties of Three-Stranded Turn Sequence Peptides**

Peptide	Turn 1	Turn 2	$\Delta G_T$ [kcal/mol] (octanol to water)	Storage Modulus G' (Pa) 1wt%, pH 9, 50 °C
EMAX 2	-V <sup>D</sup> P <sup>L</sup> PT-	-K <sup>D</sup> P <sup>L</sup> PK-	2.24	4700 (500)
EMAX 4	-V <sup>D</sup> PGT-	-K <sup>D</sup> P <sup>L</sup> PK-	1.04	3400 (100)
EMAX 6	-V <sup>D</sup> P <sup>L</sup> PT-	-K <sup>D</sup> PGK-	1.10	3400 (500)
EMAX 3	-V <sup>D</sup> PGT-	-K <sup>D</sup> PGK-	0.00	1850 (350)

The data in Table 5.2 shows that the rigidity of the EMAX peptides ranges from 1850-4700 Pa depending upon the turn regions of the peptides. The bulk material properties are dependent upon the number of physical crosslinks as well as the persistence length of the self-assembled fibrils. In the case of EMAX peptides, the kinetics of folding and self-assembly is almost the same. Thus, the data suggests that the mechanical rigidity of the hydrogels is related to both the hydrophobicity and the available surface area of the turn region residues incorporated into the three-stranded peptide sequence.

## 5.4 Conclusions

This chapter discussed the effect of turn sequence hydrophobicity and the surface area available for intermolecular packing on the mechanical rigidity of designed three-stranded peptide hydrogels. Two different turn forming dipeptide

sequences, -<sup>D</sup>P<sup>L</sup>P- and -<sup>D</sup>PG-, were employed to design four three-stranded peptides. Both the turn forming sequences have a high propensity to form a type II' turn. Yet, the mechanical rigidity of the 1 wt% EMAX peptide hydrogels varies based on the turn sequence(s) employed. The results show that the mechanical rigidity of the hydrogels depends on the hydrophobicity and displayed surface area of the turn region. More hydrophobic turns having larger surface areas form stiffer hydrogels.

## 5.5 Experimental Section

**Materials.** Rink amide resin was purchased from Polymer Laboratories. Trifluoroacetic acid (TFA), piperidine, thioanisole, ethanedithiol, and anisole were purchased from Acros. Appropriately side-chain-protected Fmoc-amino acids were obtained from Novabiochem. 1-H-Benzotriazolium-1-[bis(Dimethylamino)Methylene]-5-Chloro-Hexafluorophosphate-(1-),3-Oxide (HCTU) was purchased from Peptide International. D<sub>2</sub>O was purchased from Aldrich. Dulbecco's Modified Eagle's Medium (DMEM), Boric acid and Bis-Tris Propane (BTP) were purchased from Sigma. MilliQ (Millipore) with a resistivity of 18.2 MΩ.cm was used for all experiments and is referred to as "water" in this paper.

**Peptide Synthesis and Purification.** Peptides were prepared on Rink amide resin via automated Fmoc peptide synthesis employing an ABI 433A peptide synthesizer and HCTU activation.<sup>14</sup> The resulting dry resin-bound peptides were cleaved and side-chain-deprotected using a cocktail of TFA/thioanisole/ethanedithiol/anisole (90:5:3:2) for 2 hrs under nitrogen. The resin was filtered and peptide precipitated from the filtrate using cold diethyl ether. Crude peptide was subsequently purified by Reverse Phase-HPLC (Waters 600 series) using a semi-preparative Vydac C18 peptide/protein column. The resulting peptide solution was frozen with liquid nitrogen and lyophilized to afford pure peptide. The purity of the peptide was established using Electrospray ionization mass spectrometry and analytical HPLC.

**Circular Dichroism Studies.** CD spectra were collected on a Jasco model J-810 spectropolarimeter. A 1 mM peptide stock of EMAX peptide was prepared by dissolving the appropriate amount of purified peptide in water. UV-Vis spectroscopy was employed to determine the concentration of the peptide stock solution using the extinction coefficient ( $\epsilon$ ) of EMAX peptide at 220 nm [ $\epsilon_{220} = 20350 \text{ cm}^{-1} \text{ M}^{-1}$  (EMAX2 peptide)].  $\epsilon_{220}$  was determined by amino acid analysis. This 1 mM peptide stock was diluted to afford a 300  $\mu\text{M}$  peptide final stock solution, which was used to prepare all of the CD samples. For each CD sample, 300  $\mu\text{M}$  stock of peptide was mixed with an equal volume of pH 9.0 buffer (250 mM Borate, 20 mM NaCl) to afford a final concentration of 150  $\mu\text{M}$  peptide solution at pH 9 (125 mM Borate, 10 mM NaCl). Mean residue ellipticity  $[\theta]$  was calculated from the equation  $[\theta] = (\theta_{\text{obs}}/10lc)/r$ , where  $\theta_{\text{obs}}$  is the measured ellipticity in millidegrees,  $l$  is the length of the cell (centimeters),  $c$  is the molar concentration, and  $r$  is the number of residues.

Wavelength spectra from 260 to 190 nm were obtained in a 0.1 cm path length quartz cell at 5 and 50  $^{\circ}\text{C}$  to assess the secondary structure of the EMAX peptides. Temperature-dependent spectra were recorded by measuring the mean residual ellipticity  $[\theta]$  at 216 nm as a function of temperature using a step size of 5  $^{\circ}\text{C}$  and an equilibration time of 10 minutes at all pH values. The pH-dependent spectra were plotted by extracting the mean residual ellipticity  $[\theta_{216}]$  at 50  $^{\circ}\text{C}$  as a function of pH from the previous experiment.

**Procedure for Hydrogel Preparation.** Generally, basic solutions (low ionic strength) or neutral solutions (high ionic strength) of the peptides will undergo gelation at concentrations of 1 wt% or greater. For example, 300  $\mu\text{L}$  of 1 wt% hydrogels can be prepared as follows: To a solution of 3.0 mg of peptide in 150  $\mu\text{L}$  of MilliQ water, 150  $\mu\text{L}$  of a buffer stock solution (pH 9.0, 250 mM Borate, 20 mM NaCl) was added resulting in a 1 wt% solution (pH 9.0, 125 mM borate, 10 mM NaCl of peptide). After minimal pipet mixing, this solution was allowed to stand for 10 minutes (pH 9.0) in a sand bath pre-equilibrated to 50  $^{\circ}\text{C}$  until gelation was complete.

**Infrared Spectroscopy.** IR spectra were collected on a Nicolet Magna-IR 860 spectrometer employing a 30  $\mu\text{m}$  path length zinc-selenide flow cell. Deuterated peptide\* $\text{nDCl}$  was prepared by lyophilizing the TFA salt of the EMAX peptide once from 0.1 M HCl and twice from  $\text{D}_2\text{O}$ . The samples were prepared by dissolving the deuterated chloride salt of the peptide in  $\text{D}_2\text{O}$  to obtain a 2 wt% solution. To this solution an equal volume of pH 9.0 buffer (250 mM Borate and 20 mM NaCl) in  $\text{D}_2\text{O}$  was added and the contents were gently mixed and incubated on a sand bath at 50  $^{\circ}\text{C}$ . IR measurements were taken at room temperature. Spectra were collected at 1  $\text{cm}^{-1}$  resolution, and the spectrum recorded was an average of 100 scans.

**Oscillatory Shear Rheology.** Dynamic time, frequency, and strain sweep experiments were performed on a Paar-Physica MCR 500 rheometer with a 25 mm parallel plate geometry and 0.5 mm gap distance. The peptide was first dissolved in ice-cold water

to obtain a concentration that is twice the final peptide concentration in the gel. Then, an equal amount of ice-cold buffer pH 9 (250mM Borate, 20mM NaCl) was added to the peptide stock solution, mixed gently and immediately loaded onto the rheometer plate equilibrated to 5 °C. After the sample was loaded and the parallel plate lowered, standard low-viscosity mineral oil was used to insulate the sides of the parallel plate in order to prevent evaporation. The temperature was then increased to 50 °C to initiate folding, assembly and gelation. Control experiments show that the mineral oil has no effect on the rheological measurements. Gelation was observed by monitoring the evolution of the storage modulus ( $G'$ ) with time, in a dynamic time sweep experiment performed at an angular frequency of 6 rad/s and strain of 0.2 %. Storage moduli values ( $G'$ ) obtained at the end of 1 hr are reported with standard deviation values in parentheses obtained from experiments performed in triplicate. Frequency sweep experiments were performed by varying the frequency from 0.1-100 rad/s at a constant strain of 0.2 % and strain sweep experiments were performed by varying the strain from 0.01 to 100 % at a constant frequency of 6 rad/s. The frequency and strain sweep experiments verified that all time sweep experiments were performed within the linear viscoelastic regime.

## References

1. Choo, D. W.; Schneider, J. P.; Graciani, N. R.; Kelly, J. W., Nucleated Antiparallel  $\beta$ -Sheet That Folds and Undergoes Self-Assembly: A Template Promoted Folding Strategy toward Controlled Molecular Architectures. *Macromolecules* **1996**, 29, (1), 355-366.
2. Lamm, M. S.; Rajagopal, K.; Schneider, J. P.; Pochan, D. J., Laminated morphology of nontwisting  $\beta$ -sheet fibrils constructed via peptide self-assembly. *J. Am. Chem. Soc.* **2005**, 127, (47), 16692-16700.
3. Schneider, J. P.; Pochan, D. J.; Ozbas, B.; Rajagopal, K.; Pakstis, L.; Kretsinger, J., Responsive hydrogels from the intramolecular folding and self-assembly of a designed peptide. *J. Am. Chem. Soc.* **2002**, 124, (50), 15030-15037.
4. Karle, I.; Gopi, H. N.; Balaram, P., Supramolecular Chemistry And Self-assembly Special Feature: Infinite pleated  $\beta$ -sheet formed by the  $\beta$ -hairpin Boc- $\beta$ -Phe- $\beta$ -Phe-D-Pro-Gly- $\beta$ -Phe- $\beta$ -Phe-OMe. *Proc. Natl. Acad. Sci. U. S. A.* **2002**, 99, (8), 5160-5164.
5. Gibbs, A. C.; Bjorndahl, T. C.; Hodges, R. S.; Wishart, D. S., Probing the Structural Determinants of Type II'  $\beta$ -Turn Formation in Peptides and Proteins. *J. Am. Chem. Soc.* **2002**, 124, (7), 1203-1213.
6. Stanger, H. E.; Gellman, S. H., Rules for Antiparallel  $\beta$ -Sheet Design: D-Pro-Gly Is Superior to L-Asn-Gly for  $\beta$ -Hairpin Nucleation. *J. Am. Chem. Soc.* **1998**, 120, (17), 4236-4237.
7. Espinosa, J. F.; Syud, F. A.; Gellman, S. H., Analysis of the factors that stabilize a designed two-stranded antiparallel  $\beta$ -sheet. *Protein Sci.* **2002**, 11, (6), 1492-1505.
8. de Alba, E.; Rico, M.; Jimenez, M. A., The turn sequence directs  $\beta$ -strand alignment in designed  $\beta$ -hairpins. *Protein Sci* **1999**, 8, (11), 2234-2244.
9. Venkatraman, J.; Shankaramma, S. C.; Balaram, P., Design of Folded Peptides. *Chem. Rev.* **2001**, 101, (10), 3131-3152.
10. Schenck, H. L.; Gellman, S. H., Use of a Designed Triple-Stranded Antiparallel  $\beta$ -Sheet To Probe  $\beta$ -Sheet Cooperativity in Aqueous Solution. *J. Am. Chem. Soc.* **1998**, 120, (19), 4869-4870.
11. Yang, Z. M.; Liang, G. L.; Ma, M. L.; Gao, Y.; Xu, B., Conjugates of naphthalene and dipeptides produce molecular hydrogelators with high efficiency of hydrogelation and superhelical nanofibers. *J. Mater. Chem.* **2007**, 17, (9), 850-854.
12. Collier, J. H.; Messersmith, P. B., Self-assembling polymer-peptide conjugates: Nanostructural tailoring. *Adv. Mater.* **2004**, 16, (11), 907-910.
13. Surewicz, W. K.; Mantsch, H. H.; Chapman, D., Determination of protein secondary structure by Fourier transform infrared spectroscopy: A critical assessment. *Biochemistry* **1993**, 32, (2), 389-394.

14. Nagarkar, R. P.; Schneider, J. P., Synthesis and Primary Characterization of Self-Assembled Peptide-based hydrogels. In *Nanostructure Design, Methods and Protocols*, Gazit, E.; Nussinov, R., Eds. Humana Press: 2008; pp 61-77.

## Chapter 6

### ROLE OF CELL CULTURE CONDITIONS IN ENHANCING THE MECHANICAL PROPERTIES OF SELF-ASSEMBLED B-HAIRPIN PEPTIDE HYDROGELS AS A FUNCTION OF TIME

#### 6.0 Introduction

As discussed in previous chapters, MAX1, a  $\beta$ -hairpin with two  $\beta$ -strands of alternating valine and lysine residues, remains unfolded in aqueous solution at low pH and ionic strength (10 mM NaCl). Under these conditions, the positively lysines inhibit peptide folding and subsequent self-assembly. However, addition of cell culture media such as Dulbecco's Modified Essential Medium (DMEM), which contains about 160 mM mono and divalent salts, effectively screens the lysine-based charges and allows peptide to fold and self-assemble at 37 °C to form a mechanically rigid hydrogel.

Preliminary studies by Kretsinger et al.<sup>1</sup> showed that a 2 wt% MAX1 hydrogel fabricated with 0.5XDMEM (~ 80 mM mono and divalent salts) at 37 °C achieved an average storage modulus of about 2200 Pa after 60 min of gelation. However, 2 wt% MAX1 hydrogels fabricated under identical conditions but incubated under cell culture conditions (5% CO<sub>2</sub>, 37 °C) were significantly more rigid. A storage modulus of about 10,000 Pa was realized after 24 hrs of incubation. In general,

dynamic time sweep experiments of MAX1 hydrogels fabricated with DMEM show a small time dependent increase in storage modulus even after 60 minutes of gelation, normally referred to as “aging” process. Although, this aging process may be responsible for a moderate increase in rigidity of MAX1 hydrogels over extended periods of time, the large increase in modulus due to gel incubation under cell culture conditions cannot be explained by this aging process. In this chapter, we probe the factor(s) responsible for causing the significant increase in the storage modulus of MAX1 hydrogels under cell culture conditions.

### **6.1 Self-Assembly and Hydrogelation of MAX1 under Cell Culture Conditions**

The material properties of MAX1 hydrogels formed using DMEM were assessed by circular dichroism spectroscopy and oscillatory rheology. For these experiments, MAX1 is first dissolved in water to give a 4 wt% peptide solution. To this, an equal volume of 2XDMEM is added to give a 2 wt% MAX1 solution containing 1XDMEM (160 mM mono and divalent salts). The gelation of this solution is then triggered to by increasing the temperature to 37 °C. Hereafter, 1XDMEM is referred to as DMEM. Figure 6.1 shows a circular dichroism wavelength spectrum and a dynamic time sweep experiment of a 2 wt% MAX1 hydrogel formed with DMEM cell culture media at 37 °C. Figure 6.1(a) shows a CD spectrum where the mean residual ellipticity [ $\theta$ ] is measured as a function of wavelength (nm). The data shows that MAX1 forms a  $\beta$ -sheet secondary structure in DMEM at 37 °C as indicated by a

minimum at 216 nm. Figure 6.1(b) shows the kinetics of hydrogelation assessed by oscillatory shear rheology. The data shows that 2 wt% MAX1 solutions acquire a storage modulus of  $6000 \pm 1300$  Pa after 60 min of gelation at 37 °C. Note that gels containing 1X DMEM instead of 0.5X DMEM afford an approximately 3 fold increase in modulus value.

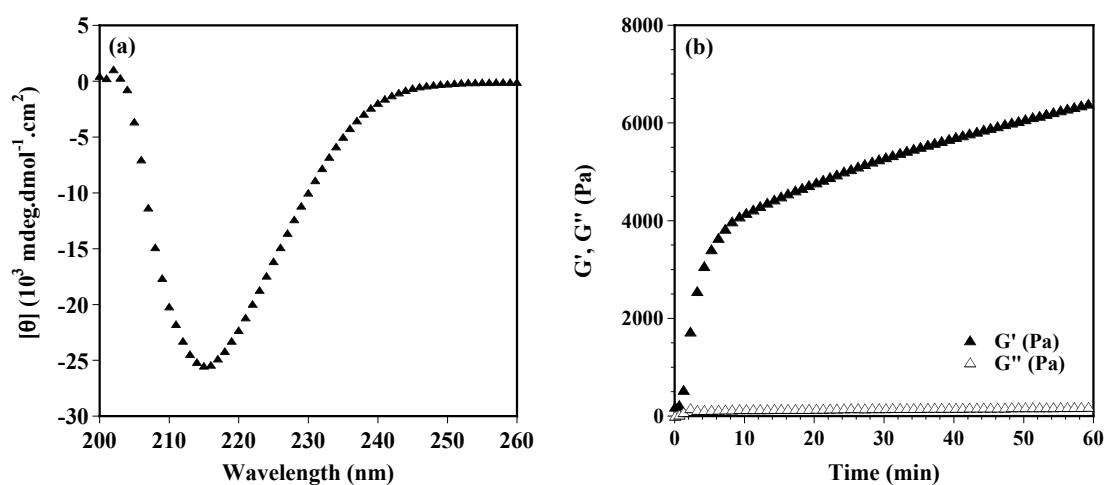


**Figure 6.1 (a) CD spectra and (b) Bulk material properties of 2 wt% MAX1 hydrogels formed with DMEM at 37 °C**

The material properties of 2 wt% MAX1 hydrogels were then investigated under cell culture conditions. Hydrogels were prepared in the same manner as described for Figure 6.1 and were then incubated under cell culture conditions [5% CO<sub>2</sub>, 37 °C] for a period of up to 48 hrs prior to rheological characterization. Figure 6.2 shows dynamic frequency sweep data that measures the storage modulus of the incubated MAX1 hydrogels as a function of angular frequency. The data shows that

storage moduli of  $13200 \pm 1700$  Pa and  $17700 \pm 1700$  Pa were realized for 2 wt% MAX1 hydrogels after 24 and 48 hrs of incubation respectively. These results indicate that the rigidity of MAX1 hydrogels increases significantly during the incubation period.

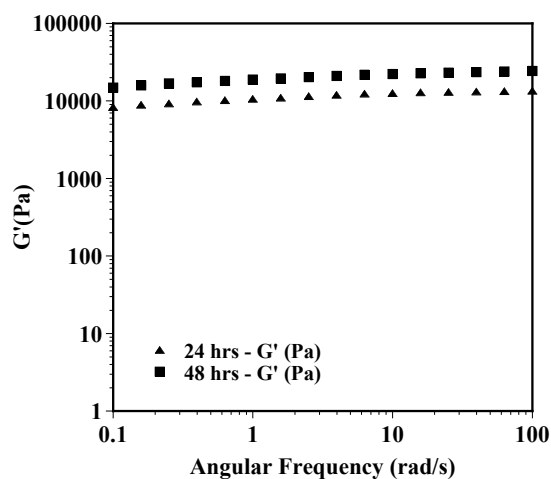


**Figure 6.2 Dynamic frequency sweep of 2 wt% MAX1 hydrogels incubated under cell culture conditions for 24 and 48 hrs**

## **6.2 Increase in Storage Modulus of MAX1 Hydrogels over Time: Effect of Normal Aging**

Figure 6.1(b) shows a dynamic time sweep experiment in which a gel is formed under non-cell culturing conditions. The storage modulus increases rapidly during the first 10 min of gelation and then gradually stiffens with time while the gel “ages”. If this aging process was responsible for the dramatic increase in rigidity

observed for gels incubated under cell culture conditions. Over time the storage modulus of the hydrogels at 24 and 48 hrs would be about 12000 and 14000 Pa respectively. These values were calculated by the slope of the line defining the increase in  $G'$  during the aging phase (e.g. from 50-60 min). The equation of the line extending from 50 to 60 minutes of the time sweep in Figure 6.1(b) is found to be

$$G' = 1942.9\ln(t) - 1536.3 [r^2 = 0.9994] \quad (1)$$

Using equation (1),

At 24 hrs,  $t = 1440$  min,  $G' = 12593$  Pa [Experimental:  $13200 \pm 1700$  Pa (Figure 8.2)]

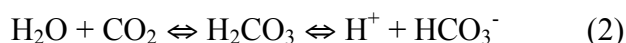
At 48 hrs,  $t = 2880$  min,  $G' = 13939$  Pa [Experimental:  $17700 \pm 1700$  Pa (Figure 8.2)]

Although the calculated storage modulus value at 24 hrs is comparable to the experimental value, the calculated modulus value at 48 hrs is lower than the experimental value. This suggests that the time dependent increase in storage modulus seen in this aging phase may not be the only factor responsible for dramatic increase in rigidity of MAX1 hydrogels under cell culture conditions.

### **6.3 Effect of Sodium Bicarbonate on the Kinetics of Self-Assembly and Hydrogelation of MAX1**

The DMEM buffer contains various vitamins, inorganic salts and amino acids for its function. However, the major constituents of DMEM buffer include NaCl

and NaHCO<sub>3</sub>. Sodium bicarbonate in conjunction with gaseous carbon dioxide at 37 °C maintains the pH of the media at 7.4. Carbon dioxide in the gas phase dissolves in the medium to establish equilibrium with bicarbonate anions to regulate the pH, equation (2).<sup>2</sup>



Since sodium bicarbonate and sodium chloride are the major constituents of the DMEM, its effect on the kinetics of self-assembly and hydrogelation of MAX1 was assessed using circular dichroism and oscillatory rheology. For these experiments, BTP buffer containing varying concentrations of sodium bicarbonate and a physiologically relevant concentration of 150 mM NaCl is used. Figure 6.3(a) shows sodium bicarbonate concentration dependent kinetics of folding and self-assembly of 0.25 wt% MAX1 monitored at 216 nm as a function of time. A lower peptide concentration is used since the kinetics of folding and self-assembly at a concentration of 2 wt% is very fast, which made it difficult to load the sample into the CD cell. The data shows that MAX1 exhibits minimal  $\beta$ -sheet formation in absence of NaHCO<sub>3</sub>. However, upon increasing the concentration of sodium bicarbonate, MAX1 exhibits faster kinetics of folding and self-assembly as observed by the change in mean residual ellipticity  $[\theta]$  at 216 nm as a function of time. However, no significant increase in kinetics of folding and self-assembly is observed when the concentration of sodium bicarbonate is increased from 22 to 44 mM. The DMEM buffer contains 44

mM NaHCO<sub>3</sub> and therefore a maximum of 44 mM NaHCO<sub>3</sub> was used for the circular dichroism and rheological measurements. Similar to the CD experiments, dynamic time sweep experiments with 2 wt% MAX1 at pH 7.4 and 37 °C show a bicarbonate concentration dependent increase in material rigidity, Figure 6.3(b). Two wt% MAX1 hydrogels prepared with DMEM buffer (44 mM NaHCO<sub>3</sub>) and the BTP buffer (44 mM NaHCO<sub>3</sub>) at pH 7.4 exhibit similar storage moduli values i.e. 6000 ± 1300 and 5400 ± 100 Pa respectively, Figure 6.1(b) and Figure 6.3(b). This result suggests that sodium bicarbonate may be the major contributor to the rigidity of the hydrogels.

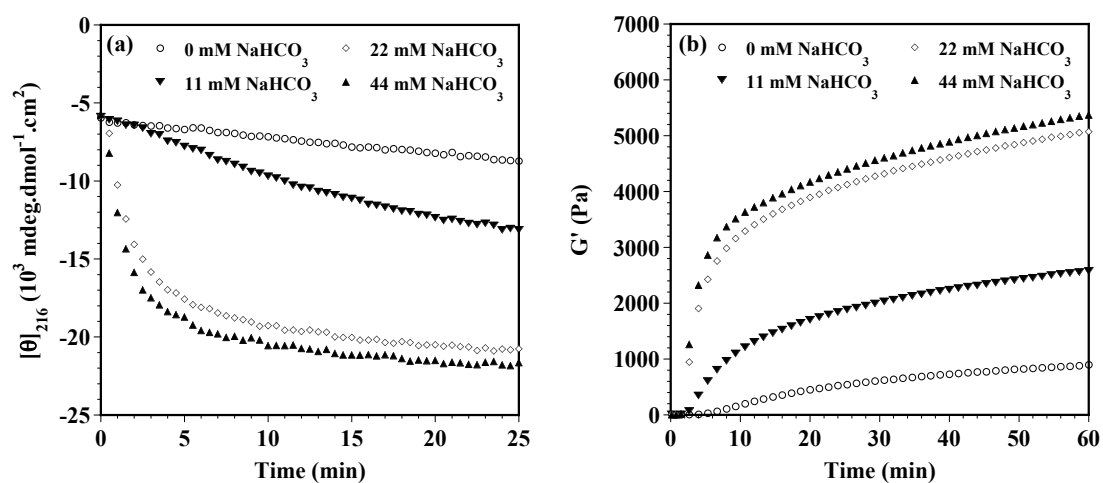


**Figure 6.3 Sodium bicarbonate concentration dependent kinetics of self-assembly and hydrogelation of MAX1 at pH 7.4 (50mM BTP, 150 mM NaCl) and 37 °C (a) 0.25 wt% MAX1 (b) 2 wt% MAX1**

To further investigate the contribution of sodium bicarbonate only, CD and rheology experiments were performed using BTP buffer (50 mM BTP, 44 mM

NaHCO<sub>3</sub>) in presence and absence of salt. Figure 6.4(a) shows kinetic scans of 0.25 wt% MAX1 solutions monitoring the  $\beta$ -sheet formation  $[(\theta)_{216}]$  as a function of time. The data shows that the NaCl does not influence the kinetics of folding and self-assembly of MAX1 in the presence of 44 mM NaHCO<sub>3</sub>. Similarly, the kinetics of hydrogelation and thus the ultimate rigidity of MAX1 hydrogel is independent of NaCl in presence of NaHCO<sub>3</sub>. These results indicate that sodium bicarbonate plays an important role in positively affecting the kinetics of self-assembly and hydrogelation of MAX1.

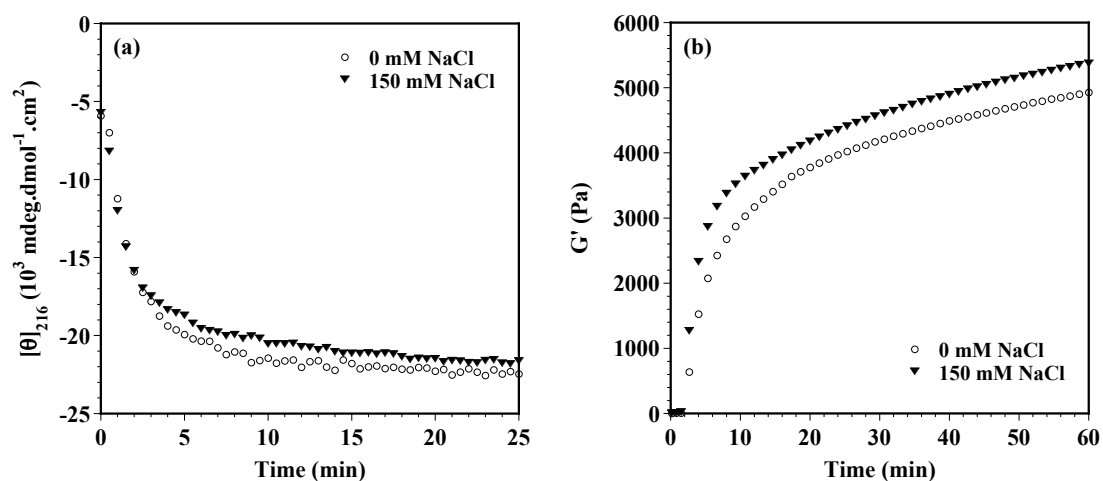


**Figure 6.4 Effect of NaCl on the kinetics of self-assembly and hydrogelation of 2 wt% MAX1 hydrogels at pH 7.4 (50mM BTP) in presence of 44 mM NaHCO<sub>3</sub> and 37 °C**

In addition to the rate of folding and self-assembly, the mechanical rigidity of self-assembled hydrogels is also influenced by the nanoscale morphology of

the peptide fibrils in self-assembled state. Figure 6.5 shows the transmission electron micrographs of diluted 2 wt% MAX1 hydrogels prepared at pH 7.4 (50 mM BTP, 150 mM NaCl) in presence and absence of 44 mM NaHCO<sub>3</sub>. The data shows that in absence of sodium bicarbonate, typical monodispersed fibrils of MAX1 are obtained.<sup>3</sup> However, in presence of 44 mM sodium bicarbonate, the fibrils appear to be undergoing some interfibrillar associations, which may be contributing to the mechanical rigidity of the MAX1 hydrogels. Collectively, data from Figure 6.3, 6.4 and 6.5 suggest that sodium bicarbonate has a significant effect on the self-assembly, hydrogelation and nanoscale morphology of MAX1 hydrogels.

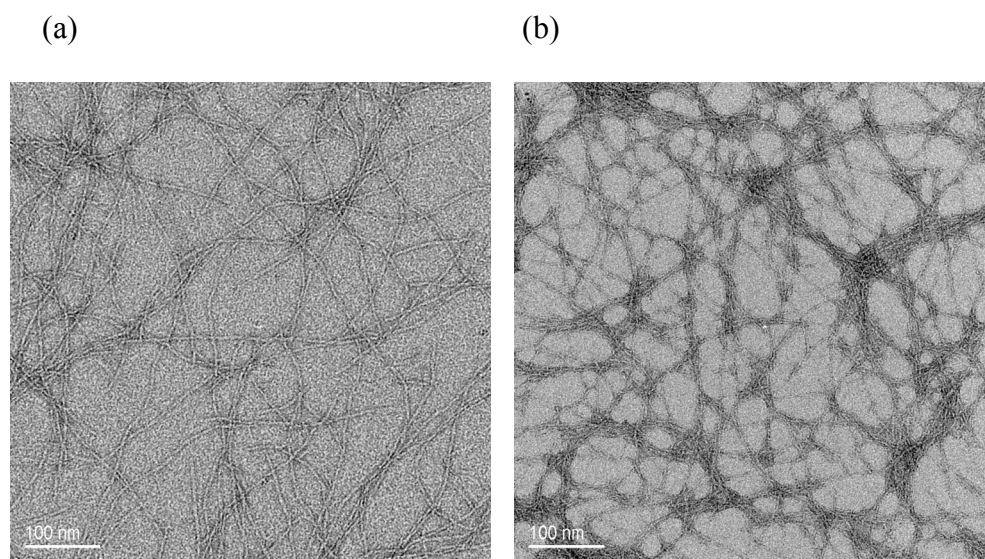


**Figure 6.5 Nanoscale morphology of MAX1 hydrogels prepared at pH 7.4 in (a) absence and (b) presence of 44 mM NaHCO<sub>3</sub>**

Based on the TEM data, it appears that the self-assembled fibrils of MAX1 seem to undergo an interfibrillar association event in presence of  $\text{NaHCO}_3$ . This may be due to the possible interactions of the bicarbonate anion with the positively charged lysine side chain of the self-assembled fibrils of MAX1 as shown in Figure 6.6. However, a cryoTEM experiment will further confirm the above hypothesis.

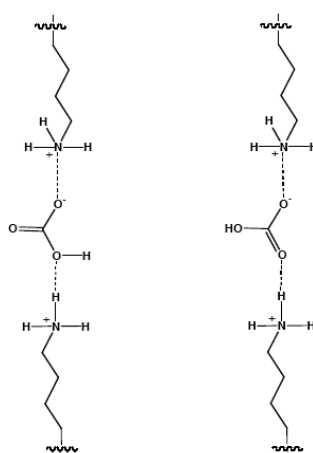


**Figure 6.6 Proposed interaction of bicarbonate anion with lysine side chain**

#### **6.4 Influence of Gaseous Carbon Dioxide on Storage Modulus of MAX1 Hydrogels**

Under cell culture conditions, carbon dioxide is known to dissolve into the media and establish equilibrium with the bicarbonate anions. However, if sodium bicarbonate interacts with the peptide fibrils as proposed, this may lead to reduction in bicarbonate concentration in the buffer. Therefore, more carbon dioxide may dissolve

into the media to increase the effective concentration of the bicarbonate anions and regulate the pH. To investigate the possible effect of dissolved carbon dioxide on the rigidity of 2 wt% MAX1 hydrogels at 37 °C, three sets of hydrogels were prepared. The first set (I) of hydrogels is prepared with DMEM that does not contain sodium bicarbonate but supplemented with 44 mM BTP or 44 mM HEPES only (again, no NaHCO<sub>3</sub>). The second set (II) of hydrogels is prepared with DMEM supplemented with 44 mM BTP or 44 mM HEPES and 44 mM NaHCO<sub>3</sub>. Sodium bicarbonate is included in the second set of MAX1 hydrogels to investigate its effect on the material rigidity of the resultant hydrogels. The third set (III) of MAX1 hydrogels is prepared with DMEM supplemented with either 44 mM NaHCO<sub>3</sub>, 44 mM BTP and 44 mM HEPES and exposed to 5% gaseous carbon dioxide. This set of gels is incubated with 5% carbon dioxide to show the effect of dissolved carbon dioxide on the rigidity of the resultant hydrogels over time. Samples from each of MAX1 hydrogels were subjected to oscillatory rheology measurements to determine their storage moduli after 24 and 48 hrs of incubation under their respective conditions. Figure 6.7 shows the material properties of the 2 wt% hydrogels investigated under different conditions. Discussing the data from right to left, MAX1 hydrogels prepared with DMEM supplemented with BTP and HEPES only acquired storage modulus in the range of 4000-5500 Pa after 48 hrs of gelation time. However, gels prepared with BTP and HEPES but in the presence of 44 mM NaHCO<sub>3</sub> resulted in more rigid hydrogels (7000-9600 Pa). This is expected since sodium bicarbonate positively affects the material rigidity of MAX1 hydrogels as shown in Figure 6.3. On the other hand, gels exposed to CO<sub>2</sub> were only slightly less

rigid than those made in presence of  $\text{NaHCO}_3$  (5400-7800 Pa). But the gels prepared with DMEM media supplemented with 44 mM  $\text{NaHCO}_3$  and also exposed to 5%  $\text{CO}_2$  were significantly more rigid than the BTP and HEPES containing hydrogels (13200-17700 Pa). This data indicates that both  $\text{NaHCO}_3$  and  $\text{CO}_2$  individually enhance the rigidity of MAX1 hydrogels but show a synergistic enhancement when used in conjunction.

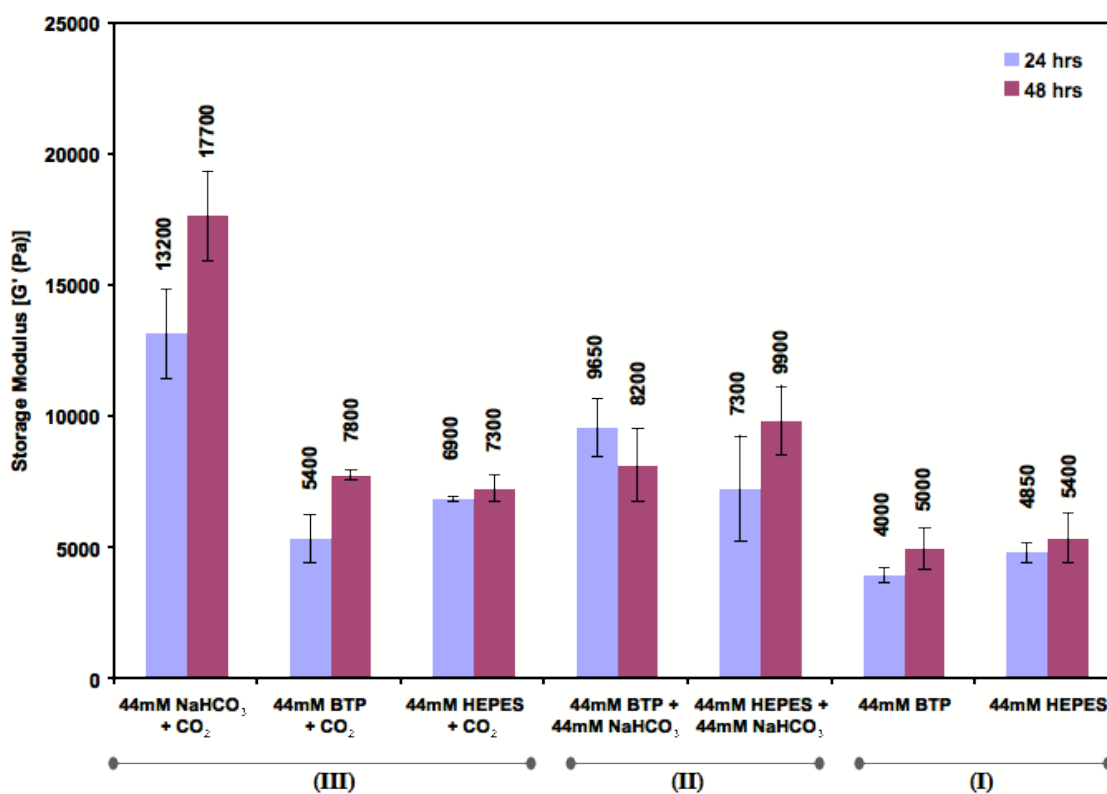


**Figure 6.7 Mechanical properties of 2 wt% MAX1 hydrogels at pH 7.4 and 37 °C based on incubation conditions**

## 6.5 Role of Dissolved Carbon Dioxide on Storage Modulus of MAX1 Hydrogels

Under cell culture conditions, CO<sub>2</sub> dissolves into the media and forms carbonic acid, which further dissociates to regulate the bicarbonate concentration. In this case, carbon dioxide may be increasing the effective concentration of the bicarbonate anions in the media, which in turn affects the rigidity of the MAX1 hydrogels. If true then under saturated bicarbonate concentrations, equation (2) will be pushed to the left and no more carbon dioxide will dissolve into the media. To demonstrate this, a rheological study was performed wherein the material rigidity of 2 wt% MAX1 hydrogels at pH 7.4 and 37 °C (60 min time sweep) were determined at increasing concentration of sodium bicarbonate in the buffer till a saturation in the storage modulus is obtained. The data in Figure 6.8(a) shows that the storage modulus of the gels reached a constant saturation value around 10,000 Pa with 88-132 mM sodium bicarbonate concentration. With saturated bicarbonate conditions, carbon dioxide will not dissolve into the media to regulate the bicarbonate concentration i.e equation (2) should be pushed to the left to maintain the pH at 7.4. Figure 6.8(b) shows the storage moduli of 2 wt% MAX1 gels prepared in presence of 100 mM NaHCO<sub>3</sub> and then incubated for 48 hrs in presence and absence of carbon dioxide. The data shows that the rigidity of hydrogels is comparable irrespective of whether the gel is exposed to gaseous CO<sub>2</sub> or not. This data suggests that the carbon dioxide dissolves to increase the local concentration of the bicarbonate anions and thus rigidity of the

hydrogels as a function of time. The rigidity of hydrogels in Figure 6.8(b) is higher than the rigidity of hydrogels in Figure 6.8(a), since the gels were aged for 48 hrs prior to analysis.

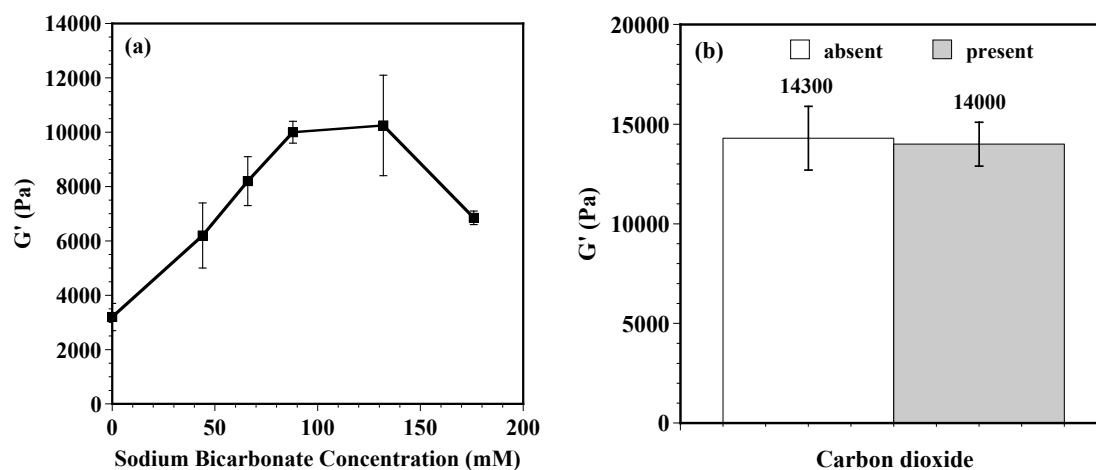


**Figure 6.8 Mechanical properties of 2 wt% MAX1 hydrogels at pH 7.4 and 37 °C (a)  $G'$  as a function of sodium bicarbonate concentration (b) Effect of CO<sub>2</sub> on rigidity of hydrogels with saturated concentration of sodium bicarbonate**

## 6.6 Conclusions

This chapter discusses the possible factor(s) that are responsible for the enhancement of mechanical properties of MAX1 hydrogels upon exposure to cell culture conditions. Self-assembled hydrogels display an increase in storage modulus over time following initial hydrogelation via an aging process still not fully understood. However, the calculated and experimental values of storage moduli indicated that this aging process is not the only responsible factor for the large increase in  $G'$  when gels are incubated

in presence of cell culture media under cell culture conditions. Hydrogels scaffolds for cell culture experiments are prepared using cell culture media (DMEM), the major constituents of which include sodium bicarbonate and sodium chloride. In addition, the fabricated hydrogels are exposed to 5% gaseous carbon dioxide to maintain the pH of the buffer at 7.4 during cell culture. Therefore, the effect of sodium chloride, sodium bicarbonate and gaseous carbon dioxide on the material properties of MAX1 gels was probed. The results demonstrated that sodium bicarbonate positively affects the self-assembly kinetics and hydrogelation of MAX1 whereas sodium chloride had minimal contribution. In addition, the material rigidity of MAX1 hydrogels were higher when exposed to gaseous carbon dioxide, which is known to dissolve into the media to maintain the pH by increasing the bicarbonate concentration. However, in presence of both sodium bicarbonate and carbon dioxide, the mechanical properties of the gel were significantly enhanced as observed under cell culture conditions. But it is the local bicarbonate anion concentration in the gel, which increases due to dissolved carbon dioxide and enhances the mechanical rigidity of the hydrogel till a saturation level is reached. Hydrogels prepared with saturated concentration of sodium bicarbonate, when exposed to gaseous carbon dioxide showed no enhancement in rigidity. This demonstrated that no more carbon dioxide could dissolve in to the media to increase the local bicarbonate anion concentration and enhance the gel rigidity. In addition, nanostructure analysis revealed that the self-assembled fibrils associated in presence of bicarbonate anions, which may be contributing to the increase in mechanical properties.

## 6.7 Experimental Section

**Materials.** Rink amide resin was purchased from Polymer Laboratories. Trifluoroacetic acid (TFA), piperidine, thioanisole, ethanedithiol, and anisole were purchased from Acros. Appropriately side-chain-protected Fmoc-amino acids were obtained from Novabiochem. 1-H-Benzotriazolium-1-[bis(Dimethylamino)Methylene]-5-Chloro-Hexafluorophosphate-(1-),3-Oxide (HCTU) was purchased from Peptide International. D<sub>2</sub>O was purchased from Aldrich. Dulbecco's Modified Eagle's Medium (DMEM), Boric acid and Bis-Tris Propane (BTP) were purchased from Sigma. MilliQ (Millipore) with a resistivity of 18.2 MΩ.cm was used for all experiments and is referred to as "water" in this paper.

**Peptide Synthesis and Purification.** Peptides were prepared on Rink amide resin via automated Fmoc peptide synthesis employing an ABI 433A peptide synthesizer and HCTU activation.<sup>4</sup> The resulting dry resin-bound peptides were cleaved and side-chain-deprotected using a cocktail of TFA/thioanisole/ethanedithiol/anisole (90:5:3:2) for 2 hrs under nitrogen. The resin was filtered and peptide precipitated from the filtrate using cold diethyl ether. Crude peptide was subsequently purified by Reverse Phase-HPLC (Waters 600 series) using a semi-preparative Vydac C18 peptide/protein column. The resulting peptide solution was frozen with liquid nitrogen and lyophilized

to afford pure peptide. The purity of the peptide was established using Electrospray ionization mass spectrometry and analytical HPLC.

**Circular Dichroism Studies.** CD spectra were collected on a Jasco model J-810 spectropolarimeter. A 1 mM peptide stock of MAX1 was prepared by dissolving the appropriate amount of purified peptide in water. UV-Vis spectroscopy was employed to determine the concentration of the peptide stock solution using the extinction coefficient ( $\epsilon$ ) of MAX1 at 220 nm [ $\epsilon_{220} = 15750 \text{ cm}^{-1} \text{ M}^{-1}$  (MAX1 peptide)].  $\epsilon_{220}$  was determined by amino acid analysis. This 1 mM peptide stock was diluted to afford a 300  $\mu\text{M}$  peptide final stock solution, which was used to prepare all of the CD samples. For each CD sample, 300  $\mu\text{M}$  stock of peptide was mixed with an equal volume of pH 7.4 buffer or DMEM to afford a final concentration of 150  $\mu\text{M}$  peptide solution at pH 7.4. A similar procedure was adopted for pH 7.4 studies except that an equal volume of pH 7.4 buffer (100 mM BTP, 300 mM NaCl or 2X DMEM) was used and the final concentration of peptide employed was 2 wt%. Mean residue ellipticity  $[\theta]$  was calculated from the equation  $[\theta] = (\theta_{\text{obs}}/10lc)/r$ , where  $\theta_{\text{obs}}$  is the measured ellipticity in millidegrees,  $l$  is the length of the cell (centimeters),  $c$  is the molar concentration, and  $r$  is the number of residues.

Wavelength spectra from 260 to 190 nm were obtained in a 0.1 cm path length quartz cell at 37 °C to assess the secondary structure of MAX1. The rate of  $\beta$ -sheet formation was assessed by monitoring  $[\theta]_{216}$  as a function of time at 37 °C. Sodium

bicarbonate concentration-dependent spectra were collected in a 0.1 mm quartz cell by measuring  $[\theta]_{216}$  of 2 wt% peptide preparations at pH 7.4 (50 mM BTP) as a function of sodium bicarbonate concentration.

**Oscillatory Shear Rheology.** Dynamic time, frequency, and strain sweep experiments were performed on a Paar-Physica MCR 500 rheometer with a 25 mm parallel plate geometry and 0.5 mm gap distance. The peptide was first dissolved in ice-cold water to obtain a concentration that is twice the final peptide concentration in the gel. Then, an equal amount of ice-cold buffer pH 7.4 (2X DMEM) was added to the peptide stock solution, mixed gently and immediately loaded onto the rheometer plate equilibrated to 5 °C. After the sample was loaded and the parallel plate lowered, standard low-viscosity mineral oil was used to insulate the sides of the parallel plate in order to prevent evaporation. The temperature was then increased to 37 °C to initiate folding, assembly and gelation. Control experiments show that the mineral oil has no effect on the rheological measurements. Gelation was observed by monitoring the evolution of the storage modulus ( $G'$ ) with time, in a dynamic time sweep experiment performed at an angular frequency of 6 rad/s and strain of 0.2 %. Storage moduli values ( $G'$ ) obtained at the end of 1 hr are reported with standard deviation values in parentheses obtained from experiments performed in triplicate. Frequency sweep experiments were performed by varying the frequency from 0.1-100 rad/s at a constant strain of 0.2 % and strain sweep experiments were performed by varying the strain from 0.01 to 100 % at a constant frequency of 6 rad/s. The frequency and strain sweep

experiments verified that all time sweep experiments were performed within the linear viscoelastic regime.

**Mechanical properties of Pre-formed gels:**

The peptide was first dissolved in ice-cold water to obtain a concentration that is twice the final peptide concentration in the gel. Then, an equal amount of ice-cold buffer pH 7.4 (2X DMEM or appropriate BTP buffer) was added to the peptide stock solution, mixed gently and 350  $\mu$ L was transferred into a confocal plate. The confocal plate was immediately covered and the pplate was placed in the incubator at 37 °C in presence or absence of CO<sub>2</sub>. The gels were allowed to cure for 2 hrs and then 700  $\mu$ L of buffer was added on top of the gel to prevent the gels from drying over time. The gels were incubated for either 24 or 48 hrs prior to rheological analysis. A dynamic time sweep experiment was first performed to allow the gel to achieve equilibrium modulus and thereafter a dynamic frequency sweep was performed.

**Transmission Electron Microscopy.** 1 wt% hydrogels were incubated for at least 24 hours prior to sample preparation. A 2-5  $\mu$ L aliquot of diluted gel was applied to carbon-coated copper grids. The samples were negatively stained by placing a drop of 2 % (w/v) uranyl acetate aqueous solution on the grid. The excess of the solution was blotted with filter paper, and the sample was subsequently left to dry. Concentrated samples were diluted to 0.1 % (w/v) with deionized water prior to staining. Bright field images of the fibril nanostructure were taken on a JEOL 2000-FX transmission

electron microscope (TEM) at 200 kV accelerating voltage on both a Gatan CCD camera and Kodak negative films.

## References

1. Kretsinger, J. K.; Haines, L. A.; Ozbas, B.; Pochan, D. J.; Schneider, J. P., Cytocompatibility of self-assembled b-hairpin peptide hydrogel surfaces. *Biomaterials* **2005**, 26, (25), 5177-5186.
2. Freshney, R. I., *Culture of Animal Cells, A Manual of Basic Technique*. 5th ed.; John Wiley & Sons, Inc.: New Jersey, 2005; p 627.
3. Ozbas, B.; Rajagopal, K.; Schneider, J. P.; Pochan, D. J., Semiflexible chain networks formed via self-assembly of beta-hairpin molecules. *Phys. Rev. Lett.* **2004**, 93, (26).
4. Nargarkar, R. P.; Schneider, J. P., Synthesis and Primary Characterization of Self-Assembled Peptide-based hydrogels. In *Nanostructure Design, Methods and Protocols*, Gazit, E.; Nussinov, R., Eds. Humana Press: 2008; pp 61-77.

## Chapter 7

### CONCLUSIONS

The material properties self-assembling peptide hydrogels presented in this thesis demonstrate that structure based design of the peptides can be employed to create functional materials with enhanced mechanical properties for biomedical applications. Gelation of these peptides can be triggered in response to environmental cues such as pH, ionic strength and cell culture media. The resultant peptides can be syringe delivered with spatial and temporal resolution making them attractive candidates as injectable biomaterials.

Self-assembled physically crosslinked hydrogels are self-supporting and moderately rigid but mechanically weak and therefore yield easily. Peptides were covalently modified at the molecular level to modulate the mechanical properties following photopolymerization. Hydrogels prepared using a N-terminal modified  $\beta$ -hairpin peptide (M1NA) had higher mechanical rigidity upon polymerization. However, these gels lacked the ability to be syringe delivered prior to irradiation. Hydrophilic face modification of the  $\beta$ -hairpin peptide with a lysine-diene (MLD) showed potential to be syringe delivered but did not exhibit significant increase in the mechanical rigidity of the hydrogels following polymerization. MKA peptides with

strategically placed N $\epsilon$ -acryloyl-L-lysine along the lysine face not only afforded syringe deliverable scaffolds but also with mechanical rigid hydrogels following polymerization. Although the resultant hydrogels exhibited enhanced mechanical rigidity following polymerization, they still yielded at lower strain values.

The peptide-polymer hydrogels were designed to impart enhanced mechanical properties as well as resistance to strain compared to the physically crosslinked hydrogels. MKA based hydrogels incorporated with increasing concentration of a high molecular weight bifunctional PEG (PEGDVB) afforded hydrogels that could be syringe delivered as well as polymerized to achieve a synergistic increase in the mechanical rigidity as compared to the individual networks. The surfaces of the resultant soft gels were found to be cytocompatible, thus making them attractive candidates as injectable scaffolds for tissue engineering applications. Another approach employed to fabricate mechanically robust hydrogels was through preparation of interpenetrating dual-networks. Self-assembled MAX1 hydrogels were polymerized in presence of diffused short PEG-diacrylate (PEGDA) to result in two physically interacting networks. Hydrogels with exhibited a significant non-linear increase in mechanical rigidity, which could be modulated by the concentration of PEGDA employed. These hydrogels have the ability to withstand high fracture and strain making them beneficial for use as load-bearing substitutes such as intervertebral discs.

Utilizing peptide design principles, three-stranded peptide (EMAX2) capable of folding and subsequent self-assembly was designed. The three-stranded

peptide (EMAX2) exhibited faster kinetics of self-assembly and resulted in mechanically enhanced hydrogels compared to MAX1. In addition, EMAX2 hydrogels could be syringe delivered with spatial and temporal resolution. EMAX2 hydrogel surfaces were found to be non-cytotoxic to mesenchymal stem cells and supported cell adhesion and proliferation events. The mechanical properties of the three-stranded peptides could be further tuned by incorporating turn sequences of varying hydrophobicity. These studies demonstrated that design principles and structural considerations from both, non-assembling *de novo* designed  $\beta$ -sheets and naturally occurring self-assembling proteins, can be employed as a useful source to create responsive functional materials.